



The University of  
**Nottingham**

UNITED KINGDOM • CHINA • MALAYSIA

**Phytochemical Investigation of Alkaloids  
from the Leaves of *Elaeocarpus tectorius*  
(Lour.) Poir. and *Elaeocarpus angustifolius*  
Blume**

MARGRET CHINONSO EZEIKE

BSc

School of Pharmacy

The University of Nottingham Malaysia Campus

Thesis submitted to the University of Nottingham for the degree of  
Master of Philosophy

February 2018

## PREFACE

This thesis is submitted for the degree of Master of Philosophy at the University of Nottingham. The study described herein was conducted under the supervision of Dr Lim Kuan Hon of the Faculty of Science, University of Nottingham Malaysia.

This work is to the best of my knowledge original, except where acknowledgements and references are made to previous work. This thesis has not been submitted for any degree and is not concurrently submitted in candidature of any other degree.

Part of this work has been presented in the following publication:

Ezeoke, M. C.; Krishnan, P.; Sim, D. S.-Y.; Lim, S.-H.; Low, Y.-Y.; Chong, K.-W.; Lim, K.-H. *Phytochemistry*, **2018**, *146*, 75–81.

## **ACKNOWLEDGEMENTS**

This research study was conducted with the assistance of many whose names may not all be mentioned. Their contributions are sincerely appreciated.

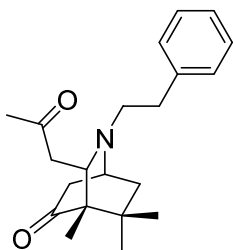
I would like to express my gratitude to my research supervisor, Dr. Lim Kuan Hon, for his patience, guidance and support throughout the duration of this research. I would also like to express my appreciation to Dr. Mai Chun Wai from School of Pharmacy, International Medical University for carrying out the biological assay reported in this thesis.

My greatest appreciation also goes out to Prof. T.S. Kam, Dr Y.Y. Low and their research team at Chemistry Department, University of Malaya for aiding the collection of most of the spectroscopic data. I also appreciate Dr K.T. Yong from Institute of Biological Sciences, University of Malaya for aiding the identification of the plant materials used in this project.

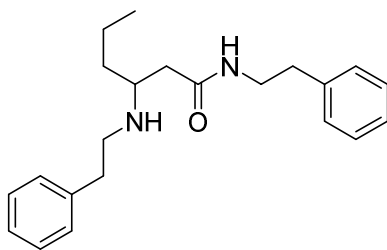
My deepest appreciation goes to my co-supervisor, Mr. Premanand Krishnan for his assistance all through my period of lab work. Also to I thank my colleagues, friends and family, as I owe them a lot for their unceasing support and encouragement.

## ABSTRACT

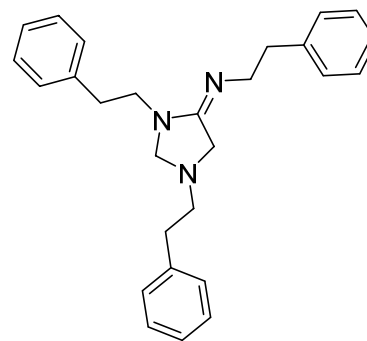
The genus *Elaeocarpus* (Elaeocarpaceae) has been reported as a producer of interesting indolizidine alkaloids. The leaves of *Elaeocarpus tectorius* (Lour.) Poir and *Elaeocarpus angustifolius* Blume were not previously phytochemically investigated. Preliminary test for presence of alkaloids on the leaf samples of both plants collected in Malaysia yielded positive results. The present study was therefore aimed at isolation and identification of new and bioactive compounds from the leaves of both plant species. A total of 16 alkaloids were identified in the present study. The leaves of *E. tectorius* yielded four new phenethylamine-containing alkaloids, namely, tectoricine (**1**), tectoraline (**2**), tectoramidine A (**3**) and tectoramidine B (**4**). These compounds represent the first occurrence of phenylethylamine-containing alkaloids from Elaeocarpaceae. Tectoricine (**1**) represents a novel isoquinuclidinone incorporating a phenethylamine moiety, while tectoraline (**2**) represents a rare alkamide incorporating two phenethylamine moieties. Tectoramidines A and B (**3** and **4**) represent the first naturally occurring trimeric and dimeric phenethylamine alkaloids incorporating an amidine function. The leaves of *E. angustifolius* yielded a total of 12 alkaloids, nine of which are new compounds. Seven of the nine new compounds obtained were indolizidine alkaloids, namely, carpusinine A (**5**), carpusinine B (**6**), carpusinine C (**7a**), epicarpusinine C (**7b**), carpusinine D (**8**), carpusinine E (**9**) and carpusidine (**14**), while the two remaining new compounds are pyrrolidine alkaloids, namely, carpusinine F (**10a**) and epicarpusinine F (**10b**). The three known alkaloids were identified as elaeokanine A (**11**), elaeokanine C (**12**) and elaeokanine D (**13**). The new carpusinine compounds (**5 – 10**) are alkyindolizidines that can be classified as elaeokanine-type alkaloids. Carpusidine (**14**) on the other hand represents the first simple indolizidine alkaloid isolated from Elaeocarpaceae. Compounds **5, 6, 7a/7b, 9, 11, 12, 13** and **14** were found to be non-cytotoxic when assessed using the CellTiter-Glo Luminescent Cell Viability Assay against a panel of 20 cancer cell lines and two normal human cell lines. In conclusion, chromatographic fractionation and purification of the alkaloid mixtures of the leaves of *E. tectorius* and *E. angustifolius* gave a total of 16 alkaloids including four phenylethylamine alkaloids, two pyrrolidine alkaloids and ten indolizidine alkaloids.



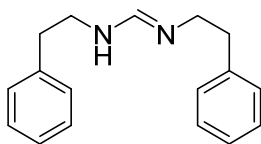
1



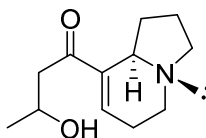
2



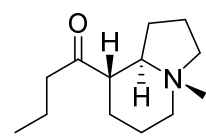
3



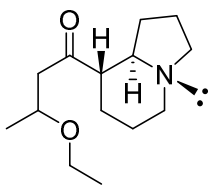
4



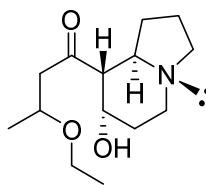
5



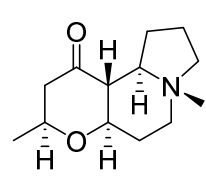
6



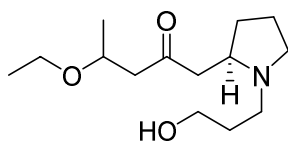
7a/7b



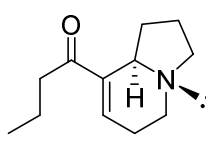
8



9



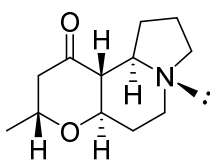
10a/10b



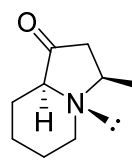
11



12



13



14

## TABLE OF CONTENTS

PREFACE.....	i
ACKNOWLEDGEMENTS.....	iii
ABSTRACT.....	iv
TABLE OF CONTENTS.....	vi
LIST OF FIGURES.....	ix
LIST OF TABLES.....	xiii
LIST OF SCHEMES.....	xv
LIST OF APPENDICES.....	xvi
<b>CHAPTER 1: INTRODUCTION.....</b>	<b>1</b>
1.1 Natural product from plants.....	1
1.2 Alkaloids.....	2
1.2.1 History and significance.....	2
1.2.2 Natural occurrence, distribution and localisation of alkaloids.....	5
1.2.3 Ecological roles of alkaloids in plants.....	6
1.2.4 Classification of alkaloids .....	7
1.2.4.1 Pyrrolidine alkaloids.....	12
1.2.4.2 Phenylethylamine alkaloids.....	13
1.2.5 Indolizidine alkaloids and classification of indolizidine alkaloids.....	14
1.2.5.1 Phenanthroindolizidine alkaloids.....	16
1.2.5.2 Polyhydroxylated indolizidine alkaloids.....	16
1.2.5.3 Steroidal indolizidine alkaloids.....	17
1.2.5.4 Alkylindolizidine alkaloids.....	18

1.2.5.5 Polycyclic indolizidine alkaloids.....	13
1.3 Indolizidine alkaloids from the <i>Elaeocarpus</i> genus.....	19
1.3.1 Biosynthesis of <i>Elaeocarpus</i> polycyclic indolizidine and alkyindolizidine alkaloids.....	20
1.4 The <i>Elaeocarpus</i> genus.....	21
1.4.1 Natural occurrence, morphological appearance and ethnomedicinal use.....	21
1.4.2 <i>Elaeocarpus angustifolius</i> Blume.....	22
1.4.3 <i>Elaeocarpus tectorius</i> (Lour.) Poir.....	23
1.4.4 Alkaloids from <i>Elaeocarpus</i> genus.....	25
1.5 Research objectives.....	30
<b>CHAPTER 2: EXPERIMENTAL.....</b>	<b>31</b>
2.1 General.....	31
2.2 Dragendorff's reagent.....	31
2.3 Plant material.....	31
2.4 Screening of plant material.....	32
2.5 Extraction of plant material.....	32
2.6 Isolation of alkaloids.....	33
2.6.1 Chromatographic procedures.....	33
2.6.1.1 Thin layer chromatography (TLC).....	33
2.6.1.2 Column chromatography.....	33
2.6.2 Isolation of alkaloids from the leaves of <i>E. tectorius</i> .....	36
2.6.3 Isolation of alkaloids from the leaves of <i>E. angustifolius</i> .....	37
2.7 Compound data.....	40
2.8 Cytotoxicity assay.....	42

2.8.1 Cell lines and cell culture.....	42
2.8.2 Luminescent cell viability assay.....	42
<b>CHAPTER 3: RESULTS AND DISCUSSION.....</b>	<b>43</b>
3.1 Alkaloids from <i>Elaeocarpus tectorius</i> .....	43
3.1.1 Tectoricine ( <b>1</b> ) .....	43
3.1.2 Tectoraline ( <b>2</b> ) .....	51
3.1.3 Tectoramidine A ( <b>3</b> ) .....	56
3.1.4 Tectoramidine B ( <b>4</b> ) .....	61
3.1.5 Biosynthetic pathway to tectoramidines A and B ( <b>3</b> and <b>4</b> ) .....	65
3.2 Alkaloids from <i>Elaeocarpus angustifolius</i> .....	66
3.2.1 Carpusinine A ( <b>5</b> ) .....	66
3.2.2 Carpusinine B ( <b>6</b> ) .....	73
3.2.3 Carpusinine C ( <b>7a</b> ) and epicarpusinine C ( <b>7b</b> ).....	79
3.2.4 Carpusinine D ( <b>8</b> ).....	85
3.2.5 Carpusinine E ( <b>9</b> ) .....	91
3.2.6 Carpusinine F ( <b>10a</b> ) and epicarpusinine F ( <b>10b</b> ) .....	97
3.2.7 (+)-Elaeokanine A ( <b>11</b> ) .....	105
3.2.8 Elaeokanine C ( <b>12</b> ) .....	108
3.2.9 Elaeokanine D ( <b>13</b> ) .....	111
3.2.10 Carpusidine ( <b>14</b> ) .....	114
3.3 Cytotoxic evaluation of alkaloids from <i>Elaeocarpus angustifolius</i> on cancer cell lines .....	121

<b>CHAPTER 4: CONCLUSION AND FUTURE STUDIES.....</b>	<b>123</b>
4.1 Future studies.....	125
<b>REFERENCES.....</b>	<b>126</b>
<b>APPENDIX.....</b>	<b>132</b>

## LIST OF FIGURES

**Figure 1.1:** Some structural variation encountered in alkaloids.

**Figure 1.2:** Structures of some alkaloids isolated from various sources.

**Figure 1.3:** Structures of **31**, **32** and **33**.

**Figure 1.4:** Examples of C<sub>16</sub> and C<sub>12</sub> carbon skeletons found in *Elaeocarpus* indolizidine alkaloids.

**Figure 1.5:** A - Flowers and leaves of *E. angustifolius*; B – Flowers, leaves and fruit of *E. tectorius*.

**Figure 1.6:** Structure of elaeocarpidine (**53**).

**Figure 2.1:** TLC plates of crude alkaloid mixtures of *E. angustifolius* (**A**) and *E. tectorius* (**B**).

**Figure 2.2:** Leaves of *E. angustifolius* and *E. tectorius* soaked in 95% ethanol.

**Figure 2.3:** Typical set up of column chromatography.

**Figure 2.4:** Isolation of alkaloids from the leaf extract of *E. tectorius*

**Figure 2.5:** Isolation of alkaloids from the leaf extract of *E. angustifolius*.

**Figure 3.1:** Structure of tectoricine (**1**).

**Figure 3.2:** COSY (bold bonds) and key HMBC <sup>1</sup>H-<sup>13</sup>C correlations (arrows) of tectoricine (**1**).

**Figure 3.3:** Selected NOESY correlations of tectoricine (**1**).

**Figure 3.4:** Experimental and calculated ECD spectra of tectoricine (**1**) in MeCN.

**Figure 3.5:** Structures of **54** and **55**.

**Figure 3.6:** <sup>1</sup>H NMR (600 MHz, CDCl<sub>3</sub>) spectrum of tectoricine (**1**).

**Figure 3.7:** <sup>13</sup>C NMR (150 MHz, CDCl<sub>3</sub>) spectrum of tectoricine (**1**).

**Figure 3.8:** Structure of tectoraline (**2**).

**Figure 3.9:** COSY (bold bonds) and key HMBC  $^1\text{H}$ - $^{13}\text{C}$  correlations (arrows) of tectoraline (2).

**Figure 3.10:**  $^1\text{H}$  NMR (600 MHz,  $\text{CDCl}_3$ ) spectrum of tectoraline (2).

**Figure 3.11:**  $^{13}\text{C}$  NMR (150 MHz,  $\text{CDCl}_3$ ) spectrum of tectoraline (2).

**Figure 3.12:** Structure of tectoramidine A (3).

**Figure 3.13:** COSY (bold bonds) and HMBC  $^1\text{H}$ - $^{13}\text{C}$  correlations (arrows) of tectoramidine A (3).

**Figure 3.14:**  $^1\text{H}$  NMR (600 MHz,  $\text{CDCl}_3$ ) spectrum of tectoramidine A (3).

**Figure 3.15:**  $^{13}\text{C}$  NMR (150 MHz,  $\text{CDCl}_3$ ) spectrum of tectoramidine A (3).

**Figure 3.16:** Structure of tectoramidine B (4).

**Figure 3.17:** HMBC  $^1\text{H}$ - $^{13}\text{C}$  correlations (arrows) of tectoramidine B (4).

**Figure 3.18:**  $^1\text{H}$  NMR (600 MHz,  $\text{CDCl}_3$ ) spectrum of tectoramidine B (4).

**Figure 3.19:**  $^{13}\text{C}$  NMR (150 MHz,  $\text{CDCl}_3$ ) spectrum of tectoramidine B (4).

**Figure 3.20:** Structure of carpusinine A (5).

**Figure 3.21:** COSY (bold bonds) and  $^1\text{H}$  -  $^{13}\text{C}$  HMBC correlations (arrows) of carpusinine A (5).

**Figure 3.22:** Selected NOESY correlations of carpusinine A (5).

**Figure 3.23:** Structures of 13, 14 and 56.

**Figure 3.24:**  $^1\text{H}$  NMR (600 MHz,  $\text{CDCl}_3$ ) spectrum of carpusinine A (5).

**Figure 3.25:**  $^{13}\text{C}$  NMR (150 MHz,  $\text{CDCl}_3$ ) spectrum of carpusinine A (5).

**Figure 3.26:** Structure of carpusinine B (6).

**Figure 3.27:** COSY (bold bonds) and HMBC  $^1\text{H}$ - $^{13}\text{C}$  correlations (arrows) of carpusinine B (6).

**Figure 3.28:** Selected NOESY correlations of carpusinine B (**6**).

**Figure 3.29:**  $^1\text{H}$  NMR (600 MHz,  $\text{CDCl}_3$ ) spectrum of carpusinine C (**6**).

**Figure 3.30:**  $^{13}\text{C}$  NMR (150 MHz,  $\text{CDCl}_3$ ) spectrum of carpusinine B (**6**).

**Figure 3.31:** Structure of carpusinine C (**7a**) and epicarpusinine C (**7b**).

**Figure 3.32:** COSY (bold bonds) and HMBC  $^1\text{H}$ - $^{13}\text{C}$  correlations (arrows) of **7a/7b**.

**Figure 3.33:**  $^1\text{H}$  NMR (600 MHz,  $\text{CDCl}_3$ ) spectrum carpusinine C (**7a**) and epicarpusinine C (**7b**).

**Figure 3.34:**  $^{13}\text{C}$  NMR (150 MHz,  $\text{CDCl}_3$ ) spectrum of carpusinine C (**7a**) and epicarpusinine C (**7b**).

**Figure 3.35:** Structure of carpusinine D (**8**).

**Figure 3.36:** COSY (bold bonds) and HMBC  $^1\text{H}$ - $^{13}\text{C}$  correlations (arrows) of carpusinine D (**8**).

**Figure 3.37:** Selected NOESY correlations of carpusinine D (**8**).

**Figure 3.38:**  $^1\text{H}$  NMR (600 MHz,  $\text{CDCl}_3$ ) spectrum of carpusinine D (**8**).

**Figure 3.39:**  $^{13}\text{C}$  NMR (150 MHz,  $\text{CDCl}_3$ ) spectrum of carpusinine D (**8**).

**Figure 3.40:** Structure of carpusinine E (**9**).

**Figure 3.41:** COSY (bold bonds) and HMBC  $^1\text{H}$ - $^{13}\text{C}$  correlations (arrows) of carpusinine E (**9**).

**Figure 3.42:** Structures of (+)-elaeokanines D (**13**) and (+)-elaeokanine E (**57**)

**Figure 3.43:** Selected NOESY correlations (arrows) of carpusinine E (**9**).

**Figure 3.44:**  $^1\text{H}$  NMR (600 MHz,  $\text{CDCl}_3$ ) spectrum of carpusinine E (**9**).

**Figure 3.45:**  $^{13}\text{C}$  NMR (150 MHz,  $\text{CDCl}_3$ ) spectrum of carpusinine E (**9**).

**Figure 3.46:** Structures of carpusinine F (**10a**) and epicarpusinine F (**10b**).

**Figure 3.47:** COSY (bold bonds) and HMBC  $^1\text{H}$ - $^{13}\text{C}$  correlations of carpusinine F (**10a**) and epicarpusinine F (**10b**).

**Figure 3.48:** Structures of habbemines A and B (**36** and **37**), peripentadenine (**57**) and peripentonines A–C (**58**, **59** and **60**).

**Figure 3.49:**  $^1\text{H}$  NMR (150 MHz,  $\text{CDCl}_3$ ) of carpusinine F (**10a**) and epicarpusinine F (**10b**).

**Figure 3.50:**  $^{13}\text{C}$  NMR (600 MHz,  $\text{CDCl}_3$ ) of carpusinine F (**10a**) and epicarpusinine F (**10b**).

**Figure 3.51 :** Structure of (+)-elaeokanine A (**11**).

**Figure 3.52:**  $^1\text{H}$  NMR (600 MHz,  $\text{CDCl}_3$ ) spectrum of (+)-elaeokanine A (**11**).

**Figure 3.53:** Structure of elaeokanine C (**12**).

**Figure 3.54:**  $^1\text{H}$  NMR (600 MHz,  $\text{CDCl}_3$ ) spectrum of elaeokanine C (**12**).

**Figure 3.55:** Structure of (+)-elaeokanine D (**13**).

**Figure 3.56:**  $^1\text{H}$  NMR (600 MHz,  $\text{CDCl}_3$ ) spectrum to (+)-elaeokanine D (**13**).

**Figure 3.57:** Structure of carpusidine (**14**).

**Figure 3.58:** COSY (bold bonds) and HMBC  $^1\text{H}$ - $^{13}\text{C}$  correlations (arrows) of carpusidine (**14**).

**Figure 3.59:** Selected NOESY correlations of carpusidine (**14**).

**Figure 3.60:**  $^1\text{H}$  NMR (600 MHz,  $\text{CDCl}_3$ ) of carpusidine (**14**).

**Figure 3.61:**  $^{13}\text{C}$  NMR (150 MHz,  $\text{CDCl}_3$ ) of carpusidine (**14**).

**Figure 3.62:**  $^1\text{H}$  NMR (600 MHz,  $\text{CDCl}_3$ ) spectrum of ( $\pm$ )-elaeokanine C (**13**).

**Figure 3.63:** Structure of (+)-elaeokanine D (**14**).

**Figure 3.64:**  $^1\text{H}$  NMR (600 MHz,  $\text{CDCl}_3$ ) spectrum of (+)-elaeokanine D (**14**).

## LIST OF TABLES

**Table 1.1:** Structural classification of alkaloids.

**Table 1.2:** Structural classification of indolizidine alkaloids with some examples.

**Table 1.3:** Indolizidine alkaloids from the *Elaeocarpus* genus.

**Table 2.1:** Guide to CTLC plate selection and preparation.

**Table 3.1:**  $^{13}\text{C}$  (150 Hz) and  $^1\text{H}$  NMR (600 Hz) data of tectoricine (**1**) ( $\delta$  in ppm).

**Table 3.2:**  $^{13}\text{C}$  (150Hz) and  $^1\text{H}$  NMR (600 Hz) data of tectoraline (**2**) ( $\delta$  in ppm).

**Table 3.3:**  $^{13}\text{C}$  (150Hz) and  $^1\text{H}$  NMR (600 Hz) data of tectoramidine A (**3**) ( $\delta$  in ppm).

**Table 3.4:**  $^{13}\text{C}$  (150Hz) and  $^1\text{H}$  NMR (600 Hz) data of tectoramidine B (**4**) ( $\delta$  in ppm).

**Table 3.5:**  $^{13}\text{C}$  (150Hz) and  $^1\text{H}$  NMR (600 Hz) data of carpusinine A (**5**) and (+)-elaeokanine A (**11**) ( $\delta$  in ppm).

**Table 3.6:**  $^{13}\text{C}$  (150Hz) and  $^1\text{H}$  NMR (600 Hz) data of carpusinine B (**6**) ( $\delta$  in ppm).

**Table 3.7:**  $^{13}\text{C}$  (150Hz) and  $^1\text{H}$  NMR (600 Hz) data of carpusinine C and epicarpusinine C (**7a** and **7b**) ( $\delta$  in ppm).

**Table 3.8:**  $^{13}\text{C}$  (150Hz) and  $^1\text{H}$  NMR (600 Hz) data of carpusinine D (**8**) ( $\delta$  in ppm).

**Table 3.9:**  $^{13}\text{C}$  (150Hz) and  $^1\text{H}$  NMR (600 Hz) data of carpusinine E (**9**) and (+)-elaeokanine D (**13**) ( $\delta$  in ppm)

**Table 3.10:**  $^{13}\text{C}$  (150Hz) and  $^1\text{H}$  NMR (600 Hz) data of carpusinine F (**10a**) and epicarpusinine F (**10b**) ( $\delta$  in ppm).

**Table 3.11:**  $^1\text{H}$  NMR (600 MHz) data of **11** and synthetic samples of elaeokanine A ( $\delta$  in ppm).

**Table 3.12:**  $^1\text{H}$  NMR (600 MHz) data of **12** and ( $\pm$ )-elaeokanine C ( $\delta$  in ppm).

**Table 3.13:**  $^1\text{H}$  NMR (600 MHz) data of **13** and (+)-elaeokanine D ( $\delta$  in ppm).

**Table 3.14:**  $^{13}\text{C}$  (150 MHz) and  $^1\text{H}$  NMR (600 MHz) data of carpusidine (**14**) ( $\delta$  in ppm).

**Table 3.15:** Anti-proliferative activity of selected alkaloids isolated from *Elaeocarpus angustifolius* against a panel of selected cancer and normal cell lines.

## LIST OF SCHEMES

**Scheme 1.1:** Biosynthetic pathway to pyrrolidine alkaloids.

**Scheme 1.2:** Biosynthetic pathway to *Elaeocarpus* pyrrolidine alkaloids.

**Scheme 1.3:** Biosynthetic pathway to simple phenylethylamine alkaloids.

**Scheme 1.4:** Biosynthetic pathway to phenanthroindolizidine alkaloids.

**Scheme 1.5:** Biosynthetic pathway to polyhydroxylated indolizidine alkaloids.

**Scheme 1.6:** Biosynthetic pathway to steroidal indolizidine alkaloids.

**Scheme 1.7:** Biosynthetic pathway to alkylindolizidine alkaloids.

**Scheme 1.8:** Biosynthesis pathway to dihydropyrrole and polyketide.

**Scheme 1.9:** Proposed biosynthetic pathway to selected alkylindolizidines from *E. kaniensis*.

**Scheme 3.1:** Plausible biosynthetic pathway to tectoricine (**1**).

**Scheme 3.2:** Plausible biosynthesis pathway to tectoraline (**2**).

**Scheme 3.3:** Plausible biosynthetic pathway to tectoramidines A and B (**3** and **4**).

**Scheme 3.4:** Plausible biosynthetic pathway to carpusinine A (**5**).

**Scheme 3.5:** Plausible biosynthetic pathway to carpusinine B (**6**).

**Scheme 3.6:** Plausible biosynthetic pathway to carpusinine C and epicarpusinine C (**7a** and **7b**).

**Scheme 3.7:** Plausible biosynthetic pathway to carpusinine F (**11**).

**Scheme 3.8:** Plausible biosynthetic pathway to carpusinine E (**9**).

**Scheme 3.9:** Plausible epimerization of a  $\beta$ -amino carbonyl moiety.

**Scheme 3.10:** Plausible biosynthetic pathway to carpusinine F (**10a**) and epicarpusinine F (**10b**).

**Scheme 3.11:** Plausible biosynthetic pathway to carpusidine (**14**).

## LIST OF APPENDICES

- Appendix 1:** UV spectrum of tectoricine (1).
- Appendix 2:** IR spectrum of tectoricine (1).
- Appendix 3:** MS spectrum of tectoricine (1).
- Appendix 4:** HSQC spectrum of tectoricine (1).
- Appendix 5:** COSY spectrum of tectoricine (1).
- Appendix 6:** HMBC spectrum of tectoricine (1).
- Appendix 7:** NOESY spectrum of tectoricine (1).
- Appendix 8:** UV spectrum of tectoraline (2).
- Appendix 9:** IR spectrum of tectoraline (2).
- Appendix 10:** MS spectrum for tectoraline (2).
- Appendix 11:** HSQC spectrum for tectoraline (2).
- Appendix 12:** COSY spectrum of tectoraline (2).
- Appendix 13:** HMBC spectrum of tectoraline (2).
- Appendix 14:** NOESY spectrum of tectoraline (2).
- Appendix 15:** UV spectrum of tectoramidine A (3).
- Appendix 16:** IR spectrum for tectoramidine A (3).
- Appendix 17:** MS spectrum of tectoramidine A (3).
- Appendix 18:** HSQC spectrum of tectoramidine A (3).
- Appendix 19:** COSY spectrum of tectoramidine A (3).
- Appendix 20:** HMBC spectrum of tectoramidine A (3).

**Appendix 21:** IR spectrum of tectoramidine B (4).

**Appendix 22:** MS spectrum of tectoramidine B (4).

**Appendix 23:** HSQC spectrum of tectoramidine B (4).

**Appendix 24:** HMBC spectrum of tectoramidine B (4).

**Appendix 25:** IR spectrum of carpusinine A (5).

**Appendix 26:** UV spectrum of carpusinine A (5).

**Appendix 27:** MS spectrum of carpusinine A (5).

**Appendix 28:** HSQC spectrum of carpusinine A (5).

**Appendix 29:** COSY spectrum of carpusinine A (5).

**Appendix 30:** HMBC spectrum of carpusinine A (5).

**Appendix 31:** NOESY spectrum of carpusinine A (5).

**Appendix 32:** IR spectrum of carpusinine B (6).

**Appendix 33:** MS spectrum of carpusinine B (6).

**Appendix 34:** HSQC spectrum of carpusinine B (6).

**Appendix 35:** COSY spectrum of carpusinine B (6).

**Appendix 36:** HMBC spectrum of carpusinine B (6).

**Appendix 37:** NOESY spectrum of carpusinine B (6).

**Appendix 38:** IR spectrum of carpusinine C (7a and 7b).

**Appendix 39:** MS spectrum of carpusinine C (7a and 7b).

**Appendix 40:** HSQC spectrum of carpusinine C (7a and 7b).

**Appendix 41:** COSY spectrum of carpusinine C (**7a** and **7b**).

**Appendix 42:** HMBC spectrum of carpusinine C (**7a** and **7b**).

**Appendix 43:** NOESY spectrum of carpusinine C (**7a** and **7b**).

**Appendix 44:** IR spectrum of carpusinine D (**8**).

**Appendix 45:** MS spectrum of carpusinine D (**8**).

**Appendix 46:** HSQC spectrum of carpusinine D (**8**).

**Appendix 47:** COSY spectrum of carpusinine D (**8**).

**Appendix 48:** HMBC spectrum of carpusinine D (**8**).

**Appendix 49:** NOESY spectrum of carpusinine D (**8**).

**Appendix 50:** IR spectrum of carpusinine E (**9**).

**Appendix 51:** MS spectrum of carpusinine E (**9**).

**Appendix 52:** HSQC spectrum of carpusinine E (**9**).

**Appendix 53:** COSY spectrum of carpusinine E (**9**).

**Appendix 54:** HMBC spectrum of carpusinine E (**9**).

**Appendix 55:** NOESY spectrum of carpusinine E (**9**).

**Appendix 56:** IR spectrum of carpusinine F and epicarpusinine F (**10a** and **10b**).

**Appendix 57:** MS spectrum of carpusinine F (**10a** and **10b**).

**Appendix 58:** HSQC spectrum of carpusinine F and epicarpusinine F (**10a** and **10b**).

**Appendix 59:** COSY spectrum of carpusinine F and epicarpusinine F (**10a** and **10b**).

**Appendix 60:** HMBC spectrum of carpusinine F and epicarpusinine F (**10a** and **10b**).

**Appendix 61:** NOESY spectrum of carpusinine F and epicarpusinine F (**10a** and **10b**).

**Appendix 62:** UV spectrum for elaeokanine A (**11**).

**Appendix 63:** IR spectrum for elaeokanine A (**11**).

**Appendix 64:** MS spectrum for elaeokanine A (**11**).

**Appendix 65:** <sup>1</sup>R spectrum for elaeokanine C (**12**).

**Appendix 66:** MS spectrum for elaeokanine C (**12**).

**Appendix 67:** IR spectrum for elaeokanine D (**13**).

**Appendix 68:** MS spectrum for elaeokanine D (**13**).

**Appendix 69:** IR spectrum of carpusidine (**14**).

**Appendix 70:** MS spectrum of carpusidine (**14**).

**Appendix 71:** HSQC spectrum of carpusidine (**14**).

**Appendix 72:** COSY spectrum of carpusidine (**14**).

**Appendix 73:** HMBC spectrum of carpusidine (**14**).

**Appendix 74:** NOESY spectrum of carpusidine (**14**).

## CHAPTER 1: INTRODUCTION

### 1.1 Natural product from plants

Plants are valuable resources for satisfying the many needs of humanity.<sup>1</sup> The tendency for humans to rely on plants for many purposes such as food and medicine is ancient and universal.<sup>2</sup> Human beings have always utilised their vegetation, not just as a source of nutrition, but also for chemical production, clothing, dwelling and fuel. The knowledge of the traditional usage of plants and their properties has always been passed down from generation to generation through the natural course of everyday life.<sup>3</sup> This reliance on plants for many basic necessities gave rise to the development of ancient medicinal systems such as Egyptian, Chinese and Ayurveda medicine. The traditional medicines produced by these systems are usually made in the form of tea, tinctures, powders, poultices and other formulations produced from whole plant.<sup>4</sup>

The use of herbal formulation for therapeutic or experimental reasons has recorded several disadvantages over the years.<sup>5</sup> The concentration of the active constituents of plants often varies between geographical regions, resulting in irreproducible effect of the medicinal products. Additionally, other plant constituents can produce a counter effect to that of the active compound which can be synergistic or antagonistic. These irregularities resulted in the need to isolate pure bioactive substances from plants.<sup>6</sup>

After centuries of empirical use of herbal preparations, the beginning of isolation of active principles marked a new era of modern medicinal plant research referred to as phytochemistry.<sup>2</sup> In pure forms, administration of bioactive compounds is reproducible and accurate. It permits structure determination of the compounds which can be utilised in study of structure-activity relationship. Additionally, it can be used as leads in the synthesis of semi-synthetic drugs. The use of refined analytical techniques has made phytochemistry a subject of immense interest universally.<sup>7</sup> The process typically begins with a botanist who aids in the identification of the plant of interest. Plant selection is sometimes based on the biological activities encountered in the crude plant extracts where the active principles have not been isolated.<sup>8</sup> Selection can also be done taxonomically where researchers choose close relatives of species with known valuable bioactive substances. The extraction of the

plant materials collected is sometimes followed by biological screening for pharmacologically relevant assays. In other cases, isolation and purification of pure compounds are carried out before such assays.<sup>9</sup>

The advantage of phytochemicals over other sources of drug-leads lies in their structural diversity.<sup>10</sup> Plants have been shown to produce small molecular weight compounds with intrinsic *in vivo* solubility which allow for absorption and metabolism. As a result of these qualities, plant-derived natural products also play an important role in the elucidation of complex biological mechanisms.<sup>11</sup> The main classes of natural products often encountered in phytochemistry include alkaloids, terpenoids, glycosides, flavonoids, etc. Their study is generally associated with natural distribution, chemical structure, biosynthesis, metabolism and biochemical functions of the individual compounds.<sup>12</sup>

## 1.2 Alkaloids

### 1.2.1 History and significance

The word 'alkaloid' was first defined in 1882 as *any plant-derived substance with the ability to react like an alkali*.<sup>13</sup> During this period, only a few impure forms of plant-derived alkalis were discovered such as morphine (**15**). These alkaline substances obtained from plants were described to possess mainly three features: Their structures were unknown, they were physiologically active and they were alkaline.<sup>14</sup> This large group of unknown compounds was categorised as alkaloids. They were further classified based on plant families or the similarities in their chemical properties.<sup>10</sup>

With the advancement of medicinal chemistry, a wider definition was adopted. This described the word 'alkaloid' to mean "*any alkaline, organic compound obtained artificially or from nature*". This definition was further broadened to include only "*compounds with valuable physiological effects and a complex molecular structure isolated from plants which had a nitrogen atom bound within a heterocycle, with a greater or lesser degree of basicity and are characteristic for particular plant species, genera, or families*".<sup>16</sup>

A cursory look at these definitions provides a fundamental understanding of the nature of the compound class referred to as alkaloids (Figure 1.1). However, these definitions do not satisfactorily include many structures into the alkaloid class of compounds. Several alkaloids

are neither cyclic (putrescine **(16)**, a polyamine produced from tissue decarboxylation of amino acids) nor heterocyclic (acylpolyamines such as argiotoxin-636 **(17)**, a polyamine alkaloid from spider toxins).<sup>17,18,19</sup> Also some alkaloids have very simple structures while some are not physiologically active. It has also been discovered that many other organisms outside the plant kingdom produce alkaloids, such as microorganisms (pyocyanine **(18)**, *Pseudomonas aeruginosa*)<sup>20</sup> and animals (castoramine **(19)**, *Castor canadensis*<sup>21</sup>). In most cases, many alkaloids have been described as compounds with intrinsic basicity. This description also has a few exceptions. Some alkaloids are amine oxides such as kopsinoline<sup>22</sup> **(20)** from *Pleiocarpa mutica*, some are salts (stachydrine<sup>23</sup> **(21)**, *Stachys sieboldin*) and some are nitro compounds (aristolochic acid I **(22)**, *Aristolochia* species<sup>16,24</sup>). Therefore, in view of all these consideration, a more general definition was established which defines alkaloids as “organic substances of limited distribution from natural origin containing nitrogen, with a greater or lesser degree of basic property”.<sup>25</sup>

The first study directed at the isolation of alkaloid from plants was conducted in Paris. This study reported that the main active constituent of many plants used for medicinal purposes were alkaloids.<sup>26</sup> Since then, a variety of medicinal plants have also been phytochemically studied worldwide for the purpose of isolating various bioactive alkaloids present in them. For instance, *Papaver somniferum* is a medicinal plant used for its antitussive and analgesic property. This plant contains the narcotic analgesic, morphine **(15)**, and the cough suppressant, codeine **(23)** as its major constituent. Also *Ephedra sinica* used for asthma contains ephedrine **(24)**, a bronchodilator, and *Atropa belladonna* L. used as an anti-spasm contains atropine **(25)**, an anticholinergic. Due to this intrinsic ability to produce valuable biological activity, many alkaloids have already been developed into therapeutic drugs.<sup>27</sup>

The significance of alkaloids in drug discovery continuously increases over the years as many pharmacological and biological properties are encountered within this class of phytochemicals.<sup>28</sup> Many derivatives of alkaloids with pharmaceutical importance are currently being used as therapeutic agents.<sup>29</sup> As more biological assays are conducted using both old and new compounds, many unknown pharmacological properties are discovered in alkaloids. The structural diversity of alkaloids remains largely untapped from a biological perspective. This makes alkaloids a valuable resource for finding new lead in drug discovery as alkaloid producing plants continue to generate new skeleta.<sup>30</sup>

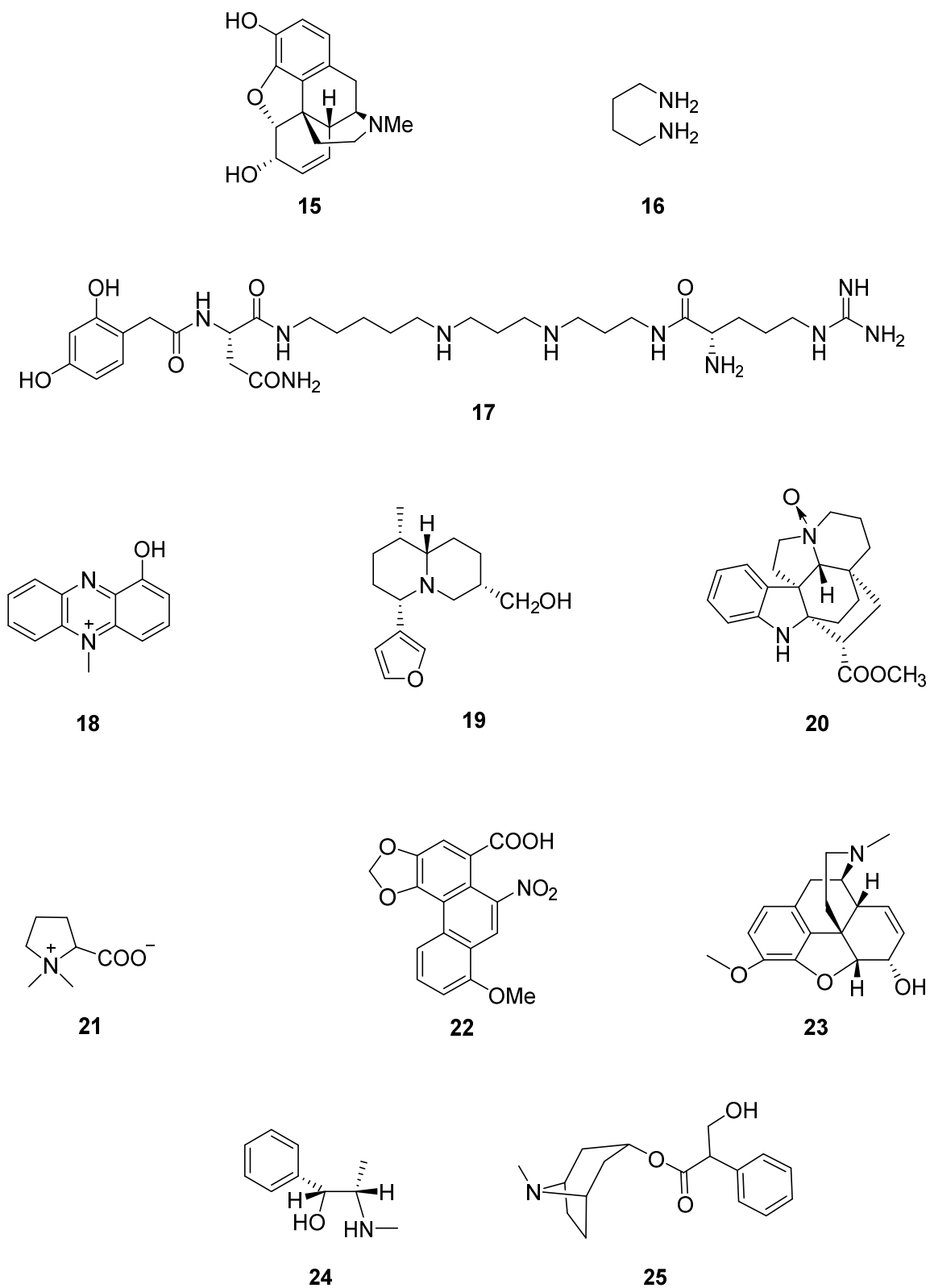


**Figure 1.1:** Some structural variation encountered in alkaloids.

### 1.2.2 Natural occurrence, distribution and localisation of alkaloids

Outside the plant kingdom, producers of alkaloids include microorganisms such as bacteria (e.g., pyocyanine **(18)** isolated from *Pseudomonas aeruginosa*<sup>31</sup>) and fungi (e.g., psilocin **(26)** from *Psilocybe subcubensis*<sup>32</sup>). In some instances, alkaloids such as castoramine **(19)** (Figure 1.2), produced by some mammals have been revealed to originate from the plants (water-lilies) the animals (beavers) feed on.<sup>33</sup>

Within the plant kingdom, the pteridophytes are not known producers of alkaloids, although Lycopodiaceae have been reported to contain some lysine derived alkaloids such as huperzine A **(27)** isolated from *Huperzia serrata*.<sup>34</sup> Majority of alkaloids discovered in the plant kingdom were obtained from Angiosperms. Certain families of the Angiosperms have a higher tendency to produce alkaloids such as Monocotyledons (Liliaceae and Amaryllidaceae) and Dicotyledons (Apocynaceae, Annonaceae, Fumariaceae, Rubiaceae, Lauraceae, Magnoliaceae, Loganiaceae, Papaveraceae, Menispermaceae, Ranunculaceae, Rutaceae, Solanaceae, etc.). Not all genera within these families produce alkaloids and some alkaloids are produced in several genera of different families.<sup>35</sup> Some of the families producing the same alkaloid are sometimes taxonomically distant (e.g., caffeine **(28)** is found in plants from Theaceae and Aquifoliaceae),<sup>36</sup> but most often they are closely related. The production of some alkaloid by plants is highly specific (morphine **(15)**), some are produced by a group of species within one genera (thebaine **(29)**) while some are produced by a limited number of genera within the same family (hyoscyamine **(30)**).<sup>37</sup>

The concentration of alkaloids encountered in nature has a wide variation. This ranges from a few parts per million (alkaloids from *Catharanthus roseus*) to more than 15% in the bark of *Cinchona ledgeriana*. Alkaloid-producing plants rarely synthesize one alkaloid. Generally, plants produce a complex mixture of related compounds dominated by one major compound. All alkaloids from one plant usually have the same biosynthetic origin, even in cases where there is a wide structural variation.<sup>37</sup> In plants, alkaloids occur in combinations with soluble salts (maleates, citrates, tartrates, isobutyrate, meconates, benzoates, etc.) or as tannins. They are mostly found in the peripheral tissues of plants such as the seed tegument and the external layers of the bark of roots and stems. Alkaloid synthesis occurs at specific sites in plants (chloroplasts, growing roots and laticiferous cells), after which they are transported to storage sites such as cell vacuoles.<sup>38</sup>

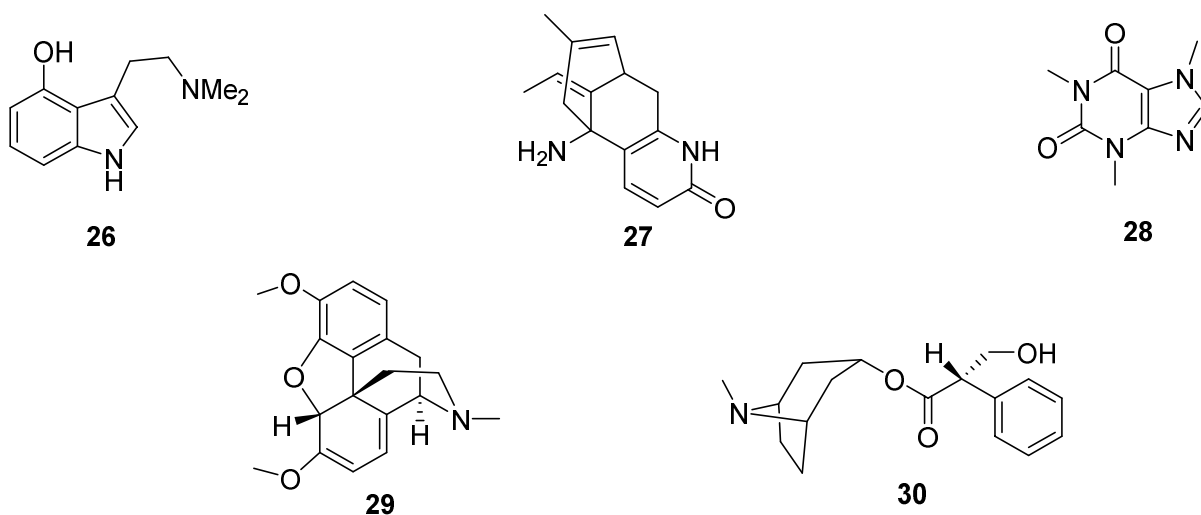


**Figure 1.2:** Structures of some alkaloids isolated from various sources.

### 1.2.3 Ecological roles of alkaloids in plants

Alkaloids possess a wide variety of structures which is often accompanied by marked pharmacological activity in humans. This valuable attribute brings about the need to understand the role alkaloids play in the plants they originated from. Previous researchers have demonstrated that alkaloids are an active part of plant metabolism. For this reason, many species vary in their daily production of alkaloids to suit their metabolic needs. The implication of this behaviour is that plants do not only synthesize alkaloids as waste products but also as an active part of their metabolic system.<sup>39</sup>

Alkaloids are necessary in plants for chemical defence against predators and herbivores. Some alkaloids are antifungal, antibacterial and antiviral. Some of them are not only toxic to microorganisms but also to animals. Physiologically, alkaloids could serve as storage and transport agents for nitrogen. Nitrogen is a limiting factor to plant growth and survival. Therefore, alkaloids are stored together with proteins, lipids and carbohydrates. In many plant species, nitrogen storage in alkaloids occurs in the leaves. This often requires a seasonal remobilisation of these compounds to internal storage organs prior to the leaves dropping in fall season.<sup>40</sup>

Isoquinoline, quinolone and indole alkaloids which contain aromatic and phenolic functional groups were found to be concentrated in plants located in high altitudes. These alkaloids

thus function as UV-absorbing agents for these plants whose environmental niche exposes them to high levels of UV radiation.<sup>40</sup>

#### 1.2.4 Classification of alkaloids

The necessity to categorise alkaloids into groups arises from the wide variation in chemical structure, botanical origin and pharmacological activities encountered within them. The classification systems adopted are mostly based on their biogenesis, structural variations and taxonomical origins.<sup>41</sup>

The biogenetic classification of alkaloids (Figure 1.3) is based on the precursor amino acids from which they originate. This system of classification often disregards similarities in pharmacological activities or taxonomic distribution within groups. Some biogenetic classifications of alkaloids are:

- i. Alkaloids derived from ornithine, e.g., grandisine D (**31**)
- ii. Alkaloids derived from tyrosine, e.g., hordenine (**32**)
- iii. Alkaloids derived from lysine, e.g., (-)-swainsonine (**33**)

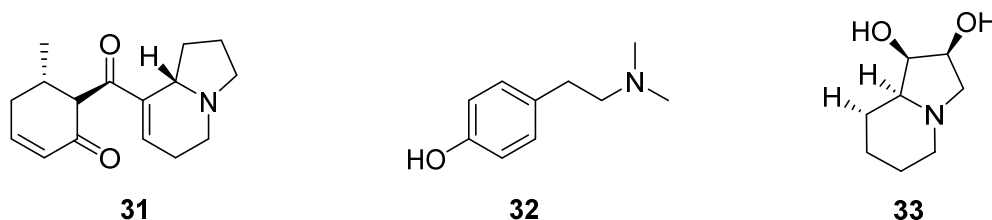


**Figure 1.3:** Structures of **31**, **32** and **33**.

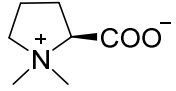
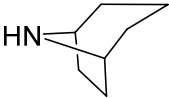
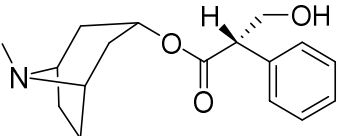
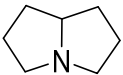
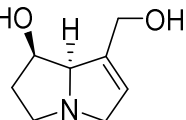
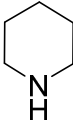
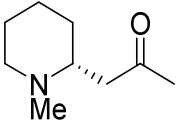
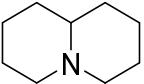
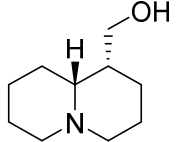
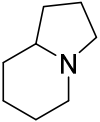
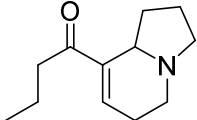
Pharmacologically, alkaloids are often classified based on their bioactivity. Such classifications are exemplified by morphine (**15**) being grouped under narcotic analgesic, codeine (**23**) as cough suppressant, etc. This classification system is not common and had become obsolete with the increasing variations in pharmacological activities produced by various alkaloids.<sup>41</sup>

Taxonomical classification of alkaloids is based on genus, subgenus, species and subspecies of plants producing alkaloids. This mode of classification often include alkaloids with little or no structural similarity within one group as many plant families are known to produce more

than one particular type of alkaloids. A few examples of taxonomic classes of alkaloids include Rubiaceae alkaloids, Cannabinoid alkaloids, etc.<sup>41</sup>

The most commonly used mode of alkaloid classification is by chemical structure. This method focuses on the immediate environment of nitrogen atom present in the alkaloid structure. They are broadly divided in two main classes: The heterocyclic alkaloids and the non-heterocyclic alkaloids (Table 1.1). Classification by chemical structure often associates each class with their biogenetic precursor as shown below.<sup>42</sup>

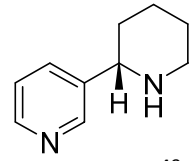
**Table 1.1:** Structural classification of alkaloids.

Heterocyclic alkaloids			
Class	Core structure	Biosynthetic precursor	Structural examples
Pyrrolidine alkaloids		Ornithine	 (-)-Stachydrine ( <i>Cadaba fruticosa</i> ) <sup>43</sup>
Tropane alkaloids		Ornithine	 (-)-Hyoscyamine ( <i>Hyoscyamus niger</i> ) <sup>44</sup>
Pyrrolizidine alkaloids		Ornithine	 Retronecine <sup>45</sup> ( <i>Heliotropium</i> )
Piperidine alkaloids		Lysine	 N-Methylpelletierine <sup>46</sup> ( <i>Punica granatum</i> )
Quinolizidine alkaloids		Lysine	 (-)-Lupinine <sup>47</sup> ( <i>Lupinus luteus</i> )
Indolizidine alkaloids		Lysine	 Elaeokanine A ( <i>Elaeocarpus kaniensis</i> ) <sup>48</sup>

Pyridine alkaloids

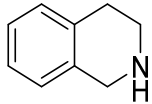


Nicotinic acid

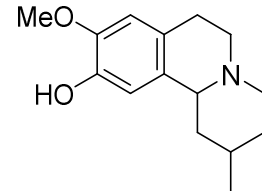


Anabasine<sup>49</sup>  
(*Nicotiana tabacum*)

Isoquinoline alkaloids

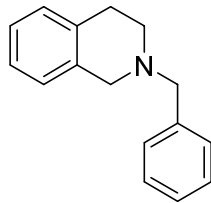


Tyrosine

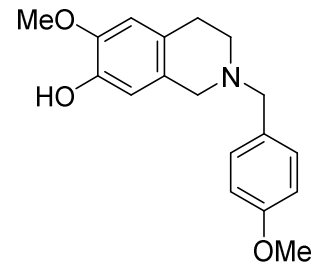


Lophocerine<sup>50</sup>  
(*Lophophora schottii*)

Benzyloisoquinoline alkaloids

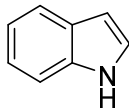


Tyrosine

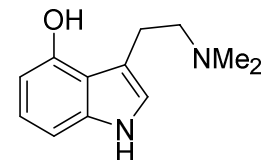


Sendaverine<sup>51</sup>  
(*Ceratocarpus heterocarpus*)

Indole alkaloids

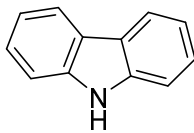


Tryptophan

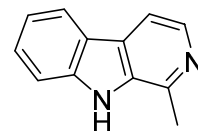


Psilocin<sup>32</sup>  
(*Psilocybe subcubensis*)

$\beta$ -Carboline alkaloids

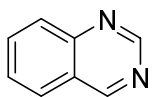


Tryptophan

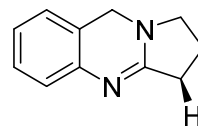


Harman  
(*Peganum harmala*)

Quinazoline alkaloids

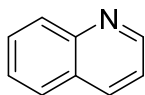


Anthranilic acid

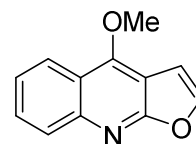


Deoxyenganine<sup>52</sup>  
(*Peganum harmala*)

Quinoline alkaloids

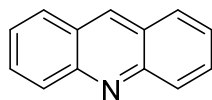


Anthranilic acid

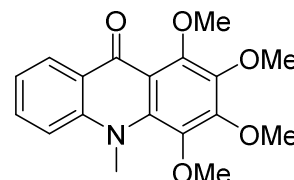


Dictamine<sup>53</sup>  
(*Dictamnus dasycarpus*)

Acridone Alkaloids



Anthranilic acid

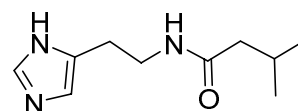


Melicopicine  
(*Melicope fareana*)

Imidazole alkaloids

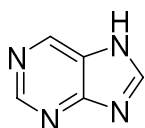


Histidine

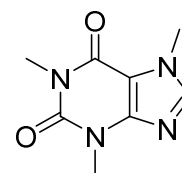


Dolichothele<sup>54</sup>  
(*Dolichothele sphaerica*)

Purine alkaloids



Purine



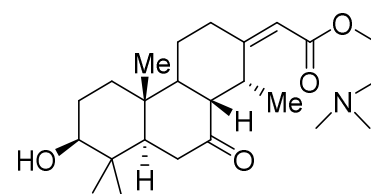
Caffeine  
(*Coffea arabica*)<sup>55</sup>

---

### Non-heterocyclic alkaloids

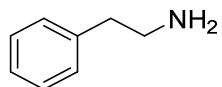
---

Erythrophleum alkaloids

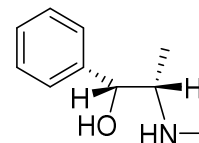


Cassaine  
(*Erythrophleum*)

Phenylethylamine alkaloids

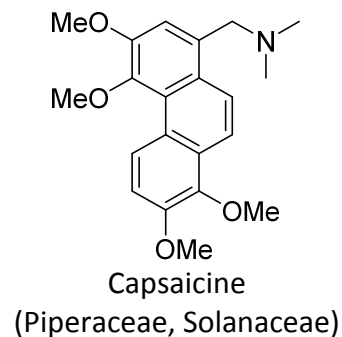
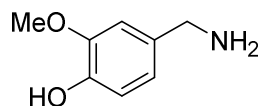


Tyrosine

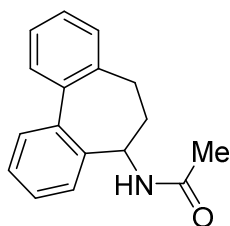


Ephedrine  
(*Ephedra* (Ephedraceae))

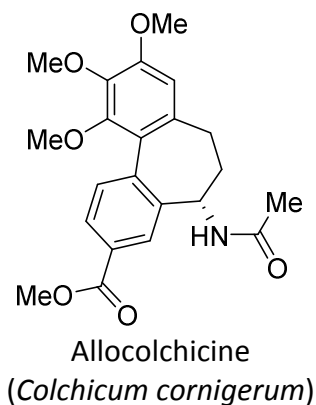
Benzylamine-type  
alkaloids



Colchicines



Tyrosine

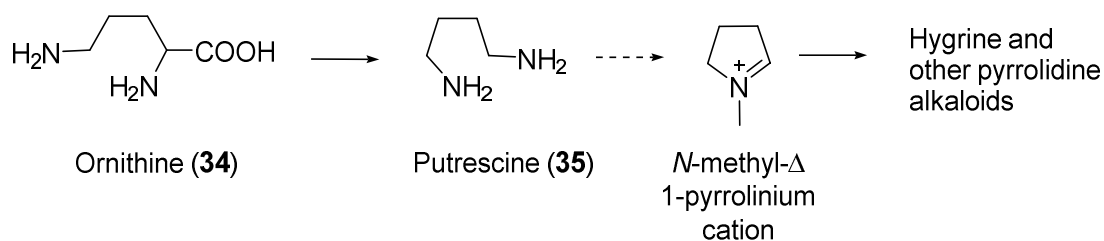


In the present study, three structural classes of alkaloids were isolated from the leaves of *E. angustifolius* and *E. tectorius*, namely, pyrrolidine, phenylethylamine and indolizidine. Therefore, the next three sections will focus on these three classes.

#### 1.2.4.1 Pyrrolidine alkaloids

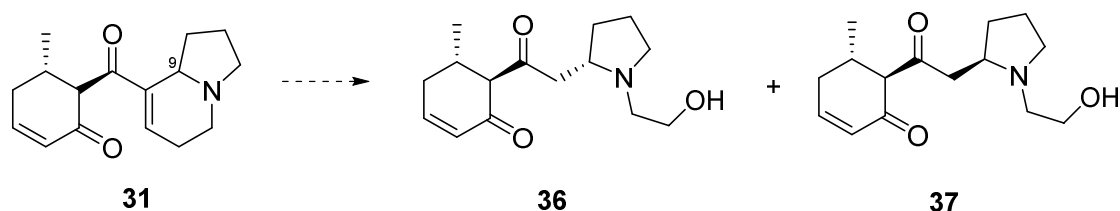
Pyrrolidine alkaloids contain a nitrogen atom as part of a 5-membered heterocyclic ring.<sup>16</sup> This class of alkaloids are biosynthetically derived from ornithine (**34**), which is a non-protein amino acid produced from glutamate in plants. It can be found in animals as a product of urea cycle produced by enzymes involved in arginine synthesis.<sup>56</sup>

The reported plausible biosynthesis to pyrrolidine alkaloids (Scheme 1.1) involves decarboxylation of ornithine by pyridoxal phosphate to putrescine (**35**). Further modifications usually involve the formation of *N*-methyl- $\Delta^1$ -pyrrolinium cation by diamine oxidase. From the *N*-methyl- $\Delta^1$ -pyrrolinium cation, other pyrrolidine alkaloids subsequently arise from reaction mechanisms such as hydrolysis, acetylation, mannich reactions etc.<sup>57</sup>



**Scheme 1.1:** Biosynthetic pathway to pyrrolidine alkaloids.

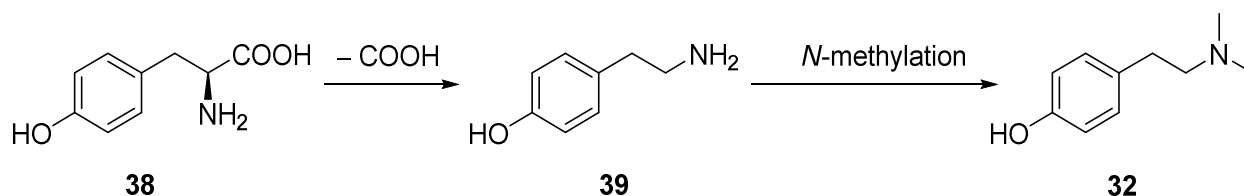
The *Elaeocarpus* genus has two reported pyrrolidine alkaloids in literature. These are habbemine A (**36**) and habbemine B (**37**) (Scheme 1.2) which were isolated from *E. habbemensis*. Both compounds are epimers reported to be derived from an intramolecular retro-aldol reaction of the parent indolizidine alkaloid, grandisine D (**31**).<sup>56</sup> Epimerisation of **36** and **37** at C-9 is reported as typical in the biosynthesis of pyrrolidine alkaloids with an unstrained monocyclic ring.



**Scheme 1.2:** Biosynthetic pathway to *Elaeocarpus* pyrrolidine alkaloids.<sup>56</sup>

#### 1.2.4.2 Phenylethylamine alkaloids

The phenylethylamine (or phenethylamine) moiety contains a benzene ring which is substituted with an ethylamine side chain. These alkaloids can be found in both plants and animals. Their structures allow for substitution on the aromatic ring and the terminal amino group. This gives rise to a high degree of structural diversity which is often accompanied with unique biological activity. In plants, phenylethylamine alkaloids are mostly produced by the genus *Ephedra* (Ephedraceae). *Ephedra* drugs have historically been a part of Chinese traditional medicine exemplified by ephedrine (**24**), which is an orally active sympathomimetic.<sup>58</sup>



**Scheme 1.3:** Biosynthetic pathway to simple phenylethylamine alkaloids.<sup>44</sup>

Phenylethylamine alkaloids are biosynthetically derived from the amino acid tyrosine (**38**) as shown in Scheme 1.3. The pyridoxal phosphate dependent decarboxylation of tyrosine produces simple phenylethylamine alkaloids such as tyramine (**39**). This subsequently undergoes *N*-methylation to yield hordenine (**32**) found in *Hordeum vulgare* (*Graminae/Poaceae*). Some phenylethylamine also originate from *Hoffmann* degradation of the corresponding isoquinoline alkaloids.<sup>41</sup>

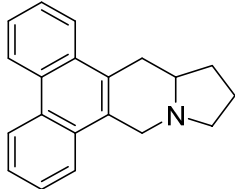
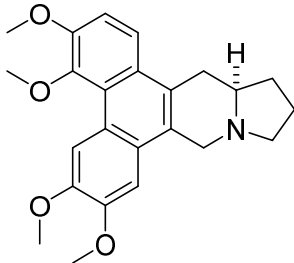
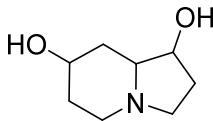
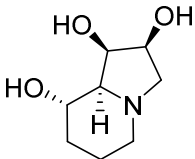
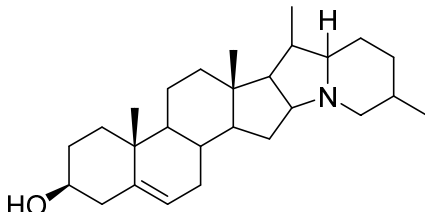
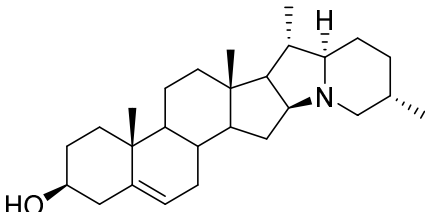
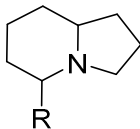
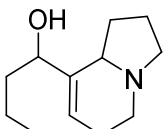
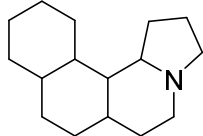
*Elaeocarpus* species have not been reported to produce phenylethylamine alkaloids in the past. The compounds isolated from this project mark the first occurrence of this type of alkaloid in this genus.

### 1.2.5 Indolizidine alkaloids and classification of indolizidine alkaloids

Indolizidine alkaloids have been obtained from various sources, such as higher plants, bacteria, fungi, vertebrates, and invertebrates. Their indolizidine motif is made up of one cyclohexane ring and one cyclopentane ring merged together with a nitrogen atom positioned at the ring junction.<sup>59</sup>

For the purpose of this report, naturally occurring indolizidine alkaloids were classified based on the substituents attached on the indolizidine nucleus, as presented in Table 1.2. The various classes of indolizidine alkaloids have been reported to come from unrelated plant sources and varying biogenetic origins, which are discussed under each class in the subsequent section.

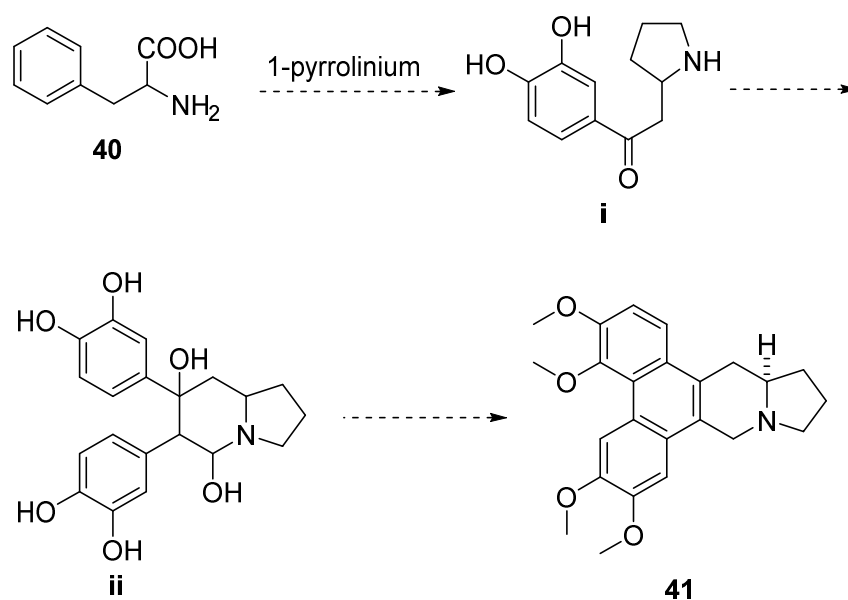
**Table 1.2:** Structural classification of indolizidine alkaloids with some examples

Classes of indolizidine alkaloids	Structural examples
	
Phenanthroindolizidine alkaloids	(+)-Isotyrolocrebrine
	
Polyhydroxylated indolizidine alkaloids	(-)-Swainsonine
	
Steroidal indolizidine alkaloids	Solanidine
	
Alkylindolizidine alkaloids	Elaeokanine B
	
Polycyclic indolizidine alkaloids	Mersicarpine

### 1.2.5.1 Phenanthroindolizidine alkaloids

Plants of the family Asclepiadaceae, serve as natural hosts for danaid butterflies as they contain mainly phenanthroindolizidine alkaloids that stimulate egg-laying. Phenanthroindolizidine alkaloids represent a class of pentacyclic natural products attached to the core indolizidine structure. They are obtained mainly from the genera *Pergularia*, *Cynanchum* and *Tylophora* with diverse biological activities, exemplified by (+)-isotylocrebrine (**41**) isolated from *Tylophora tanakae*.<sup>60</sup>

The proposed biosynthesis to phenanthroindolizidine alkaloids (Scheme 1.4) involves the hydroxylation of phenylalanine (**40**) followed by incorporation of 1-pyrrolinium to yield **i**. A second molecule of **40** is then incorporated onto **i** followed by a series of hydroxylation and cyclisation reactions to produce **41** and other phenanthroindolizidine alkaloids.

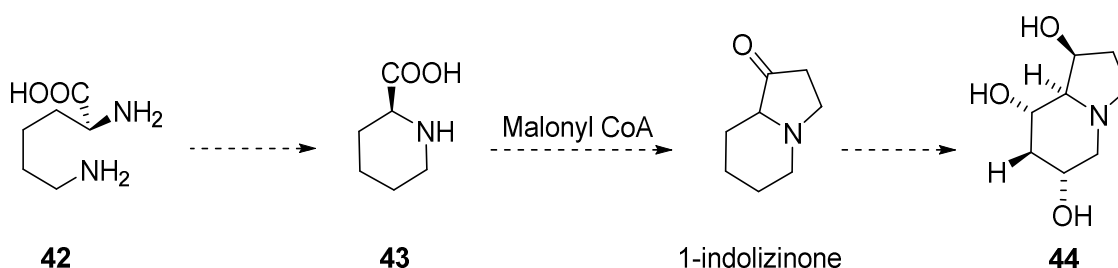


**Scheme 1.4:** Biosynthetic pathway to phenanthroindolizidine alkaloids.<sup>61</sup>

### 1.2.5.2 Polyhydroxylated indolizidine alkaloids

Polyhydroxylated indolizidine alkaloids are compounds with multiple hydroxyl groups attached to the core indolizidine structure. Previous reports showed high content of polyhydroxylated indolizidine alkaloids in several species of *Ipomoea*, one of the largest

genera of the Convolvulaceae. Polyhydroxylated indolizidine alkaloids are a growing group of natural products whose importance is reflected in an impressive number of review articles and research papers dealing with their isolation, biological evaluation and syntheses.<sup>62,63,59,64</sup>

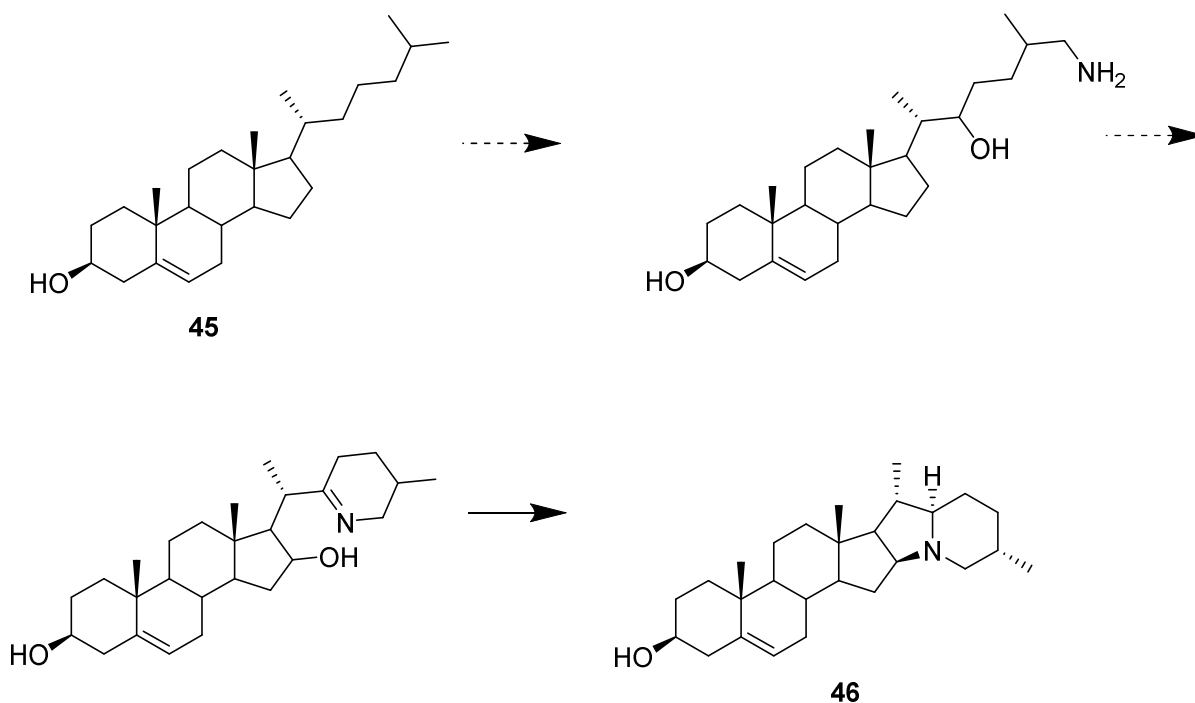


**Scheme 1.5:** Biosynthetic pathway to polyhydroxylated indolizidine alkaloids.<sup>65</sup>

A representative of this compound class is (+)-castanospermine (**44**). Polyhydroxylated indolizidine alkaloids are biosynthetically derived from the amino acid, lysine (**42**), which generally involves the condensation of pipecolic acid (**43**) and malonyl CoA (Scheme 1.5). A sequence of hydroxylation reaction follows to produce the various polyhydroxylated indolizidine alkaloids.<sup>66</sup>

### 1.2.5.3 Steroidal indolizidine alkaloids

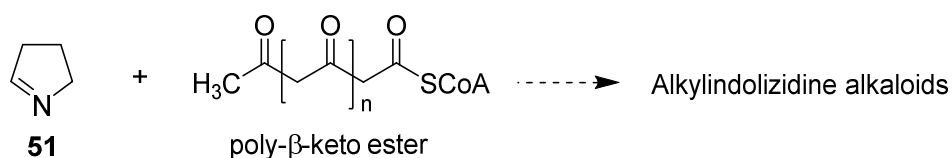
Steroidal alkaloids are mostly produced by the Solanaceae plant family, particularly by *Solanum tuberosum*. They either contain an oxo-aza spiro substitution or an indolizidine substitution (e.g., solanidine (**46**)). Biosynthetically, steroidal indolizidine alkaloids are derived from cholesterol (**45**) via oxidation, amination, glycosylation reactions, etc. (Scheme 1.6).<sup>67</sup>



**Scheme 1.6:** Biosynthetic pathway to steroidal indolizidine alkaloids.<sup>67</sup>

#### 1.2.5.4 Alkylindolizidine alkaloids

Alkylindolizidine alkaloids possess an alkyl chain attached to the indolizidine core structure. They have been shown to be the most structurally diverse of all the indolizidine alkaloids. The structural diversity of alkylindolizidine alkaloids arises from the variety in the length of the side chain and functional groups substituted to both the side chain and indolizidine nucleus. The vast majority of alkylindolizidine alkaloids were obtained from the skin of amphibians where the alkaloids function as defence chemicals against predators.<sup>63</sup>



**Scheme 1.7:** Biosynthetic pathway to alkylindolizidine alkaloids.<sup>68</sup>

The only representatives of alkyindolizidine alkaloids reported within the *Elaeocarpus* were obtained from the leaves of *E. kaniensis*. These compounds were described as low-melting point oily bases with little structural similarity as the rest of *Elaeocarpus* alkaloids. The biosynthesis to *Elaeocarpus* alkyindolizidine alkaloids (Scheme 1.7) however has a clear relationship with other *Elaeocarpus* alkaloids. This generally involves the condensation of dihydropyrrole (**51**) (derived from ornithine) and a C<sub>8</sub> polyketide (derived from acetyl CoA or malonyl CoA).<sup>69</sup>

#### 1.2.5.5 Polycyclic indolizidine alkaloids

Polycyclic indolizidine alkaloids are indolizidine alkaloids whose structural features include three or more rings, including cycloalkanes and aromatic rings attached to the indolizidine core structure. These compounds are highly complex alkaloids with a plethora of functional groups. Polycyclic indolizidine alkaloids have been isolated from a variety of natural sources of both terrestrial and marine origin. Some polycyclic indolizidine alkaloids are thought to be biosynthetically related to alkyindolizidine alkaloids. For example, *E. kaniensis* has been reported to produce both types of indolizidine alkaloids. *Elaeocarpus* alkaloids are mostly polycyclic indolizidine alkaloids, therefore this class of compounds is further discussed below.

### 1.3 Indolizidine alkaloids from the *Elaeocarpus* genus

Previous phytochemical studies reveal that the only class of indolizidine alkaloids represented within the *Elaeocarpus* genus are alkyindolizidine and polycyclic indolizidine alkaloids. Polycyclic indolizidine alkaloids are the main class of alkaloids produced by this genus. Out of all alkaloid-producing species within the genus, alkyindolizidine alkaloids were only reported from *E. kaniensis*.

*Elaeocarpus* indolizidine alkaloids (Table 1.3) are a closely interrelated group of compounds comprising mostly either a C<sub>16</sub> carbon skeleton, such as isoelaecarpine (**47**) (*E. fuscooides*), or a C<sub>12</sub> carbon skeleton, such as elaeokanine B (**48**) (*E. kaniensis*). Alkaloids with the C<sub>16</sub> carbon skeleton are polycyclic indolizidine alkaloids, while those with the C<sub>12</sub> carbon skeleton are either polycyclic and alkyindolizidine alkaloids (Figure 1.4).

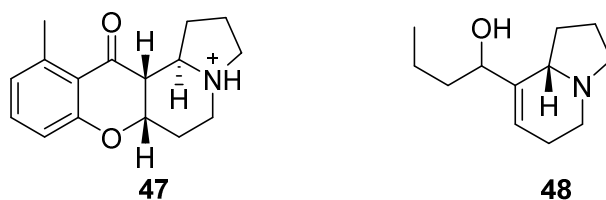
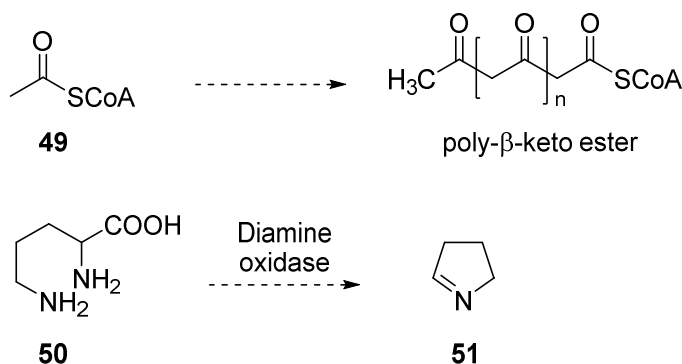


**Figure 1.4:** Examples of  $C_{16}$  and  $C_{12}$  carbon skeletons found in *Elaeocarpus* alkaloids.

### 1.3.1 Biosynthesis of *Elaeocarpus* polycyclic indolizidine and alkylindolizidine alkaloids.

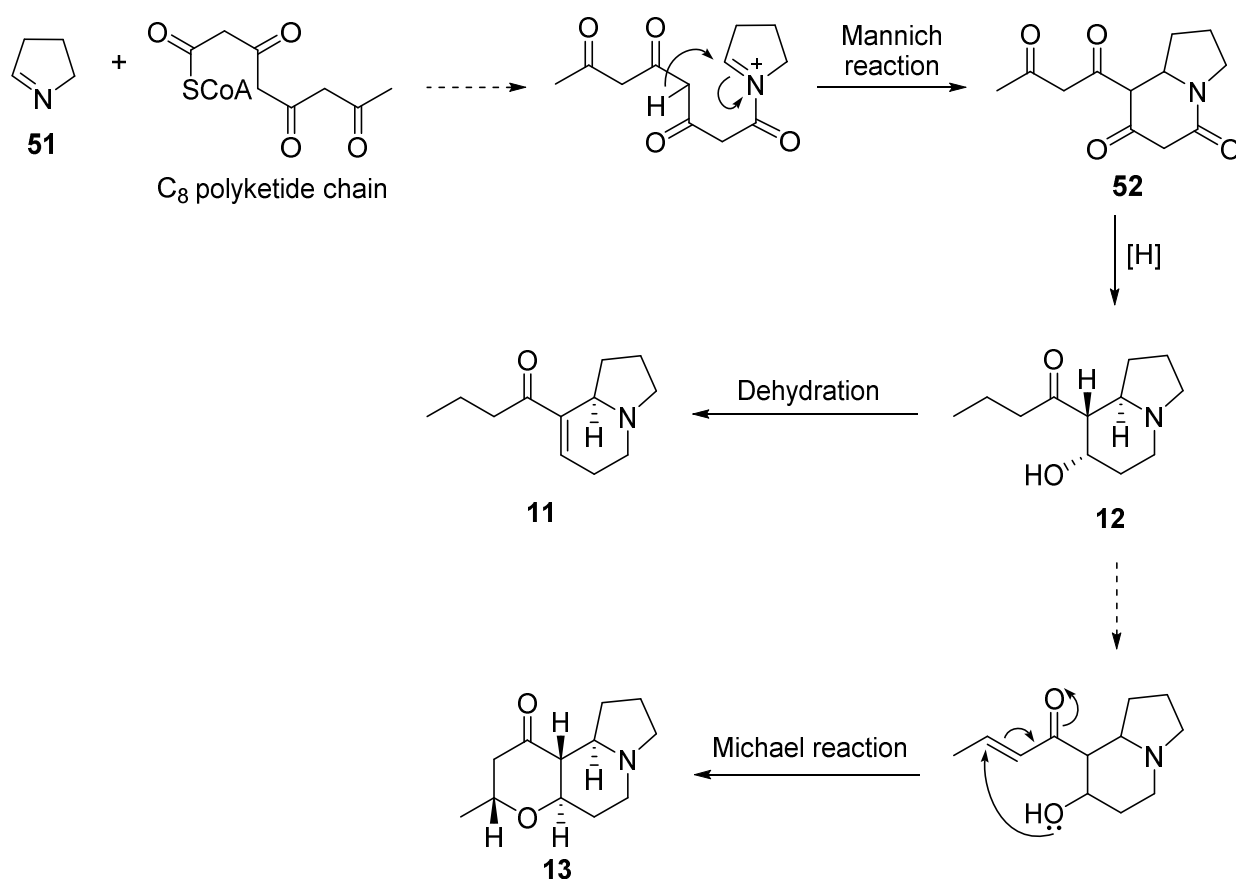
Previous reports have suggested that *Elaeocarpus* indolizidine alkaloids are biosynthetically derived from acetyl CoA (**49**) and ornithine (**50**). The process has been proposed to involve the condensation of dihydropyrrole (**51**) and a  $C_{12}$  or  $C_8$  polyketide chain (Scheme 1.8).<sup>68</sup>



**Scheme 1.8:** Biosynthetic pathway to dihydropyrrole and polyketide.

The biosynthetic pathway proposed for *Elaeocarpus* indolizidine alkaloids with the  $C_{16}$  carbon skeleton have been extensively postulated by different researchers as this is the most frequently encountered class of indolizidine alkaloids within the *Elaeocarpus* genus.<sup>70,71,72</sup> As this project has only isolated derivatives of indolizidine alkaloid with the  $C_{12}$  carbon skeleton, the proposed biosynthetic pathway will only focus on this group, specifically the known compounds isolated from this study.

It was suggested that the biosynthesis of (+)-elaeokanine A (**11**) and (-)-elaeokanine C (**12**), like the rest of *Elaeocarpus* indolizidine alkaloids, involves the condensation of dihydropyrrole (**51**) and a C<sub>8</sub> polyketide chain to give an iminium ion which cyclizes via a Mannich reaction to yield the common precursor (**52**), which is regarded as a key intermediate to other alkylindolizidine alkaloids. Subsequent reductive and dehydration transformations of **52** produce **11** and **12**. Alternatively, (-)-elaeokanine D (**13**) is formed via a Michael reaction with an  $\alpha,\beta$ -unsaturated ketone intermediate of **12** (Scheme 1.9).<sup>68</sup>



**Scheme 1.9:** Proposed biosynthetic pathway to selected alkylindolizidines from *E. kaniensis*.

## 1.4 The *Elaeocarpus* genus

### 1.4.1 Natural occurrence, morphological appearance and ethnomedicinal use

*Elaeocarpus* genus is the largest genus of Elaeocarpaceae plant family. There are over 200 species within this genus which spread throughout the tropical and subtropical areas of Southwest Pacific, East Asia and Oceania. Other names such as mendong, medang kelawar, setui tupai and sanga are local names indigenous to trees found in Malaysia. There are 27

*Elaeocarpus* species in Malaysia with a few other uncharacterised ones found in all habitats from coastal and secondary forests to a few mountain tops.<sup>73</sup>

*Elaeocarpus* species are small to large trees with twigs mostly curving up and leaves spirally arranged. The buds are sometimes coated with resin. The leaves often kneed at the top of the stalk, withering red with toothed or notched margins. The flowers are mostly medium sized and faces down. The fruits are usually small to large drupes with a hard stone, bearing one to five seeds.<sup>74</sup>

Some species are edible while others have found minor uses in traditional medicine. The hard stones are often used for ornamental purposes. *E. macrocerus* is sometimes used in the production of matchsticks. An infusion of the leaves, bark and stem of *E. floribundus* is used as mouthwash while the fruit is used as antiseptic in wound dressing. *E. grandiflora* possesses antibacterial and antiviral properties. The Leaf, fruit and twig extracts are also used to treat diabetic patients due it its hypoglycaemic effects. The fruits of *E. oblongus* are used as antiseptic administered in cases of pneumonia, rheumatism, gastric ulcers, leprosy and haemorrhoids.<sup>73</sup>

#### **1.4.2 *Elaeocarpus angustifolius* Blume**

The trees are mainly lowlands and mostly found near water bodies. Sometimes they are found on hill tops of up to 1000 meter. Some trees have been encountered in north-east India, New Caledonia and Australia. Malaysian species are found in Terenganu, Kedah, Perak, Selangor and Pahang (Figure 1.5A). Morphologically, they are medium trees of up to 30 m in height. The girth is about 1.7 m and bole is columnar, with symmetrical plank buttresses of up to 1.2 m. The bark is often smooth, while the inner bark is often pale brown and slightly fibrous and soft.<sup>73</sup>

The leafy part of the twig is often 0.15 to 0.4 cm in diameter and angular due to the extension of the leaf stalk down the internode. The leaf blade is narrowly obovate and can be papery thin or membranous. The base of the leaf is tapered to the stalk and the margin is shallowly toothed. The racemes are 3.6 cm long and are mostly seen in the axils behind existing leaves.<sup>73</sup>

The flowers are five-merous and have petals of about 0.8 cm in length. The stamens are numerous. Ovary is hairy and the style is much longer than the ovary. The flower stalks are about 0.4 to 1cm in length. The fruits are globose with firm glabrous surface.<sup>74</sup>

Traditionally, the fruits are used for ornamental purposes in India. Ethnomedicinally, the seeds have been used to alleviate blood pressure and heart related diseases while the leaf sap has stomachic properties.<sup>75</sup>

#### **1.4.3 *Elaeocarpus tectorius* (Lour.) Poir.**

They are usually seen in forests, both in lowlands and mountain summits in countries such as Bangladesh, China, Andaman Island and Sumatra. Some trees are wild while others are cultivated (Figure 1.5B). Some trees are shrubby and found on mountain summit forests where they flower from one meter. Others are found on lowland forests where they flower from three meters. The boles are columnar or fluted and sometimes possess steep plank buttresses of up to one meter in height. The bark is smoothly or shallowly fissured. The inner bark is often coloured pink, red or brown while the sapwood is usually pale yellow or white. The leafy part of the twigs is usually about 0.8 cm thick, glabrous, thinly or densely appressed with hairs.<sup>73</sup>

The leaf blades measure about 7.5 x 3.5 cm and are usually oblong, elliptic or ovate but rarely obovate in shape. The base of the leaves often withers red or yellow, the apex is acuminate. The margins are often slightly or strongly-toothed. The racemes are usually 7 – 17 cm long located in the axils of existing leaves. The flowers have 22 – 48 stamens and the petals are 0.4 – 0.8 cm. The ovaries are hairy and the stalk is about 0.6 cm. The fruits are ellipsoid and have two varieties which are designate **Var. "A"** (large fruits) or **Var. "B"** (smaller fruits).<sup>74</sup>

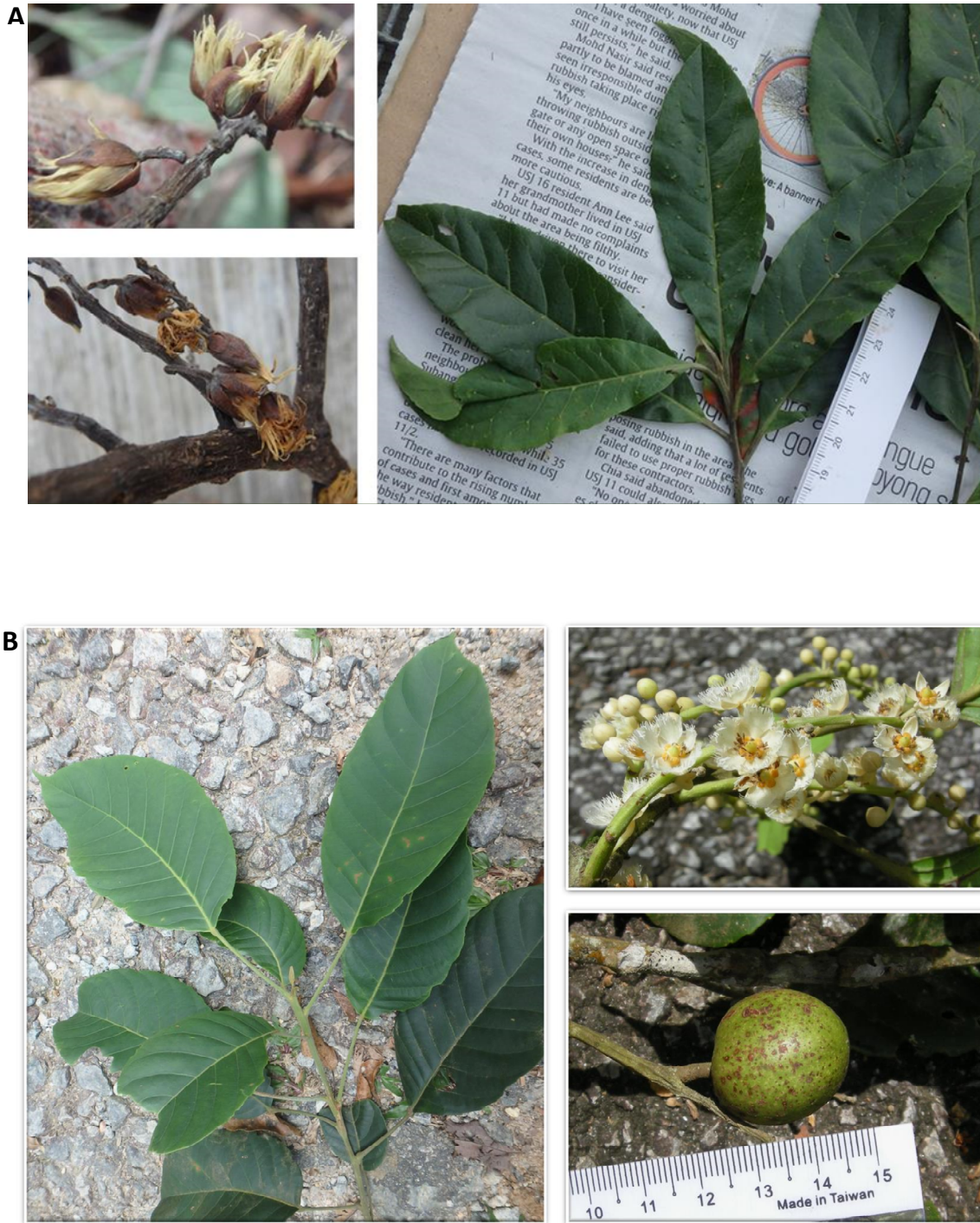
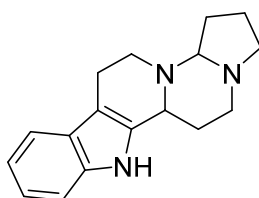


**Figure 1.5: A - Flowers and leaves of *E. angustifolius*; B – Flowers, leaves and fruit of *E. tectorius*.**

#### 1.4.4 Alkaloids from *Elaeocarpus* genus

Extracts of some species of *Elaeocarpus* genus have been previously studied as discussed in section 1.4.1 to reveal good biological activities. As a result of these beneficial properties, some species have been phytochemically investigated for their alkaloid content.<sup>76</sup>



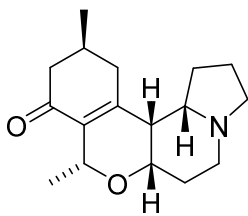
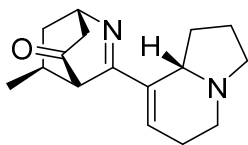
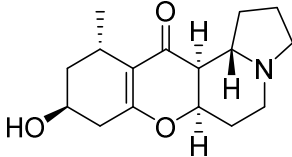
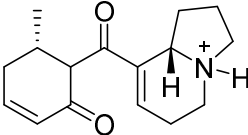
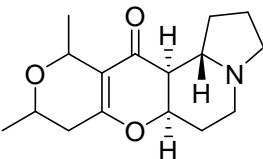
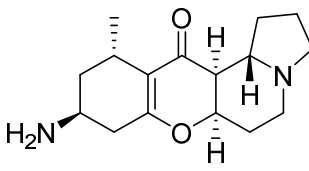
**53**

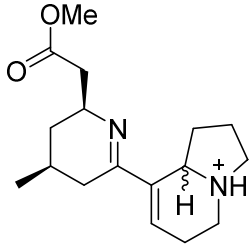
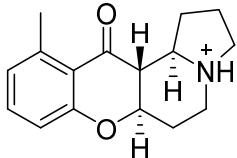
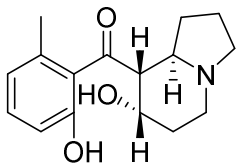
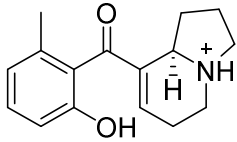
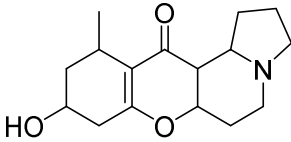
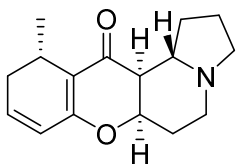
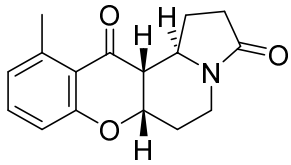
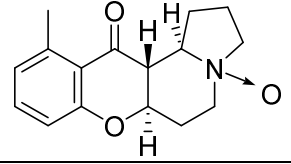
**Figure 1.6:** Structure of elaeocarpidine (**53**).

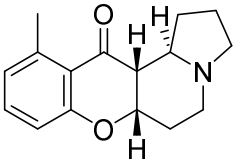
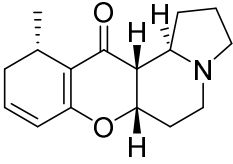
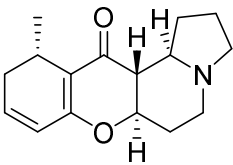
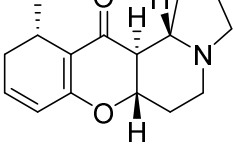
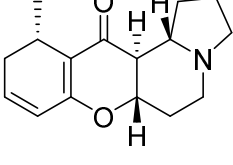
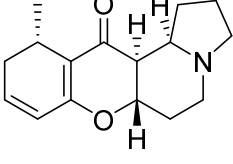
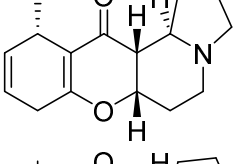
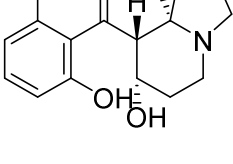
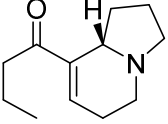
Some of the alkaloids isolated from the *Elaeocarpus* genus were identified as new polycyclic indolizidine alkaloids with good affinity for the  $\delta$ -opioid receptor. The two exceptions to the indolizidine class of alkaloids found in this genus were obtained from the phytochemical investigation of the leaves of *E. habbemensis* and *E. densiflorus*. The leaves of *E. habbemensis* collected from Papua New Guinea were found to contain pyrrolidine alkaloids namely, habbemines A and B (**36** and **37**).<sup>56,57</sup> On the other hand, *E. densiflorus* (also known as *E. archbodianus*) yielded one indole alkaloid, elaeocarpidine (**53**) as its major alkaloid (Figure 1.6).<sup>73,77</sup>

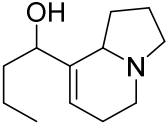
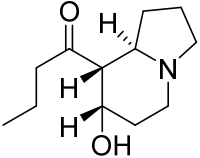
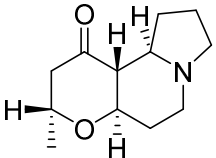
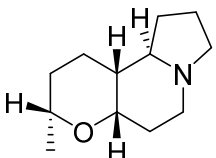
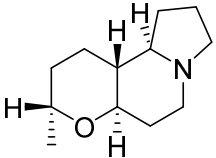
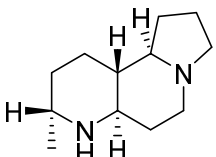
Out of the 200 characterised species, only nine *Elaeocarpus* species have been phytochemically studied for their alkaloid content. Therefore, the purpose of this study is to identify novel bioactive alkaloids from other *Elaeocarpus* sp. that are yet to be studied and uncharacterised. The alkaloids isolated to date from previous investigations of *Elaeocarpus* species are presented in Table 1.3.

**Table 1.3:** Indolizidine alkaloids from the *Elaeocarpus* genus.

Plant species	Compound name	Structure	Ref.
<i>E. grandis</i>	Grandisine A		71
<i>E. grandis</i>	Grandisine B		71
<i>E. grandis</i>	Grandisine C		72
<i>E. grandis</i>	Grandisine D		72
<i>E. grandis</i>	Grandisine E		72
<i>E. grandis</i>	Grandisine F		72

<i>E. grandis</i>	Grandisine G		72
<i>E. fuscoides</i>	(-)-Elaeocarpine		78
<i>E. fuscoides</i>	Isoelaecarpine		78
<i>E. fuscoides</i>	Elaeocarpine		78
<i>E. ganitrus</i>	Rudrakine		79
<i>E. sphaericus</i>	(-)-Isoelaecarpiline		80
<i>E. sphaericus</i>	(±)-3-Oxoisoelaecarpine		80
<i>E. sphaericus</i>	(±)-Elaeocarpine N-oxide		80

<i>E. sphaericus</i>	(±)-Isoelaeocarpine		80
<i>E. sphaericus</i>	(+)-Epiisoelaeocarpiline		80
<i>E. sphaericus</i>	(+)-Elaeocarpiline		80
<i>E. sphaericus</i>	(+)-Epielaeocarpiline		80
<i>E. sphaericus</i>	(-)-Epielaeocarpiline		80
<i>E. sphaericus</i>	(+)-Epialloelaeocarpiline		80
<i>E. sphaericus</i>	(+)-Pseudoepiisoelaeocarpiline		80
<i>E. polydactylus</i>	(+)-Isoelaeocarpicine		80
<i>E. kaniensis</i>	(+)-Elaeokanine A		48

<i>E. kaniensis</i>	Elaeokanine B		
<i>E. kaniensis</i>	(-)-Elaeokanine C		48
<i>E. kaniensis</i>	(+)-Elaeokanine D		48
<i>E. kaniensis</i>	Elaeokanine E		48
<i>E. kaniensis</i>	Elaeokanidine A		48
<i>E. kaniensis</i>	Elaeokanidine B		48

---

## 1.5 Research objectives

There are approximately 27 species of *Elaeocarpus* that are native to Peninsular Malaysia. However, to date there is no phytochemical report on any of the Malaysian samples. Additionally, some of these species are used in traditional medicine in Malaysia to treat headaches (*E. mastersii*), fever (*E. petiolatus*), poultice sores (*E. stipularis*) and as general tonic (*E. floribundus* and *E. grandiflorus*).<sup>81</sup> This has led to the search for alkaloid-containing *Elaeocarpus* species occurring in Peninsular Malaysia. The focus of this project was therefore to investigate the alkaloid composition of the leaves of *Elaeocarpus tectorius* and *Elaeocarpus angustifolius* collected in Malaysia. The specific objectives of the present project are to:

- Obtain crude alkaloid extracts from the dried-ground leaf material of *E. tectorius* and *E. angustifolius*.
- Perform chromatographic fractionation of the crude alkaloid extracts until pure alkaloids are obtained.
- Characterise and determine the structures of the pure alkaloids isolated by using various spectroscopic methods.
- Evaluate the cytotoxic property of the pure alkaloids obtained on a panel of human cancer cell lines.
- Propose plausible biosynthetic pathways to the alkaloids isolated.

## CHAPTER 2: EXPERIMENTAL

### 2.1 General

Optical rotations were measured with a JASCO P-1020 automatic digital polarimeter equipped with a 2 cm microcell. IR spectra were recorded on a Perkin Elmer Spectrum RX1 FT-IR Spectrophotometer. UV spectra were acquired on a GE Ultrospec 8000 spectrophotometer. ECD spectra were obtained on a J-815 circular dichroism spectrometer. NMR spectra were recorded on a Bruker 600 AVANCE III operating at 600 MHz ( $^1\text{H}$ ) and 150 MHz ( $^{13}\text{C}$ ). Chemical shifts were reported as  $\delta$  values (ppm) with TMS (for 600 MHz NMR) as internal reference and  $J$  in Hz. HRESIMS were obtained on a JEOL Accu TOF-DART mass spectrometer.

### 2.2 Dragendorff's reagent

0.85 g of bismuth subnitrate was mixed with 40 mL of distilled water and 10 mL of glacial acetic acid to produce solution A. 8 g of potassium iodide was dissolved in 20 mL of water to prepare solution B. Solution A and solution B were then mixed in a ratio of 1:1 to produce the stock solution.

To produce 100 mL of the reagent, 10 mL of the stock solution was added to 20 mL of acetic acid (glacial) and topped up to 100 mL with distilled water.

Dragendorff's reagent is a solution of heavy metals which act by forming a complex with the nitrogen atoms in the compounds to produce ion pairs. The precipitation of the complex produces orange-red colour after reacting with alkaloids.

### 2.3 Plant material

The leaf samples of *E. tectorius* were collected in June 2014 from Jelevu, Negeri Sembilan, while the leaf samples of *E. angustifolius* were collected in June 2015 from Hulu Langat, Selangor. Both plants were identified by Dr K. T. Yong from Institute of Biological Sciences, University of Malaya, Malaysia. The herbarium voucher specimens for both species, i.e., UNMC77 for *E. tectorius* and UNMC 96 for *E. angustifolius*, were deposited at the Herbarium of the University of Malaya.

## 2.4 Screening of plant material

For small scale screening of the plant material, 500 g of dried leaves of *E. tectorius* and *E. angustifolius* were extracted with the same method described in section 2.5 to give the desired alkaloid crude mixtures. The crude mixtures were then analysed by using thin layer chromatography (TLC), while the developed TLC plates were sprayed with Dragendorff's reagent. Orange stained spots on TLC plates indicated the presence of alkaloids in the leaves of both plants (Figure 2.1).

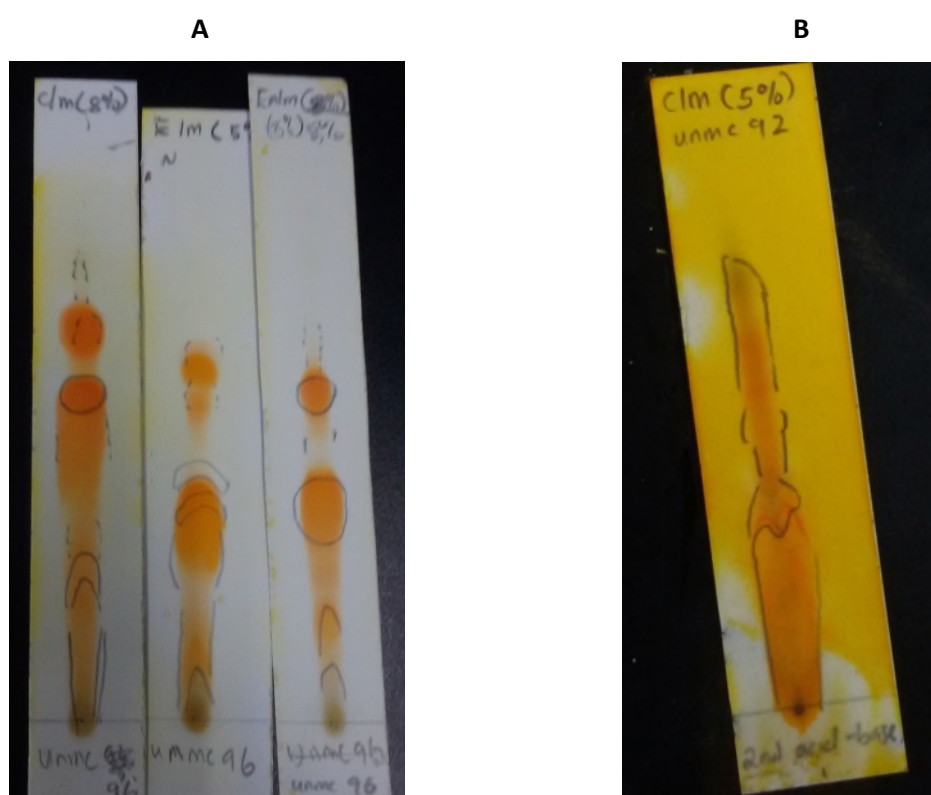


**Figure 2.1:** TLC plates of crude alkaloid mixtures of *E. angustifolius* (A) and *E. tectorius* (B).

## 2.5 Extraction of plant material

The dried-ground leaves of *E. tectorius* (15 kg) and *E. angustifolius* (9.5 kg) were individually soaked in 95% ethanol (15 L) for 48 hours (Figure 2.2). The ethanol extract was concentrated using rotatory evaporator at 40 °C. The leaf materials were re-extracted three times. The combined concentrated ethanoic extract was added into 3% tartaric acid solution (1 L) with vigorous stirring. The acidic solution was then filtered through kieselguhr (60 g) to remove the insoluble non-alkaloidal substances. Concentrated NH<sub>3</sub> solution was then added to the acidic filtrate until pH 10 was achieved. The liberated mixture of alkaloids was exhaustively

extracted with  $\text{CHCl}_3$ , washed with water, dried over anhydrous  $\text{Na}_2\text{SO}_4$ , and concentrated to afford the basic crude alkaloid mixtures (5.1 g for *E. tectorius*; 13 g for *E. angustifolius*).



**Figure 2.2:** Leaves of *E. angustifolius* and *E. tectorius* soaked in 95% ethanol.

## **2.6 Isolation of alkaloids**

### **2.6.1 Chromatographic procedures**

#### **2.6.1.1 Thin layer chromatography (TLC)**

TLC was used for detection and monitoring of alkaloids in the crude extracts and fractions. The sample for analysis was loaded on to a TLC aluminium sheet (pre-coated with silica gel 60 F<sub>254</sub> 0.20 mm thickness) and developed in a tank saturated with the appropriate solvent system. The developed spots on the TLC plate were examined under UV light (254 nm), followed by spraying with Dragendorff's reagent (see section 2.2).

#### **2.6.1.2 Column chromatography**

Column chromatography was performed using silica gel 60 (Merck 9385, 230-400 mesh). The ratio of silica gel to sample was about 30:1 by weight. The silica gel was made into a suspension by mixing with the eluting solvent before being packed into a glass column (Figure 2.3). The column was tapped gently to perfect the packing under intermittent vacuum pumping while freshly prepared solvent was introduced. This was repeated until the height of the silica gel bed reached its minimum height. The sample to be separated was

dissolved in minimum volume of chloroform and was added onto the silica gel bed followed by the addition of roughly 1 inch of fine anhydrous  $\text{Na}_2\text{SO}_4$  powder. Fractions were eluted with increasing polarity of the eluting solvent used. Fractions collected were monitored by TLC and similar fractions were combined and subjected to further separation by column chromatography or centrifugal TLC where appropriate.

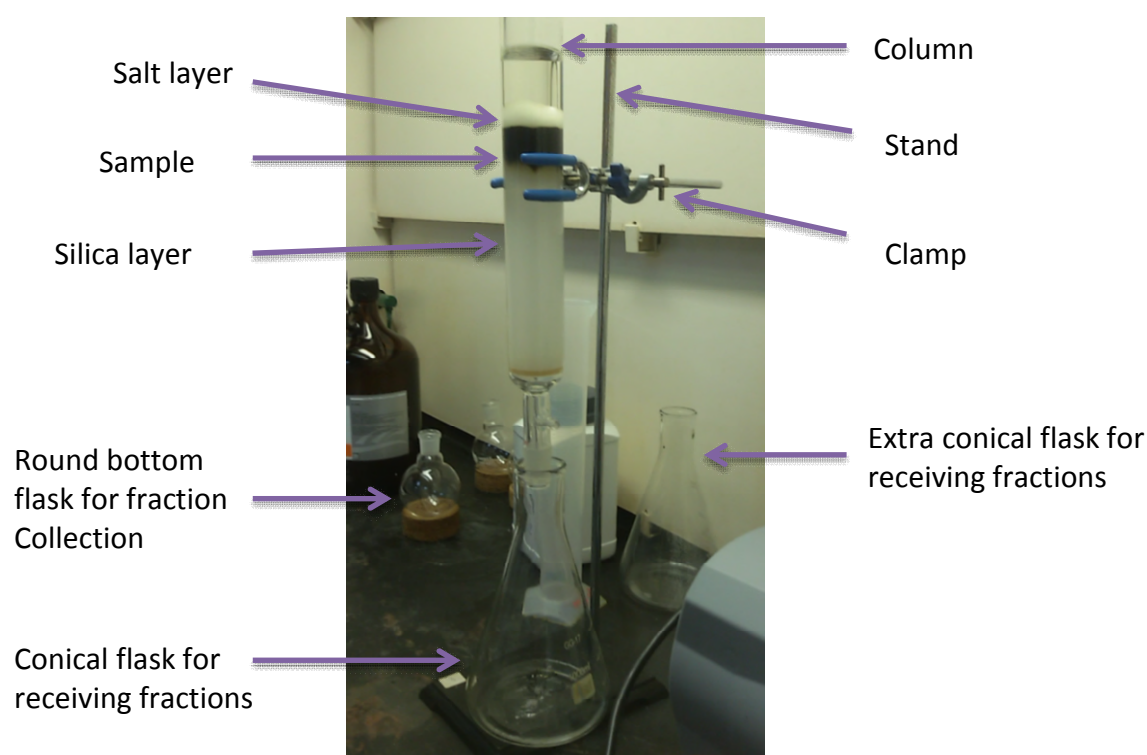


**Figure 2.3:** Typical setup of a column chromatography.

### 2.6.1.3 Centrifugal thin layer chromatography (CTLC)

Preparation of the chromatographic plate (Table 2.1) was carried out by securing the edge of the plate with cellophane tape to form a mould. Silica gel (Merck 7759) suspension was prepared by mixing silica gel powder with cold distilled water. The quantity of both silica gel and the water used are varied based on the desired plate height (Table 2.1). The suspension produced was poured onto the previously prepared mould while rotating the plate to obtain an even setting. The plate was then left to air dry prior to being dried in an oven at  $80\text{ }^{\circ}\text{C}$

overnight. The newly prepared plate was then shaved to the desired thickness before being mounted to the chromatotron.

Semi-purified fractions from column chromatography were subjected to further fractionation with CTLC, which works using the same principle as TLC, except that CTLC incorporates centrifugal force for elution and UV imaging during separation. CTLC was carried out using a round chromatographic plate measuring 24 cm in diameter. A UV transparent lid enabled visualisation and monitoring of individual UV-active bands during the separation process. Depending on the weight of the sample to be separated, the thickness of the sorbent can be increased up to 4 mm as shown in Table 2.1.

**Table 2.1:** Guide to CTLC plate selection and preparation.

<b>Ideal weight of sample</b>	<b>Height of silica layer (Mm)</b>	<b>Weight of silica (g)</b>	<b>Volume of cold distilled water (mL)</b>
< 400 mg	1	40	90
400 mg – 800 mg	2	60	100
800 mg – 1.500 g	4	110	250

Separation of a semi-purified fraction was carried out by dissolving the sample in minimum volume of the eluting solvent (NH<sub>3</sub>-saturated). This was loaded on the centre of the spinning silica plate to form a thin band. Elution was then carried out with the appropriate solvent system. Fractions were collected, concentrated by rotary evaporation, monitored by TLC and combined where appropriate. Solvents systems used as eluents were:

1. Chloroform : Hexane
2. Chloroform (NH<sub>3</sub>-saturated)
3. Chloroform : Methanol
4. Diethyl ether : Hexane
5. Diethyl ether : Methanol
6. Diethyl ether (NH<sub>3</sub>-saturated)
7. Ethyl acetate : Hexane

8. Ethyl acetate : Methanol
9. Ethyl acetate (NH<sub>3</sub>-saturated)

### 2.6.2 Isolation of alkaloids from the leaves of *E. tectorius*

The crude alkaloid mixture (5.1 g) obtained from the extraction process of the leaves of *E. tectorius* (section 2.5) was fractionated by column chromatography (8 x 12 cm). The starting solvent used for elution was CHCl<sub>3</sub> and polarity was increased gradually with addition of increasing volume of MeOH. A total of 54 fractions were collected and fractions with similar TLC profiles were combined, which resulted in a total of ten combined fractions (Figure 2.4). Only the main combined fractions 2 and 9 (labelled as ER2 and ER9, respectively) showed significant presence of alkaloids based on TLC profiles.

Fraction 2 (ER2), which weighed 0.98 g, was chromatographed with CTLC on a 4 mm plate, eluted with ethyl acetate/hexane (NH<sub>3</sub>-saturated), followed by ethyl acetate/MeOH (NH<sub>3</sub>-saturated) to produce six combined fractions. Fraction ER2/3 (0.08 g) was re-chromatographed using CTLC (1 Mm plate), eluted with ethyl acetate/hexane (NH<sub>3</sub>-saturated) and followed by ethyl acetate/MeOH (NH<sub>3</sub>-saturated) to give five fractions. Fraction ER2/3/2 (0.06 g) was again re-chromatographed using CTLC (1 Mm plate), eluted with CHCl<sub>3</sub>/hexane (NH<sub>3</sub>-saturated) and followed by CHCl<sub>3</sub>/MeOH (NH<sub>3</sub>-saturated) to yield tectoricine (**1**, 0.003 g) and tectoraline (**2**, 0.003 g).

Fraction 9 (ER9), which weighed 4.8 g, was fractionated by a second column chromatography. The starting solvent used for elution was 100% CHCl<sub>3</sub> with increasing percentage of MeOH. A total of 14 combined fractions were obtained. Fraction ERb9/10 (0.39 g) was re-chromatographed using CTLC (1 Mm plate), eluted with Et<sub>2</sub>O/hexane (NH<sub>3</sub>-saturated) and followed by Et<sub>2</sub>O/MeOH (NH<sub>3</sub>-saturated) to give seven combined fractions. Fraction ER9/10/4 (0.027 g) was further purified using CTLC (1 Mm plate), eluted with CH<sub>2</sub>Cl<sub>2</sub>/MeOH (NH<sub>3</sub>-saturated) to give tectoramidine A (**3**, 0.005 g). Fraction ER9/11 (0.039 mg) was also further purified using CTLC (1 Mm plate), eluted with CHCl<sub>3</sub>/MeOH (NH<sub>3</sub>-saturated) to give tectoramidine B (**4**, 0.002 g).

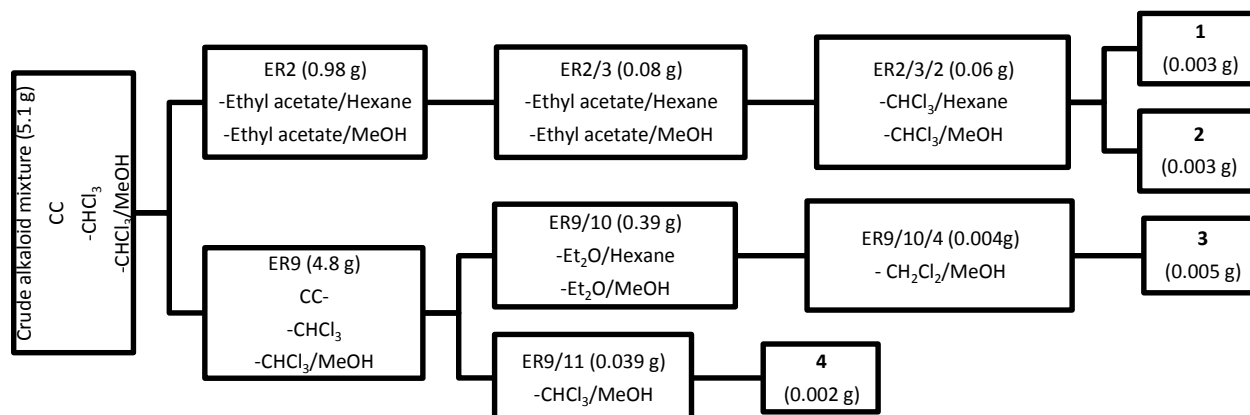


**Figure 2.4:** Isolation of alkaloids from the leaf extract of *E. tectorius*.

### 2.6.3 Isolation of alkaloids from the leaves of *E. angustifolius*

The crude alkaloid mixture (13 g) obtained from the extraction process of the leaves of *E. angustifolius* (section 2.5) was fractionated by column chromatography (8 x 12 cm). The starting solvent used for elution was CHCl<sub>3</sub>/hexane (4:1) and polarity was increased gradually with reducing the percentage of hexane. A total of 44 fractions were collected and fractions with similar TLC profiles were combined, which resulted in a total of eight combined fractions (Figure 2.5). Only the main combined fractions 1, 2, 3 and 5 (labelled as EA1, EA2, EA3 and EA5, respectively) showed significant presence of alkaloids based on TLC profiles.

Fraction 1 (EA1), which weighed 2.308 g, was fractionated by a second column chromatography. The starting solvent used for elution was CHCl<sub>3</sub> with increasing percentage of MeOH. A total of seven combined fractions were obtained. Fraction EA1/1 (0.171 g), was re-chromatographed using CTLC (1 Mm plate), eluted with CH<sub>2</sub>Cl<sub>2</sub>/CHCl<sub>3</sub>/MeOH/hexane to yield carpusidine (**14**, 0.003 g). Fraction EA1/2 (0.718 g) was fractionated using CTLC (2 Mm plate), eluted with Et<sub>2</sub>O/hexane (NH<sub>3</sub>-saturated) to give five combined fractions. Fraction EA1/2/2 (0.061 g) was purified with Et<sub>2</sub>O/hexane (NH<sub>3</sub>-saturated) to give carpusinine E (**9**,

0.003 g). Fraction EA1/2/5 (0.405 g) was fractionated using CTLC (1 Mm plate), eluted with Et<sub>2</sub>O/hexane (NH<sub>3</sub>-saturated) to yield seven fractions. Fraction EA1/2/5/1 (0.027 g) was further purified with CHCl<sub>3</sub>/hexane to yield elaeokanine D (**13**, 0.003 g).

Fraction 2 (EA2), which weighed 1.947 g, was fractionated by a second column chromatography. The starting solvent used for elution was CHCl<sub>3</sub> with increasing percentage of MeOH. A total of five combined fractions were obtained. Fraction EA2/1 (0.100 g) was chromatographed using CTLC (1 Mm plate), eluted with Et<sub>2</sub>O/hexane (NH<sub>3</sub>-saturated) and followed by Et<sub>2</sub>O/MeOH (NH<sub>3</sub>-saturated) to give five combined fractions. Fraction EA2/1/2 was purified further with CHCl<sub>3</sub>/hexane (NH<sub>3</sub>-saturated) to yield carpusinine B (**6**, 0.011 g). Fraction EA2/2 (0.577 g) was purified using CTLC (2 Mm plate), eluted with CHCl<sub>3</sub>/hexane (NH<sub>3</sub>-saturated) to give carpusinine C (**7**, 0.011 g).

Fraction 3 (EA3), which weighed 1.523 g, was further fractionated using CTLC (4 mm plate), eluted with CHCl<sub>3</sub>/hexane (NH<sub>3</sub>-saturated) to give eight combined fractions. Fraction EA3/1 (0.197 g) was further purified using CTLC (1 Mm plate), eluted with CHCl<sub>3</sub>/hexane (NH<sub>3</sub>-saturated) to yield (+)-elaekanine A (**11**, 0.036 g). Fraction EA3/3 (0.443 g) was fractionated using CTLC (1 mm plate), eluted with Et<sub>2</sub>O/hexane (NH<sub>3</sub>-saturated), followed by re-chromatography with a Sephadex LH-20 column, and re-chromatography using CTLC (1 Mm plate), eluted with CH<sub>2</sub>Cl<sub>2</sub>/CHCl<sub>3</sub>/MeOH/hexane (isocratic) to yield carpusinine D (**8**, 0.003 g), carpusinine F (**10**, 0.004 g) and elaeokanine C (**12**, 0.011 g).

Fraction 5 (EA5), which weighed 0.529 g, was fractionated with CTLC (2 Mm plate), eluted with Et<sub>2</sub>O (NH<sub>3</sub>-saturated) and followed by Et<sub>2</sub>O/MeOH (NH<sub>3</sub>-saturated) to give five combined fractions. Fraction EA5/3 (0.057 g) was further purified using CTLC (1 Mm plate), eluted with CHCl<sub>3</sub>/hexane (NH<sub>3</sub>-saturated) to yield carpusinine A (**5**, 0.032 g).

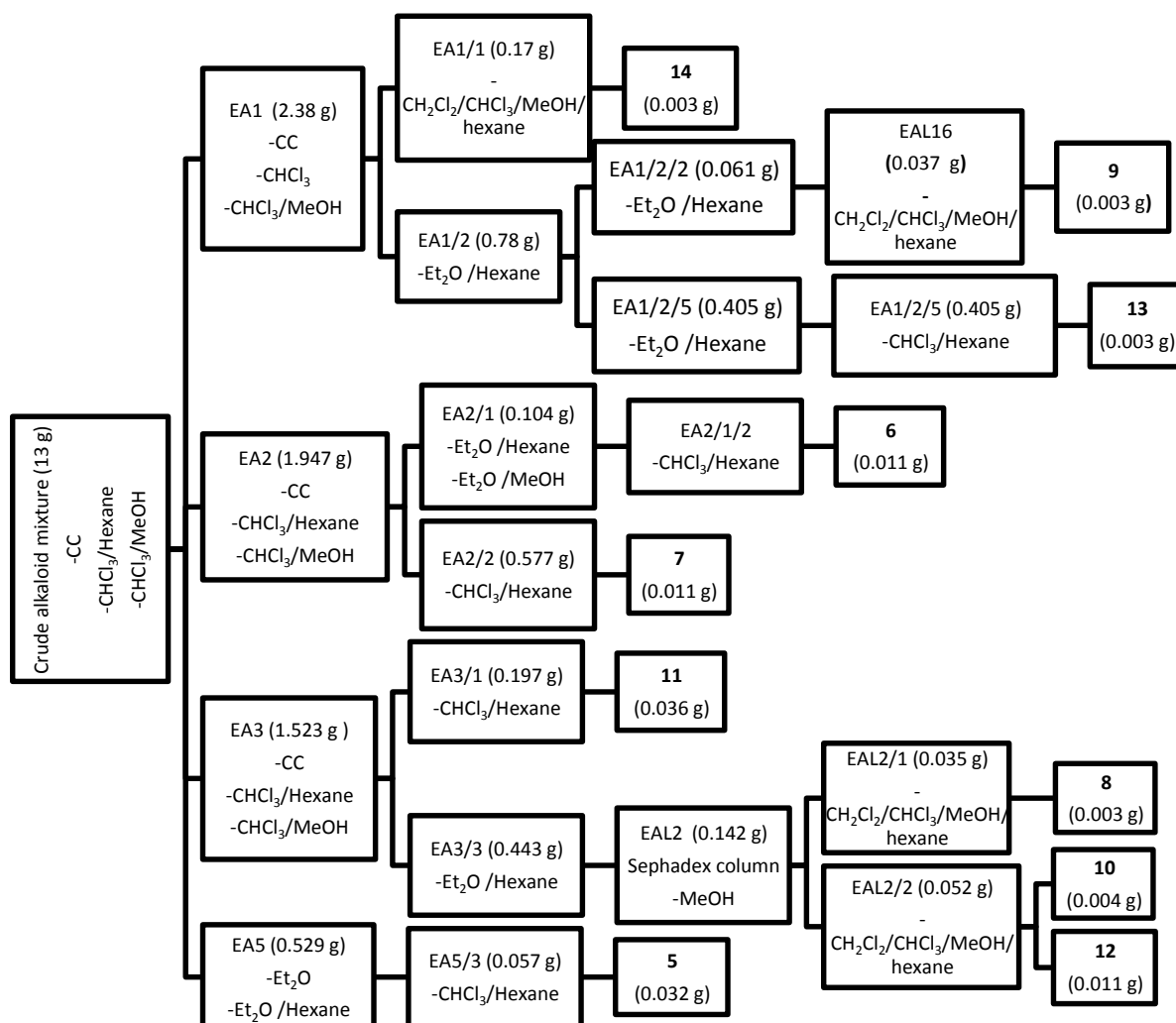


**Figure 2.5:** Isolation of alkaloids from the leaf extract of *E. angustifolius*.

## 2.7 Compound data

Tectoricine (**1**): colorless oil;  $[\alpha]_D^{25} +4$  (c 0.05, CHCl<sub>3</sub>); UV (EtOH)  $\lambda_{\max}$  (log  $\epsilon$ ) 227 (3.77) nm; IR (dry film)  $\nu_{\max}$  1735 (ketone), 1364, 1377 (*gem*-dimethyl), 701, 754 (unsubstituted phenyl) cm<sup>-1</sup>; <sup>1</sup>H and <sup>13</sup>C NMR data, see Table 3.1; HRESIMS  $m/z$  328.2284 [M+H]<sup>+</sup> (calcd for C<sub>21</sub>H<sub>29</sub>NO<sub>2</sub> + H, 328.2277).

Tectoraline (**2**): light yellowish oil;  $[\alpha]_D^{25} -21$  (c 0.12, CHCl<sub>3</sub>); UV (EtOH)  $\lambda_{\max}$  (log  $\epsilon$ ) 227 (3.85) nm; IR (dry film)  $\nu_{\max}$  3279 (NH), 1650 (amide), 701, 751 (unsubstituted phenyl) cm<sup>-1</sup>; <sup>1</sup>H and <sup>13</sup>C NMR data, see Table 3.2; HRESIMS  $m/z$  361.2232 [M+Na]<sup>+</sup> (calcd for C<sub>22</sub>H<sub>30</sub>N<sub>2</sub>O + Na, 361.2256).

Tectoramidine A (**3**): colorless oil;  $[\alpha]_D^{25} 0$  (c 0.25, CHCl<sub>3</sub>); UV (EtOH)  $\lambda_{\max}$  (log  $\epsilon$ ) 229 (3.79) nm; IR (dry film)  $\nu_{\max}$  1687 (C=N), 701, 752 (unsubstituted phenyl) cm<sup>-1</sup>; <sup>1</sup>H and <sup>13</sup>C NMR data, see Table 3.3; HRESIMS  $m/z$  398.2593 [M+H]<sup>+</sup> (calcd for C<sub>27</sub>H<sub>31</sub>N<sub>3</sub> + H, 398.2596).

Tectoramidine B (**4**): colorless oil;  $[\alpha]_D^{25} 0$  (c 0.15, CHCl<sub>3</sub>); IR (dry film)  $\nu_{\max}$  3324 (NH), 1644 (C=N), 698, 748 (unsubstituted phenyl) cm<sup>-1</sup>; <sup>1</sup>H and <sup>13</sup>C NMR data, see Table 3.4; HRESIMS  $m/z$  253.1700 [M+H]<sup>+</sup> (calcd for C<sub>17</sub>H<sub>20</sub>N<sub>2</sub> + H, 253.1705).

Carpusinine A (**5**): colorless oil;  $[\alpha]_D^{25} +2$  (c 0.24, CHCl<sub>3</sub>); UV (EtOH)  $\lambda_{\max}$  (log  $\epsilon$ ) 228 (3.97) nm; IR (dry film)  $\nu_{\max}$  3366 (OH), 2879, 2822, 2733 (Bohlmann bands) and 1656 ( $\alpha,\beta$ -unsaturated ketone) cm<sup>-1</sup>; <sup>1</sup>H and <sup>13</sup>C NMR data, see Table 3.5; HRESIMS  $m/z$  210.1495 [M+H]<sup>+</sup> (calcd for C<sub>12</sub>H<sub>19</sub>NO<sub>2</sub> + H, 210.1494).

Carpusinine B (**6**): light yellowish oil;  $[\alpha]_D^{25} -47$  (c 0.46, CHCl<sub>3</sub>); IR (dry film)  $\nu_{\max}$  2877, 2787, 2725 (Bohlmann bands) and 1708 (ketone) cm<sup>-1</sup>; <sup>1</sup>H and <sup>13</sup>C NMR data, see Table 3.6; HRESIMS  $m/z$  196.1700 [M+H]<sup>+</sup> (calcd for C<sub>12</sub>H<sub>22</sub>NO + H, 196.1701).

Carpusinine C and epicarpusinine C (**7a** and **7b**): colorless oil;  $[\alpha]_D^{25} -40$  (c 0.46, CHCl<sub>3</sub>); IR (dry film)  $\nu_{\max}$  2788, 2875, 2858 (Bohlmann bands), 1708 (ketone) and 1032 (C-O) cm<sup>-1</sup>; <sup>1</sup>H and

$^{13}\text{C}$  NMR data, see Table 3.7; HRESIMS  $m/z$  240.1970  $[\text{M}+\text{H}]^+$  (calcd for  $\text{C}_{14}\text{H}_{26}\text{NO}_2 + \text{H}$ , 240.1701).

Carpusinine D (**8**): light yellowish oil;  $[\alpha]_{\text{D}}^{25} -7$  ( $c$  0.11,  $\text{CHCl}_3$ ); IR (dry film)  $\nu_{\text{max}}$  3418 (OH), 2854, 2874 (Bohlmann bands), 1651 (H-bonded C=O) and 1088 (C-O)  $\text{cm}^{-1}$ ;  $^1\text{H}$  and  $^{13}\text{C}$  NMR data, see Table 3.8; HRESIMS  $m/z$  256.1911  $[\text{M}+\text{H}]^+$  (calcd for  $\text{C}_{14}\text{H}_{26}\text{NO}_3 + \text{H}$ , 256.1913).

Carpusinine E (**9**): colorless oil;  $[\alpha]_{\text{D}}^{25} -25$  ( $c$  0.11,  $\text{CHCl}_3$ ); IR (dry film)  $\nu_{\text{max}}$  2876, 2793, 2728 (Bohlmann bands), 1713 (ketone) and 1073 (C-O)  $\text{cm}^{-1}$ ;  $^1\text{H}$  and  $^{13}\text{C}$  NMR data, see Table 3.9; HRESIMS  $m/z$  210.1500  $[\text{M}+\text{H}]^+$  (calcd for  $\text{C}_{12}\text{H}_{19}\text{NO}_2 + \text{H}$ , 210.1494).

Carpusinine F and epicarpusinine F (**10a** and **10b**): light yellowish oil;  $[\alpha]_{\text{D}}^{25} +2$  ( $c$  0.27,  $\text{CHCl}_3$ ); IR (dry film)  $\nu_{\text{max}}$  3405 (OH), 1710 (ketone) and 1070 (C-O)  $\text{cm}^{-1}$ ;  $^1\text{H}$  and  $^{13}\text{C}$  NMR data, see Table 3.10; HRESIMS  $m/z$  258.2074  $[\text{M}+\text{H}]^+$  (calcd for  $\text{C}_{14}\text{H}_{28}\text{NO}_3 + \text{H}$ , 258.2059).

(+)-Elaeokanine A (**11**): light yellowish oil;  $[\alpha]_{\text{D}}^{25} +46$  ( $c$  0.50,  $\text{CHCl}_3$ ); UV (EtOH)  $\lambda_{\text{max}}$  ( $\log \epsilon$ ) 228 (1.63) nm; IR (dry film)  $\nu_{\text{max}}$  2874, 2792, 2728 (Bohlmann bands) and 1662 ( $\alpha,\beta$ -unsaturated ketone)  $\text{cm}^{-1}$ ;  $^1\text{H}$  and  $^{13}\text{C}$  NMR data, see Table 3.11; HRESIMS  $m/z$  194.1536  $[\text{M}+\text{H}]^+$  (calcd for  $\text{C}_{14}\text{H}_{28}\text{NO}_3 + \text{H}$ , 194.1545).

Elaeokanine C (**12**): light yellowish oil;  $[\alpha]_{\text{D}}^{25} +3^\circ$  ( $c$  0.30,  $\text{CHCl}_3$ ); IR (dry film)  $\nu_{\text{max}}$  3384 (OH) and 1708 (ketone)  $\text{cm}^{-1}$ ;  $^1\text{H}$  and  $^{13}\text{C}$  NMR data, see Table 3.12; HRESIMS  $m/z$  212.1661  $[\text{M}+\text{H}]^+$  (calcd for  $\text{C}_{12}\text{H}_{21}\text{NO}_2 + \text{H}$ , 212.1651).

Elaeokanine D (**13**): light yellowish oil;  $[\alpha]_{\text{D}}^{25} +2$  ( $c$  0.20,  $\text{CHCl}_3$ ); IR (dry film)  $\nu_{\text{max}}$  2855, 2790, 2717 (Bohlmann bands), 1711 (ketone) and 1073 (C-O)  $\text{cm}^{-1}$ ;  $^1\text{H}$  and  $^{13}\text{C}$  NMR data, see Table 3.13; HRESIMS  $m/z$  210.1502  $[\text{M}+\text{H}]^+$  (calcd for  $\text{C}_{12}\text{H}_{20}\text{NO}_2 + \text{H}$ , 210.1494).

Carpusidine (**14**): light yellowish oil;  $[\alpha]_{\text{D}}^{25} +1$  ( $c$  0.56,  $\text{CHCl}_3$ ); IR (dry film)  $\nu_{\text{max}}$  2851, 2792, 2708 (Bohlmann bands) and 1717 (ketone)  $\text{cm}^{-1}$ ;  $^1\text{H}$  and  $^{13}\text{C}$  NMR data, see Table 3.14; HRESIMS  $m/z$  154.1228  $[\text{M}+\text{H}]^+$  (calcd for  $\text{C}_9\text{H}_{15}\text{NO} + \text{H}$ , 154.1232).

## **2.8 Cytotoxicity assay**

### **2.8.1 Cell lines and cell culture**

A panel of human breast cancer (MCF7, MDA-MB-231, MDA-MB-468, SKBR3, T47D), colorectal cancer (Caco2, HCT116, HT29, Sw48), lung cancer (A549, H1299), nasopharyngeal cancer (CNE1, HK1, SUNE1), neuroblastoma (SHSY5Y), pancreatic cancer (AsPC1, BxPC3, SW1990), human non-tumorigenic breast epithelial cells (MCF10A) and lung fibroblast cells (MRC5) were purchased from the American Type Culture Collection. All cancer cells including MRC5 cells were maintained in RPMI 1640 medium with 10% fetal bovine serum (FBS), 100 IU/mL penicillin, and 100 µg/mL streptomycin (Sigma-Aldrich, St. Louis, MO, USA), while MCF10A cells were cultured with 5% horse serum, 20 ng/mL epidermal growth factor, 0.5 µg/mL hydrocortisone, 10 µg/mL insulin, 100 IU/mL penicillin, and 100 µg/mL streptomycin. All cells were maintained in an incubator at 37°C and 5% carbon dioxide.

### **2.8.2 Luminescent cell viability assay**

Cell viability of cells after treatment with compounds **5**, **6**, **7a/7b**, **9**, **11**, **12**, **13** and **14** were determined using the CellTitre-Glo® Luminescent Cell Viability Assay kit (Promega, USA). All compounds were prepared as a stock solution of 100 mM in DMSO and diluted to 100 µM using sterile phosphate buffer solution. All cancer or non-tumorigenic cells were seeded in 384-well opaque plates for 24 h at a density of 1000 cells/well and followed by treatment with the individual compound for 72 hours. Cells treated with 0.1% DMSO were the negative controls. Luminescence reading was measured using SpectraMax M3 Multi-Mode Microplate Reader (Radnor, USA). The percentage cell viability was determined based on the luminescent reading of treated cells and cells treated with negative control.

## CHAPTER 3: RESULTS AND DISCUSSION

### 3.1 Alkaloids from *Elaeocarpus tectorius*

Investigation of the alkaloidal content of the leaves of *Elaeocarpus tectorius* has provided four new phenylethylamine-containing alkaloids, namely, tectoricine (**1**), tectoraline (**2**), tectoramidine A (**3**) and tectoramidine B (**4**).

#### 3.1.1 Tectoricine (**1**)

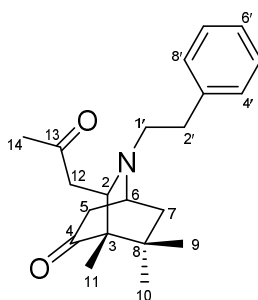


**Figure 3.1:** Structure of tectoricine (**1**).

Tectoricine (**1**) (Figure 3.1) was obtained as a colourless oil,  $[\alpha]_D +4$  (c 0.05,  $\text{CHCl}_3$ ). The IR spectrum (Appendix 2) showed absorption bands due to a ketone carbonyl ( $1735\text{ cm}^{-1}$ ), an unsubstituted phenyl ring ( $701, 754\text{ cm}^{-1}$ ) and a *gem*-dimethyl group ( $1364, 1377\text{ cm}^{-1}$ ). The HRESIMS data ( $[\text{M}+\text{H}]^+$   $m/z$  328.2284) of **1** established the molecular formula as  $\text{C}_{21}\text{H}_{29}\text{NO}_2$  (Appendix 3), requiring eight degrees of unsaturation. The  $^{13}\text{C}$  NMR data of **1** (Table 3.1 and Figure 3.7) indicated the presence of 19 discrete carbon signals, of which two are due to two pairs of equivalent aromatic methine carbons. In agreement with the HRESIMS data, the total number of carbons in **1** was therefore determined as 21, comprising four methyls, five methylenes, two aliphatic methines, five aromatic methines, two aliphatic quaternary carbons, one quaternary aromatic carbon and two ketone carbonyls. The presence of two pairs of equivalent methine carbons at  $\delta_{\text{C}} 128.4$  and  $128.9$ , a methine carbon at  $\delta_{\text{C}} 126.1$  and a quaternary carbon at  $\delta_{\text{C}} 140.4$  suggested the presence of an unsubstituted phenyl group. This was further supported by the  $^1\text{H}$  NMR data (Table 3.1 and Figure 3.6), which also showed

signals due to an unsubstituted phenyl group ( $\delta_{\text{H}}$  7.15–7.26, 5H). In addition, the  $^1\text{H}$  NMR data revealed the presence of four distinct 3H singlet signals at  $\delta_{\text{H}}$  0.71, 0.87, 1.12 and 2.00 due to four isolated methyl groups. The three methyl signals at  $\delta_{\text{H}}$  0.71, 0.87 and 1.12 were determined to be associated with a 2,3,3-trimethylpropanone fragment, corresponding to the O=C-4-C-3(Me-11)-C-8(Me-10)-Me-9 partial structure in **1**, on the basis of the observed correlations from Me-11 to C-3, C-4 and C-8; Me-9 to C-3, C-8 and C-10; and Me-10 to C-3, C-8 and C-9 in the HMBC spectrum (Figure 3.2). Furthermore, the presence of the *gem*-dimethyl group (Me-9-C-8-Me-10) was supported by the observation of two absorption bands at 1364 and 1377  $\text{cm}^{-1}$  in the IR spectrum of **1**.

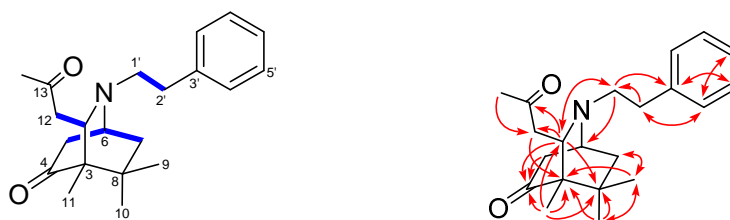


**Figure 3.2:** COSY (bold bonds) and key HMBC  $^1\text{H}$ - $^{13}\text{C}$  correlation (arrows) of tectoricine (**1**).

Examination of the HSQC and COSY data of **1** (Figure 3.2) revealed three additional partial structures, namely, an  $\text{NCH}_2\text{CH}_2$  fragment corresponding to  $\text{NC-1}'\text{-C-2}'$ , an  $\text{NCHCH}_2$  fragment corresponding to  $\text{NC-2-C-12}$ , and a  $\text{CH}_2\text{CH}(\text{N})\text{CH}_2$  fragment corresponding to  $\text{C-5-C-6-C-7}$ . The  $\text{NC-1}'\text{-C-2}'$  partial structure was established to be part of the phenethylamino side chain based on the observed HMBC correlations from H-1' and H-5'/7' to C-3'; H-2' and H-6' to C-4'/8'; and H-4'/8' to C-2', while the  $\text{NC-2-C-12}$  partial structure was determined to be associated with the acetyl side chain based on the observed HMBC correlations from H-14 to C-12 and from H-2 to C-13. The observed correlations from H-5 and H-11 to C-4 and from H-9 to C-7 in the HMBC spectrum allowed assembly of the cyclohexanone moiety by connecting the  $\text{C-5-C-6-C-7}$  partial structure to the ketonic C-4 and quaternary C-8 of the 2,3,3-trimethylpropanone partial structure. The observed correlations from H-2 to C-1' and from H-1' to C-2 and C-6 indicated that C-2, C-6 and C-1' were attached to a tertiary N atom. Finally, the linkage between C-2 and C-3, which completed the assembly of the isoquinuclidinone ring system of **1**, was shown by the

observed HMBC correlations from H-2 to C-4, C-6 and C-8; H-11 to C-2; and H-12 to C-3. The proposed structure of **1** is consistent with the full HMBC data (Figure 3.2).

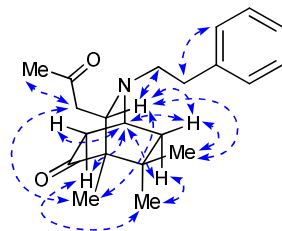


**Figure 3.3:** Selected NOESY correlations of tectoricine (**1**).

The relative configurations at the three stereocenters in **1** (i.e., C-2, C-3 and C-6) were established based on the NOESY data (Figure 3.3). The rigid architecture of the isoquinuclidinone ring system required the configurations at C-3 and C-6 to be 3*S*,6*S* or 3*R*,6*R*. This leaves only the relative configuration at C-2 to be considered. The NOEs observed for H-2/Me-9 and H-2/H-7 $\beta$  required that H-2, H-7 $\beta$  and Me-9 to be directed into the same face of the isoquinuclidinone ring system (the acetyl group is oriented away from Me-9), thus restricting the number of possible structures of **1** to one enantiomeric pair, which corresponded to the relative configuration 2*S*,3*S*,6*S* (or 2*R*,3*R*,6*R*). Additionally, since both H-7 $\beta$  ( $\delta_{\text{H}}$  2.12) and Me-9 ( $\delta_{\text{H}}$  1.12) were equatorially  $\beta$ -oriented, both H-7 $\alpha$  ( $\delta_{\text{H}}$  1.40) and Me-10 ( $\delta_{\text{H}}$  0.87) must therefore be axially  $\alpha$ -oriented. This deduction was supported by the NOEs observed for H-10/H-5 $\alpha$  and H-10/H-7 $\alpha$ . On the other hand, based on the overall geometry of the isoquinuclidinone ring system of **1**, the Me-11 group is oriented in the anisotropic shielding zone of the adjacent ketone at C-4, thus providing an explanation for the notably shielded resonances observed for Me-11 ( $\delta_{\text{H}}$  0.71,  $\delta_{\text{C}}$  10.7) in the  $^1\text{H}$  and  $^{13}\text{C}$  NMR spectra. Other NOEs observed are in complete agreement with the structure and relative configuration of **1**. Finally, the absolute configuration of **1** was established as 2*S*,3*S*,6*S* by comparing the experimental and calculated electronic circular dichroism (ECD) spectra of **1** (Figure 3.4).

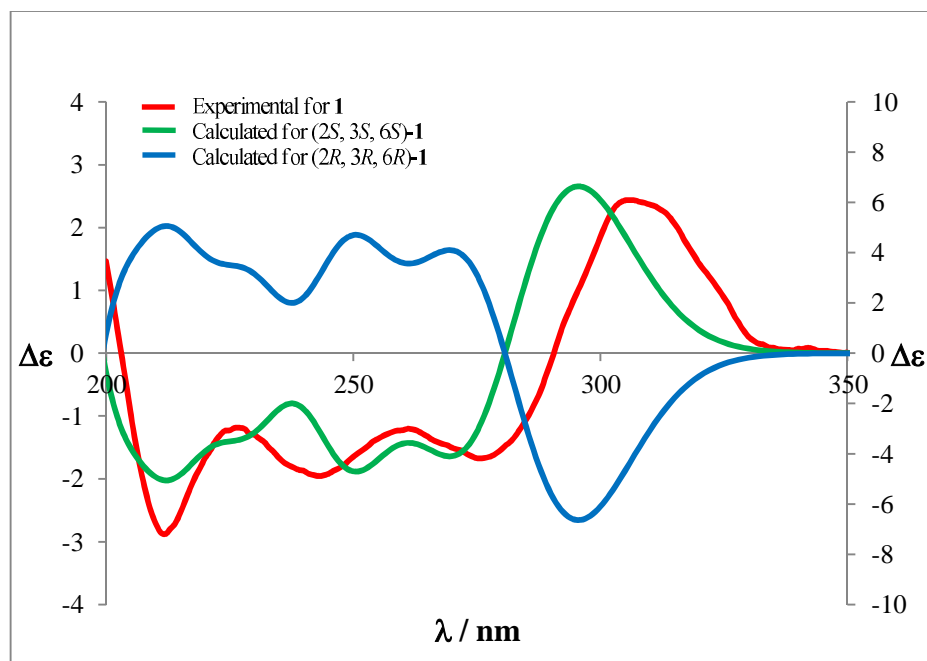


**Figure 3.4:** Experimental and calculated ECD spectra of tectoricine (**1**) in MeCN.

Tectoricine (**1**) represents a new class of alkaloids in which the phenethylamine nitrogen atom is incorporated into a novel isoquinuclidinone ring system that is substituted with three methyl groups (1,1,2-trisubstitution) and an acetyl side chain. Alkaloids that possess an isoquinuclidine moiety as a standalone unit without being part of a larger fused-ring system are rare and are only to date represented by mearsine (**54**) obtained from *Peripentadenia mearsii* and grandisine B (**55**) isolated from *Elaeocarpus grandis* (Figure 3.5).<sup>71,82</sup>

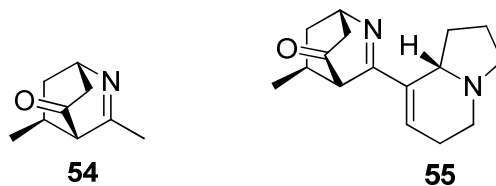
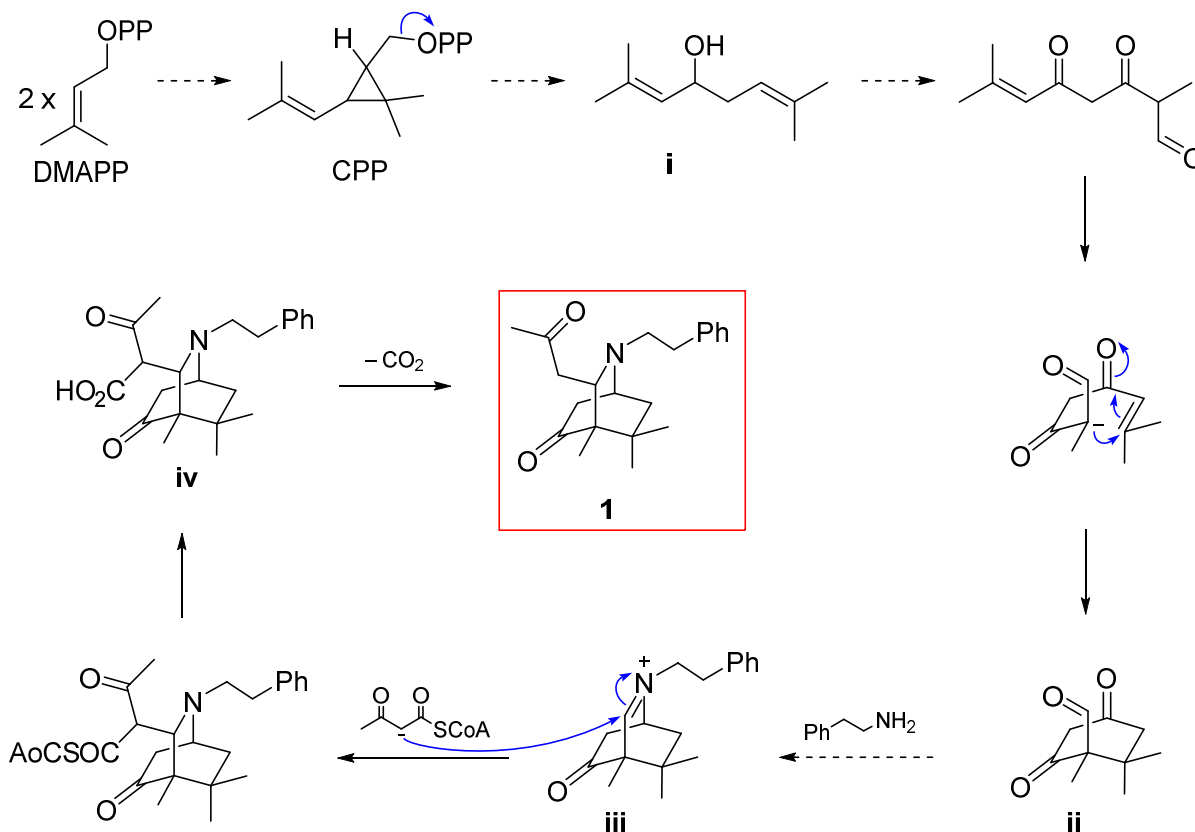


**Figure 3.5:** Structures of **54** and **55**.

The structure of tectoricine (**1**) suggests that it is a monoterpene phenethylamine. However, the monoterpene moiety in **1** appears to possess an irregular monoterpene skeleton, which

was mostly found to be present in monoterpenoids represented in plants of the family Asteraceae. A plausible pathway to **1** from two molecules of dimethylallyl pyrophosphate (DMAPP) is presented in Scheme 3.1. It was previously proposed that the biosynthesis of irregular monoterpenes starts with the condensation of two molecules of DMAPP to give chrysanthemyl diphosphate (CPP). Subsequent elimination of diphosphate from CPP gives rise to a carbocation that undergoes multiple rearrangements and trapping by a molecule of water to give the allylic alcohol **i**, which in the present case is regarded as the key intermediate to **1**. A series of oxidative transformations and cyclization then follow to give the cyclohexadione **ii**, which on a double reductive amination with phenethylamine furnishes the cyclic iminium ion, **iii**. Nucleophilic attack of acetoacetyl-CoA on **iii** followed by hydrolysis give the  $\beta$ -keto acid **iv**, after which decarboxylation leads to tectoricine (**1**).<sup>83,84</sup>



**Scheme 3.1:** Plausible biosynthetic pathway to tectoricine (**1**).

**Table 3.1:**  $^{13}\text{C}$  (150 MHz) and  $^1\text{H}$  NMR (600 MHz) data of tectoricine (**1**) ( $\delta$  in ppm).<sup>a</sup>

Position	$\delta_{\text{C}}$	$\delta_{\text{H}}$ ( <i>J</i> in Hz)
2	58.9	3.46, dd (6.9, 4.2)
3	54.8	-
4	215.4	-
5	45.5	2.32, m 2.37, m
6	49.8	3.14, t (3.0)
7 $\beta$	36.4	2.12, dt (14.0, 3.0)
7 $\alpha$		1.40, dd (14.0, 3.0)
8	33.4	-
9	25.7	1.12 s
10	29.6	0.87 s
11	10.7	0.71 s
12	49.9	2.03, dd (18.5, 4.1) 2.39, m
13	207.9	-
14	31.0	2.00, s
1'	55.2	2.99, m 2.70, m
2'	35.9	2.65, m 2.65, m
3'	140.4	-
4'	128.9	7.15, d (7.5)
5'	128.4	7.26, m
6'	126.1	7.19, m
7'	128.4	7.26, m
8'	128.9	7.15, d (7.5)

<sup>a</sup> Measured in  $\text{CDCl}_3$ .

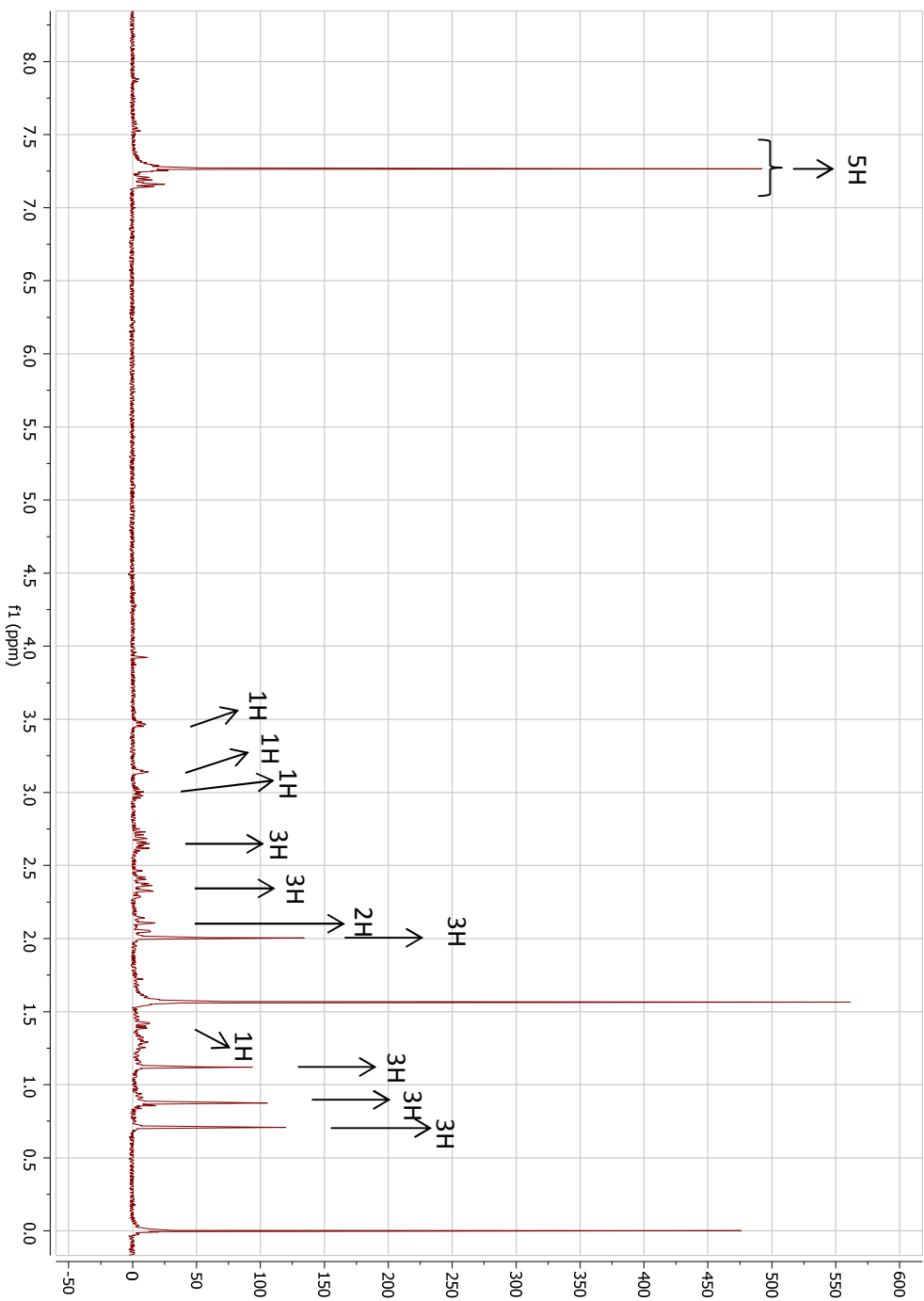
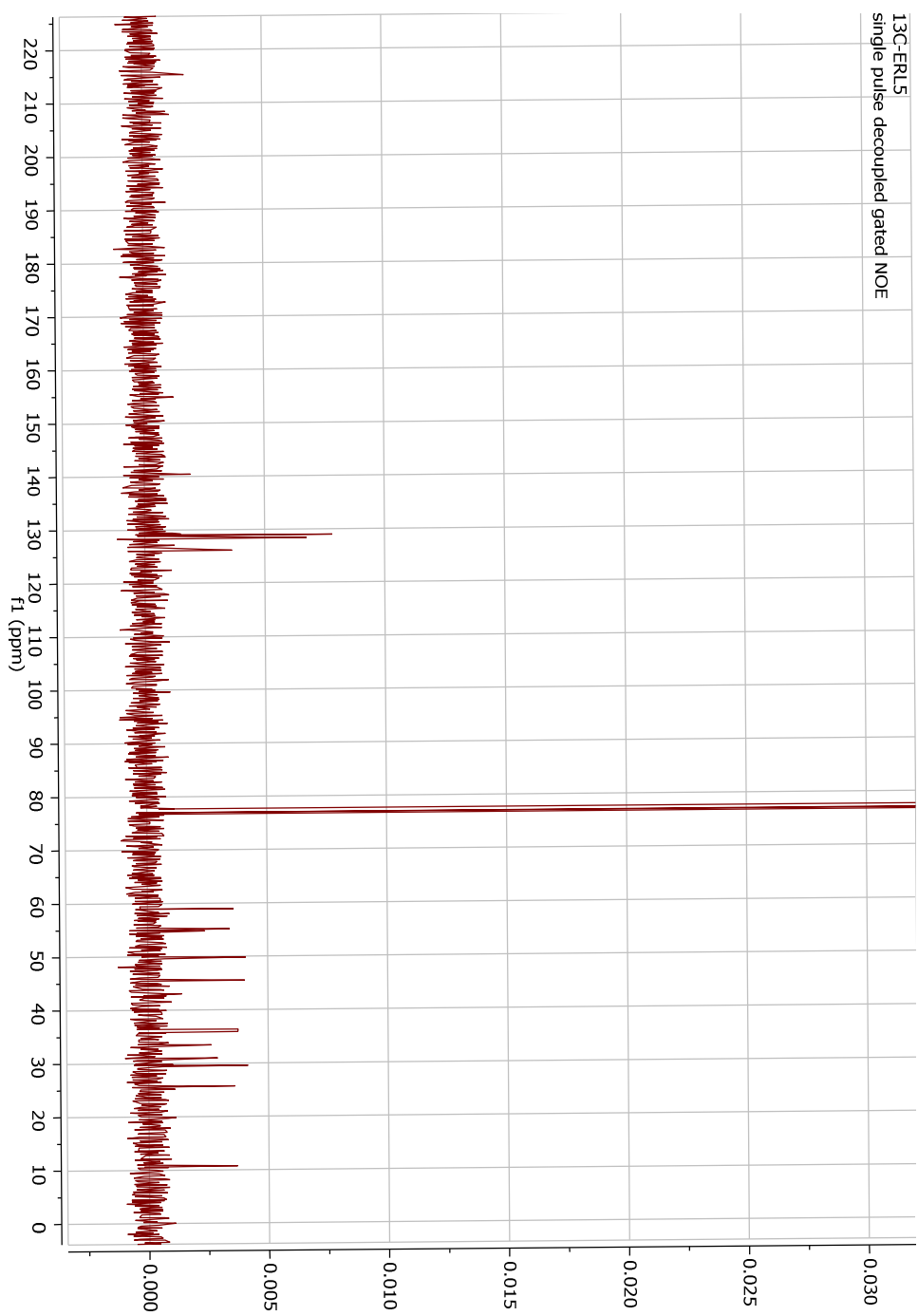
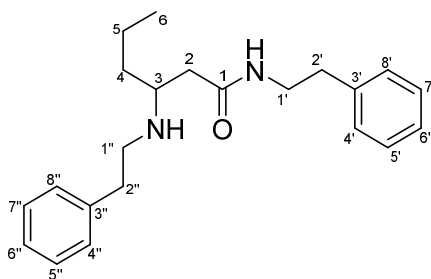


Figure 3.6:  $^1\text{H}$  NMR (600 MHz,  $\text{CDCl}_3$ ) spectrum of tectoricine (**1**).



**Figure 3.7:**  $^{13}\text{C}$  NMR (150 MHz,  $\text{CDCl}_3$ ) spectrum of tectoricine (**1**).

### 3.1.2 Tectoraline (2)



**Figure 3.8:** Structure of tectoraline (**2**).

Tectoraline (**2**) (Figure 3.8) was obtained as a light yellowish oil,  $[\alpha]_D -21$  ( $c$  0.12,  $\text{CHCl}_3$ ). The IR spectrum (Appendix 9) showed the presence of unsubstituted phenyl rings ( $701$  and  $751\text{ cm}^{-1}$ ), an amide carbonyl ( $1650\text{ cm}^{-1}$ ) and an NH group ( $3279\text{ cm}^{-1}$ ). The HRESIMS data ( $[\text{M}+\text{Na}]^+$   $m/z$  361.2232) of **2** established the molecular formula as  $\text{C}_{22}\text{H}_{30}\text{N}_2\text{O}$  (Appendix 10), requiring nine degrees of unsaturation. The  $^{13}\text{C}$  NMR data of **2** (Table 3.2 and Figure 3.11) indicated the presence of 18 discrete carbon signals, four of which are due to four pairs of equivalent aromatic methine carbons. The total number of carbons in **2** was therefore determined as 22 (comprising one methyl, seven methylenes, one aliphatic methine, ten aromatic methines, two quaternary aromatic carbons and one amide carbonyl), which agrees with the molecular formula. The presence of four pairs of equivalent methine resonances at  $\delta_{\text{C}}$  128.4, 128.5, 128.6 and 128.7, two methine resonances at  $\delta_{\text{C}}$  126.3 and 126.4, and two quaternary carbon resonances at  $\delta_{\text{C}}$  139.3 and 139.5, suggested the presence of two unsubstituted phenyl groups with a similar chemical environment. The presence of 10 aromatic signals in the  $^1\text{H}$  NMR spectrum ( $\delta_{\text{H}}$  7.14–7.29) (Table 3.2 and Figure 3.10) provided further support for this suggestion. The  $^{13}\text{C}$  NMR spectrum also exhibited the presence of an amide/ester carbonyl resonance at  $\delta_{\text{C}}$  172.0. However, since the molecular formula contains only one O atom, the carbonyl resonance was attributed to an amide function. In addition to the methyl triplet observed at  $\delta_{\text{H}}$  0.85, the  $^1\text{H}$  NMR spectrum also revealed the presence of a methylene group adjacent to a carbonyl function, as inferred by the observation of a large  $J_{\text{gem}}$  value, i.e., 16.0 Hz, for the pair of geminally coupled H atoms.

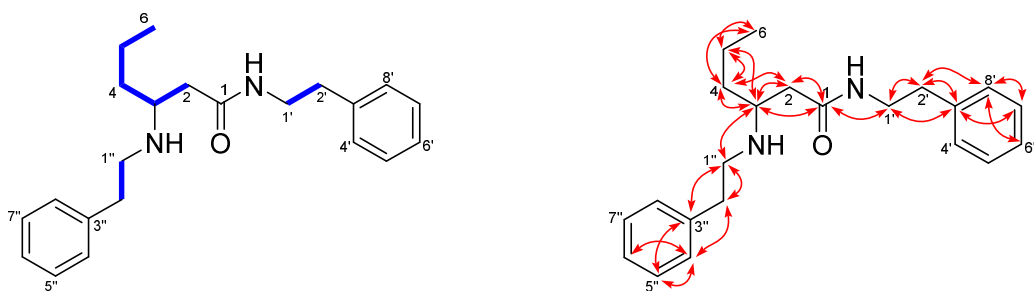
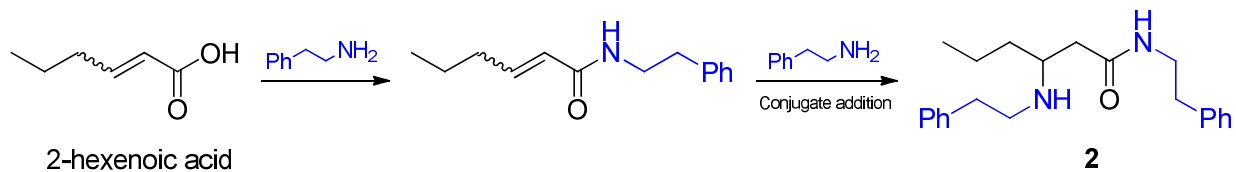


**Figure 3.9:** COSY (bold bonds) and key HMBC  $^1\text{H}$ - $^{13}\text{C}$  correlation (arrows) of tectoraline (**2**).

The COSY and HSQC data revealed two  $\text{CH}_2\text{CH}_2\text{N}$  fragments corresponding to the C-2'-C-1'-N and C-2''-C-1''-N partial structures, and a  $\text{CH}_2\text{CH}(\text{N})\text{CH}_2\text{CH}_2\text{CH}_3$  fragment corresponding to the C-2-C-3-C-4-C-5-C-6 partial structure in **2** (Figure 3.9). The presence of two phenethylamine moieties in **2** was readily established by the HMBC data (Figure 3.9), which connected C-2' to C-3' and C-2'' to C-3'', from the observed three-bond correlations from H-4'/8' to C-2'; H-2' to C-4'/8'; H-1' to C-3'; H-4''/8'' to C-2''; H-2'' to C-4''/8''; and H-1'' to C-3''. The attachment of the C-2-C-3-C-4-C-5-C-6 partial structure to the amide carbonyl C-1 was revealed by the HMBC correlation from H-3 to C-1. This is also consistent with the large  $J_{gem}$  value observed for both H-2 (*vide supra*). On the other hand, the amide function was established to be associated with the Ph-C-2'-C-1'-N partial structure based on the observed correlation from H-1' to C-1 in the HMBC spectrum. Finally, the Ph-C-2''-C-1''-N partial structure was connected to C-3 based on the observed correlation from H-1'' to C-3. The proposed structure for tectoraline (**2**) is therefore *N*-phenethyl-3-(phenethylamino)hexanamide and is entirely consistent with the full HMBC data (Figure 3.9). Tectoraline (**2**) represents a new alkamide that appears to be derived from a molecule of 2-hexenoic acid and two molecules of phenethylamine (Scheme 3.2).



**Scheme 3.2:** Plausible biosynthetic pathway to tectoraline (**2**).

**Table 3.2:**  $^{13}\text{C}$  (150 MHz) and  $^1\text{H}$  NMR (600 MHz) data of tectoraline (**2**) ( $\delta$  in ppm).<sup>a</sup>

Position	$\delta_{\text{C}}$	$\delta_{\text{H}}$ ( <i>J</i> in Hz)
2	38.7	2.35, dd (16.0, 3.4) 2.12, dd (16.0, 7.2)
3	54.7	2.76, m
4	35.7	1.34, m
5	19.0	1.19, m
6	14.0	0.85, t (7.3)
1'	39.9	3.41, m
2'	35.6	2.73, t (7.0)
3'	139.3 <sup>d</sup>	-
4'	128.6 <sup>e</sup>	7.14, d (7.5) <sup>b</sup>
5'	128.4 <sup>f</sup>	7.29, t (7.5) <sup>c</sup>
6'	126.3 <sup>g</sup>	7.22, t (7.5)
7'	128.4 <sup>f</sup>	7.29, t (7.5) <sup>c</sup>
8'	128.6 <sup>e</sup>	7.14, d (7.5) <sup>b</sup>
1''	47.0	2.85, dt (11.2, 6.7) 2.75, m
2''	36.2	2.65 t (6.7)
3''	139.5 <sup>d</sup>	
4''	128.7 <sup>e</sup>	7.18 d (7.5) <sup>b</sup>
5''	128.5 <sup>f</sup>	7.30 t (7.5) <sup>c</sup>
6''	126.4 <sup>g</sup>	7.22 t (7.5)
7''	128.5 <sup>f</sup>	7.30 t (7.5) <sup>c</sup>
8''	128.7 <sup>e</sup>	7.18 d (7.5) <sup>b</sup>
<u>CONH</u>	172.0	-
NH	-	8.06 br s

<sup>a</sup> Measured in  $\text{CDCl}_3$ .<sup>b-g</sup> Signals are interchangeable within the same column.

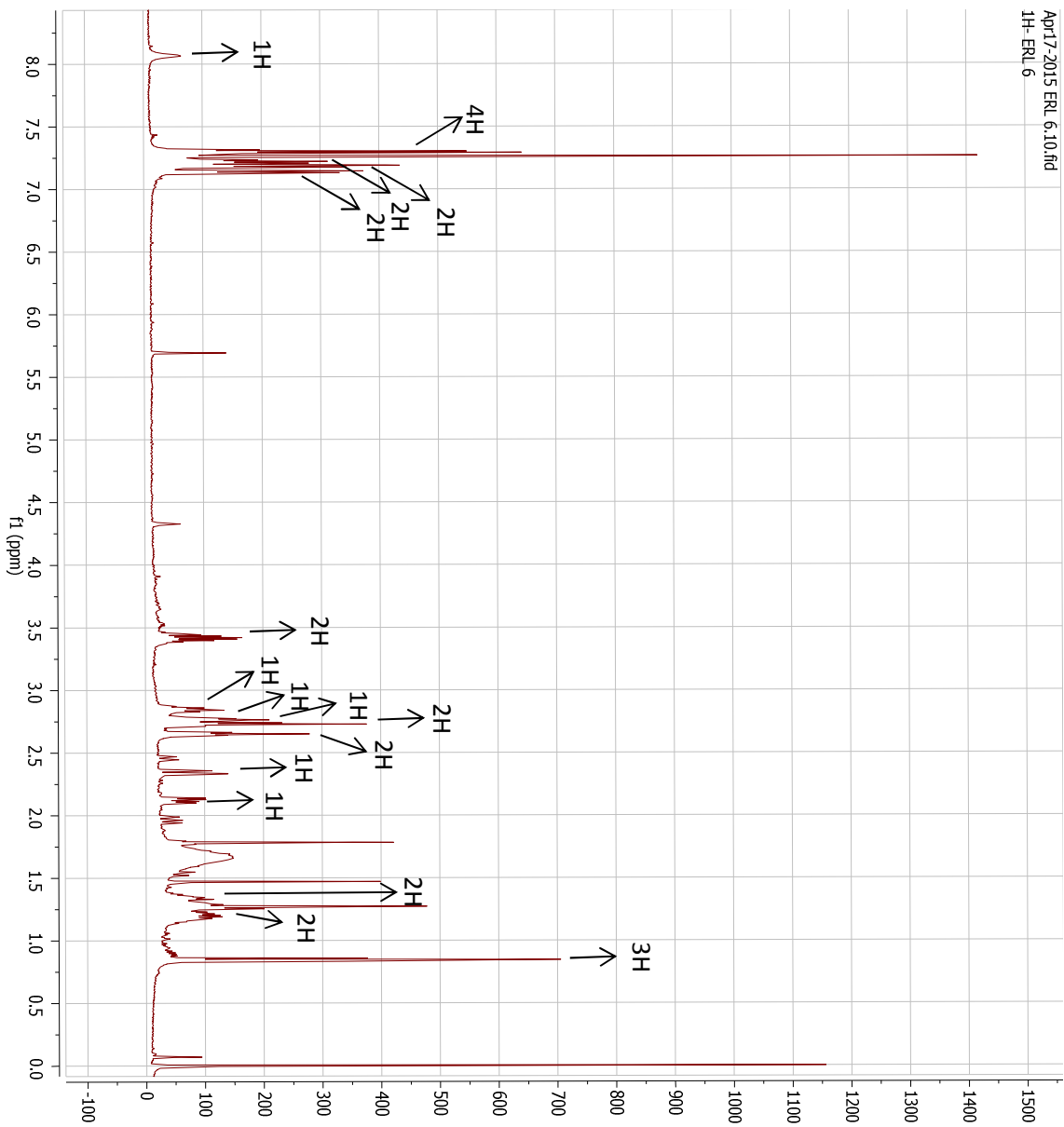
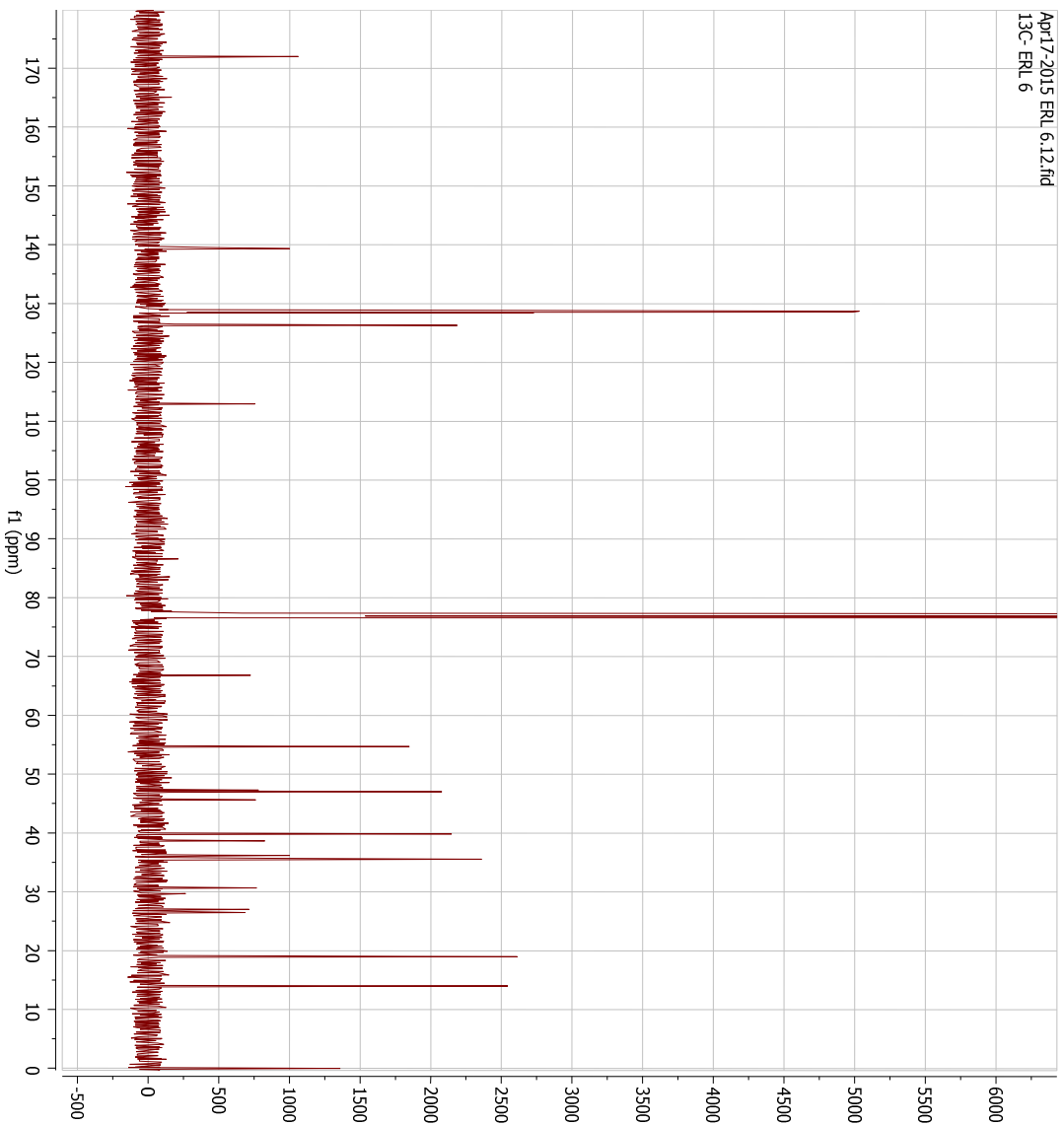
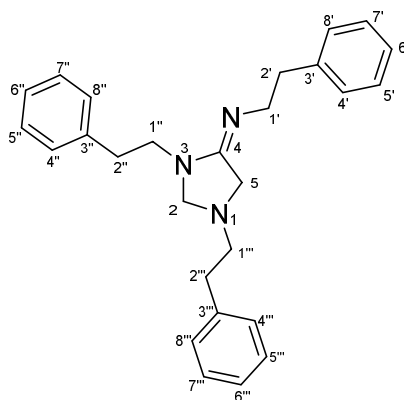


Figure 3.10:  $^1\text{H}$  NMR (600 MHz,  $\text{CDCl}_3$ ) spectrum of tectoraline (2).



**Figure 3.11:**  $^{13}\text{C}$  NMR (150 MHz,  $\text{CDCl}_3$ ) spectrum of tectoraline (**2**).

### 3.1.3 Tectoramidine A (**3**)



**Figure 3.12:** Structure of tectoramidine A (**3**).

Tectoramidine A (**3**) (Figure 3.12) was obtained as a colorless oil. The IR spectrum (Appendix 16) showed the presence of bands due to unsubstituted phenyl rings ( $701$  and  $752\text{ cm}^{-1}$ ) and an amidine  $\text{C}=\text{N}$  ( $1687\text{ cm}^{-1}$ ). The HRESIMS data ( $[\text{M}+\text{H}]^+$   $m/z$  398.2593) of **3** established the molecular formula as  $\text{C}_{27}\text{H}_{31}\text{N}_3$  (Appendix 17), requiring 14 degrees of unsaturation. The  $^{13}\text{C}$  NMR data of **3** (Table 3.3 and Figure 3.15) indicated the presence of 21 discrete carbon signals, six of which are due to six pairs of equivalent aromatic methine carbons. The total number of carbons in **3** was therefore determined as 27 (comprising eight methylenes, 15 aromatic methines, three quaternary aromatic carbons and one amidine carbon), which agrees with the molecular formula. The presence of six pairs of equivalent methine resonances at  $\delta_{\text{C}}$  128.5, 128.6, 128.89, 128.91, 129.1 and 129.4, three methine resonances at  $\delta_{\text{C}}$  126.7, 127.0 and 127.2, and three quaternary carbon resonances at  $\delta_{\text{C}}$  137.3, 138.2 and 138.4, revealed the presence of three unsubstituted phenyl groups. The  $^{13}\text{C}$  NMR spectrum also showed the presence of the amidine  $\text{N}=\text{C}-\text{N}$  resonance at  $\delta_{\text{C}}$  163.0.

The COSY and HSQC data of **3** revealed the presence of three  $\text{CH}_2\text{CH}_2\text{N}$  fragments corresponding to the three phenethylamine moieties in **3**, i.e.,  $\text{Ph}-\text{C}-2'-\text{C}-1'-\text{N}$ ,  $\text{Ph}-\text{C}-2''-\text{C}-1''-\text{N}$ , and  $\text{Ph}-\text{C}-2'''-\text{C}-1'''-\text{N}$  (Figure 3.13). This was confirmed by the HMBC data (Figure 3.13), which showed three-bond correlations from  $\text{H}-1'$  to  $\text{C}-3'$ ;  $\text{H}-1''$  to  $\text{C}-3''$ ;  $\text{H}-1'''$  to  $\text{C}-3'''$ ;  $\text{H}-4'/8'$  to

C-2'; H-4''/8'' to C-2''; and H-4'''/8''' to C-2'''. By subtracting the three phenethylamine moieties ( $C_{24}H_{27}N_3$ , corresponding to 12 degrees of unsaturation) and the amidine carbon from the molecular formula of **3**, only two methylene groups ( $\delta_C$  55.6,  $\delta_H$  3.02;  $\delta_C$  74.8,  $\delta_H$  3.86) and one degree of unsaturation remained to be considered. Therefore, it could be deduced that to complete the construction of the entire structure of **3**, formation of another ring involving the two methylene groups (C-2 and C-5), the amidine function (C-4) and the three phenethylamine moieties was required. The Ph-C-2''-C-1''-N fragment was deduced to be connected to C-2 ( $\delta_C$  74.8,  $\delta_H$  3.86) and C-4 ( $\delta_C$  163.0) as a result of the correlations from H-1'' to C-2 and C-4; and from H-2 to C-4, while the attachment of the Ph-C-2'''-C-1'''-N fragment to C-2 and C-5 ( $\delta_C$  55.6,  $\delta_H$  3.02) was deduced from the correlations from H-1''' to C-2 and C-5; H-2 to C-1'''; and H-5 to C-1''' and C-2. Finally, the linkage between C-4 and C-5, which completed the assembly of the imidazolidinyl ring, was shown by the observed HMBC correlation from H-5 to C-4. Other HMBC correlations (Figure 3.13) are entirely consistent with the structure of tectoramidine A (**3**). Additionally, the structure of **3** is consistent with the observation that the signal of H-1'' was notably deshielded compared to that of H-1' ( $\delta_H$  4.16 *versus*  $\delta_H$  3.29, respectively) in the  $^1H$  NMR spectrum (Table 3.3 and Figure 3.14). This observation can be rationalized by the fact that C-1'' is attached to the electron-deficient N-3 of the amidine function, while C-1' is attached to the electron-rich N-1. Tectoramidine A (**3**) represents the first naturally occurring trimeric phenethylamine alkaloid incorporating a rare trisubstituted amidine function with an exocyclic C=N as a partial structure.

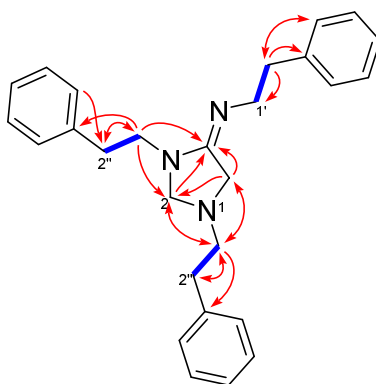


**Figure 3.13:** COSY (bold bonds) and HMBC  $^{13}C$ - $^1H$  correlation (arrows) of tectoramidine A (**3**).

**Table 3.3:**  $^{13}\text{C}$  (150 MHz) and  $^1\text{H}$  NMR (600 MHz) data of tectoramidine A (**3**) ( $\delta$  in ppm).<sup>a</sup>

Position	$\delta_{\text{C}}$	$\delta_{\text{H}}$ ( <i>J</i> in Hz)
2	74.8	3.86, br s
3	-	-
4	163.0	-
5	55.6	3.02, br s
1'	48.2	3.49, m
2'	35.8	3.06, t (6.3)
3'	138.2	-
4'	129.1	7.19, m
5'	129.4	7.30, m
6'	127.0 <sup>b</sup>	7.24, m <sup>d</sup>
7'	129.4	7.30, m
8'	129.1	7.19, m
1''	46.8	4.16, t (6.0)
2''	33.2	3.04, t (6.0)
3''	137.3	-
4''	128.89 <sup>c</sup>	7.29, m
5''	128.91 <sup>c</sup>	7.23, m
6''	126.7 <sup>b</sup>	7.24, m <sup>d</sup>
7''	128.91 <sup>c</sup>	7.23, m
8''	128.89 <sup>c</sup>	7.29, m
1'''	56.1	2.34, t (7.3)
2'''	34.8	2.45, t (7.3)
3'''	138.4	-
4'''	128.5 <sup>c</sup>	7.03, m
5'''	128.6 <sup>c</sup>	7.30, m
6'''	127.2 <sup>b</sup>	7.22, m <sup>d</sup>
7'''	128.6 <sup>c</sup>	7.30, m
8'''	128.5 <sup>c</sup>	7.03, m

<sup>a</sup> Measured in  $\text{CDCl}_3$ .<sup>b-d</sup> Signals are interchangeable within the same column.



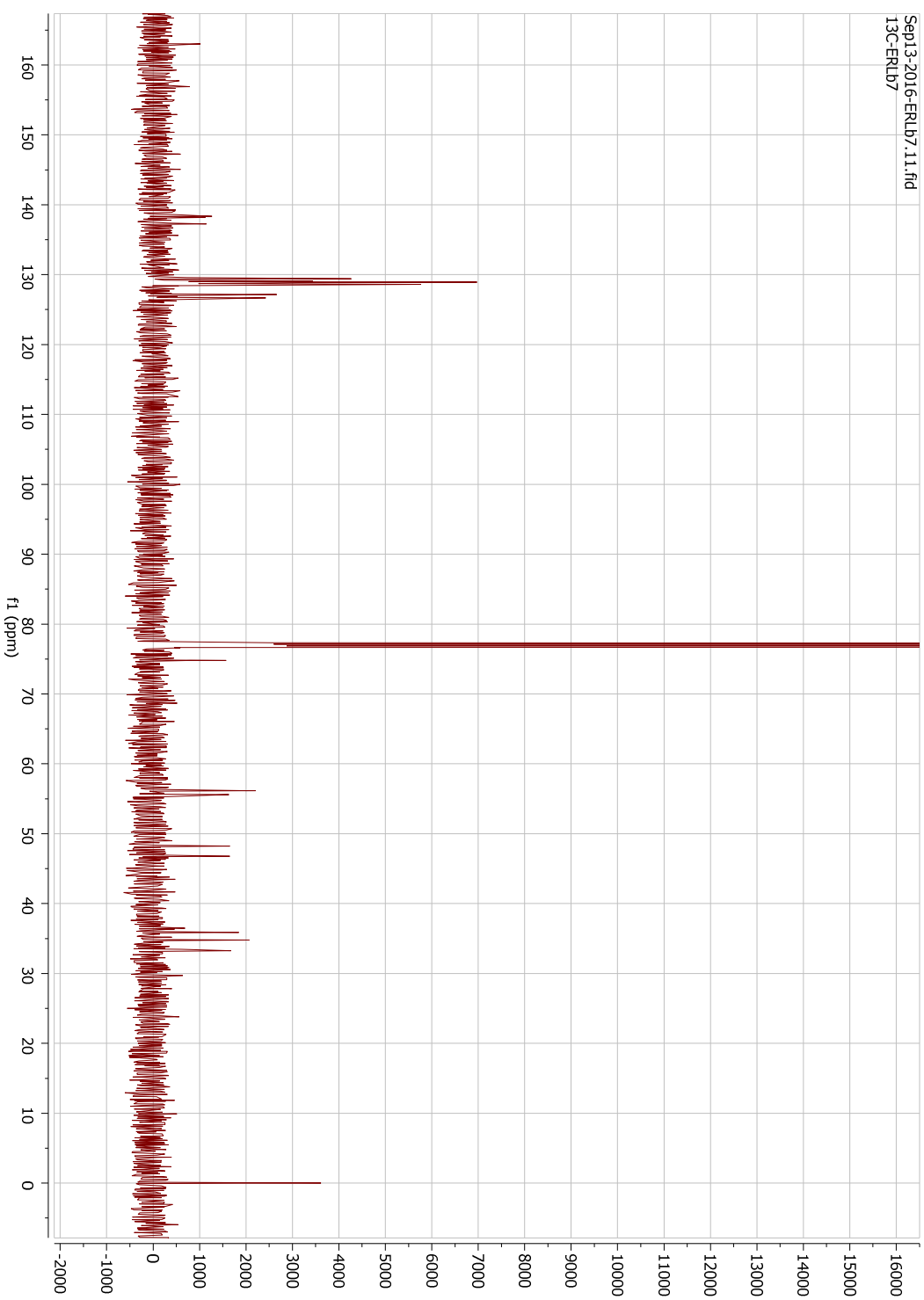


**Figure 3.15:**  $^{13}\text{C}$  NMR (150 MHz,  $\text{CDCl}_3$ ) spectrum of tectoramidine A (**3**).

### 3.1.4 Tectoramidine B (4)

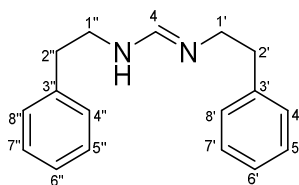


**Figure 3.16:** Structure of tectoramidine B (**4**).

Tectoramidine B (**4**) (Figure 3.16) was obtained as a colorless oil. As in the case for **3**, the IR spectrum (Appendix 21) of **4** showed the presence of unsubstituted phenyl rings (698 and 748  $\text{cm}^{-1}$ ) and an amidine C=N (1644  $\text{cm}^{-1}$ ). The HRESIMS data ( $[\text{M}+\text{H}]^+$   $m/z$  253.1700) of **4** established the molecular formula as  $\text{C}_{17}\text{H}_{20}\text{N}_2$  (Appendix 22), requiring nine degrees of unsaturation.

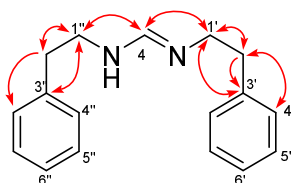


**Figure 3.17:** HMBC  $^{13}\text{C}$ - $^1\text{H}$  correlation (arrows) of tectoramidine B (**4**).

The  $^1\text{H}$  NMR of **4** (Table 3.4 and Figure 3.18) revealed the presence of two pairs of mutually coupled triplets at  $\delta_{\text{H}}$  2.848/2.852 and 3.56/3.57 (each pair integrated for 4H), suggesting the presence of two closely comparable phenethylamine moieties in **4**. This was further supported by the presence of three clusters of aromatic resonances at  $\delta_{\text{H}}$  7.20 (4H), 7.24 (2H) and 7.31 (4H) in the  $^1\text{H}$  NMR. The  $^1\text{H}$  NMR also showed a 1H singlet at  $\delta_{\text{H}}$  8.13, attributed to an amidine N=CH–N moiety. In addition to the resonances due to the two phenethyl units, the  $^{13}\text{C}$  NMR (Table 3.4 and Figure 3.19) showed a resonance at  $\delta_{\text{C}}$  161.1, which correlated to  $\delta_{\text{H}}$  8.13 in the HSQC spectrum of **4**. Therefore, the resonance at  $\delta_{\text{C}}$  161.1 was deduced to be attributed to the amidine N=CH–N moiety. This deduction was further confirmed by the observed three-bond

correlations from H-1'/1'' to  $\delta_C$  161.1 and from  $\delta_H$  8.13 to C-1'/1'' in the HMBC spectrum of **4** (Figure 3.17). These HMBC correlations also established that the amidine N=CH–N is bridging the two phenethyl units. To the best of our knowledge, tectoramidine B (**4**) represents the first dimeric phenethylamine alkaloid incorporating a formamidine core from plants.

**Table 3.4:**  $^{13}\text{C}$  (150 MHz) and  $^1\text{H}$  NMR (600 MHz) data of tectoramidine B (**4**) ( $\delta$  in ppm).

Position	$\delta_C$	$\delta_H$ (J in Hz)
4	161.1	8.13, s
1'	39.2 <sup>b</sup>	3.56, t (7.0) <sup>e</sup>
2'	35.4 <sup>c</sup>	2.848, t (7.0) <sup>f</sup>
3'	138.1	-
4'	128.6 <sup>d</sup>	7.20, m
5'	128.7 <sup>d</sup>	7.31, m
6'	126.7	7.24, m
7'	128.7 <sup>d</sup>	7.31, m
8'	128.6 <sup>d</sup>	7.20, m
1''	40.8 <sup>b</sup>	3.57, t (7.0) <sup>e</sup>
2''	35.5 <sup>c</sup>	2.852, t (7.0) <sup>f</sup>
3''	138.1	-
4''	128.6 <sup>d</sup>	7.20, m
5''	128.7 <sup>d</sup>	7.31, m
6''	126.7	7.24, m
7''	128.7	7.31, m
8''	128.6	7.20, m
NH		7.50, br s

<sup>a</sup> Measured in  $\text{CDCl}_3$ .

<sup>b-f</sup> Signals are interchangeable within the same column.

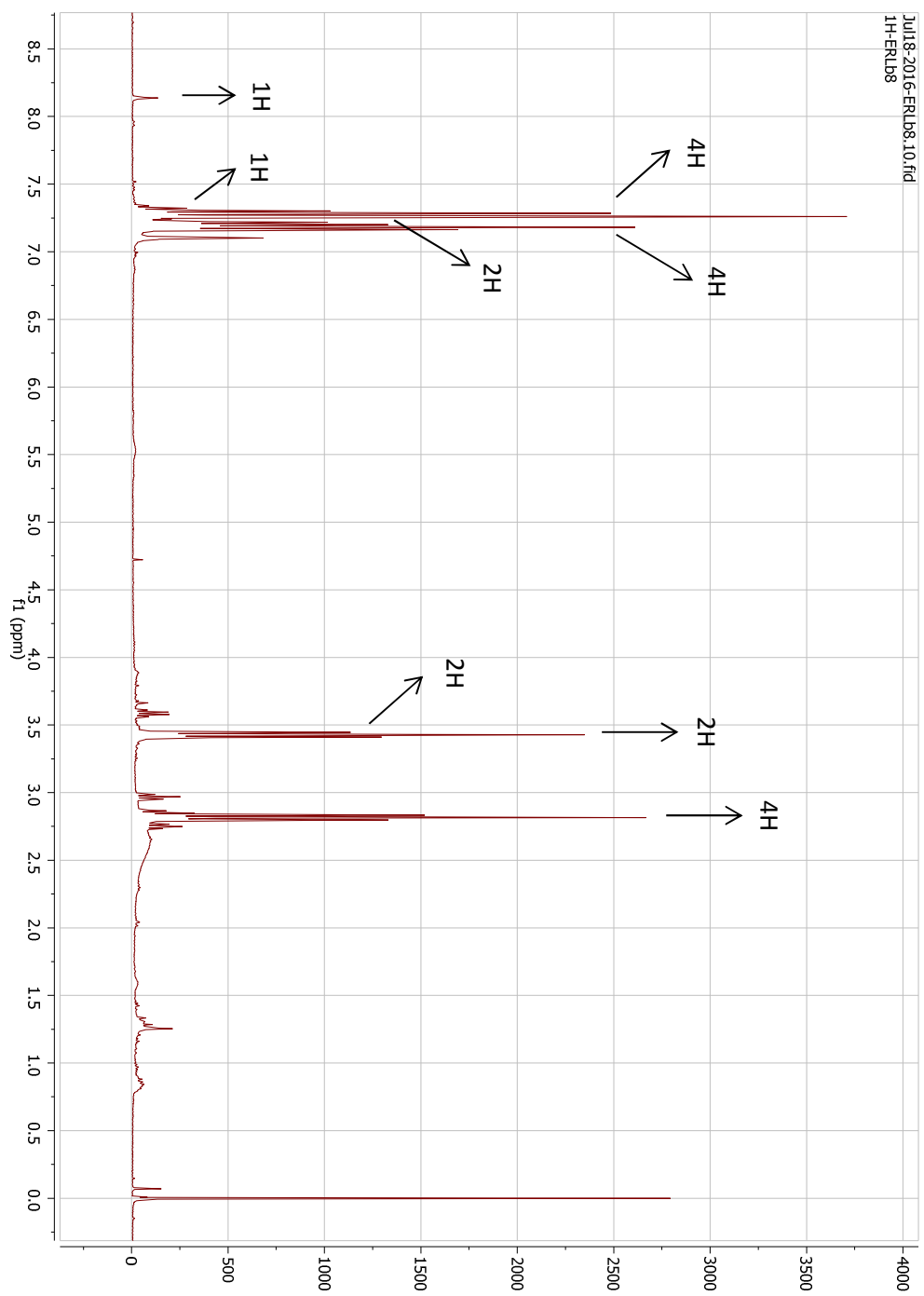


**Figure 3.18:** <sup>1</sup>H NMR (600 MHz, CDCl<sub>3</sub>) spectrum of tectoramidine B (4).

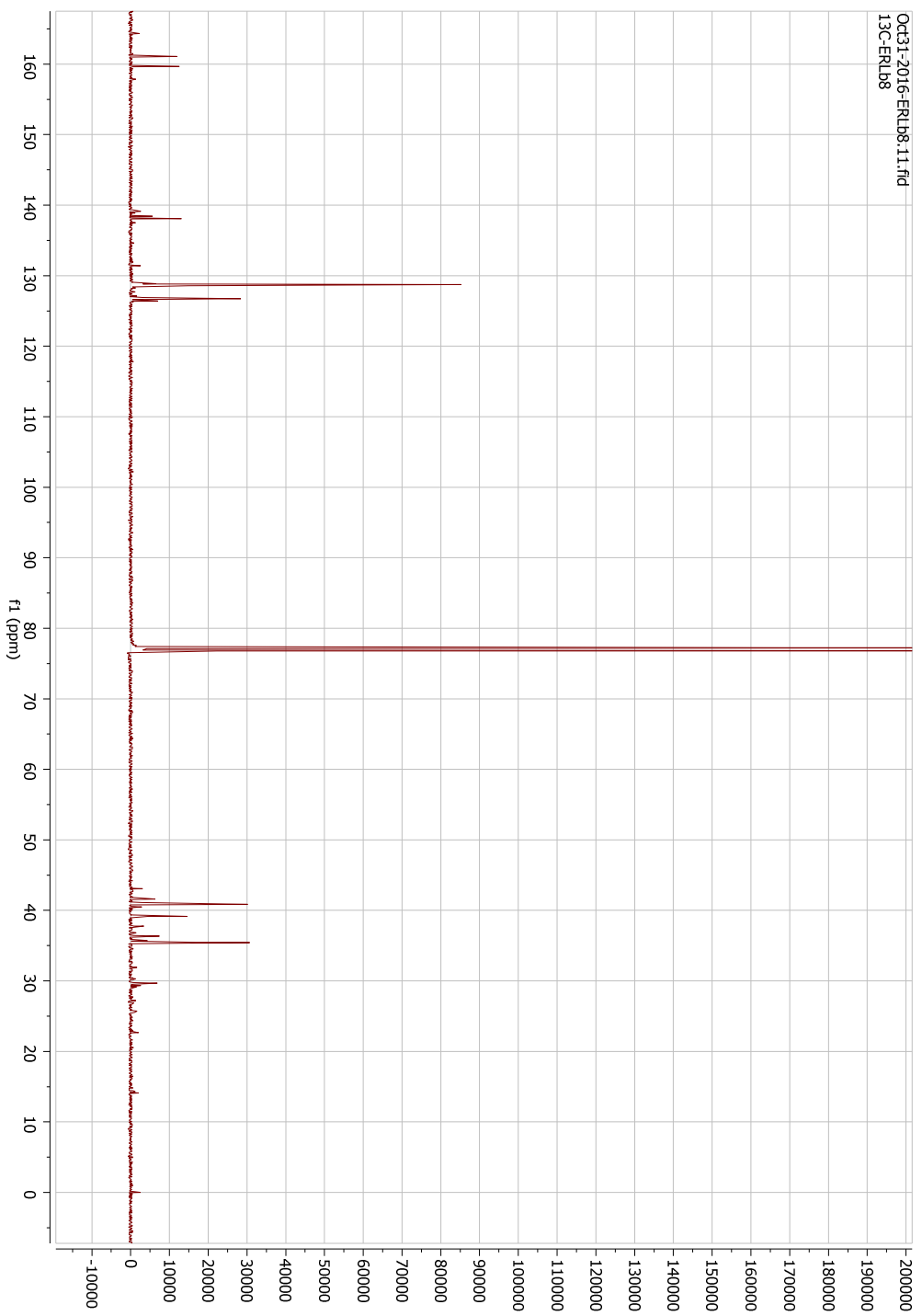
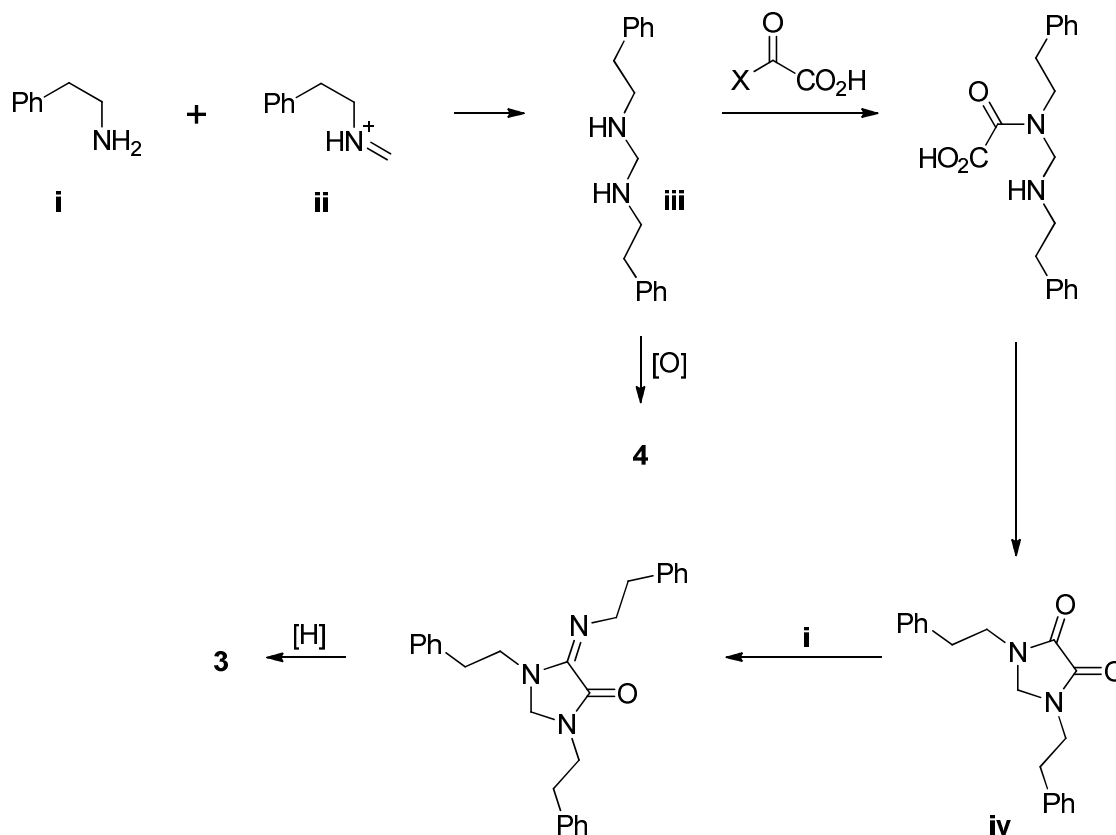


**Figure 3.19:**  $^{13}\text{C}$  NMR (150 MHz,  $\text{CDCl}_3$ ) spectrum of tectoramidine B (**4**).

### 3.1.5 Biosynthetic pathway to tectoramidines A and B (3 and 4)

It is envisaged that both tectoramidines A and B (**3** and **4**), which appear to be structurally related, share a common biosynthetic origin. A plausible pathway to the tectoramidines starting from phenethylamine (**i**) and the iminium ion of N-methylphenethylamine (**ii**) is presented in Scheme 3.3. Nucleophilic addition of **i** onto the iminium ion **ii** gives the dimeric aminoacetal **iii**, which on subsequent dehydrogenation/oxidation furnishes tectoramidine B (**4**). Alternatively, intermolecular and intramolecular coupling reactions (nucleophilic substitution) involving **iii** and oxalic acid or an oxalate ester (including oxalyl-CoA) gives the symmetrical imidazolidinyl ring intermediate **iv**. Finally, reductive amination of **iv** with another molecule of phenethylamine (**i**) followed by ketone reduction furnishes tectoramidine A (**3**).



**Scheme 3.3:** Plausible biosynthetic pathway to tectoramidines A and B (**3** and **4**).

### 3.2 Alkaloids from *Elaeocarpus angustifolius*

A total of 12 alkaloids were obtained from the leaves of *Elaeocarpus angustifolius*. Seven of these are new indolizidine alkaloids, namely, carpusinine A (**5**), carpusinine B (**6**), carpusinine C (**7a**), epicarpusinine C (**7b**), carpusinine D (**8**), carpusinine E (**9**) and carpusidine (**14**), while two are new pyrrolidine alkaloids, namely, carpusidine F (**10a**) and epicarpusinine F (**10b**). The remaining three alkaloids are known compounds previously isolated from *E. kaniensis*, namely, (+)-elaeokanine A (**11**), elaeokanine C (**12**) and elaeokanine D (**13**).

#### 3.2.1 Carpusinine A (**5**)

Carpusinine A (**5**) (Figure 3.20) was obtained as a colourless oil with  $[\alpha]_D^{25} +2$  (*c* 0.24, CHCl<sub>3</sub>). The very small optical rotation measured suggested that carpusinine A (**5**) was isolated as a racemate. The IR spectrum of **5** (Appendix 25) showed the characteristic of Bohlmann bands (2879, 2822 and 2733 cm<sup>-1</sup>), which suggested the presence of a *trans*-fused ring junction in an indolizidine ring system.<sup>48,70</sup> Additionally, the IR spectrum showed absorption bands due to OH and  $\alpha,\beta$ -unsaturated ketone (H-bonded) at 3366 and 1656 cm<sup>-1</sup>, respectively. The UV spectrum of **5** showed an absorption maximum at 228 nm, which is characteristic of an  $\alpha,\beta$ -unsaturated ketone moiety. The molecular formula of **5** was determined by HRESIMS ( $m/z$  210.1495 [M+H]<sup>+</sup>) to be C<sub>12</sub>H<sub>19</sub>NO<sub>2</sub> (Appendix 27), corresponding to four degrees of unsaturation.

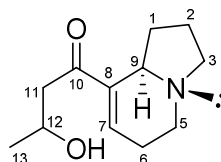


**Figure 3.20:** Structure of carpusinine A (**5**).

<sup>1</sup>H NMR for carpusinine A (**5**) (Table 3.5 and Figure 3.24) revealed the presence of a distinct doublet at  $\delta_H$  1.22, attributed to CH<sub>3</sub>-13. The doublet signal of CH<sub>3</sub>-13 implied that C-12 is a

methine group. The most deshielded upfield signal observed at  $\delta_{\text{H}}$  4.25 (H-12) is characteristic of an oxymethine group, while the only downfield signal observed at  $\delta_{\text{H}}$  6.92 (H-7) is characteristic of a trisubstituted olefinic hydrogen. The very large germinal coupling constants observed for the methylene hydrogens at C-11 ( $J = 17$  Hz) and C-6 ( $J = 19$  Hz) are consistent with the fact that both methylene groups are adjacent to a ketone group and the double bond of an  $\alpha,\beta$ -unsaturated ketone moiety, respectively. The  $^{13}\text{C}$  NMR (Table 3.5 and Figure 3.25) revealed the presence of 12 carbon resonances, in agreement with the molecular formula established by HRESIMS. With the aid of the HSQC data, the  $^{13}\text{C}$  NMR data revealed the presence of one methyl group, six methylene groups, three methine groups (i.e., olefinic methine,  $\delta_{\text{C}}$  138.7; oxymethine,  $\delta_{\text{C}}$  64.1; aminomethine,  $\delta_{\text{C}}$  58.4), one ketone group ( $\delta_{\text{C}}$  200.8) and one olefinic quaternary carbon ( $\delta_{\text{C}}$  142.0). Comparison of the  $^1\text{H}$  and  $^{13}\text{C}$  NMR spectra of **5** with those of elaeokanine A (**11**),<sup>85</sup> revealed that **5** has an additional hydroxymethine group (CHOH) in place of a methylene group in **11**.



**Figure 3.21:** COSY (bold bonds) and HMBC  $^1\text{H}$ - $^{13}\text{C}$  correlations (arrows) of carpusinine A (**5**).

Detailed analysis of the COSY and HSQC data revealed the presence of  $\text{CHCH}_2\text{CH}_2\text{CH}_2$ ,  $\text{CH}_2\text{CH}_2\text{CH}=\text{CH}$  and  $\text{CH}_2\text{CH}(\text{OH})\text{CH}_3$  fragments (Figure 3.21), which corresponded to the C-9–C-1–C-2–C-3, C-5–C-6–C-7 and C-11–C-12–C-13 partial structures in **5**. The presence of the indolizidine ring system with a trisubstituted double bond at C-7 and C-8 was firmly established based on the HMBC correlations from H-1 to C-8 and C-9; from H-3 to C-5 and C-9; from H-2 to C-9; from H-5 to C-3 and C-9; from H-7 to C-9; and from H-9 to C-1, C-2, C-3, C-5, C-7 and C-8 (Figure 3.21). The indolizidine moiety was shown to be connected to the C-11–C-12–C-13 partial structure at C-8 via the C-10 ketone group by the HMBC correlation from H-7, H-9, H-11

and H-12 to C-10. The gross structure established for **5** is entirely consistent with the full HMBC data (Figure 3.21).

The Bohlmann bands observed in the IR spectrum indicated a *trans*-fused ring junction in the indolizidine ring system of **5** (i.e., H-9 is  $\alpha$ -axial-oriented, while N lone pair is  $\beta$ -axial-oriented, Figure 3.22).<sup>48</sup> This conclusion is consistent with the NOEs observed for H-9/H-3 $\alpha$  and H-9/H-5 $\alpha$ , suggesting the presence of 1,3-diaxial interactions amongst the three hydrogens, which will not be possible in a *cis*-fused ring junction (at most, only either one of the two NOEs would be observed) (Figure 3.22). The relative configuration at C-12 was not assignable based on the NOESY data due to the inherent flexibility of the side chain. Carpusinine A (**5**) is therefore a 12-hydroxy derivative of elaeokanine A (**11**).

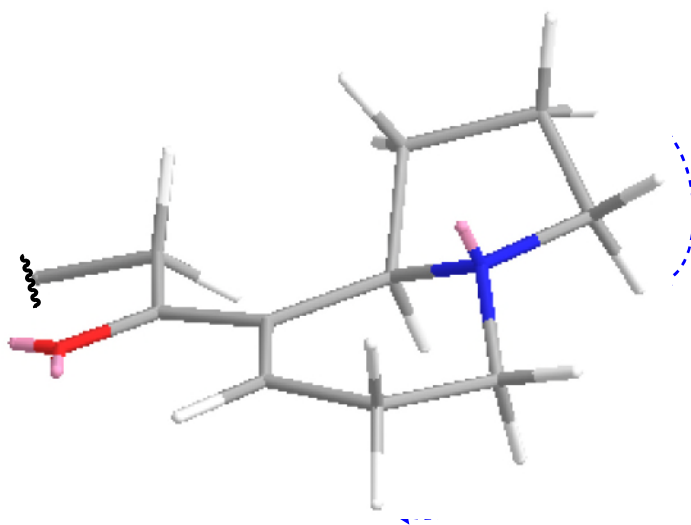


**Figure 3.22:** Selected NOESY correlations of carpusinine A (**5**).

Carpusinine A (**5**) represents the first *Elaeocarpus* alkyindolizidine alkaloid with a hydroxyl group attached to its side chain at C-12. Compound **5** shares a marked similarity with alkaloids obtained from *Elaeocarpus kaniensis* such as (+)-elaekanine A and B (**11** and **48**) (Figure 3.23).

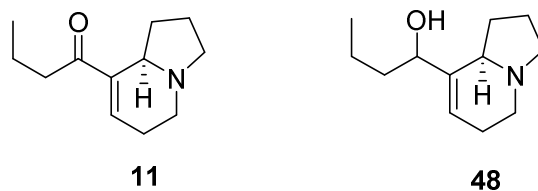
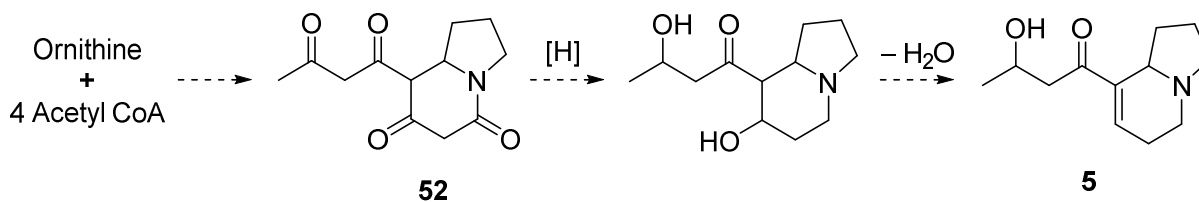


**Figure 3.23:** Structures of **11** and **48**.

Since it was previously proposed that *Elaeocarpus* alkaloids are originated from condensation of a polyketomethylene chain derived from acetyl CoA with ornithine,<sup>71</sup> it was reasonable to postulate that carpusinine A (**5**) is derived from the same biosynthetic root, i.e., from the common polyketoindolizidine precursor (**52**) (refer to section 1.3.1), following a series of reductive and dehydration transformations (Scheme 3.4).



**Scheme 3.4:** Plausible biosynthetic pathway to carpusinine A (**5**)

**Table 3.5:**  $^{13}\text{C}$  (150 MHz) and  $^1\text{H}$  NMR (600 MHz) data of carpusinine A (**5**) and (+)-elaekanine A (**11**) ( $\delta$  in ppm).<sup>a</sup>

Position	Carpusinine A ( <b>5</b> )		(+)-Elaekanine A ( <b>11</b> ) <sup>85</sup>	
	$\delta_{\text{C}}$	$\delta_{\text{H}}$ (J in Hz)	$\delta_{\text{C}}$	$\delta_{\text{H}}$ (J in Hz)
1 $\alpha$	29.5	2.33, dddd (13, 9.7, 7.4, 4)	29.5	2.30 – 2.50, m
1 $\beta$		1.38, dtd (13, 10.2, 7.6)		1.40, m
2 $\beta$	22.4 <sup>b</sup>	1.87, m	21.8	1.70 – 1.90, m
2 $\alpha$		1.79, m		1.70 – 1.90, m
3 $\beta$	52.7	2.91, ddd (10.2, 8.0, 4.3)	53.1	2.80 – 3.00, m
3 $\alpha$		2.77, dt (10.2, 8.0)		2.60, td (9, 3)
5 $\beta$ (eq)	45.1 <sup>c</sup>	2.84, dt (11.5, 5.5)	44.9	2.80 – 3.00, m
5 $\alpha$ (ax)		2.60, ddd (11.5, 6.2, 5.5)		2.60, td (9, 3)
6 $\beta$ (ax)	25.5	2.48, br d (19)	24.1	2.30 – 2.50, m
6 $\alpha$ (eq)		2.38, br d (19)		2.30 – 2.50, m
7	138.7	6.92, td (4.0, 1.2)	136.0	6.87, s
8	142.0	-	139.0	-
9 (ax)	58.4	3.50, m	58.7	3.52, br s
10	200.8	-	199.4	-
11	44.9 <sup>c</sup>	2.89, dd (17, 2.9)	39.1	2.80 - 3.00, m
		2.65, dd (17, 9)		2.30 – 2.50, m
12	64.1	4.25, dqd (9, 6.3, 2.9)	17.8	1.61, q (7)
13	22.5 <sup>b</sup>	1.22, d (6.3)	13.7	0.93, t (7)

<sup>a</sup> Measured in  $\text{CDCl}_3$ .

<sup>b-c</sup> Signals are interchangeable within the same column.

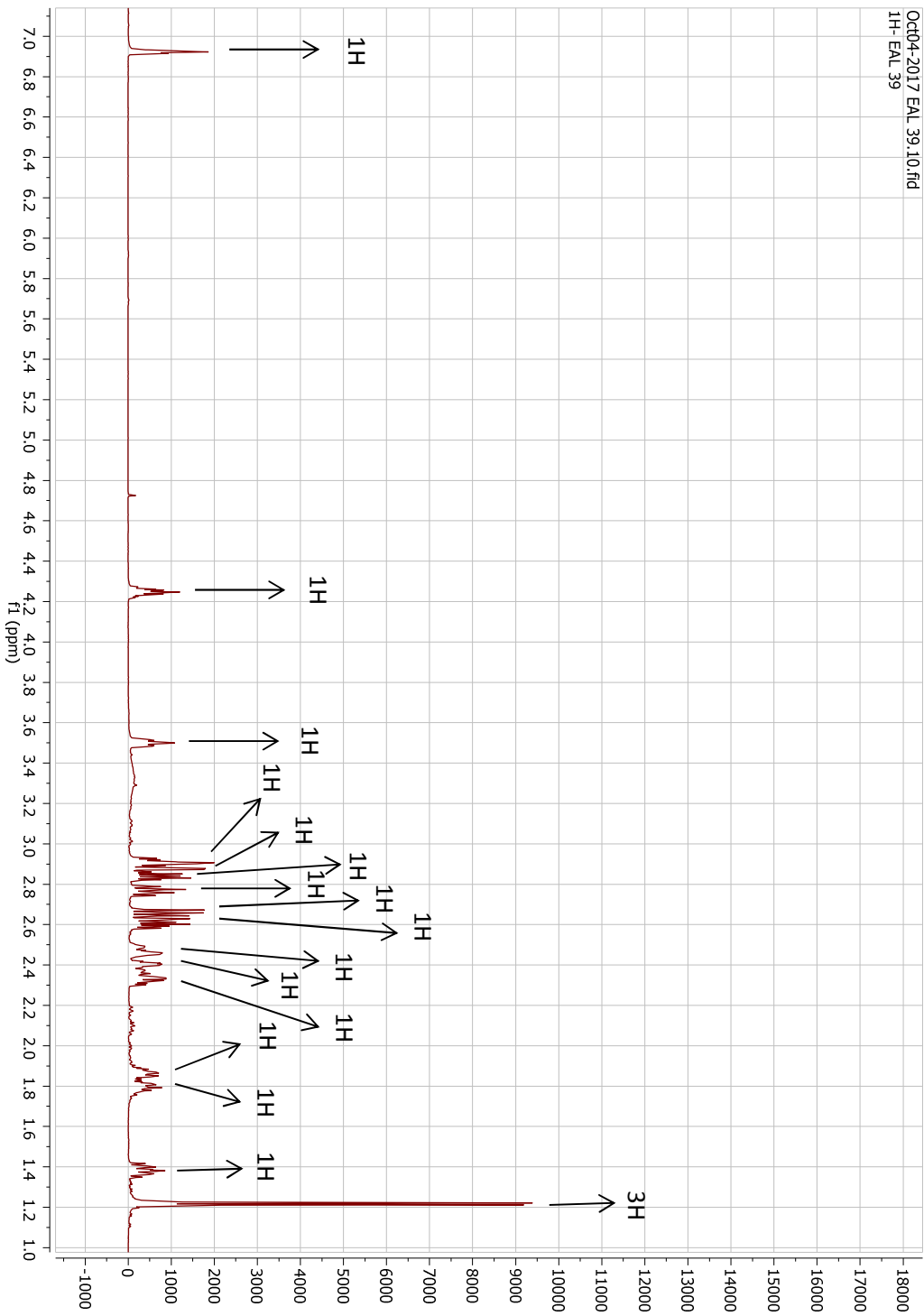
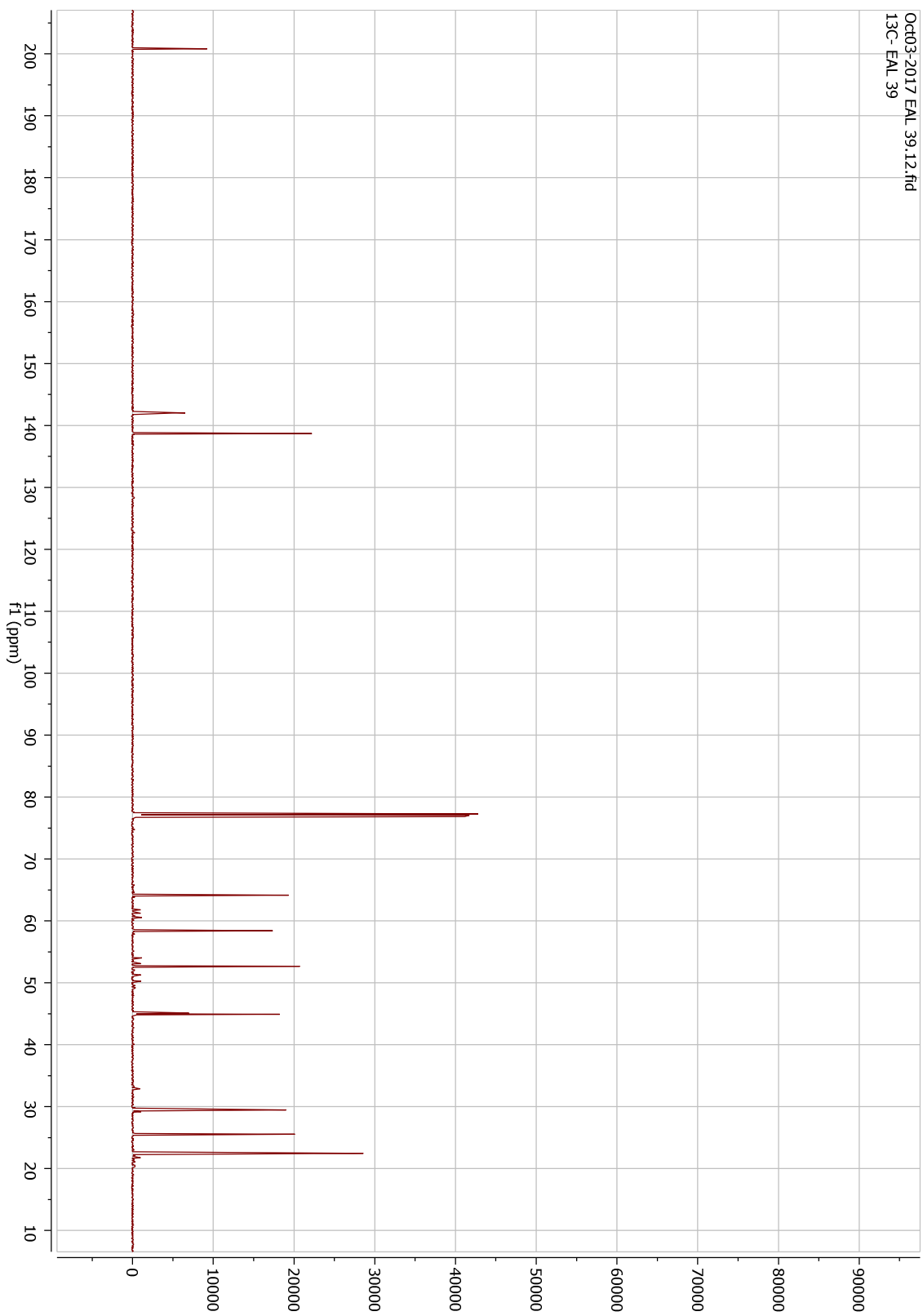


Figure 3.24: <sup>1</sup>H NMR (600 MHz, CDCl<sub>3</sub>) spectrum of carpusinine A (5).



**Figure 3.25:**  $^{13}\text{C}$  NMR (150 MHz,  $\text{CDCl}_3$ ) spectrum of carpusinine A (5)

### 3.2.2 Carpusinine B (6)

Carpusinine B (**6**) (Figure 3.26) was obtained as a light yellowish oil with  $[\alpha]_D^{25} -47$  (c 0.46,  $\text{CHCl}_3$ ). The molecular formula of **6** was determined by HRESIMS data ( $m/z$  196.1700  $[\text{M}+\text{H}]^+$ ) to be  $\text{C}_{12}\text{H}_{22}\text{NO}$  (Appendix 33), corresponding to three degrees of unsaturation. In addition to an absorption band due to a ketone function at  $1708\text{ cm}^{-1}$ , the IR spectrum (Appendix 32) showed absorption bands characteristic of Bohlmann bands ( $2877$ ,  $2787$  and  $2725\text{ cm}^{-1}$ )<sup>70</sup>, which suggested the presence of a *trans*-fused ring junction in **6**.<sup>48</sup>

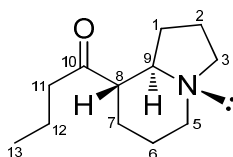


**Figure 3.26:** Structure of carpusinine B (**6**).

The  $^1\text{H}$  NMR data (Table 3.6 and Figure 3.29) revealed one distinct methyl triplet at  $\delta_{\text{H}}$  0.91, attributed to  $\text{CH}_3$ -13. The triplet signal for  $\text{CH}_3$ -13 indicated that C-12 is an unsubstituted methylene group. The  $^{13}\text{C}$  NMR data (Table 3.6 and Figure 3.30) revealed the presence of 12 carbon resonances, in agreement with the molecular formula established by HRESIMS. With the aid of the HSQC data, the  $^{13}\text{C}$  data revealed the presence of one methyl group, eight methylene groups, two methine groups and one ketone group. The most downfield carbon resonance observed at  $\delta_{\text{C}}$  212.8 is attributed to the C-10 ketone group. The  $^1\text{H}$  and  $^{13}\text{C}$  NMR data of **6** are largely similar to those of elaeokanine C (**12**),<sup>86</sup> except that the resonances due to the hydroxymethine group in **12** were replaced by resonances due to a methylene group in **6**. This suggested that **6** is a dehydroxylated derivative of elaeokanine C (**12**).



**Figure 3.27:** COSY (bold bonds) and HMBC  $^1\text{H}$ - $^{13}\text{C}$  correlations (arrows) of carpusinine B (**6**).

Detailed analysis of the COSY and HSQC data revealed the presence of a  $\text{CH}_2\text{CH}_2\text{CH}_2\text{CHCHCH}_2\text{CH}_2\text{CH}_2$  fragment corresponding to the C-3–C-2–C-1–C-9–C-8–C-7–C-6–C-5 partial structure and a propyl fragment corresponding to the C-11–C-12–C-13 partial structure in **6** (Figure 3.27). These two partial structures are present in the structure of elaeokanine C (**12**), except that the oxymethine group at C-7 in elaeokanine C (**12**) has been replaced with a methylene group in **6**. The presence of a tertiary N atom attached to C-3, C-5 and C-9 was revealed by the three-bond HMBC correlations from H-3 to C-5 and C-9; from H-5 to C-3 and C-9; and from H-9 to C-5 (Figure 3.27), thus establishing the indolizidine moiety in **6**. The attachment of the C-11–C-12–C-13 partial structure to C-8 via the ketone C-10 was revealed by the HMBC correlations from H-8, H-11 and H-12 to C-10. The gross structure established for carpusinine A (**6**) is entirely consistent with the full HMBC data (Figure 3.27).

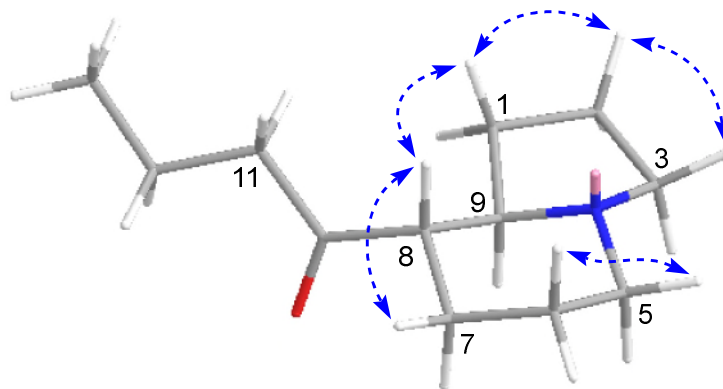
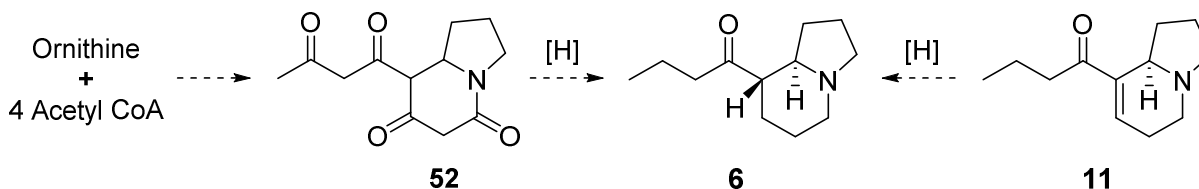


**Figure 3.28:** Selected NOESY correlations of carpusinine B (**6**).

The relative configuration of **6** was deduced from vicinal coupling constants and NOESY data (Figure 3.28). As in the case of carpusinine A (**5**), H-9 in **6** showed a large coupling constant (10 Hz) with H-8 indicating that both hydrogens are *trans*-diaxial. This deduction is further supported by the NOEs observed for H-7 $\alpha$ /H-9 and H-8/H-7 $\beta$  (alkyl side chain is equatorial) (Figure 3.28), which required H-9 to be  $\alpha$ -axial-oriented, H-8 to be  $\beta$ -axial-oriented and H-7 $\alpha$  axial-oriented. The presence of the Bohlmann bands also required that the indolizidine ring junction to be *trans*-fused, i.e., N lone pair is  $\beta$ -axial-oriented. The relative configuration of **6** at C-8 and C-9 was therefore established as 8*R*,9*S* (Figure 3.28), which correspond to a chair conformation for the piperidine ring.

Carpusinine B (**6**) represents the 7-dehydroxy-derivative of elaeokanine C (**12**). As with carpusinine A (**5**), compound **6** was postulated to be derived from the common polyketoidindolizidine precursor (**52**) (Scheme 3.5) following a series of reductive transformations. Alternatively, compound **6** could also arise from elaeokanine A (**11**) as a direct precursor via a hydrogenation step (Scheme 3.5).



**Scheme 3.5:** Plausible biosynthetic pathway to carpusinine B (**6**).

**Table 3.6:**  $^{13}\text{C}$  (150 MHz) and  $^1\text{H}$  NMR (600 MHz) data of carpusinine B (**6**) ( $\delta$  in ppm).<sup>a</sup>

Position	$\delta_{\text{C}}$	$\delta_{\text{H}}$ ( <i>J</i> in Hz)
1 $\alpha$	29.0	1.97, m
1 $\beta$		1.34, m
2 $\beta$	20.6	1.76, m
2 $\alpha$		1.66, m
3 $\beta$	53.8	3.05, td (9, 2)
3 $\alpha$		2.11, q (9)
5 $\beta$ (eq)	52.3	3.09, br d (12)
5 $\alpha$ (ax)		2.01, td (12, 3)
6 $\alpha$ (eq)	25.1	1.76, m
6 $\beta$ (ax)		1.66, m
7 $\beta$ (eq)	28.1	1.97, m
7 $\alpha$ (ax)		1.34, m
8 (ax)	55.0	2.40, m
9 (ax)	64.8	1.97, td (10, 6.6)
10	212.8	-
11	44.6	2.42, dt (17, 7.2) 2.45, dt (17, 7.2)
12	17.0	1.59, sextet (7.3)
13	13.8	0.91, t (7.4)

<sup>a</sup> Measured in  $\text{CDCl}_3$ .

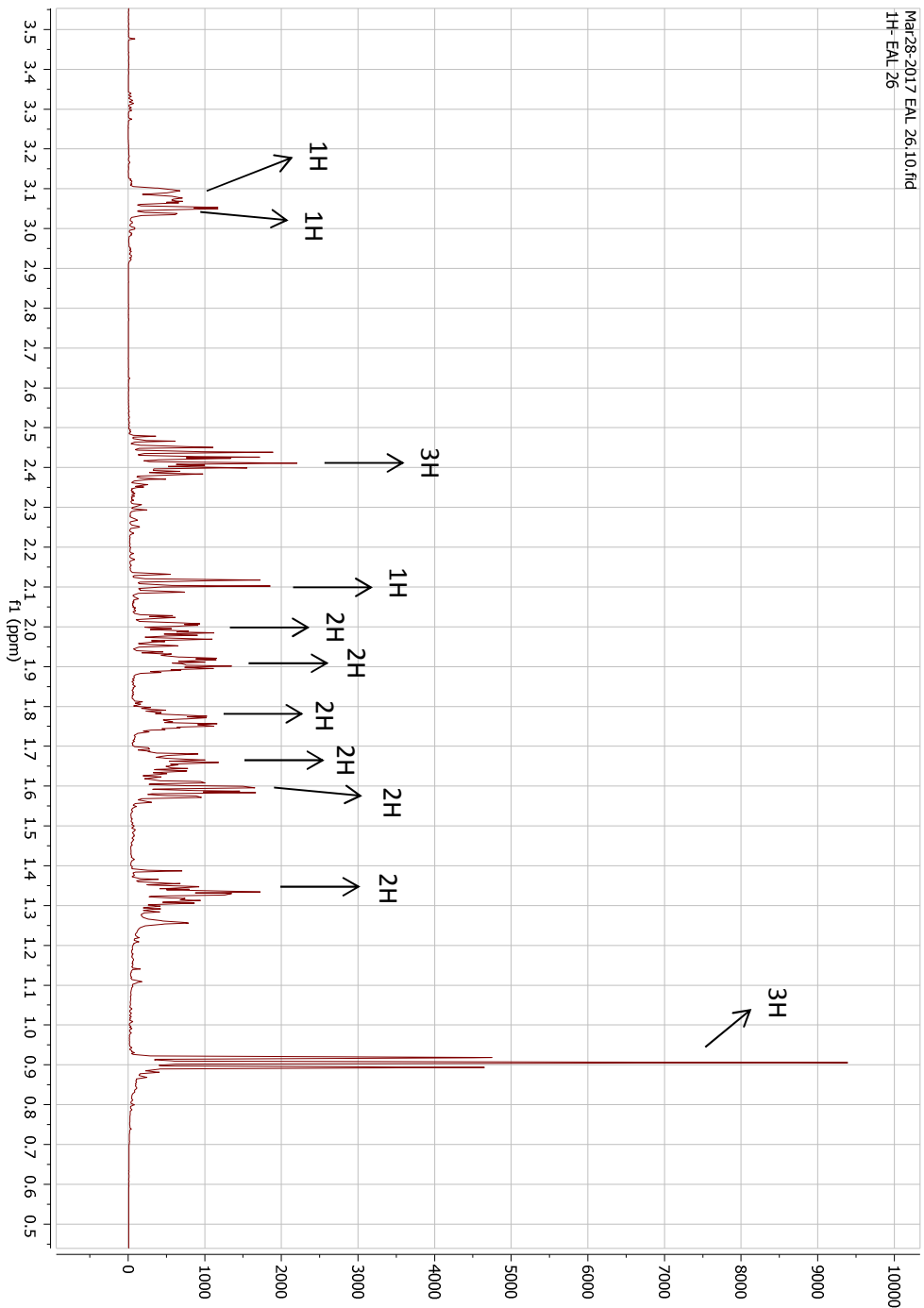
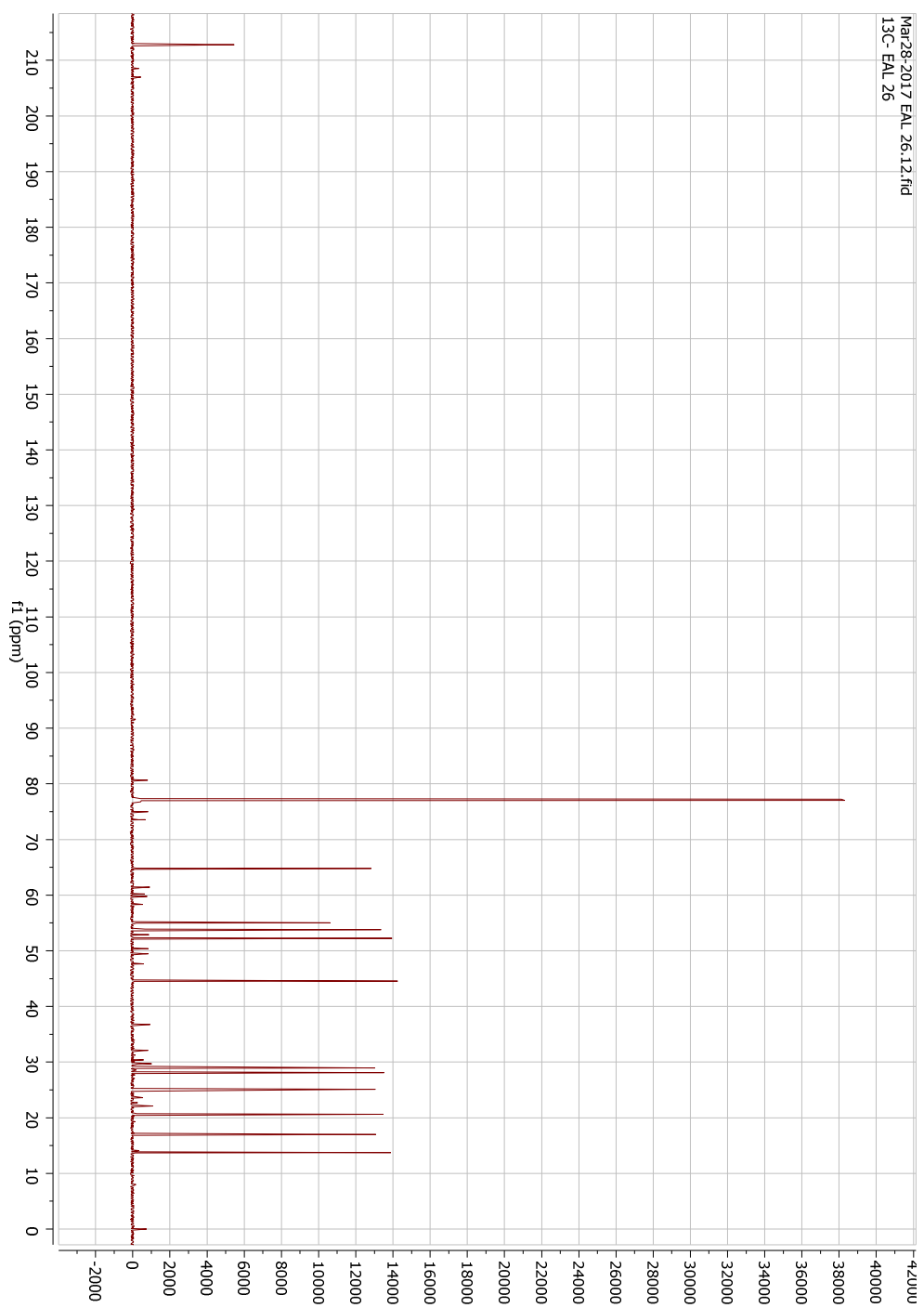


Figure 3.29:  $^1\text{H}$  NMR (600 MHz,  $\text{CDCl}_3$ ) spectrum of carpusinine B (6).



**Figure 3.30:**  $^{13}\text{C}$  NMR (150 MHz,  $\text{CDCl}_3$ ) spectrum of carpusinine B (6).

### 3.2.3 Carpusinine C (7a) and epicarpusinine C (7b)

Carpusinine C (**7a**) and epicarpusinine C (**7b**) (Figure 3.31) were obtained as a mixture of a pair of C-12 epimers (diastereomers), which could not be separated by chromatography. This was revealed by the  $^{13}\text{C}$  NMR spectrum which showed the presence of a 1:1 mixture of the two epimers (Table 3.7 and Figure 3.34). The IR spectrum (Appendix 38) showed absorption bands due to a ketone carbonyl ( $1708\text{ cm}^{-1}$ ) and a *trans*-fused indolizidine ring junction (Bohlmann bands at  $2788$ ,  $2875$  and  $2858\text{ cm}^{-1}$ )<sup>70</sup>. The HRESIMS showed a pseudo molecular ion at  $m/z$  240.1970, consistent with the molecular formula  $\text{C}_{14}\text{H}_{26}\text{NO}_2$  (Appendix 39), differing from **6** by 44 mass units and suggesting replacement of a H atom in **6** with a  $\text{C}_2\text{H}_5\text{O}$  group in **7a/7b**. Comparison of the NMR data with those of **6** (Tables 3.6 and 3.7) revealed that **6** and **7a/7b** have essentially the same structure, except that the methylene group at C-12 in **6** was substituted with an ethoxy group in **7a/7b**. This was evident from the  $^1\text{H}$  NMR spectrum of **7a/7b** which showed the presence of an oxymethine signal at  $\delta_{\text{H}}$  3.90 in place of the shielded 2H methylene signal at  $\delta_{\text{H}}$  1.59 in that of **6** (Tables 3.6 and 3.7).

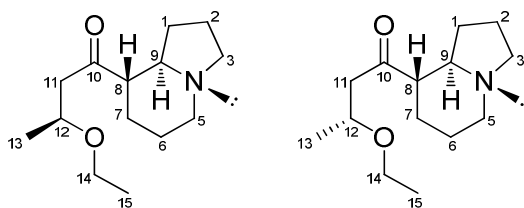


**Figure 3.31:** Structures of carpusinine C (**7a**) and epicarpusinine C (**7b**).

Complete coincidence of most of the signals for both the epimers **7a** and **7b** was observed in the  $^1\text{H}$  NMR spectrum (Figure 3.33). Although only four of the 14 signals were completely coincident in the  $^{13}\text{C}$  NMR spectrum, the remaining 10 paired signals showed very similar chemical shifts, i.e., the average chemical shift difference ( $\Delta\delta$ ) for the paired signals is 0.07 ppm. As a result, the paired signals were not distinguishable. The largest  $\Delta\delta$  was determined to

be 0.20 ppm and is due to the paired signals assigned to C-12 of both compounds (Table 3.7). This suggested that C-12 is the epimeric carbon where both the structures of **7a** and **7b** differ. The chemical shift differences for the paired signals due to C-10, C-11 and C-13 were also rather high ( $\Delta\delta_c$  ranging from 0.06 to 0.19) due to their proximity to C-12.



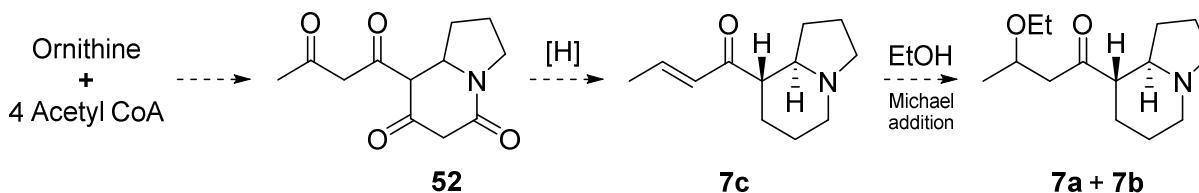
**Figure 3.32:** COSY (bold bonds) and  $^1\text{H}$ - $^{13}\text{C}$  HMBC correlations (arrows) of **7a/7b**.

The proposed structures for **7a/7b** were also supported by the 2D NMR data. The  $\text{CH}_2\text{CH}_2\text{CH}_2$ ,  $\text{CH}_2\text{CH}_2\text{CH}_2\text{CH}$ ,  $\text{CH}_3\text{CHCH}_2$  and  $\text{CH}_2\text{CH}_3$  fragments were obtained from the COSY and HSQC data (Figure 3.32), which corresponded to the C-1–C-2–C-3, C-5–C-6–C-7–C-8, C-11–C-12–C-13 and C-14–C-15 partial structures in **7a/7b**. C-3, C-5 and C-9 were deduced to be connected to the tertiary N atom by the HMBC correlations from H-3 to C-5 and C-9; and from H-5 to C-9 (Figure 3.32). The HMBC correlations from H-2 and H-1 to C-9; and from H-8 to C-9 completed the assembly of the indolizidine moiety. The indolizidine moiety was shown to be connected from C-8 to the C-10 ketone group via the HMBC correlation from H-7 to C-10. Subsequently, the  $\text{CH}_3\text{CHCH}_2$  fragment corresponding to the C-11–C-12–C-13 partial structure was deduced to be connected to C-10 by the HMBC correlations from H-11 and H-12 to C-10. Finally, the C-14–C-15 ethoxy group was connected to C-12 based on the HMBC correlations from H-14 to C-12; and from H-12 to C-14. The gross structure established for **7a/7b** is entirely consistent with the full HMBC data (Figure 3.32).

Unfortunately, due to severe overlapping of the  $^1\text{H}$  signals for H-1, H-7, H-8 and H-9, the NOESY spectrum obtained could not afford any useful information regarding the relative stereochemistry for the chiral centres at C-8 and C-9. However, based on the observation of Bohlmann bands in the IR spectrum (see above), the indolizidine ring junction was determined to be *trans*-fused. Since the NMR data of **7a/7b** (barring the C-11–C-12–C-13 partial structure)

showed a close correspondence with those of carpusinine B (**6**), the relative configurations at C-8 and C-9 were assumed to be identical to those in **6** (i.e., 8*R*,9*S*). This is somewhat consistent with the optical activity observed for **7a/7b** ( $[\alpha]_D -40$ ), which is comparable to that for **6** ( $[\alpha]_D -47$ ). Carpusinine C and epicarpusinine C (**7a** and **7b**) were therefore isolated as a pair of inseparable epimers and represent the 12-ethoxy derivatives of carpusinine B (**6**).

Compounds **7a** and **7b** are postulated to be derived from the common polyketoidindolizidine precursor (**52**), which then undergoes a series of reductive and dehydration reactions to give the hypothetical  $\alpha,\beta$ -unsaturated ketone intermediate **7c** (Scheme 3.6). A Michael addition involving an ethanol molecule onto **7c** would then give the pair of epimers **7a** and **7b** (Scheme 3.6).



**Scheme 3.6:** Plausible biosynthetic pathway to carpusinine C and epicarpusinine C (**7a** and **7b**).

**Table 3.7:**  $^{13}\text{C}$  (150 MHz) and  $^1\text{H}$  NMR (600 MHz) data of carpusinine C and epicarpusinine C (**7a** and **7b**) ( $\delta$  in ppm).<sup>a</sup>

Position	$\delta_{\text{H}}$ ( <i>J</i> in Hz)	$\delta_{\text{C}}$	$ \Delta\delta_{\text{C}} $
1 $\alpha$	1.95, m	28.94, 28.95	0.01
1 $\beta$	1.33, m		
2 $\beta$	1.76, m	20.63, 20.64	0.01
2 $\alpha$	1.65, m		
3 $\beta$	3.05, m	53.73	-
3 $\alpha$	2.10, q (8.5)		
5 $\beta$ (eq)	3.08, m	52.20, 52.22	0.02
5 $\alpha$ (ax)	1.99, m		
6 $\alpha$ (eq)	1.76, m	25.060, 25.062	0.002
6 $\beta$ (ax)	1.65, m		
7 $\beta$ (eq)	1.95, m	27.66, 27.71	0.04
7 $\alpha$ (ax)	1.29, m		
8 (ax)	2.41, m	55.82	-
9 (ax)	1.96, m	64.60, 64.65	0.05
10	-	211.22, 211.32	0.10
11	2.76, dt (16, 6.8) 2.45, dd (16, 5.5)	49.55, 49.74	0.19
12	3.90, sextet (6.1)	71.24, 71.44	<b>0.20</b>
13	1.16, d (6.1)	19.92, 19.98	0.06
14	3.54, pentet (7.3) 3.38, pentet (7.3)	63.98	-
15	1.15, t (7.3)	15.50	-

<sup>a</sup> Measured in  $\text{CDCl}_3$ .

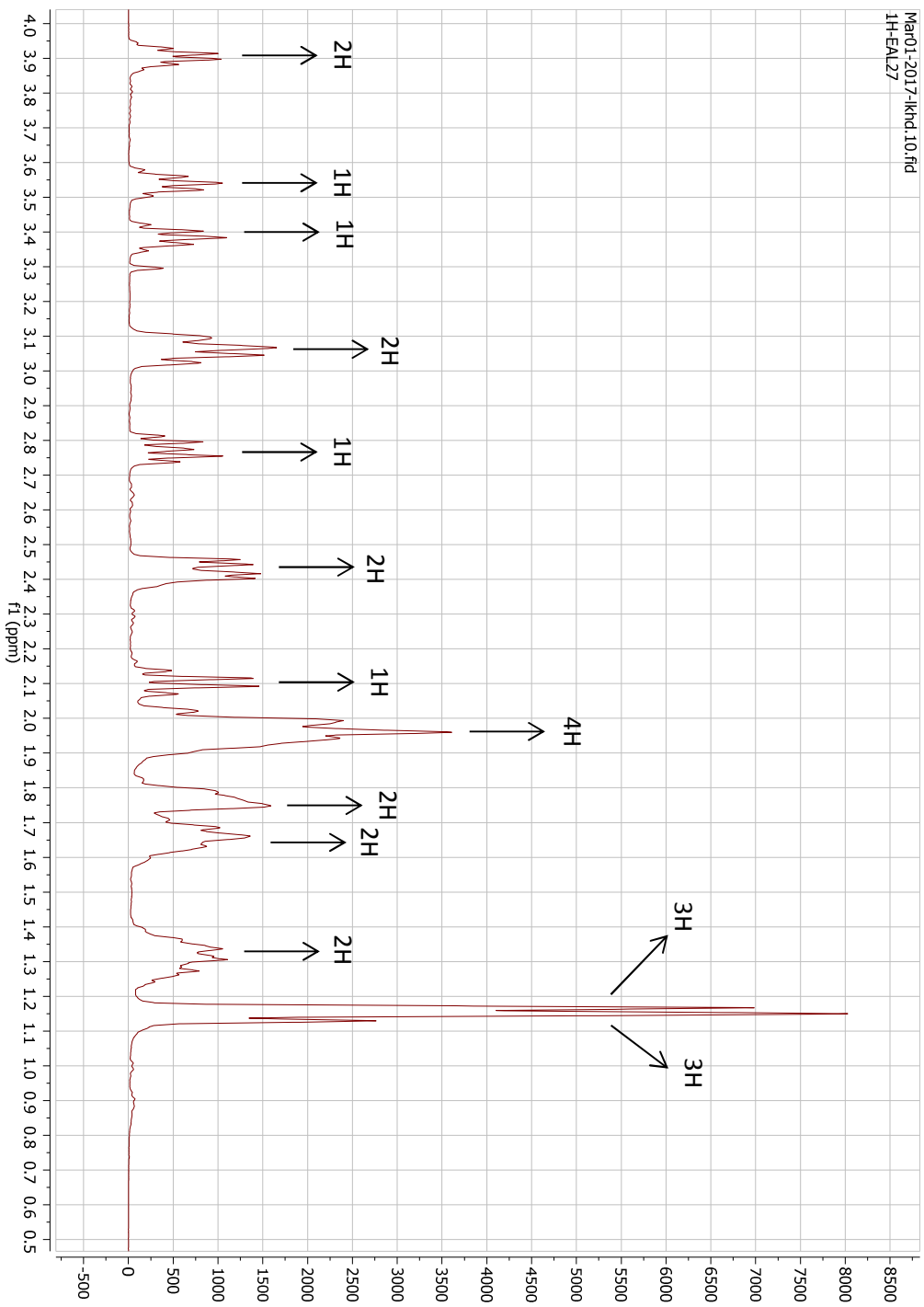


**Figure 3.33:** <sup>1</sup>H NMR (600 MHz, CDCl<sub>3</sub>) spectrum of carpusinine C (**7a**) and epicarpusinine C (**7b**).

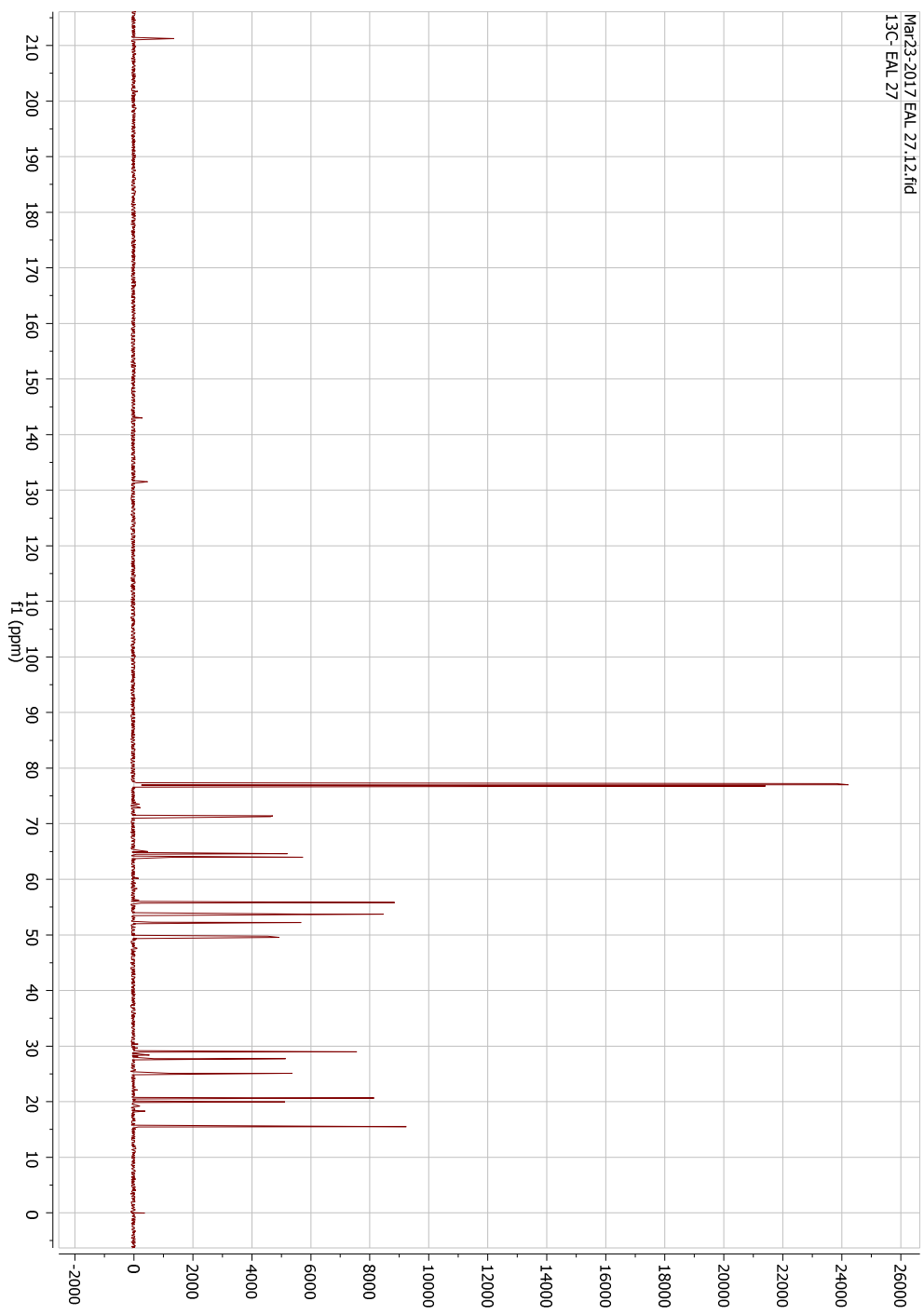


**Figure 3.34:**  $^{13}\text{C}$  NMR (150 MHz,  $\text{CDCl}_3$ ) spectrum of carpusinine C (**7a**) and epicarpusinine C (**7b**).

### 3.2.4 Carpusinine D (8)

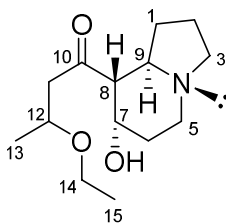


**Figure 3.35:** Structure of carpusinine D (**8**).

Carpusinine D (**8**) (Figure 3.35) was obtained in minute amounts as a light yellowish oil with  $[\alpha]_D^{25} -7$  ( $c$  0.11,  $\text{CHCl}_3$ ). The molecular formula of **8** was determined by HRESIMS ( $m/z$  256.1911  $[\text{M}+\text{H}]^+$ ) to be  $\text{C}_{14}\text{H}_{26}\text{NO}_3$  (Appendix 45), corresponding to three degrees of unsaturation. In addition to the presence of Bohlmann bands ( $2854$  and  $2874\text{ cm}^{-1}$ )<sup>70</sup>, the IR spectrum (Appendix 44) showed absorption bands due to OH ( $3418\text{ cm}^{-1}$ ) and H-bonded C=O ( $1651\text{ cm}^{-1}$ ).

The HRESIMS showed a pseudo molecular ion at  $m/z$  256.1911, in agreement with the molecular formula  $\text{C}_{14}\text{H}_{26}\text{NO}_3$ , differing from **7a/7b** by an extra O atom. Comparison of the NMR data with those of **7** (Tables 3.7 and 3.8) revealed that both **7a/7b** and **8** have very similar structures, with the main change being that the methylene group at C-7 in **7a/7b** was substituted with an OH group in **8**. This was evident from the  $^1\text{H}$  NMR spectrum of **8** (Table 3.7 and Figure 3.38), which showed the presence of a second oxymethine signal at  $\delta_{\text{H}}$  4.49 at the expense of the two shielded signals due to  $\text{CH}_2$ -7 ( $\delta_{\text{H}}$  1.29 and 1.95) in that of **7** (Table 3.7). Similarly, the  $^{13}\text{C}$  NMR (Figure 3.39) and HSQC data of **8** (Table 3.7) showed the presence of an additional oxymethine carbon at the expense of the methylene C-7 present in those of **7**.

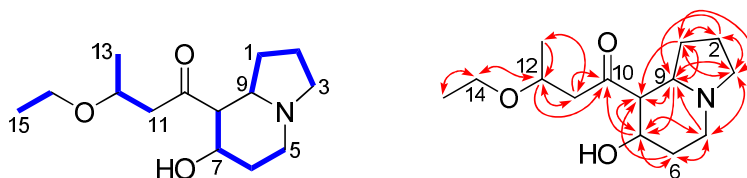


**Figure 3.36:** COSY (bold bonds) and  $^1\text{H}$  -  $^{13}\text{C}$  HMBC (arrows) correlations of carpusinine D (**8**).

Detailed analysis of the COSY and HSQC data revealed the  $\text{CHCH}_2\text{CH}_2\text{CH}_2$ ,  $\text{CH}_2\text{CH}_2\text{CHCH}$ ,  $\text{CH}_2\text{CHCH}_3$ , and  $\text{CH}_2\text{CH}_3$  fragments (Figure 3.36), which corresponded to the C-9–C-1–C-2–C-3, C-5–C-6–C-7–C-8, C-11–C-12–C-13 and C-14–C-15 partial structures in **8**. The presence of the indolizidine ring junction was firmly established based on the HMBC correlations from H-1 to C-9; from H-3 to C-5 and C-9; from H-5 to C-3 and C-9; from H-8 to C-1 and C-9; and from H-9 to C-3 (Figure 3.36). The HMBC correlations from H-5 to C-7; and from H-7 to C-9 and C-10 confirmed the location of the hydroxymethine C-7. The indolizidine moiety was shown to be connected to the C-11–C-12–C-13 partial structure at C-8 via the C-10 ketone group by the HMBC correlation from H-7, H-8, H-11 and H-12 to C-10. Finally, the C-14–C-15 ethoxy group was connected to C-12 based on the HMBC correlations from H-14 to C-12; and from H-12 to C-14. The gross structure established for **8**, which is entirely consistent with the full HMBC data (Figure 3.36), seemed to suggest that **8** was a hydroxylated derivative of carpusinine C (**7**) or one of its stereoisomers.

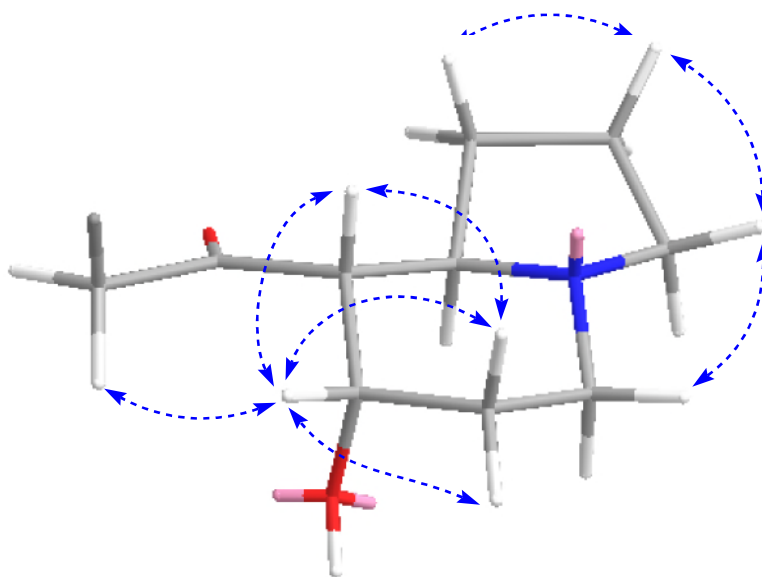
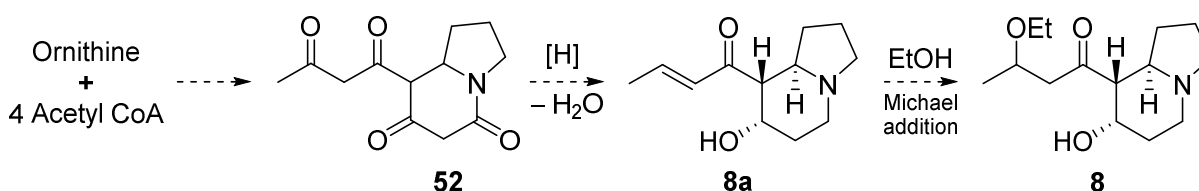


**Figure 3.37:** Selected NOESY correlations of carpusinine D (**8**).

The relative configurations at the C-7, C-8 and C-9 stereocenters as well as the N lone pair orientation in **8** were determined based on vicinal coupling constants and the NOESY data

(Figure 3.37). The NOE observed for H-8/H-6 $\beta$  not only required the piperidine ring to be in chair conformation but also indicated a 1,3-diaxial interaction between H-8 and H-6 $\beta$ . The orientation of H-8 was therefore determined as  $\beta$ . The large coupling constant (10 Hz) observed between H-8 and H-9 indicated that both the hydrogens are *trans*-diaxial. The NOEs observed for H-9/H-3 $\alpha$ , H-3 $\alpha$ /H-5 $\alpha$  and H-3 $\beta$ /H-5 $\beta$  deduced a *trans*-fused ring junction for the indolizidine moiety. This deduction is consistent with the presence of Bohlmann bands in the IR spectrum of **8**.<sup>70</sup> The NOEs observed for H-8/H-7 and H-7/H-6 $\beta$  required the hydroxyl group at C-7 to be  $\alpha$ -axial-oriented. This was supported by the small coupling constant (5.8 Hz) observed for H-8/H-7, which required H-7 to be  $\beta$ -equatorial. The relative configurations at C-7, C-8 and C-9 in **8** were therefore established as 7*S*,8*R*,9*R*. This corresponds to a chair conformation for the piperidine ring. The relative configuration at C-12 was however not assignable based on the NOESY data due to the inherent flexibility of the side chain.



**Scheme 3.7:** Plausible biosynthetic pathway to carpusinine D (**8**).

Carpusinine D (**8**) incorporates a 7-hydroxy-8-ketoindolizidine moiety with the same relative configuration as that found in elaeokanine C (**12**).<sup>86</sup> Carpusinine D (**8**) is therefore a 12-ethoxy derivative of elaeokanine C (**12**). Similar to compounds **7a/7b**, carpusinine D (**8**) is postulated to be the product of Michael addition of an ethanol molecule onto the hypothetical  $\alpha,\beta$ -unsaturated ketone **8a**, derived from the common polyketoid indolizidine precursor (**52**) (Scheme 3.7).

**Table 3.8:**  $^{13}\text{C}$  (150 MHz) and  $^1\text{H}$  NMR (600 MHz) data of carpusinine D (**8**) ( $\delta$  in ppm).<sup>a</sup>

Position	$\delta_{\text{C}}$	$\delta_{\text{H}}$ ( <i>J</i> in Hz)
1 $\alpha$	29.2	2.09, dddd (12.5, 9.5, 5.8, 3.6)
1 $\beta$		1.29, m
2 $\beta$	20.8	1.78, m
2 $\alpha$		1.74, m
3 $\beta$	53.4	3.06, td (9, 2.3)
3 $\alpha$		2.20, q (9)
5 $\beta$ (eq)	46.5	2.88, ddd (11, 4.5, 2.5)
5 $\alpha$ (ax)		2.42, td (12.5, 3)
6 $\alpha$ (eq)	32.2	1.93, dq (13.5, 3)
6 $\beta$ (ax)		1.87, tt (13.5, 3.5)
7 (eq)	64.7	4.49, q (2.4)
8 (ax)	58.3	2.50, dd (10.0, 2)
9 (ax)	61.2	2.53, td (10.0, 5.8)
10	211.1	-
11	48.8	2.96, dd (15.4, 9.4) 2.29, dd (15.4, 3.9)
12	72.3	4.01, dqd (9.4, 6.1, 3.9)
13	19.2	1.20, d (6.1)
14	64.0	3.60, dq (9.1, 7) 3.35, dq (9.1, 7)
15	15.2	1.14, t (7)

<sup>a</sup> Measured in  $\text{CDCl}_3$ .

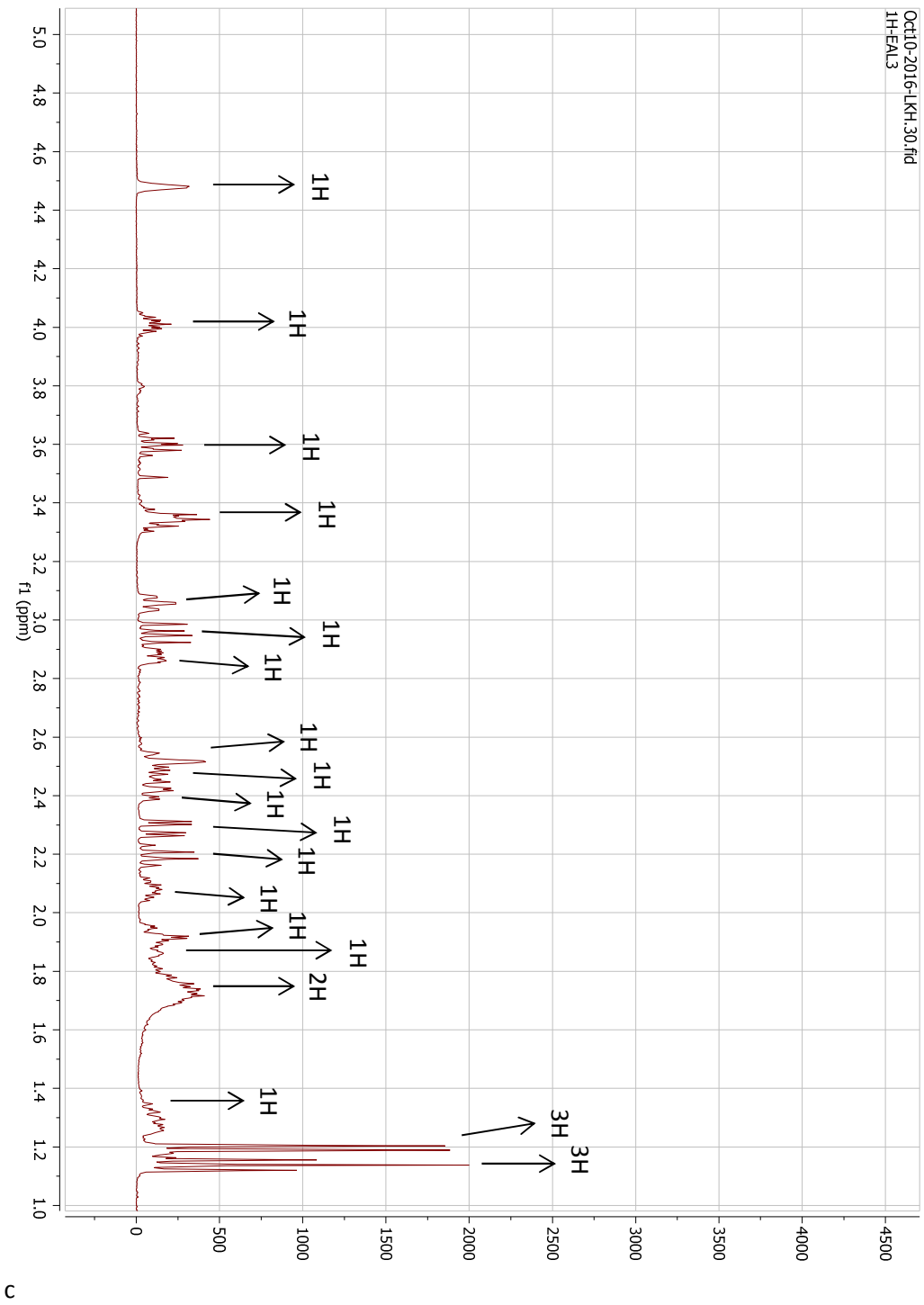
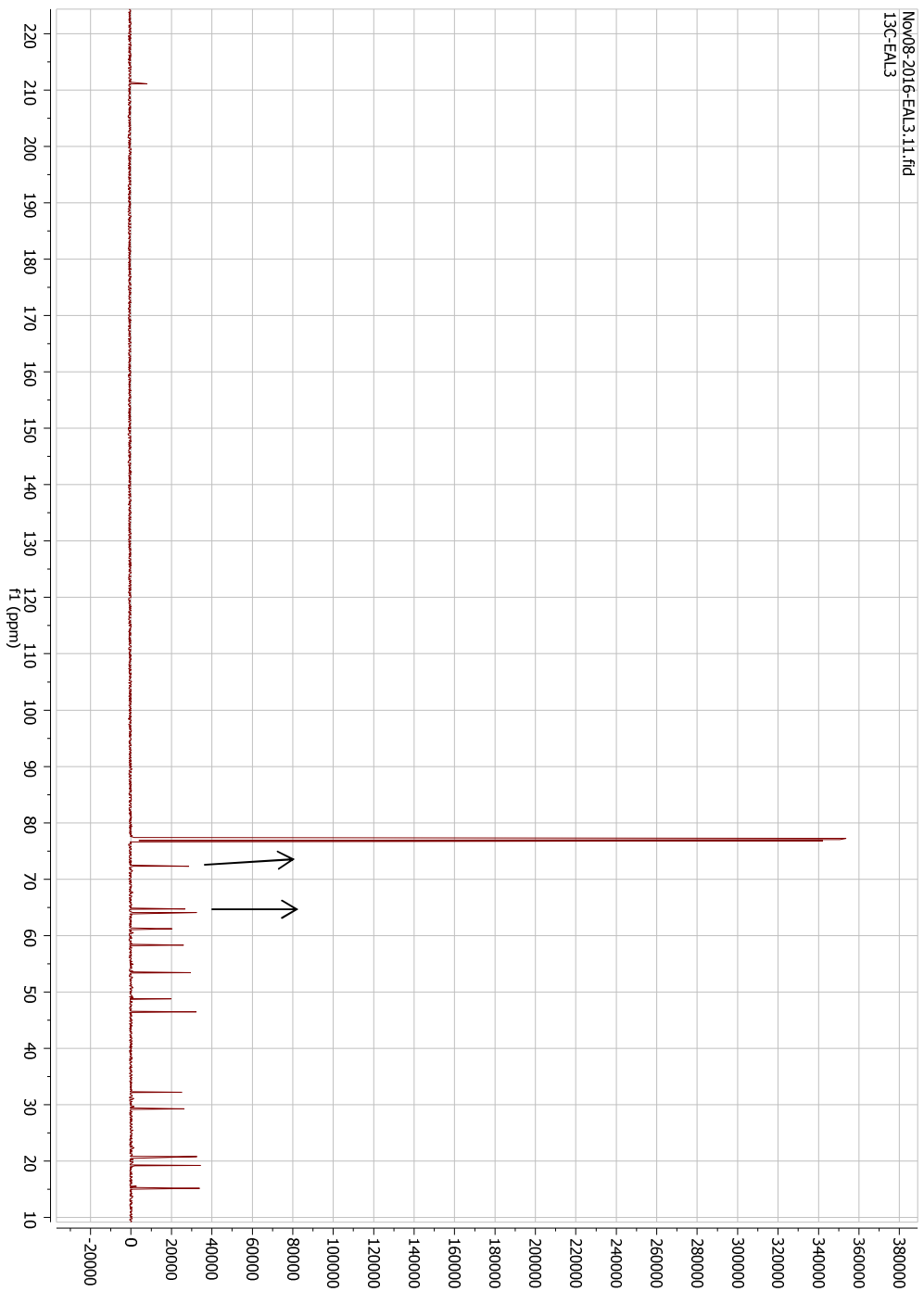


Figure 3.38: <sup>1</sup>H NMR (600 MHz, CDCl<sub>3</sub>) spectrum of carpusinine D (8).



**Figure 3.39:**  $^{13}\text{C}$  NMR (150 MHz,  $\text{CDCl}_3$ ) spectrum of carpusinine D (**8**)

### 3.2.5 Carpusinine E (9)

Carpusinine A (9) was obtained as a colourless oil with  $[\alpha]_D^{25} -25$  (c 0.11,  $\text{CHCl}_3$ ). The molecular formula of 9 was determined by HRESIMS ( $m/z$  210.1500  $[\text{M}+\text{H}]^+$ ) to be  $\text{C}_{12}\text{H}_{19}\text{NO}_2$  (Appendix 51), corresponding to four degrees of unsaturation (Figure 3.20). The IR spectrum of 9 (Appendix 50) showed absorptions characteristic of Bohlmann bands (2876, 2793 and  $2728\text{ cm}^{-1}$ ), suggesting the presence of a *trans*-fused ring junction in an indolizidine ring system.<sup>70</sup> Additionally, the IR absorption band observed at  $1713\text{ cm}^{-1}$  indicated the presence of a ketone function.

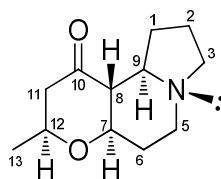


**Figure 3.40:** Structure of carpusinine E (9).

The  $^1\text{H}$  NMR data (Table 3.9 and Figure 3.44) revealed one distinct methyl doublet at  $\delta_{\text{H}}$  1.34 attributed to  $\text{CH}_3$ -13. The deshielded methine signals at  $\delta_{\text{H}}$  3.32 and 3.82 were assignable to oxymethine hydrogens (H-7 and H-12 respectively). The  $^{13}\text{C}$  NMR data (Table 3.9 and Figure 3.45) revealed the presence of 12 carbon resonances in agreement with the molecular formula established by HRESIMS. With the aid of the HSQC data, the  $^{13}\text{C}$  data revealed the presence of one methyl group, six  $\text{CH}_2$  groups, four CH groups, and one ketone group. The most downfield carbon resonance observed at  $\delta_{\text{C}}$  206.9 is attributed to the C-10 ketone group, while the resonances at  $\delta_{\text{C}}$  80.6 and 75.0 were assignable to the oxymethines C-7 and C-12.



**Figure 3.41:** COSY (bold bonds) and HMBC  $^1\text{H}$ - $^{13}\text{C}$  correlations (arrows) of carpusinine E (9).

Detailed analysis of the COSY and HSQC data revealed the presence of a propylene fragment corresponding to the C-1–C-2–C-3 partial structure, a CH<sub>2</sub>CH<sub>2</sub>CHCHCH fragment corresponding to the C-5–C-6–C-7–C-8–C-9 partial structure and a CH<sub>2</sub>CHCH<sub>3</sub> fragment corresponding to the C-11–C-12–C-13 partial structure in **9** (Figure 3.41). The presence of a tertiary N atom attached to C-3, C-5 and C-9 was supported by the three-bond HMBC correlations from H-3 to C-5 and C-9; from H-5 to C-3 and C-9; and from H-9 to C-3 (Figure 3.41). Additionally, the HMBC correlations from H-2 to C-9; and from H-9 to C-1 connected C-1 to C-9, thus establishing the indolizidine moiety in **9**. The attachment of the C-11–C-12–C-13 partial structure to C-8 via the ketone C-10 was revealed by the HMBC correlations from H-7, H-8, H-11 and H-12 to C-10. Finally, the oxymethine C-7 and C-12 were shown to be connected via an ether bridge based on the HMBC correlations from H-7 to C-12; and from H-12 to C-7. The 2D structure established for carpusinine E (**9**) is entirely consistent with the full HMBC data (Figure 3.41).

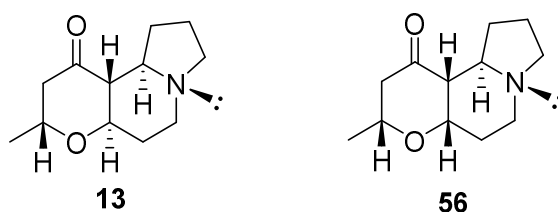


**Figure 3.42:** Structures of (+)-elaekanine D (**13**) and (+)-elaekanine E (**56**)

The gross structure of **9** was found to be identical to that of the isomeric alkaloids, elaeokanines D (**13**) and E (**56**) (Figure 3.42). The <sup>1</sup>H NMR spectrum of **9** showed a close resemblance to that of **13** (Table 3.9). However, the resonances for H-12 in both alkaloids were significantly different, i.e.,  $\delta_{\text{H}}$  3.82 in **9** versus  $\delta_{\text{H}}$  4.63 in **13**. This suggested that both **9** and **13** are epimers, with C-12 being the epimeric carbon. The relative configuration of **9** was subsequently deduced based on a combination of vicinal coupling constants and NOESY correlations (Figure 3.43). The large coupling constant (10 Hz) observed between H-9 and H-8 required both hydrogens to be *trans*-diaxial. Similarly, the large coupling constant (10 Hz) observed between H-8 and H-7 indicated that both hydrogens are also *trans*-diaxial. These observations are consistent with the

relative configuration where H-7 and H-9 are  $\alpha$ -oriented, while H-8 is  $\beta$ -oriented. Furthermore, the NOEs observed for H-7/H-9 and H-7/H-12 not only indicated that the piperidine and pyran rings were in chair conformation but also revealed the presence of 1,3-diaxial interactions between H-7 and H-9 as well as between H-7 and H-12, thus requiring H-7, H-9 and H-12 to be axially oriented at the  $\alpha$ -plane (CH<sub>3</sub>-13 is equatorial). The relative configuration of **9** at C-7, C-8, C-9 and C-12 was therefore established as *7R,8R,9R,12S* (Figure 3.43). Carpusinine E (**9**) represents the C-12-epimer of elaeokanine D (**13**), which possesses the relative configuration of *7R,8R,9R,12R*.

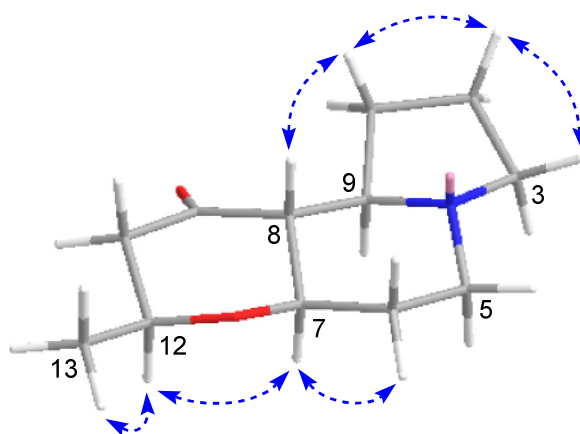
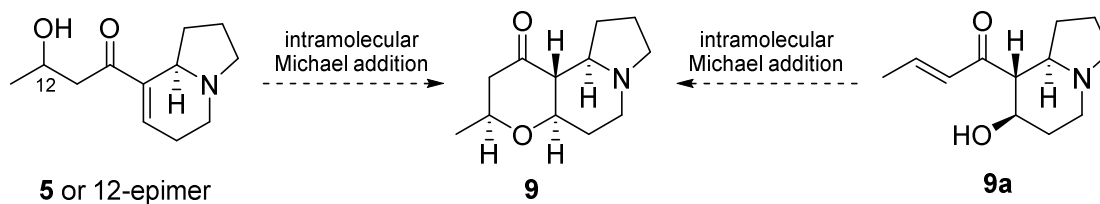


**Figure 3.43:** Selected NOESY correlations of carpusinine E (**9**).

Carpusinine E (**9**) is postulated to be derived from carpusinine A (**5**) or its C-12 epimer via an intramolecular Michael addition of the 12-OH group onto the  $\alpha,\beta$ -unsaturated ketone function (Scheme 3.8). Alternatively, compound **9** could also arise from the hypothetical hydroxyindolizidine **9a**, which is a regioisomer of **5**.



**Scheme 3.8:** Plausible biosynthetic pathway to carpusinine E (**9**).

**Table 3.9:**  $^{13}\text{C}$  (150 MHz) and  $^1\text{H}$  NMR (600 MHz) data of carpusinine E (**9**) and (+)-elaeokanine D (**13**) ( $\delta$  in ppm).<sup>a</sup>

Position	Carpusinine E ( <b>9</b> )		(+)-Elaeokanine D ( <b>13</b> )
	$\delta_{\text{C}}$	$\delta_{\text{H}}$ (J in Hz)	$\delta_{\text{H}}$ (J in Hz)
1 $\alpha$	29.2	2.33, m	2.10, m
1 $\beta$		1.36, m	1.36, qd (11.4, 7.0)
2 $\beta$	22.08	1.83, m	1.85, m
2 $\alpha$		1.76, m	1.76, m
3 $\beta$	52.9	3.00, td (8.8, 2.1)	3.00, td (8.7, 2.4)
3 $\alpha$		2.10, m	2.32, m
5 $\beta$ (eq)	49.4	3.11, ddd (11.4, 4.3, 2.4)	3.12, dt (11.6, 3.5)
5 $\alpha$ (ax)		2.09, m	2.13, m
6 $\alpha$ (eq)	32.1	2.05, m	2.10, m
6 $\beta$ (ax)		1.92, qd (12, 4.3)	1.93, dd (10.7, 4.2)
7 (ax)	80.6	3.32, td (10, 4.3)	3.65, td (10.3, 5.0)
8 (ax)	59.7	2.26, t (10)	2.34, t (9.9)
9 (ax)	61.4	1.98, td (10, 6.3)	2.00, td (9.9, 6.2)
10	206.9	-	-
11	50.3	2.36, m	2.88, dd (13.3, 7.0)
		2.36, m	2.20, dd (13.4, 1.9)
12 (ax)	75.0	3.82, dqd (10, 6.1, 2.3)	4.63, quintet of doublet (6.7, 3.4)
13 (eq)	22.11	1.34, d (6.1)	1.26, d (6.6)

<sup>a</sup> Measured in  $\text{CDCl}_3$ .

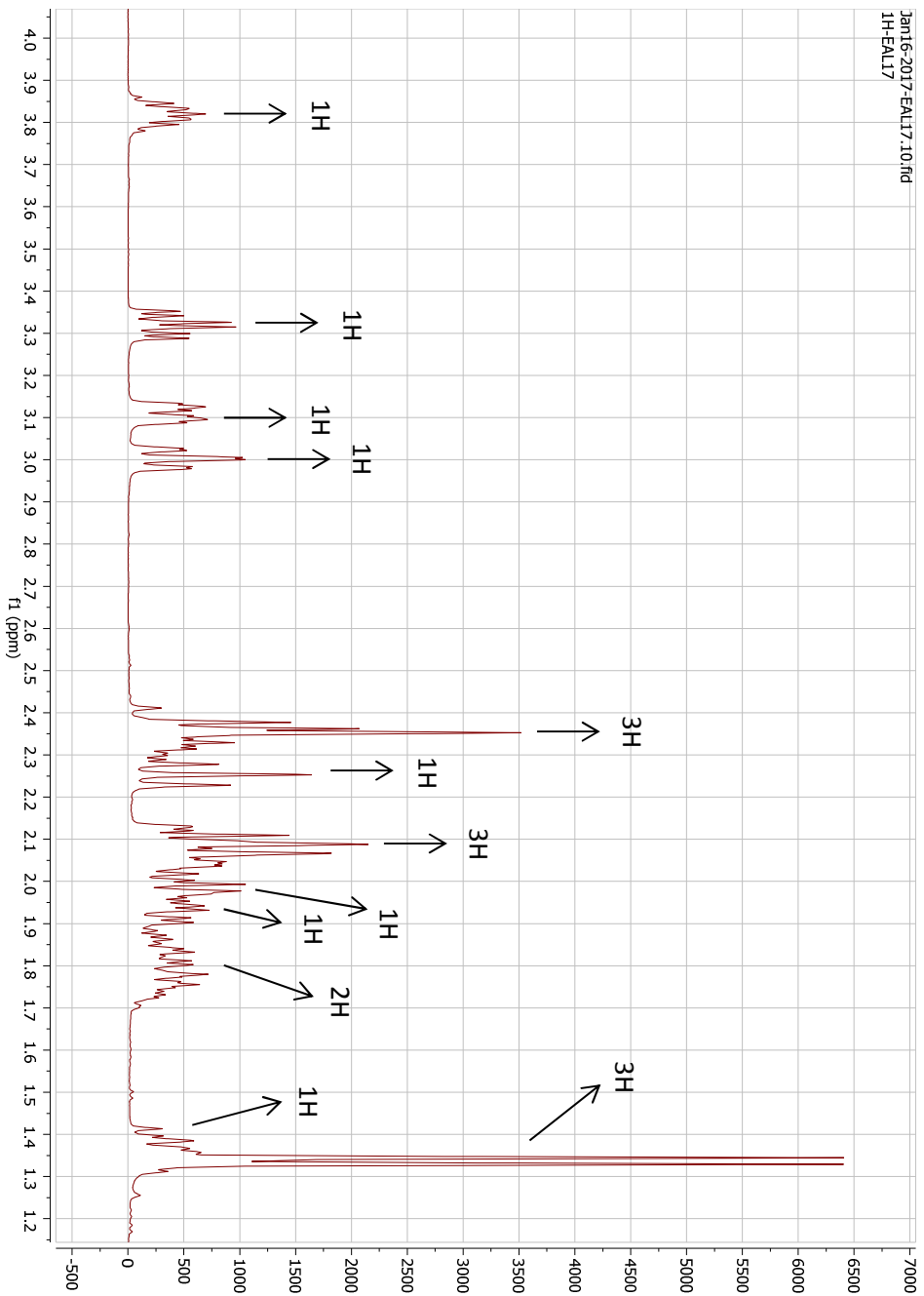
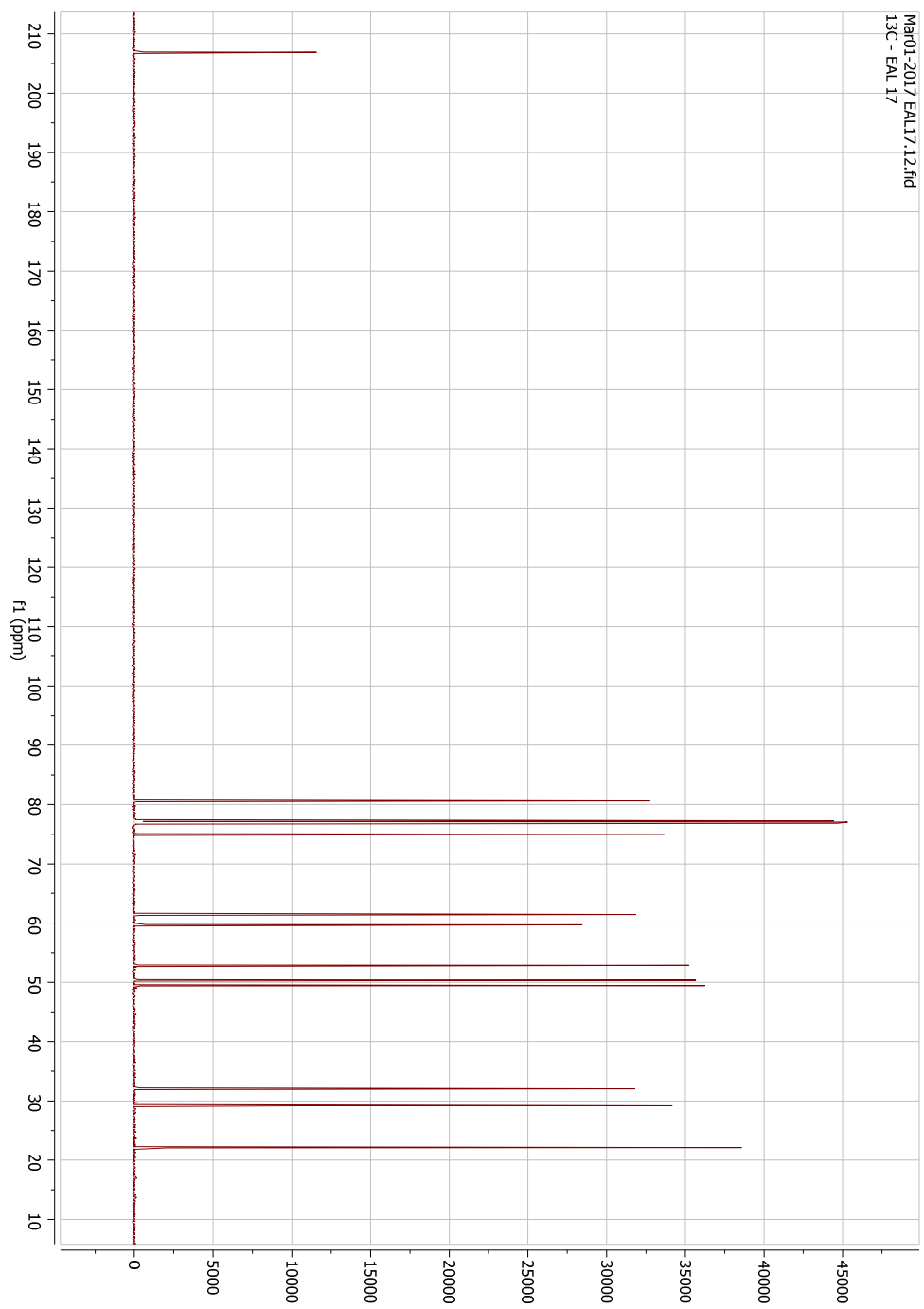


Figure 3.44:  $^1\text{H}$  NMR (600 MHz,  $\text{CDCl}_3$ ) spectrum of carpusinine E (9).



**Figure 3.45:**  $^{13}\text{C}$  NMR (150 MHz,  $\text{CDCl}_3$ ) spectrum of carpusinine E (9).

### 3.2.6 Carpusinine F (10a) and epicarpusinine F (10b)

Carpusinine F (**10a**) and epicarpusinine F (**10b**) (Figure 3.46) were obtained as a pair of diastereomers, which, like carpusinine C (**7a**) and epicarpusinine C (**7b**), was intractable to further resolution by chromatography. The IR spectrum (Appendix 56) showed absorption bands at 3405 (OH) and 1710  $\text{cm}^{-1}$  (C=O). The molecular formula of **10** was determined by HRESIMS ( $m/z$  258.2074  $[\text{M}+\text{H}]^+$ ) to be  $\text{C}_{14}\text{H}_{28}\text{NO}_3$  (Appendix 57), corresponding to two degrees of unsaturation.

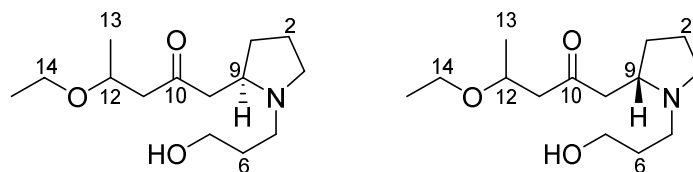


**Figure 3.46:** Structures of carpusinine F (**10a**) and epicarpusinine F (**10b**).

As in the case of carpusinine C (**7a**) and epicarpusinine C (**7b**), complete coincidence of most of the signals for both **10a** and **10b** was observed in the  $^1\text{H}$  NMR spectrum (Table 3.10 and Figure 3.49). The  $^{13}\text{C}$  NMR spectrum (Figure 3.50) showed a total of 26 distinct carbon resonances. Of these, 24 signals appeared as 12 pairs of signals with very similar chemical shifts, i.e., the average chemical shift difference ( $\Delta\delta$ ) for the paired signals is only 0.07 ppm (as a result, the paired signals were not distinguishable). The remaining two signals have double the intensity compared to the rest, indicating that each of the two signals represents a pair of signals that were completely coincident (Table 3.10). Therefore, a total of two sets of 14 carbon signals due to a mixture of two diastereomeric compounds were accounted for, which is consistent with the molecular formula established by HRESIMS. Additionally, the  $^{13}\text{C}$  NMR spectrum revealed the mixture composition to be approximately 1:1 based on the fact that the 12 paired signals have very similar signal intensity.

The  $^1\text{H}$  NMR data (Table 3.10) revealed the presence of two methyl signals at  $\delta_{\text{H}}$  1.15 (triplet) and 1.17 (doublet), attributable to  $\text{CH}_3$ -15 and  $\text{CH}_3$ -13. The most deshielded upfield signal observed at  $\delta_{\text{H}}$  3.90 (H-12) is characteristic of an oxymethine group. The very large germinal coupling constants observed for the methylene hydrogens at C-8 ( $J = 16.7$  Hz) and C-11 ( $J = 15.5$  Hz) are consistent with the fact that both methylene groups are adjacent to a ketone group. The  $^{13}\text{C}$  NMR and HSQC data (Table 3.10) established the presence of two methyl groups, nine  $\text{CH}_2$  groups (of which two are oxymethylene groups,  $\delta_{\text{C}}$  63.95/6397 and 64.51/64.51), two CH groups (i.e., oxymethine,  $\delta_{\text{C}}$  71.47/71.61; aminomethine,  $\delta_{\text{C}}$  60.52/60.58) and one ketone group ( $\delta_{\text{C}}$  208.46/208.60).

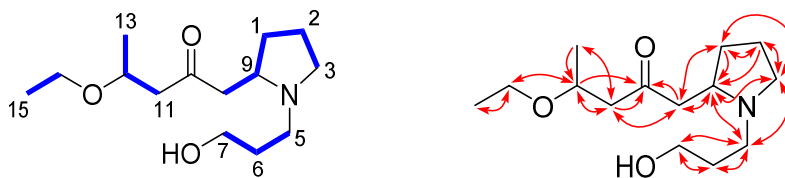
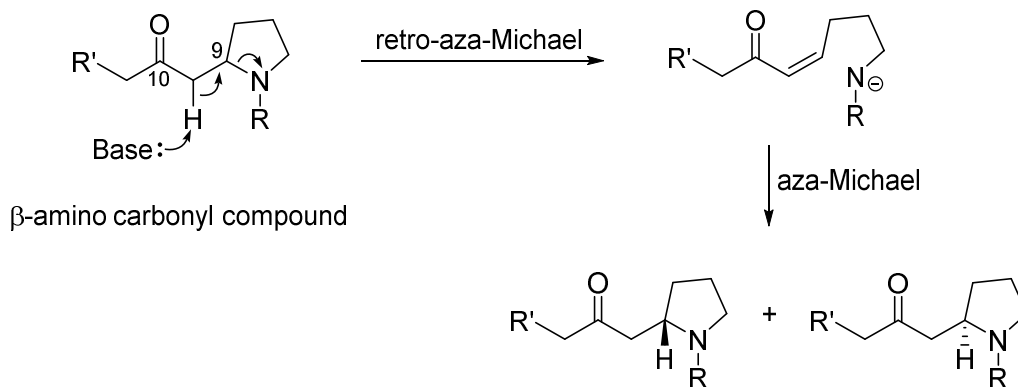


**Figure 3.47:** COSY (bold bonds) and HMBC  $^1\text{H}$ - $^{13}\text{C}$  correlations (arrows) of carpusinine F (**10a**) and epicarpusinine F (**10b**).

Detailed analysis of the COSY and HSQC data revealed the presence of  $\text{CH}_2\text{CHCH}_2\text{CH}_2\text{CH}_2$ ,  $\text{CH}_2\text{CH}_2\text{CH}_2\text{OH}$ ,  $\text{CH}_2\text{CH}(\text{OH})\text{CH}_3$  and  $\text{OCH}_2\text{CH}_3$  fragments (Figure 3.47), which corresponded to the C-8–C-9–C-1–C-2–C-3, C-5–C-6–C-7, C-11–C-12–C-13 and C-14–C-15 partial structures in **10a/10b**. While the presence of the pyrrolidine ring in **10a/10b** was firmly established by the HMBC correlations observed from H-1, H-2 and H-3 to C-9; and from H-9 to C-3, the conspicuous absence of correlations from H-6 to C-8; from H-7 to C-8, C-9 and C-10; from H-9 to C-7; and from H-8 to C-6 and C-7, strongly suggested that the indolizidine piperidine ring was absent due to the disconnection of the C-7–C-8 bond, i.e., C-7 and C-8 are both methylene groups now (Figure 3.47). The pyrrolidine moiety was shown to be connected to the C-11–C-12–C-13 partial structure at C-8 via the C-10 ketone group by the HMBC correlations from H-8, H-11 and H-12 to C-10. The C-14–C-15 ethyl fragment was deduced to be connected to C-12 via

an ether linkage based on the chemical shifts of C-12 ( $\delta_C$  71.47/71.61) and C-14 ( $\delta_C$  63.95/63.97) as well as by the HMBC correlations from H-12 to C-14; and from H-14 to C-12. Based on the  $^1\text{H}$  and  $^{13}\text{C}$  shifts observed for CH<sub>2</sub>-7 at  $\delta_H$  3.79 and  $\delta_C$  64.51/64.48, and consideration of the molecular formula, C-7 was established to be a CH<sub>2</sub>OH group (primary alcohol). The gross structure established for **10a/10b** is entirely consistent with the full HMBC data (Figure 3.47).

Since the gross structure for both **10a** and **10b** contained two chiral centres, i.e., C-9 and C-12, both compounds would only differ configurationally from each other at either one of these two carbons. Unfortunately, the NMR data did not enable the stereochemistry of the two compounds to be distinguished due to the inherent flexibility of the molecules. Furthermore, it is known that N inversion occurs rapidly in an unstrained pyrrolidine moiety like that in **10a/10b**, and as such the N atom in **10a/10b** is not regarded as a stereocentre.<sup>87</sup> However, it was previously reported that a  $\beta$ -amino carbonyl moiety such as that found in **10a/10b** can racemize/epimerize via a retro-aza-Michael ring opening reaction and subsequently re-closure via an aza-Michael reaction to give a pair of epimers (Scheme 3.9).<sup>88,89,56</sup> This epimerization could potentially occur during the acid-base extraction process where the acidic filtrate containing the alkaloid salts was treated with concentrated ammonia solution (see section 2.5.1.1), which could act as a base catalyst. Based on this knowledge, we are tempted to speculate that carpusinine F (**10a**) and epicarpusinine F (**10b**) are a pair of C-9 epimers. As with the case of carpusinine D (**8**), the relative configuration at C-12 could not be assigned.



**Scheme 3.9:** Plausible epimerization of a  $\beta$ -amino carbonyl moiety.

Previous reports revealed two incidents where pyrrolidine alkaloids were obtained from the Elaeocarpaceae family. Habbemines A and B (**36** and **37**) obtained from *Elaeocarpus habbemensis* were suggested to be an inseparable pair of C-9 epimers.<sup>56</sup> In the other instance, *Peripentadenia mearsii* produced a group of pyrrolidine alkaloids, namely, peripentadenine (**57**) and peripentonines A–C (**58**, **59** and **60**). Peripentonines A and B (**58** and **59**) are a pair of C-9 epimers. Furthermore, some partial structures in habbemines A and B (**36** and **37**) are identical to those in **10a/10b**, i.e.,  $\beta$ -aminoketone, 2-substituted pyrrolidine and N-propylene alcohol groups (Figure 3.48).

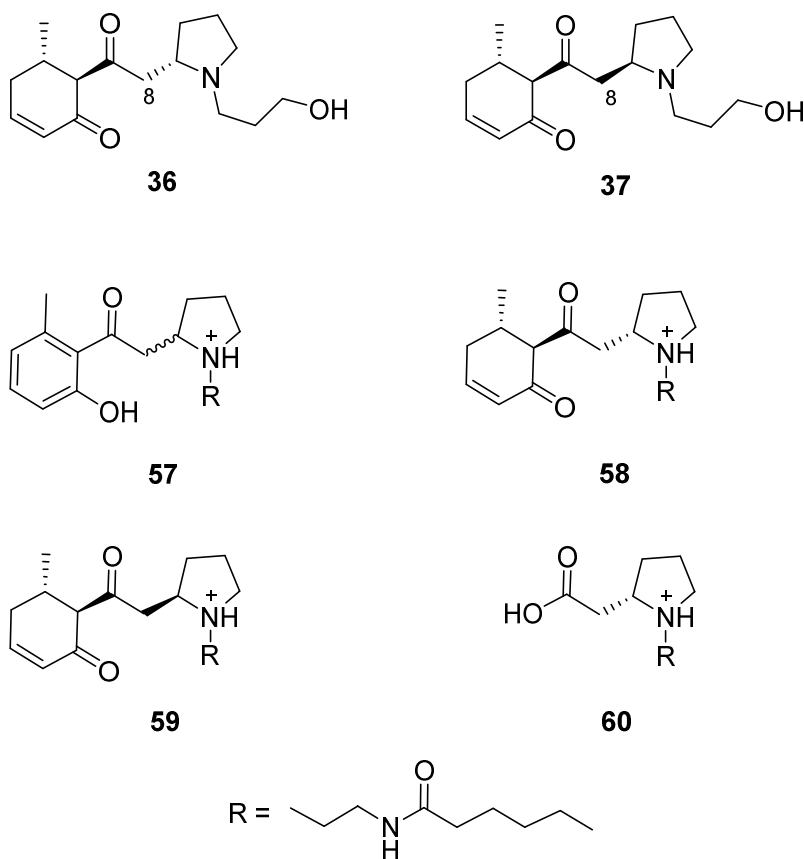
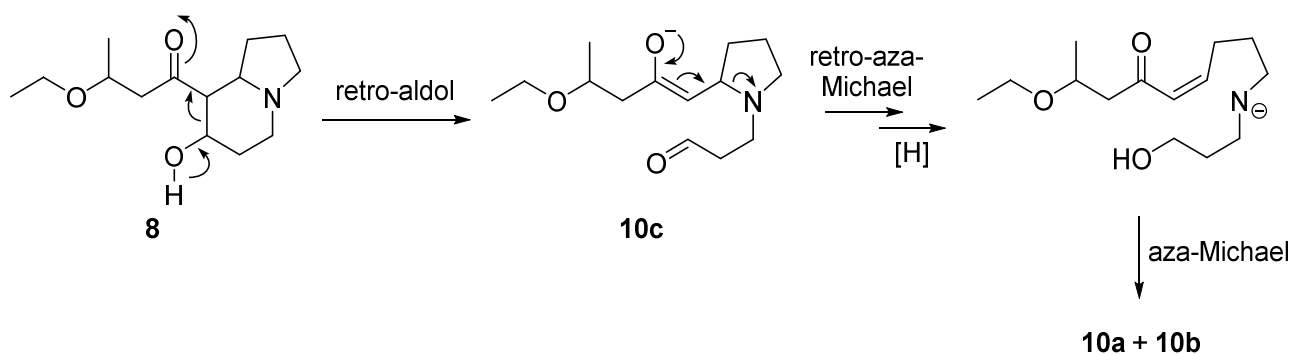


**Figure 3.48:** Structures of habbemines A and B (**36** and **37**), peripentadenine (**57**) and peripentonines A–C (**58**, **59** and **60**)

The proposed structures of **10a** and **10b** suggest that they are biosynthetically related to the other *Elaeocarpus* indolizidine alkaloids. As shown in Scheme 3.10, carpusinine D (**8**) was postulated as the precursor of **10a** and **10b** via a retro-aldol ring opening reaction as the key step. This pathway can also account for the formation of the C-9 epimeric pair of **10a** and **10b**, where the enolate intermediate **10c** formed from **8** via the retro-aldol may undergo the retro-aza Michael / aza-Michael epimerization to give the C-9 epimers of **10a** and **10b**.



**Scheme 3.10:** Plausible biosynthetic pathway to carpusinine F (**10a**) and epicarpusinine F (**10b**).

**Table 3.10:**  $^{13}\text{C}$  (150 MHz) and  $^1\text{H}$  NMR (600 MHz) data of carpusinine F (**10a**) and epicarpusinine F (**10b**) ( $\delta$  in ppm).<sup>a</sup>

Position	$\delta_{\text{H}}$ ( $J$ in Hz)	$\delta_{\text{C}}$	$ \Delta\delta_{\text{C}} $
1	2.09, tt (14, 7)	31.04	-
	1.37, tt (14, 7)		
2	1.74, m	22.32, 22.27	0.05
	1.74, m		
3	3.30, m	53.61, 53.58	0.03
	2.16, qd (8.8, 7)		
5	2.92, td (11.7, 4)	54.87, 54.77	0.10
	2.51, m		
6	1.89, m	29.14, 29.12	0.02
	1.55, dp (14.8, 4)		
7	3.79, m	64.51, 64.48	0.03
8	2.88, br dd (16.7, 3.3)	49.05, 48.92	0.13
	2.53, dd (16.7, 8.6)		
9	2.81, m	60.58, 60.52	0.06
10	-	208.60, 208.46	0.14
11	2.71, dd (15.5, 7.7); 2.72, dd (15.5, 7.7)	50.75, 50.68	0.07
	2.40, dd (15.5, 5); 2.41, dd (15.5, 5)		
12	3.90, m	71.61, 71.47	0.14
13	1.17, d (6.3)	19.88, 19.84	0.04
14	3.56, dqd (9.1, 7.0, 4.2)	63.97, 63.95	0.02
	3.39, dqd (9.5, 7.0, 2.6)		
15	1.15, t (7.0)	15.49	-

<sup>a</sup> Measured in  $\text{CDCl}_3$ .

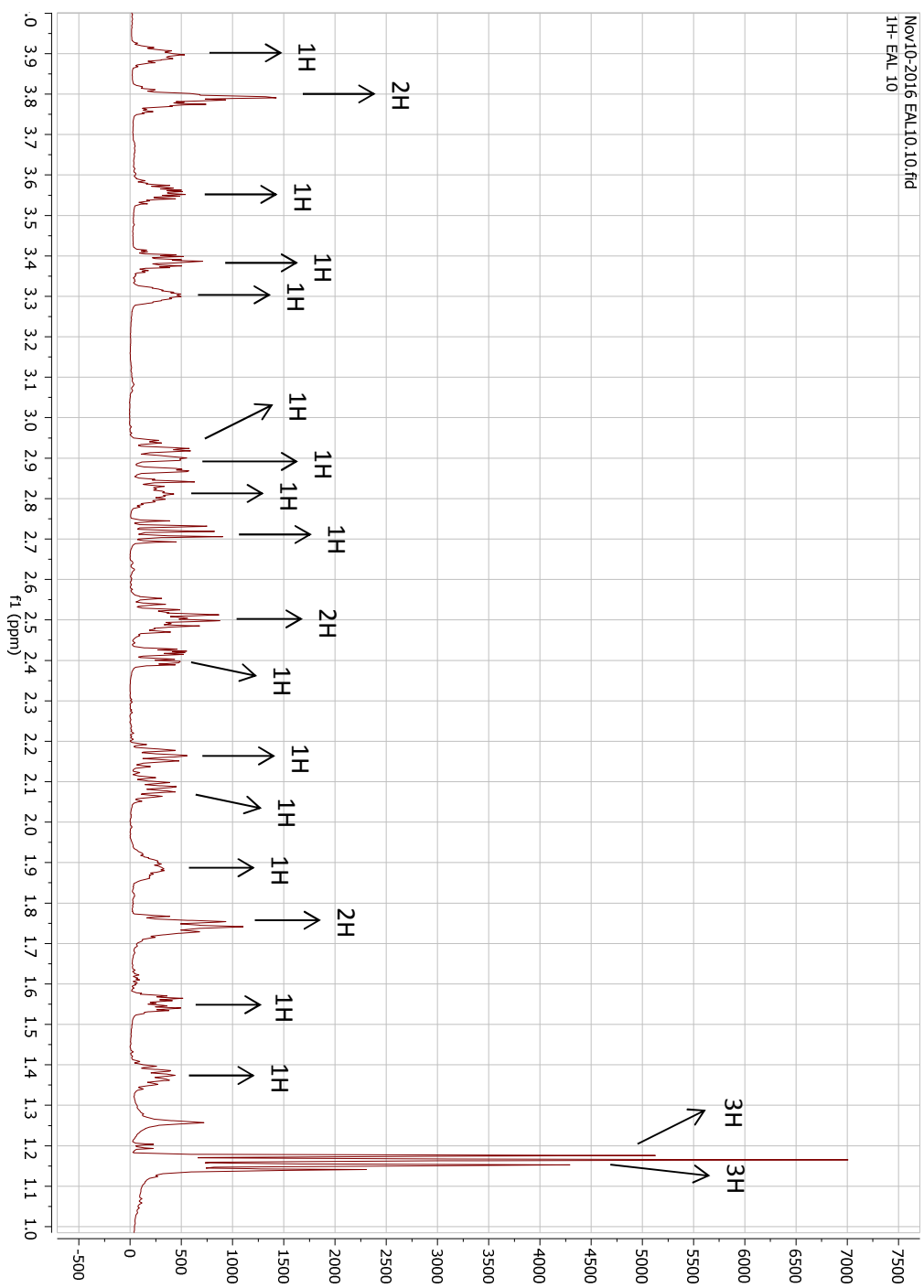


**Figure 3.49:**  $^1\text{H}$  NMR (600 MHz,  $\text{CDCl}_3$ ) spectrum of carpusinine F (**10a**) and epicarpusinine F (**10b**).

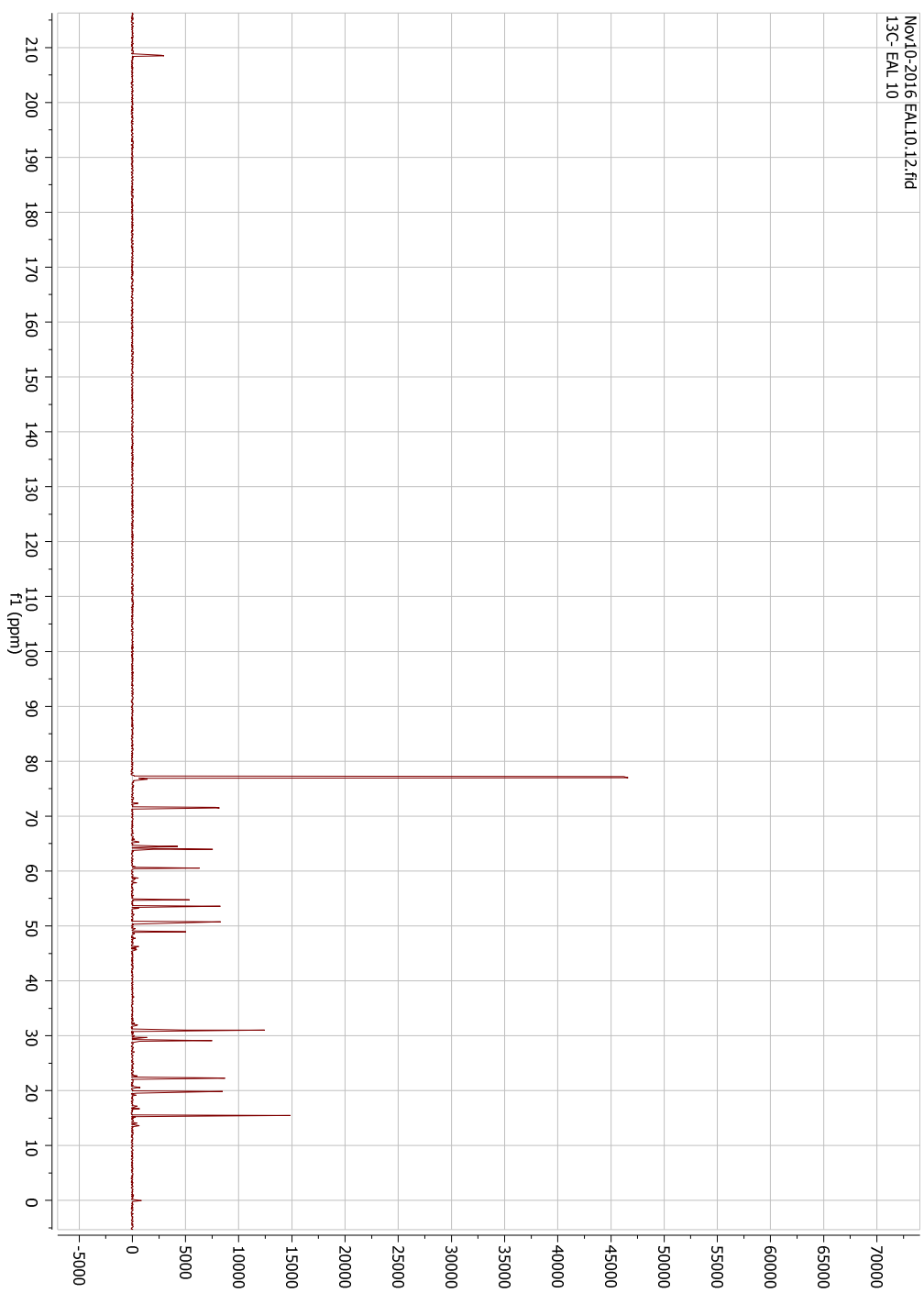


**Figure 3.50:**  $^{13}\text{C}$  NMR (150 MHz,  $\text{CDCl}_3$ ) spectrum of carpusinine F (**10a**) and epicarpusinine F (**10b**).

### 3.2.7 (+)-Elaeokanine A (**11**)

(+)-Elaeokanine A (**11**) has previously been isolated from *E. kaniensis* Schltr.<sup>85,48</sup> Compound **11** was obtained from *E. angustifolius* in the present study as a colourless oil with  $[\alpha]_D^{25} +46$  (c 0.5, CHCl<sub>3</sub>) (lit.  $[\alpha]_D +49^\circ$  (c 0.5, CHCl<sub>3</sub>)).<sup>85</sup> The UV spectrum (Appendix 62) for **11** showed an absorption maximum at 228 nm (log  $\epsilon$  1.63) which is characteristic of an  $\alpha,\beta$ -unsaturated ketone moiety.<sup>90</sup> The molecular formula of **11** was determined to be C<sub>12</sub>H<sub>19</sub>NO (Appendix 64) by HRESIMS ( $m/z$  194.1536 [M+H]<sup>+</sup>), corresponding to four degrees of unsaturation (Figure 3.51).

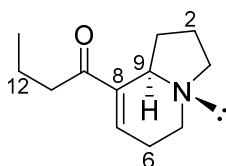


**Figure 3.51:** Structure of (+)-elaeokanine A (**11**).

The IR spectrum of **11** (Appendix 63) showed absorptions at 2874, 2792 and 2728 cm<sup>-1</sup>, which are characteristic of Bohlmann bands (lit. 2885, 2805 and 2740 cm<sup>-1</sup>). The presence of Bohlmann bands suggested a *trans*-fused ring junction for the indolizidine ring system. Additionally, the IR band observed at 1662 cm<sup>-1</sup> (lit. 1667 cm<sup>-1</sup>) indicated the presence of  $\alpha,\beta$ -unsaturated ketone moiety.<sup>48,56</sup>

The identity of compound **11** was confirmed by comparing the <sup>1</sup>H NMR data of **11** with those reported in the literature for (+)-elaeokanine A (Table 3.11 and Figure 3.52). One distinct methyl triplet was observed at  $\delta_H$  0.93 which corresponds to the methyl group at CH<sub>3</sub>-13. H-7 was observed to resonate at  $\delta_H$  6.87 which is characteristic of a trisubstituted olefinic methine hydrogen. The chemical shift of H-3 ( $\delta_H$  2.60, 2.91) and H-5 ( $\delta_H$  2.60, 2.73) are typical of aminomethylene hydrogens while the chemical shift of H-9 ( $\delta_H$  3.47) is typical of an

aminomethine hydrogen. The  $^1\text{H}$  NMR data of **11** are in good agreement with those reported in the literature, which led to the conclusion that **11** is (+)-elaekanine A.

**Table 3.11:**  $^1\text{H}$  NMR (600 MHz) data of **11** and synthetic samples of elaeokanine A ( $\delta$  in ppm).<sup>a</sup>

Position	<b>11</b>	(+)-elaekanine A <sup>85</sup>	(±)-elaekanine A <sup>91</sup>
	$\delta_{\text{H}}$ (J in Hz)	$\delta_{\text{H}}$ (J in Hz)	$\delta_{\text{H}}$ (J in Hz)
1	2.47, m	2.30 – 2.50, m	2.50, dt (8.8, 1.9)
	1.36, m	1.40, m	1.31 – 1.42, m
2	1.82, m	1.70 – 1.90, m	1.71 – 1.95, m
3	2.91, dt (10, 8)	2.80 – 3.00, m	2.70 – 3.00, m
	2.60, m	2.60, td (9, 3)	2.50, td (8.8, 1.9)
5	2.73, ddd (10.2, 8.5, 7.5)	2.30 – 2.80, m	2.70 – 3.00, m
	2.60, m	2.60, td (9, 3)	2.50, td (8.8, 1.9)
6	2.35, m	2.30 – 2.50, m	2.30 – 2.40, m
			1.71 – 1.95, m
7	6.87, td (4, 1.7)	6.87, s	6.89, t (1.8)
8	-	-	-
9	3.47, brs	3.52, brs	3.56, t (1.8 Hz)
10	-	-	-
11	2.85, m	2.80 – 3.00, m	2.70 – 3.00, m
	2.56, m	2.30 – 2.50, m	2.30 – 2.48, m
12	1.63, sextet (7.4)	1.61, q (7.0)	1.61, q (7.2)
13	0.93, t (7.4)	0.93, t (7.0)	0.93, t (7.2)

<sup>a</sup> Measured in  $\text{CDCl}_3$ .

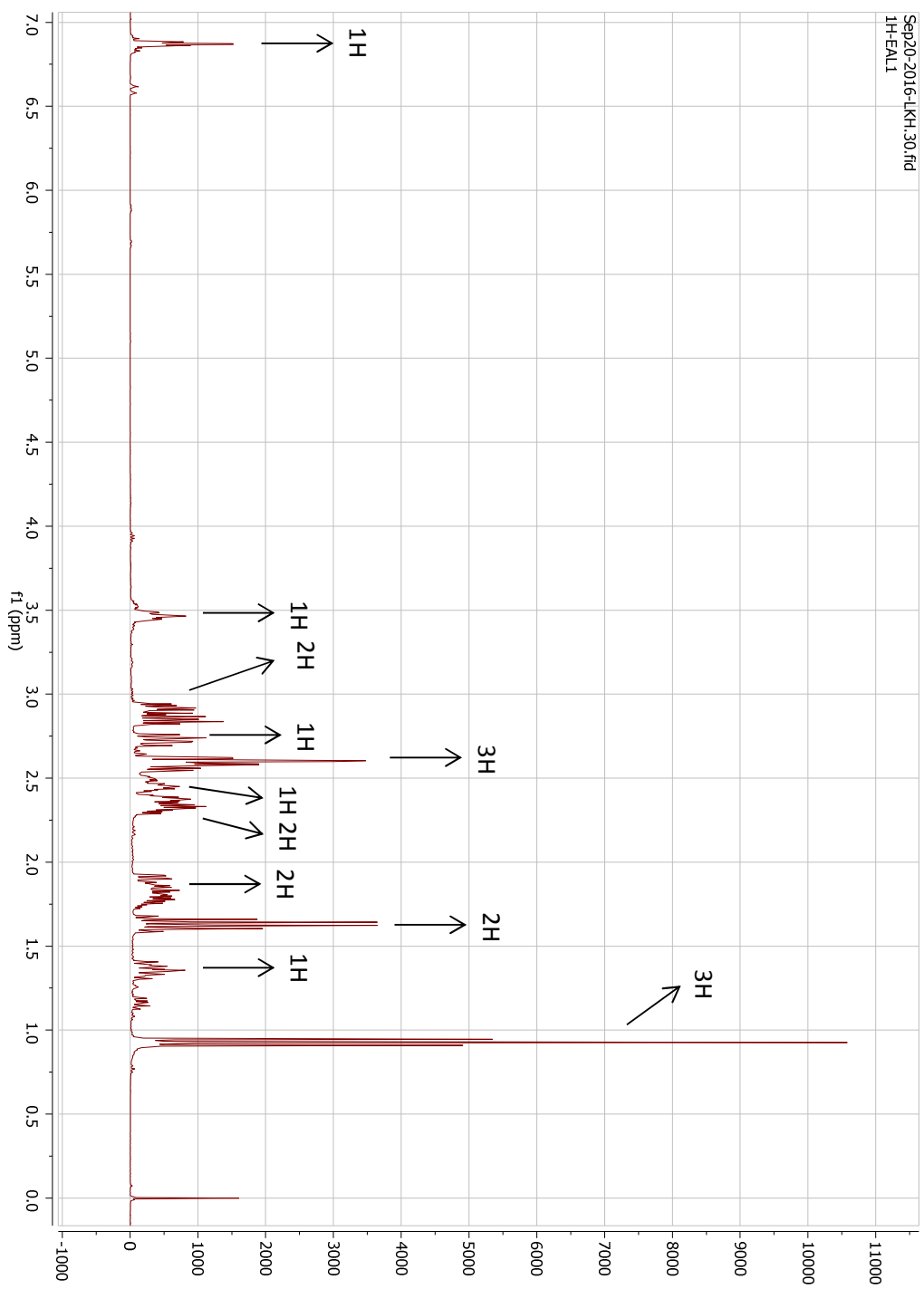


**Figure 3.52:**  $^1\text{H}$  NMR (600 MHz,  $\text{CDCl}_3$ ) spectrum to (+)-elaeokanine A (**11**).

### 3.2.8 Elaeokanine C (**12**)

Elaeokanine C (**12**) (Figure 3.53) was previously isolated from *E. kaniensis*.<sup>48</sup> It was obtained from *E. angustifolius* in the present study as a light yellowish oil with  $[\alpha]_D^{25} +3$  (c 0.3, CHCl<sub>3</sub>) (lit.  $[\alpha]_D +37^\circ$ ).<sup>70</sup> The very small optical rotation value obtained suggested that **12** was isolated as a scalemic mixture. The molecular formula of **12** was determined to be C<sub>12</sub>H<sub>21</sub>NO<sub>2</sub> (Appendix 66) by HRESIMS ( $m/z$  212. 1661 [M+H]<sup>+</sup>), corresponding to three degrees of unsaturation.

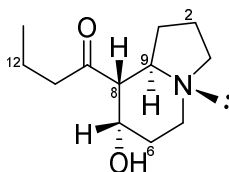


**Figure 3.53:** Structure of elaeokanine C (**12**).

The IR spectrum of **12** (Appendix 65) showed absorption bands at 3384 (OH) and 1708 cm<sup>-1</sup> (C=O).<sup>5</sup> The set of data observed for **12** is in line with those obtained for elaeokanine C reported in literature.

The identity of compound **12** was confirmed by comparing the <sup>1</sup>H NMR data of **12** with those reported in the literature for elaeokanine C (Table 3.12 and Figure 3.54). The <sup>1</sup>H NMR data of **12** revealed the presence of one methyl triplet at  $\delta_H$  0.92, attributed to CH<sub>3</sub>-13. The signal for H-7 was observed at  $\delta_H$  4.22, which is characteristic of oxymethine hydrogen. Other distinct signals observed in the <sup>1</sup>H NMR spectrum were H-3 ( $\delta_H$  2.50, 3.06), H-5 ( $\delta_H$  2.50, 2.87) and H-9 ( $\delta_H$  2.59). These are typical of aminomethylene hydrogens (H-3 and H-5) and aminomethine hydrogen (H-9). The <sup>1</sup>H NMR data of **12** are in good agreement with those reported in the literature, which led to the conclusion that **12** is elaeokanine C.

**Table 3.12:** <sup>1</sup>H NMR (600 MHz) data of **12** and (±)-elaeokanine C (δ in ppm).<sup>a</sup>

Position	<b>12</b>	(±)-Elaeokanine C <sup>86</sup>
	δ <sub>H</sub> ( <i>J</i> in Hz)	δ <sub>H</sub> ( <i>J</i> in Hz)
1	1.85, m 1.41, m	1.70 – 2.00, m 1.40, m
2	1.79, m 1.62, sextet (7.3)	1.70 – 2.00, m 1.63, sextet (8)
3	3.06, td (8.8, 2.4) 2.50, m	3.06, t (8.8) 2.40 – 2.62, m
5	2.87, ddd (11.2, 4.9, 2.1) 2.50, m	2.87, d (11.0) 2.40 – 2.62, m
6	1.62, sextet (7.3) 2.20, q (9)	1.63, sextet (8) 2.22, q (9.8)
7	4.22, brs	4.26, brs
8	2.43, m	2.40 – 2.62, m
9	2.59, m	2.40 – 2.62, m
10	-	-
11	1.79, m 2.43, m	1.70 – 2.00, m 2.40 – 2.62, m
12	1.79, m	1.70 – 2.00, m
13	0.92, t (7.4)	0.93, t (8)

<sup>a</sup> Measured in CDCl<sub>3</sub>.

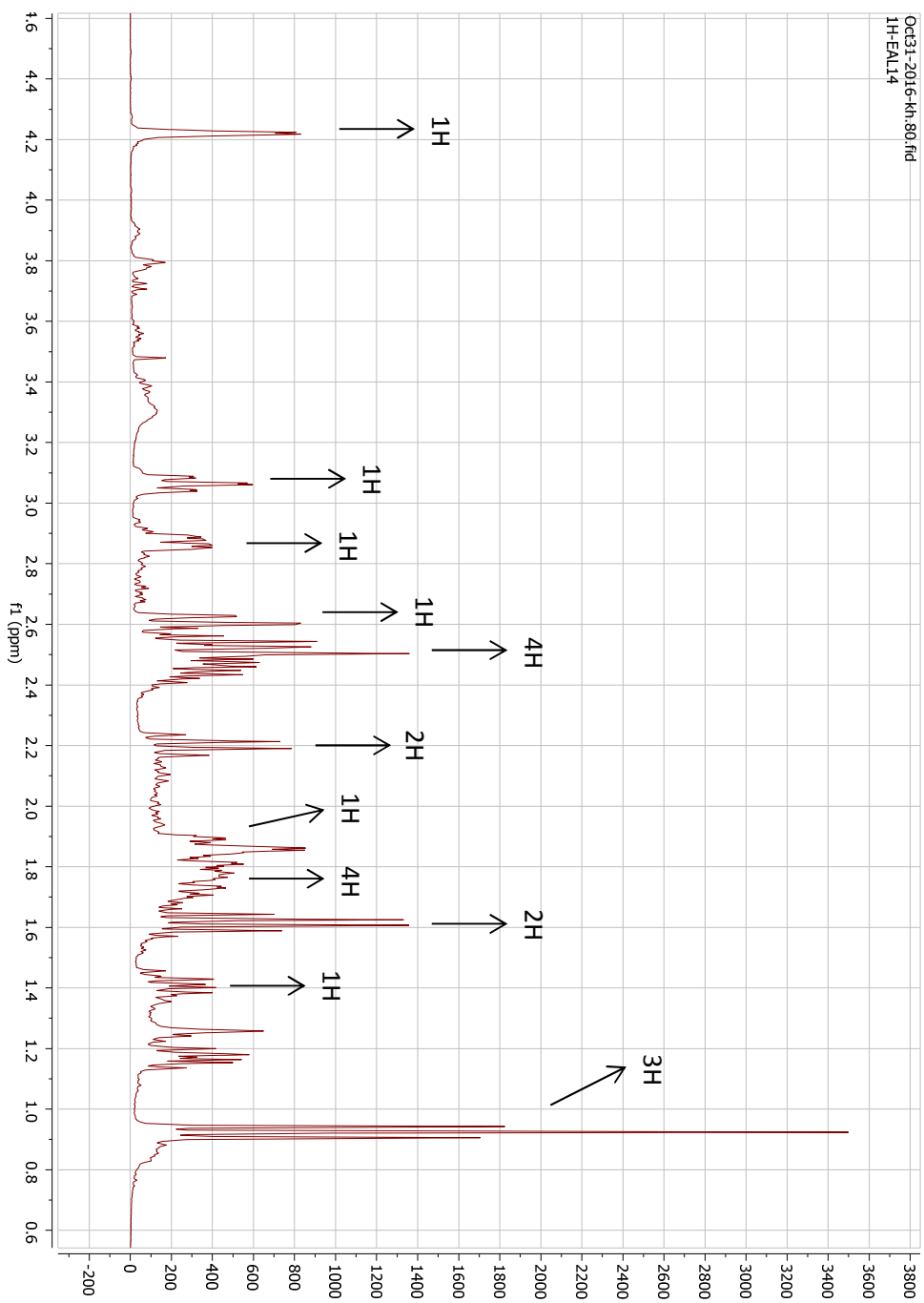
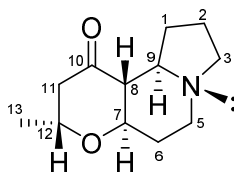


Figure 3.54:  $^1\text{H}$  NMR (600 MHz,  $\text{CDCl}_3$ ) spectrum of elaeoakanine C (**12**).

### 3.2.9 Elaeokanine D (13)

Elaeokanine D (**13**) (Figure 3.55) was previously isolated from *E. kaniensis*<sup>48</sup> and was obtained from *E. angustifolius* in the present study as a light yellowish oil with  $[\alpha]_D^{25} +2$  (c 0.2, CHCl<sub>3</sub>) (lit.  $[\alpha]_D +51$ ).<sup>48</sup> The very small optical rotation value obtained indicated that **13** was isolated as a scalemic mixture. The IR spectrum (Appendix 67) showed absorptions at 2855, 2790 and 2717 cm<sup>-1</sup> which are characteristic of Bohlmann bands (2855, 2790 and 2717 cm<sup>-1</sup>) was observed. Additionally, absorption bands at 1711 (C=O) and 1073 cm<sup>-1</sup> (C-O) were also observed. The molecular formula of **13** was determined to be C<sub>12</sub>H<sub>20</sub>NO<sub>2</sub> (Appendix 68) by HRESIMS (*m/z* 210.1502 [M+H]<sup>+</sup>), corresponding to four degrees of unsaturation.



**Figure 3.55:** Structure of (+)-elaeokanine D (**13**).

The identity of compound **13** was confirmed by comparing the <sup>1</sup>H NMR data of **13** with those reported in the literature for elaeokanine D (Table 3.13). Unfortunately, the NMR data previously reported for elaeokanine D was incomplete. However, it was still sufficient to confirm the identity of **13**. <sup>1</sup>H NMR data of **13** revealed the presence of one methyl doublet at  $\delta_H$  1.26, attributed to CH<sub>3</sub>-13. The signals due to H-7 and H-12 were observed at  $\delta_H$  3.65 and 4.63, which are characteristic of oxymethine hydrogens. Other distinct signals observed in the <sup>1</sup>H NMR were H-3 ( $\delta_H$  2.32, 3.00), H-5 ( $\delta_H$  2.13, 3.12) and H-9 ( $\delta_H$  2.00). These are typical of aminomethylene hydrogens (H-3 and H-5) and aminomethine hydrogen (H-9). The <sup>1</sup>H NMR data

of **13** are in good agreement with the key NMR data reported in the literature, which led to the conclusion that **13** is elaeokanine D.

**Table 3.13:**  $^1\text{H}$  NMR (600 MHz) data of **13** and (+)-elaekanine D ( $\delta$  in ppm).<sup>a</sup>

Position	<b>13</b>	(+)-Elaekanine D
	$\delta_{\text{H}}$ ( $J$ in Hz)	$\delta_{\text{H}}$ ( $J$ in Hz)
1	2.10, m 1.36, qd (11.4, 7)	
2	1.85, m 1.76, m	
3	3.00, td (8.7, 2.4) 2.32, m	
5	3.12, dt (11.6, 4) 2.13, m	
6	1.94, m 1.86, m	
7	3.65, td (10, 5)	3.65, td (10, 8)
8	2.34, t (10)	2.34, t (10)
9	2.00, td (10, 6.2)	
10	-	-
11	2.88, dd (13.4, 7) 2.20, dd (13.4, 2)	2.87, dd (14, 7) 2.18, dd (14, 2)
12	4.63, quintet of doublets, (7, 2)	4.62, quintet of doublets, (7, 2)
13	1.26, d (7)	1.26, d (7)

<sup>a</sup> Measured in  $\text{CDCl}_3$ .

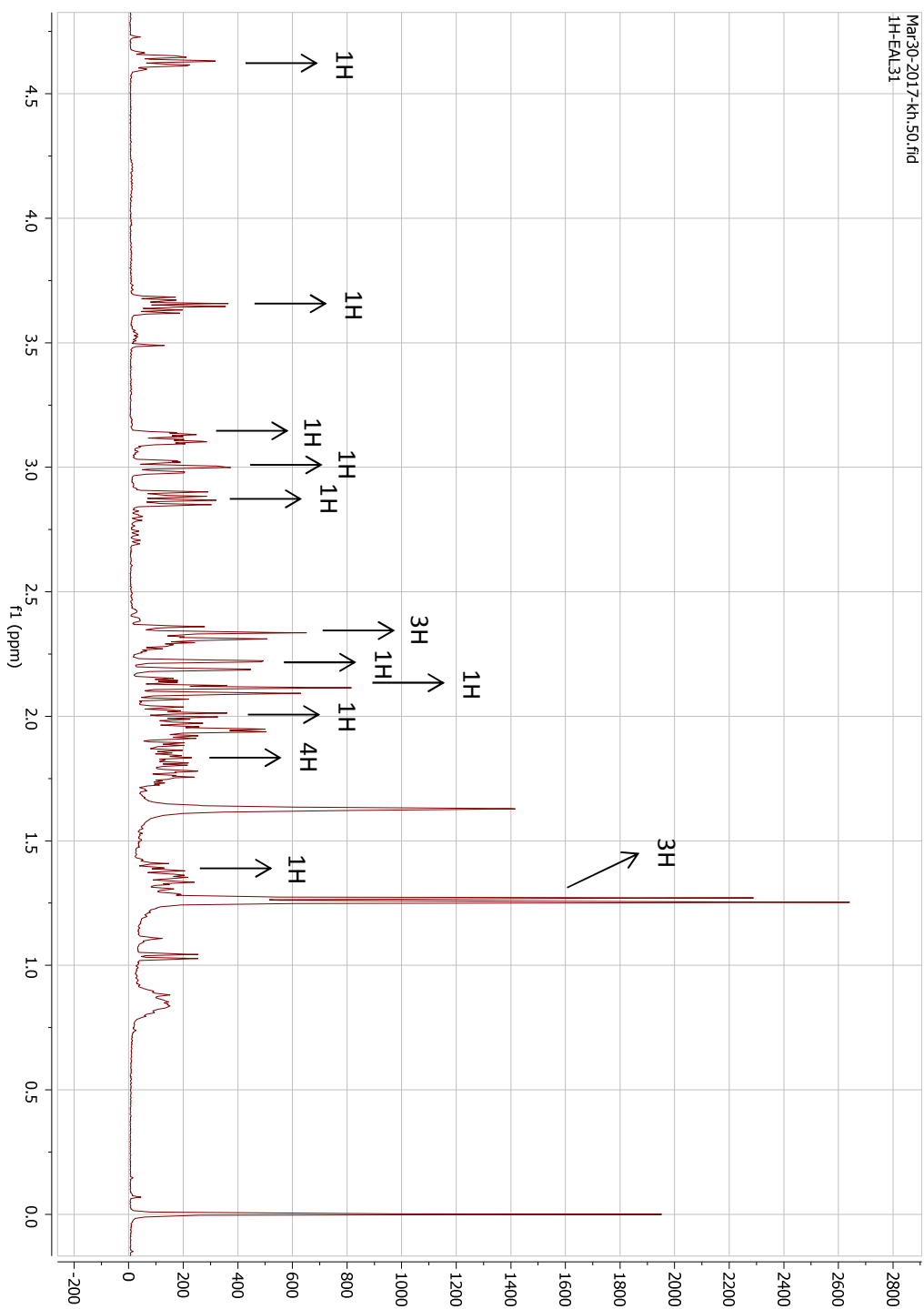


**Figure 3.56:**  $^1\text{H}$  NMR (600 MHz,  $\text{CDCl}_3$ ) spectrum to (+)-elaeokanine D (**13**).

### 3.2.10 Carpusidine (14)

Carpusidine (**14**) (Figure 3.57) is a simple indolizidine alkaloid obtained as a light yellowish oil with  $[\alpha]_D^{25} +1$  ( $c$  0.56,  $\text{CHCl}_3$ ). The very small optical rotation value suggested that carpusidine (**14**) was isolated as a racemic mixture. The molecular formula of **14** was determined by HRESIMS ( $m/z$  154.1228  $[\text{M}+\text{H}]^+$ ) to be  $\text{C}_9\text{H}_{15}\text{NO}$  (Appendix 70), corresponding to three degrees of unsaturation. In addition to the band due to a ketone group ( $1717\text{ cm}^{-1}$ ), the IR spectrum (Appendix 69) showed the presence of the characteristic Bohlmann bands at 2878, 2852 and  $2793\text{ cm}^{-1}$ .

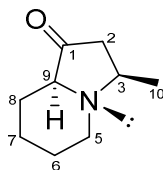


Figure 3.57: Structure of carpusidine (**14**).

The  $^1\text{H}$  NMR of carpusidine (**14**) (Table 3.14 and Figure 3.60) revealed the presence of one doublet at  $\delta_{\text{H}}$  1.21 corresponding to  $\text{CH}_3$ -10. H-3 ( $\delta_{\text{H}}$  2.42), H-5 ( $\delta_{\text{H}}$  2.14, 3.30) and H-9 ( $\delta_{\text{H}}$  2.33) all have chemical shifts typical of aminomethine groups (H-3 and H-9) and aminomethylene group (H-5). The  $^{13}\text{C}$  NMR data of carpusidine (**14**) (Table 3.14 and Figure 3.61) showed the presence of nine carbon resonances, which confirmed the molecular formula established by HRESIMS. The most downfield carbon shift was observed at  $\delta_{\text{C}}$  209.0, which was characteristic of the ketone function at C-1, while the most upfield carbon shift was observed at  $\delta_{\text{C}}$  21.4, attributed to the methyl group at C-10.

The COSY and HSQC data revealed the presence of  $\text{CHCH}_3$  and  $\text{CH}_2\text{CH}_2\text{CH}_2\text{CH}_2$  fragments corresponding to the C-3–C-10 and C-5–C-6–C-7–C-8 partial structures in **14** (Figure 3.58). The HMBC data (Figure 3.58) confirmed the partial structures established by the COSY data as well as aided in the elucidation of the gross structure of **14**. The  $\text{CH}_2\text{CH}_2\text{CH}_2\text{CH}_2$  fragment was

associated with the piperidine ring based on the chemical shift of C-5 ( $\delta_c$  50.6) which is typical of an aminomethylene group. The connectivity within this fragment (i.e., aminobutylene) was supported by the observed HMBC correlations from H-5 and H-6 to C-7; and from H-8 to C-7. The aminomethine C-9 ( $\delta_c$  63.9) was also connected to the aminobutylene fragment based on the three-bond correlations from H-7 and H-8 to C-9; and from H-9 to C-7 and C-8. C-2 was determined to be associated with the CHCH<sub>3</sub> fragment based on the three-bond correlations from H-3 and H-10 to C-2. The ketone group was assigned to C-1 based on the two-bond correlations from H-2 and H-8 to C-1; and from H-9 to C-2. Finally, the indolizidine ring junction was readily established based on the correlations from H-3 to C-5 and C-9; from H-5 to C-3 and C-9; from H-8 to C-1; and from H-9 to C-3 and C-5. Other HMBC correlations in support of the gross structure of **14** are shown in Figure 3.58.



**Figure 3.58:** COSY (bold bonds) and HMBC <sup>1</sup>H-<sup>13</sup>C correlations (arrows) of carpusidine (**14**).

Due to overlapping of several key signals, useful coupling constants could not be extracted from the <sup>1</sup>H NMR spectrum for most of the hydrogens to aid with stereochemical assignment. Fortunately, the splitting pattern and coupling constant for H-3 were determined to be dqd ( $J = 10.5, 6.2, 4.1$  Hz). The large coupling constant (10.5 Hz) observed for H-3 was due to its coupling with H-2 $\beta$  via a *trans*-diaxial-like interaction. This observation required H-3 to be  $\alpha$ -oriented, which also implied that CH<sub>3</sub>-10 is equatorially oriented ( $\beta$ ). The relative configurations of **14** at C-3 and C-9 could also be assigned based on the NOESY data (Figure 3.59). Firstly, the Bohlmann bands observed in the IR spectrum indicated a *trans*-fused ring junction. Subsequently, the NOEs observed for H-3/H-5 $\alpha$  and H-5 $\beta$ /CH<sub>3</sub>-10 confirmed the orientation of CH<sub>3</sub>-10 as  $\beta$ -equatorial. This conclusion is also consistent with the key NOEs observed for H-5 $\beta$ /H-6 $\beta$ , H-

6 $\beta$ /H-8 $\beta$ , and H-7 $\alpha$ /H-9. The relative configuration of **14** at C-3 and C-9 was therefore established as 3*R*,9*S* (Figure 3.59) with the piperidine ring being in chair conformation.

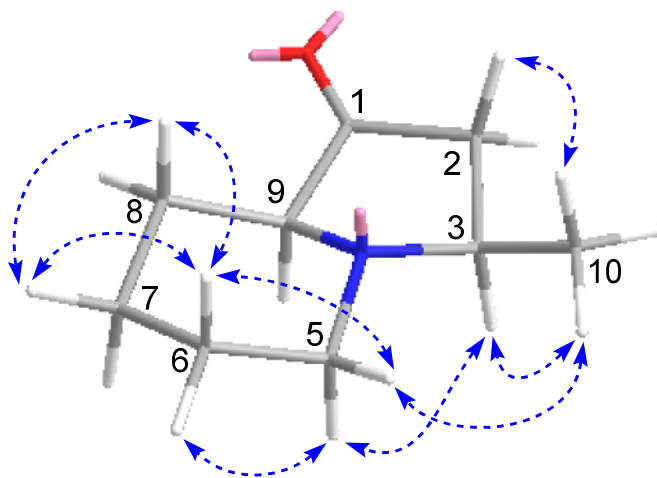
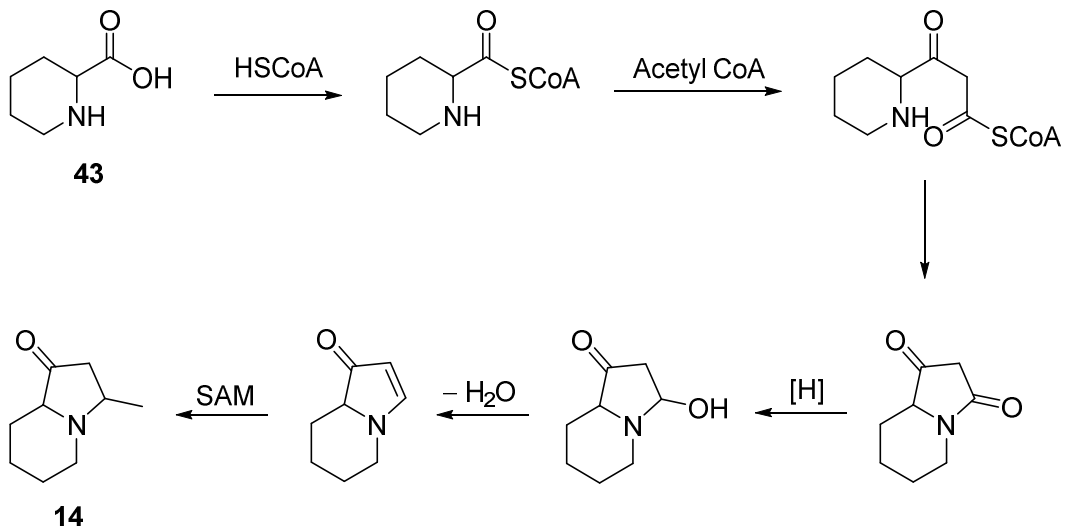


**Figure 3.59:** Selected NOESY correlations of carpusidine (**14**).

Carpusidine (**14**) represents a new compound and the first simple indolizidine compound to be isolated from Elaeocarpaceae. However, a synthetic intermediate made in an attempt to synthesize the lupin alkaloid, norlupinane, was found to possess identical 2D structure as **14**. A detailed NMR comparison of the two compounds was not possible as no NMR data was published for the synthetic work.<sup>92</sup>

Scheme 3.11 outlines the proposed biosynthetic pathway to carpusidine (**14**) which was based on the pathway to simple indolizidine alkaloids such as castanospermine (**44**) (see Scheme 1.5 in section 1.2.5.2). Pipecolic acid (**43**), derived from L-lysine, was presumed to be a key intermediate. Formation of CoA ester of **43** followed by Claisen reaction with a molecule of acetyl CoA<sup>44</sup> and ring closure via lactamization gives the indolizidine ring system. Subsequent reductive transformation and methylation by the enzyme SAM<sup>93</sup> yield carpusidine (**14**).



**Scheme 3.11:** Plausible biosynthesis pathway to carpusidine (**14**).

**Table 3.14:**  $^{13}\text{C}$  (150 MHz) and  $^1\text{H}$  NMR (600 MHz) data of carpusidine (**14**) ( $\delta$  in ppm).<sup>a</sup>

Position	$\delta_{\text{C}}$	$\delta_{\text{H}}$ ( $J$ in Hz)
1	209.0	-
2	48.6	2.29, m 2.29, m
3 (ax-like)	56.7	2.42, dqd (10.5, 6.2, 4.1)
5 $\beta$ (eq)	50.6	3.30, td (9, 2.3)
5 $\alpha$ (ax)		2.14, q (9)
6 $\beta$ (ax)	21.3	1.94, m
6 $\alpha$ (eq)		1.82, m
7 $\alpha$ (ax)	30.9	1.96, m
7 $\beta$ (eq)		1.56, m
8 $\alpha$ (eq)	47.2	2.51, br dd (11, 2)
8 $\beta$ (ax)		2.32, m
9 (ax)	63.9	2.32, m
10 (eq)	21.4	1.21, d (6.2)

<sup>a</sup> Measured in  $\text{CDCl}_3$ .

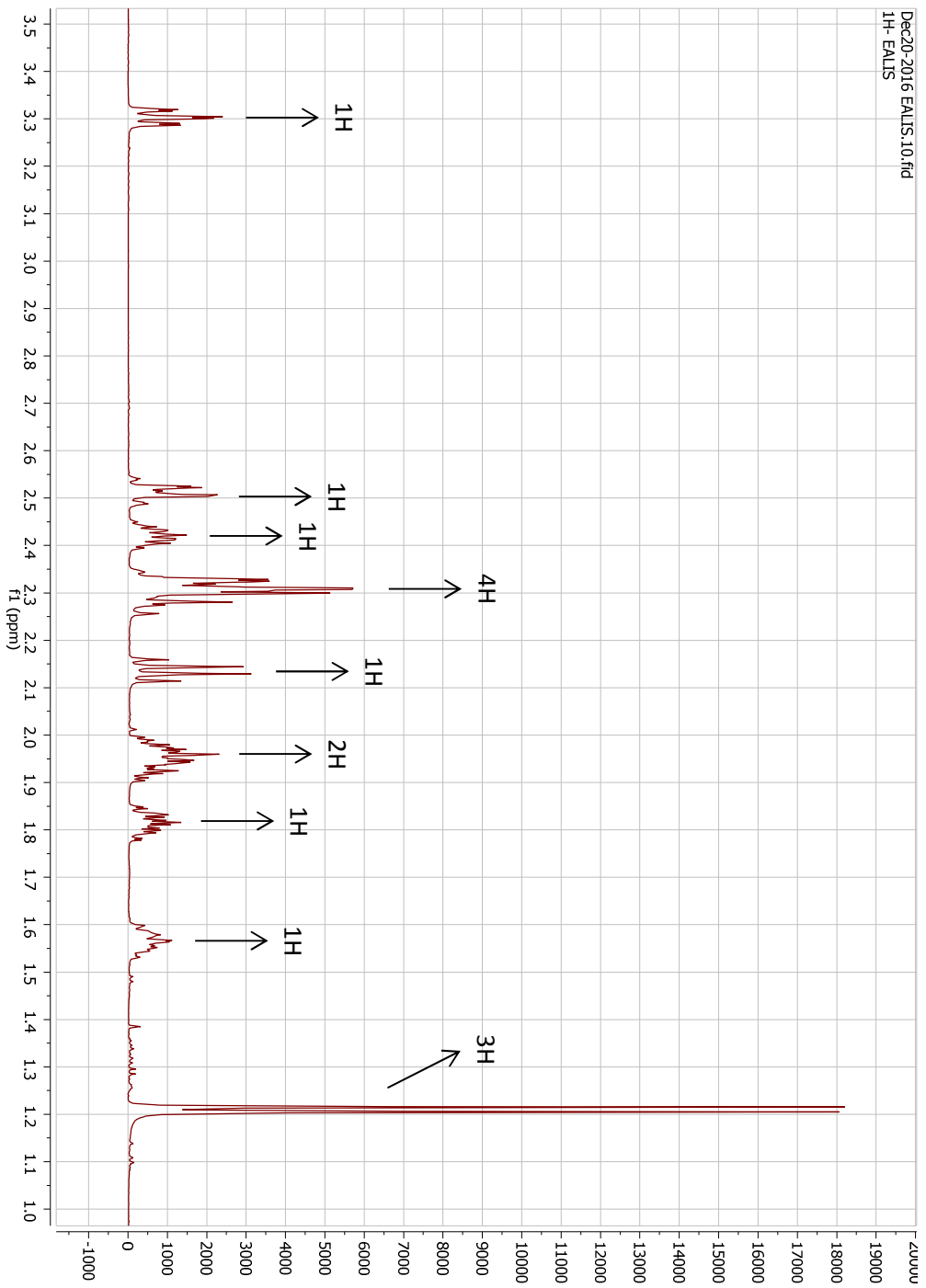


Figure 3.60: <sup>1</sup>H NMR (600 MHz, CDCl<sub>3</sub>) of carpusidine (14).



### 3.3 Cytotoxic evaluation of alkaloids from *Elaeocarpus angustifolius* on cancer cell lines

It was previously noted that indolizidine alkaloid-containing plants are toxic or poisonous to livestock.<sup>94</sup> This prompted the screening of selected indolizidine alkaloids obtained in the present study for cytotoxic activity. Compounds **5**, **6**, **7a/7b**, **9**, **11**, **12**, **13** and **14** were assessed for cytotoxic activity by using the CellTiter-Glo Luminescent Cell Viability Assay.

**Table 3.15:** Anti-proliferative activity of selected alkaloids isolated from *Elaeocarpus angustifolius* against a panel of selected cancer and normal cell lines.

	Percentage of Cell Viability (%)									
	Sample	5	6	7a/7b	9	11	12	13	14	Control (0.1% DMSO)
Breast Cancer	MCF7	41.9	78.4	34.2	54.7	55.0	56.5	48.7	33.7	100.0
	MDA-MB-231	76.4	104.6	90.6	81.2	89.0	83.3	90.2	78.7	100.0
	MDA-MB-468	60.3	116.2	50.9	55.1	75.5	67.6	80.1	50.2	100.0
	SKBR3	70.9	123.1	89.0	95.4	101.3	58.5	111.9	87.3	100.0
	T47D	60.6	74.4	34.9	81.8	73.1	67.0	73.7	66.6	100.0
Colorectal Cancer	Caco2	100.5	116.7	99.8	89.3	112.5	107.6	102.4	120.4	100.0
	HCT116	59.7	84.4	57.4	64.9	67.5	61.9	75.0	60.8	100.0
	HT29	58.5	82.1	41.5	86.2	73.8	59.8	73.8	69.2	100.0
	Sw48	59.3	93.1	<b>32.5</b>	93	89.8	69.9	79.2	69.8	100.0
Lung Cancer	A549	62.6	78.8	54.0	91.8	83.9	114.3	71.2	85.5	100.0
	H1299	110.3	151.4	112	88.6	126.3	125.7	108.7	120.1	100.0
Nasopharyngeal Cancer	CNE1	96.4	125.6	50.3	90.3	110.1	120.0	109.0	107.6	100.0
	HK1	78.6	99.8	71.3	96.2	98.7	83.1	89.5	95.1	100.0
	SUNE1	170.5	175.3	166.2	173.3	177.8	158.3	163.1	186.3	100.0
Neuroblastoma	SHSY5Y	49.8	100.6	47.1	46.1	76.0	62.3	78.9	59.8	100.0
Pancreatic Cancer	AsPC1	84.0	93.8	62.2	86.1	108.7	96.5	81.0	89.1	100.0
	BxPC3	100.9	122.2	58.3	76.4	122.5	118.3	97.3	120.8	100.0
	SW1990	50.5	79.2	43.1	68.1	62.2	54.5	56.9	53.3	100.0
Breast Cells	MCF10A	90.5	123.7	45.0	117.5	116.1	76.3	97.4	75.7	100.0
Lung Cells	MRC5	99.4	125	98.3	116.6	135.0	85.9	111.0	114.7	100.0

The panel of selected cell lines were treated with the test compounds at 100  $\mu$ M and incubated for 72 hours. The results were recorded as percentage of cell viability (Table 3.15). A potent cytotoxic compound would be expected to return a low percentage of cell viability value, i.e., 10% or lower. Unfortunately, all of the test compounds showed percentage of cell viability that is greater than 30%. This indicated that all the test compounds were essentially non-cytotoxic to both the cancer and normal cell lines tested.

Compounds **1** – **4**, **8** and **10** were not included in the cytotoxicity study due to scarcity of material (low yields).

## CHAPTER 4: CONCLUSION AND FUTURE STUDIES

### 4.1 Conclusion

Chromatographic fractionation and purification of the alkaloid mixtures of the leaves of *E. tectorius* and *E. angustifolous* gave a total of 16 alkaloids including two pyrrolidine alkaloids, four phenylethylamine alkaloids and ten indolizidine alkaloids.

The phenylethylamine alkaloids were obtained from the leaves of *E. tectorius*, namely, tectoricine (**1**), tectoraline (**2**), tectoramidine A (**3**), and tectoramidine B (**4**). These compounds represent the first occurrence of phenylethylamine alkaloids from the *Elaeocarpus* genus. With respect to alkaloid content, only indolizidine, pyrrolidine and indole alkaloids were previously reported from nine *Elaeocarpus* species. Therefore, compounds **1–4**, which display phenethylamine as a common structural feature, represent another distinct class of alkaloids from *Elaeocarpus*. Unfortunately, the lack of compounds **1–4** due to poor isolation yields and decomposition has precluded biological evaluation.

The structure of tectoricine (**1**) suggests that it is a monoterpenoid phenethylamine possessing an irregular monoterpene skeleton. Tectoricine (**1**) represents a new class of alkaloids in which the phenethylamine nitrogen atom is incorporated into a novel isoquinuclidinone ring system that is substituted with three methyl groups (1, 1, 2-trisubstitution) and an acetyl side chain. Tectoraline (**2**) represents a rare naturally occurring amide incorporating two phenethylamine moieties. It is the first example of an alkamide that appears to be derived from a molecule of 2-hexenoic acid and two molecules of phenethylamine. Tectoramidine A (**3**) represents the first naturally occurring trimeric phenethylamine alkaloid incorporating a rare trisubstituted amidine function with an exocyclic C=N as a partial structure, while tectoramidine B (**4**) is a dimeric phenethylamine alkaloid representing the first naturally occurring formamidine obtained from plants. Tectoramidines A and B (**3** and **4**) represent the first naturally occurring trimeric and dimeric phenethylamine alkaloids incorporating an amidine function.

A total of 12 alkaloids were obtained from the leaves of *Elaeocarpus angustifolius*. Seven of these are new indolizidine alkaloids, namely, carpusinine A (**5**), carpusinine B (**6**), carpusinine C (**7a**), epicarpusinine C (**7b**), carpusinine D (**8**), carpusinine E (**9**) and

carpusidine (**14**), while two are new pyrrolidine alkaloids, namely, carpusidine F (**10a**) and epicarpusidine F and (**10b**). The remaining three alkaloids are known compounds previously isolated from *E. kaniensis*, namely, (+)-elaekanine A (**11**), elaekanine C (**12**) and elaekanine D (**13**).

Apart from the simple alkylindolizidinone alkaloid, carpusidine (**14**), all the compounds isolated from *E. angustifolous* are elaekanine-type indolizidine alkaloids. Carpusidine A (**5**) represents the first *Elaeocarpus* alkylindolizidine alkaloid with a hydroxyl group attached to its side chain at C-12. Carpusidine B (**6**) represents the 7-dehydroxy-derivative of elaekanine C (**12**). Carpusidine C and epicarpusidine C (**7a** and **7b**) were isolated as a pair of inseparable epimers and represent the 12-ethoxy derivatives of carpusidine B (**6**). Carpusidine D (**8**) incorporates a 7-hydroxy-8-ketoindolizidine moiety with the same relative configuration as that found in elaekanine C (**12**) and therefore is a 12-ethoxy derivative of elaekanine C (**12**). Compounds **7a**, **7b** and **8** are the first *Elaeocarpus* alkylindolizidine alkaloids to incorporate an ethoxy functional group to their structures. The gross structure of **9** was found to be identical to that of the isomeric alkaloids, elaekanes D (**13**) and E (**57**). It represents the C-12-epimer of elaekanine D (**13**), both of which were successfully purified as single compounds from the leaves of *E. angustifolius*. Carpusidine F (**10a**) and epicarpusidine F (**10b**) were isolated as a pair of inseparable epimers and represent rare dialkylated pyrrolidine alkaloids produced by *Elaeocarpus* genus. Carpusidine (**14**) represents the first simple indolizidine alkaloid to be isolated from Elaeocarpaceae.

Compounds **5**, **6**, **7a/7b**, **9**, **11**, **12**, **13** and **14** were found to be non-cytotoxic when assessed using the CellTiter-Glo Luminescent Cell Viability Assay against a panel of 20 cancer cell lines and two normal human cell lines.

#### 4.1 Future studies

The future studies for the present project will involve the re-isolation of alkaloids from the leaves of *E. tectorius* for the purpose of biological testing. The compounds isolated from *E. angustifolius* will also be evaluated for their opioid receptor activity. The expectation is to identify some interesting structure-activity relationships from the isolated compounds as similar compounds isolated in the past from the *Elaeocarpus* species have been shown to produce similar biological activity.<sup>71,72</sup> Additionally, the absolute configuration of carpusinine A (**5**) obtained from *E. angustifolius* will be determined using experimental and theoretical ECD data.

Out of 200 characterised species, only nine species of *Elaeocarpus* have been phytochemically studied for their alkaloid content. Therefore, future studies will include phytochemical investigation of other *Elaeocarpus* species to discover other alkaloids with new structures and interesting biological activity.

## REFERENCES

- 1 Cragg, G. M.; Newman, D. J. *Biochim. Biophys. Acta - Gen. Subj.* **2013**, *1830*, 3670–3695.
- 2 Hamburger M.; Hostettmann K. *Phytochemistry*, **1991**, *30*, 3864–3874.
- 3 Tetik F.; Civelek S.; Cakilcioglu U. *J. Ethnopharmacol.*, **2013**, *146*, 331–346.
- 4 Samuelsson G.; Bohlin L. In *history of natural products in medicine: Drugs of natural origin : A treatise of Pharmacognosy*; 6th rev. ed.; Apotekarsocietete: Stockholm, 2009; pp 17 –40.
- 5 Cordell G. A. *Phytochem. Lett.*, **2015**, *11*, 332–346.
- 6 S. D. Sarker, Z. Latif and A. I. Gray, In *Natural Product Isolation: Natural Products Isolation*; 2nd ed.; S. D. Sarker, Z. Latif and A. I. Gray (Eds.) , Humana Press: Totowa, New Jersey, 2005; pp. 1–25.
- 7 Dahanukar S. A.; Kulkarni R. A.; Rege N. N. *Indian J. Pharmacol.*, **2000**, *32*, 81–118.
- 8 Jantan I. *J. Sains Kesihat. Malaysia*, **2004**, *2*, 27–46.
- 9 Balunas M. J.; Kinghorn A. D. *Life Sci.*, **2005**, *78*, 431–441.
- 10 Bindseil K. U.; Jakupovic J.; Wolf D.; Lavayre J.; Leboul J.; Van Der Pyl D. *Drug Discov. Today*, **2001**, *6*, 840–847.
- 11 Xu R., Ye Y. and Zhao W., In *Extraction and Isolation of Natural Products: Introduction to Natural Products Chemistry*, Xu R., Ye Y. and Zhao W. (Eds.), CRC Press: London, New York, 2010; pp 5.
- 12 Kar A. In *introduction: Pharmacognosy and pharmacobiotechnology*, New Age International, New Delhi, 2nd ed., 2003, pp. pp 1-40.
- 13 Sasidharan S.; Chen Y.; Saravanan D.; Sundram K. M.; Yoga Latha L. *African J. Tradit. Complement. Altern. Med.*, **2011**, *8*, 1–10.

- 14 Petrovska B. *Phcog Rev.*, **2012**, 6, 1.
- 15 Umihara H.; Yokoshima S.; Inoue M.; Fukuyama T. *Chem. Eur. J.*, **2017**, 23, 6993–6995.
- 16 M. Hesse, In *Bioactive Alkaloids: Structure and Biology: Alkaloids: Nature's curse or blessing?*, WILEY-VCH Verlag: Zurich, 2002, pp 1–22 .
- 17 Cordell G. A. In *Putrescine, spermidine, spermine, and related polyamine alkaloids: The Alkaloids: Chemistry and Biology*; Gulf Professional Publishing, 58 vol., 2002, pp. 83–338
- 18 Belebony R.; Pizzo A.; Fontana A.; Carolino R.; Coutinho-Netto J.; Santos D. W. *Eur. J. Pharmacol.*, **2004**, 493, 1–17.
- 19 Nelson J. K.; Frølund S. U.; Tikhonov D. B.; Kristensen A. S.; Strømgaard K. *Angew. Chem. Int. Ed. - Int. Ed.*, **2009**, 48, 3087–3091.
- 20 Lau G. W.; Hassett D. J.; Ran H.; Kong F. *Trends Mol. Med.*, **2004**, 10, 599–606.
- 21 Marion L. In *Sinomenine: The Alkaloids: Chemistry and Physiology*, vol. 2; Academic Press, 1952; pp 219 - 260
- 22 Thomas D. W.; Achenbach H.; Biemann K. *J. Am. Chem. Soc.*, **1966**, 88, 3423–3426.
- 23 Blunden G.; Gordon S. M.; McLean W. F. H.; Keysell G. R. *Phytochemistry*, **1983**, 22, 293.
- 24 Li W.; Gong S.; Wen D.; Che B.; Liao Y.; Liu H.; Feng X.; Hu S. *J. Chromatogr. A.*, **2004**, 1049, 211–217.
- 25 Bruneton J. In *Alkaloids: Pharmacognosy, Phytochemistry, Medicinal Plants*; 2nd ed.; Lavoisier publishing: Paris, 1999; pp 781–799.
- 26 Baker D. D.; Chu M.; Oza U.; Rajgarhia V. *Nat. Prod. Rep.*, **2007**, 24, 1225–1244.
- 27 Lu J. J.; Bao J. L.; Chen X. P.; Huang M.; Wang Y. T. *Evid. Based Complement. Alternat. Med.*, **2012**, 2012, 1–13.
- 28 Kuramoto M.; Arimoto H.; Uemura D. *Mar. Drugs*, **2004**, 2, 39–54.

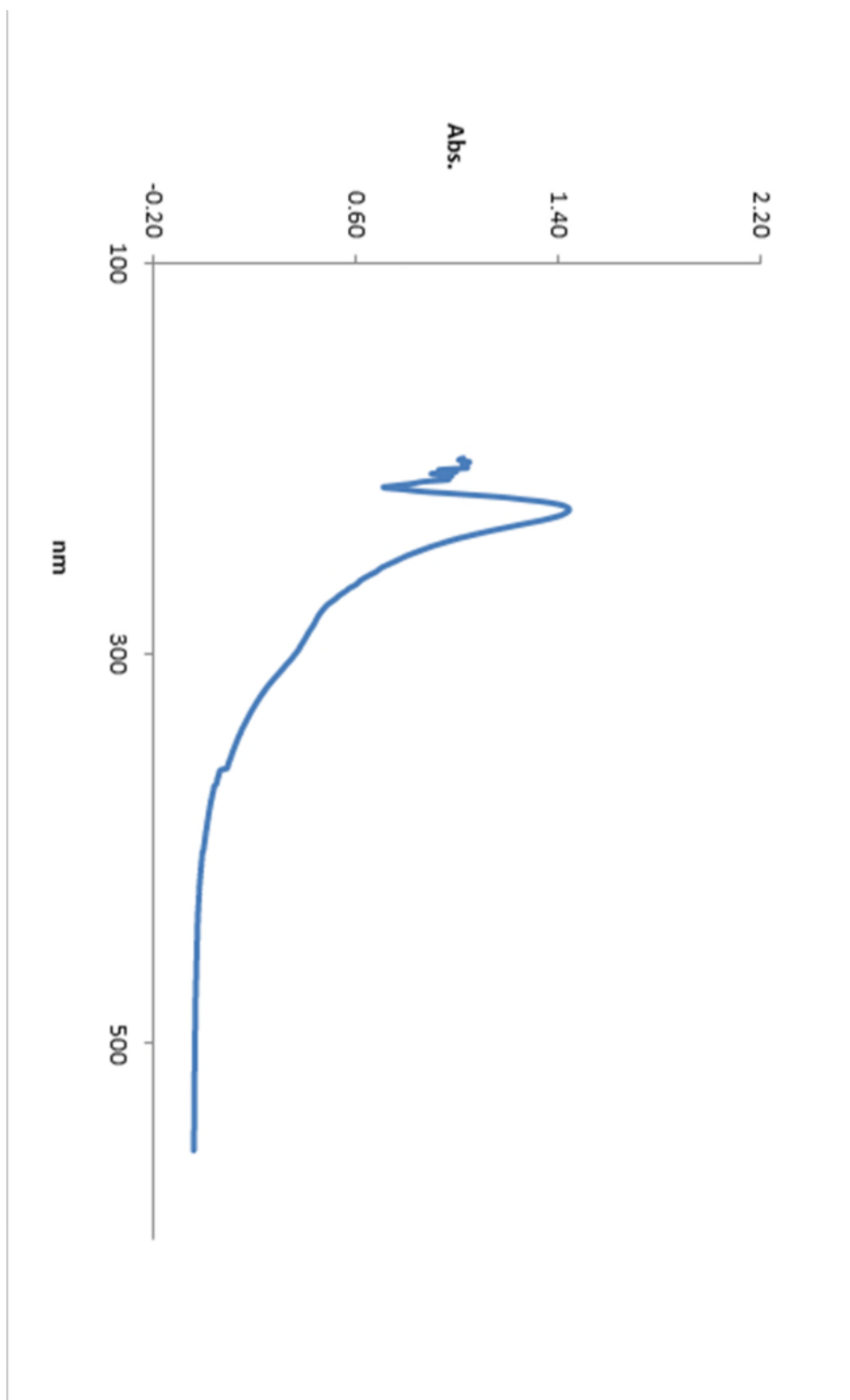
- 29 Savithramma N.; Rao M. *Middle-East J. Sci. Res.*, **2011**, *8*, 579–584.
- 30 Cordell G. A.; Quinn-Beattie M. L.; Farnsworth N. R. *Phytother. Res.*, **2001**, *15*, 183–205.
- 31 Nowroozi J.; Sepahi A. A.; Rashnonejad A. *Cell*, **2012**, *14*, 7–18.
- 32 Keller T.; Schneider A.; Regenscheit P.; Rucker T.; Jaspers J.; Kisser W. *Forensic Sci. Int.*, **1999**, *99*, 93–105.
- 33 Brahmachary R. L. *Endeavour*, **1986**, *10*, 65–68.
- 34 Shan S. M.; Luo J. G.; Pan K.; Zou H. Y.; Kong L. Y. *Biomed. Chromatogr.*, **2016**, *30*, 1861–1872.
- 35 Bourgaud F.; Gravot A.; Milesi S.; Gontier E. *Plant Sci.*, **2001**, *161*, 839–851.
- 36 Suzuki T.; Ashihara H.; Waller G. R. *Phytochemistry*, **1992**, *31*, 2575–2584.
- 37 Wink M. *Molecules*, **2012**, *17*, 12771–12791.
- 38 Evans W. C. In *pharmacopoeial and related drugs of biological origin: Trease and Evans' Pharmacognosy*; 15th ed.; W.B. Saunders: Edinburgh, 2002, pp 333–337.
- 39 Evans W. C. In *pharmacopoeial and related drugs of biological origin: Trease and Evans' Pharmacognosy*; 15th ed.; W.B. Saunders: Edinburgh, 2002; pp 337–338.
- 40 Fattorusso O.; Tagliatela-Scafati E. In *Ecological roles of alkaloids: Modern alkaloids*; Wiley-VCH: Weinheim, 2008, pp 3–4.
- 41 Kar A. In *Alkaloids: Pharmacognosy and pharmacobiotechnology*, New Age International, New Delhi, 2nd ed., **2003**, pp 1–40.
- 42 Gurib-Fakim A. *Mol Aspects Med.*, **2006**, *27*, 1–93.
- 43 Ahman V. C.; Basha C. *Phytochemistry*, **1975**, *14*, 292–293.
- 44 Dewick P. In *Alkaloids: Medicinal Natural Products*; 2nd ed.; John Wiley & Sons: Chichester, 2009, pp. 311–313.

- 45 Gunnar I. D.; Spenser G.-S. *J. Am. Chem. Soc.*, **1981**, *103*, 3208–3210.
- 46 Neuhofer H.; Witte L.; Gorunovic M.; Czygan F. C. *Pharmazie*, **1993**, *48*, 389–391.
- 47 Serrano E.; Storebakken T.; Penn M.; Landsverk T.; Hansen J. Ø.; Mydland L. T. *Aquaculture*, **2011**, *318*, 122–127.
- 48 Hart J. A.; Johns N. K.; Lamberton S. R. *J. Chem. Soc., D Chem. Commun.*, **1971**, 460–461.
- 49 Dewey R. E.; Xie J. *Phytochemistry*, **2013**, *94*, 10–27.
- 50 O'Donovan D. G.; Horan H. *J. Chem. Soc. C Org.*, **1968**, 2791–2795.
- 51 Suau R.; Silva M. V.; Valpuesta M. *Phytochemistry*, **1993**, *36*, 241–243.
- 52 Michael J. P. *Nat. Prod. Rep.*, **2008**, *25*, 166–187.
- 53 Liu J.; Liu L.D. ; Wang S. M.; Xu L. N.; Yu B.; Lin S.; Hou S. G.; Zhou N.; Jin L. L.; Yang H. *Chem. Res. Chinese Universities*, **2007**, *23*, 554–557.
- 54 Rosenberg H.; Stohs S. J.; Paul A. G. *Phytochemistry*, **1974**, *13*, 823–828.
- 55 Mazzafera P.; Crozier A.; Magalhães A. C. *Phytochemistry*, **1991**, *30*, 3913–3916.
- 56 Katavic P. L.; Venables D. A.; Rali T.; Carroll A. R. *J. Nat. Prod.*, **2007**, *70*, 866–868.
- 57 Katavic P. L.; Venables D. A.; Guymer G. P.; Forster P. I.; Carroll A. R. *J. Nat. Prod.*, **2007**, *70*, 1946–1950.
- 58 Güven K. C.; Percot A.; Sezik E. *Mar. Drugs*, **2010**, *8*, 269–284.
- 59 Ortega N.; Tang D. D.; Urban S.; Zhao D.; Glorius F. *Angewanate Commun.*, **2013**, *52*, 9500–9503.
- 60 Su B.; Cai C.; Deng M.; Liang D.; Wang L.; Wang Q. *Bioorganic Med. Chem. Lett.*, **2014**, *24*, 2881–2884.
- 61 Honda K.; Tada A.; Hayashi N.; Abe F.; Yamauchi T. *Experientia*, **1995**, *51*, 753–756.
- 62 Michael J. P. *Nat. Prod. Rep.*, **2008**, *25*, 139–165.

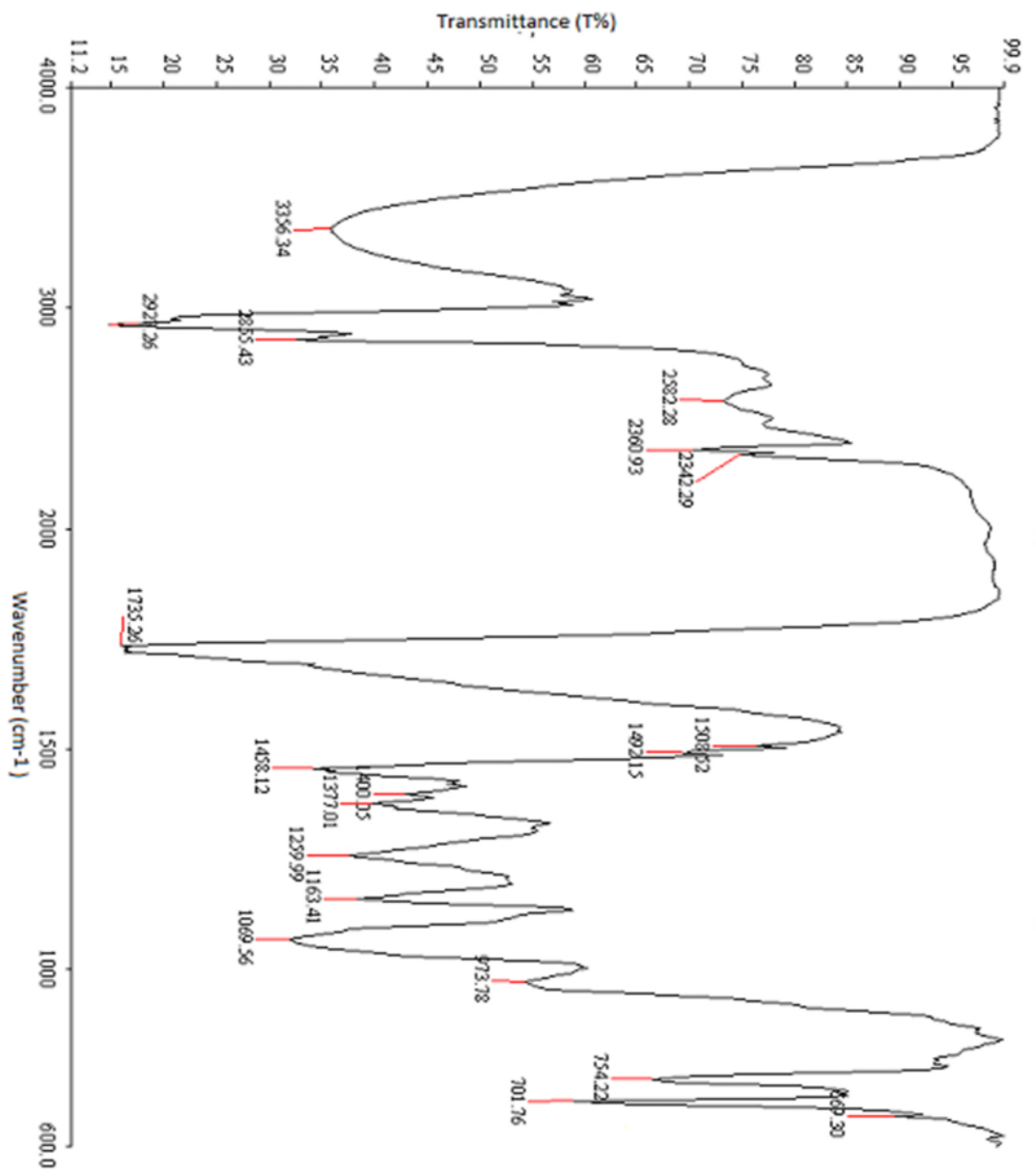
- 63 Kondakal V. V. R.; Qamar M. L; Hemming K. *Tetrahedron Lett.*, **2012**, *53*, 4100–4103.
- 64 Michael J. P. *Nat. Prod. Rep.*, **2007**, *24*, 191–222.
- 65 Dewick P. In *Alkaloids: Medicinal Natural Products*; 2nd ed.; John Wiley & Sons: Chichester, 2009; pp. 321–331.
- 66 Rassu G.; Carta P.; Pinna L.; Battistini L.; Zanardi F.; Acquotti D.; Casiraghi G. *Eur. J. Org. Chem.*, **1999**, 1395–1400.
- 67 Ohyama K.; Okawa A.; Moriuchi Y.; Fujimoto Y. *Phytochemistry*, **2013**, *89*, 26–31.
- 68 Wink M. *Planta Med.*, **1987**, *53*, 509–514.
- 69 Kumareswaran R.; Gallucci J.; RajanBabu T. V. *J. Org. Chem.*, **2004**, *69*, 9151–9158.
- 70 Hart N. K.; Johns S. R.; Lambertson J. A. *Aust. J. Chem.*, **1972**, *25*, 817–835.
- 71 Carroll A. R.; Arumugan G.; Quinn R. J.; Redburn J.; Guymer G.; Grimshaw P. *J. Org. Chem.*, **2005**, *70*, 1889–92.
- 72 Katavic P. L.; Venables D. A.; Forster P. I.; Guymer G.; Carroll A. R. *J. Nat. Prod.*, **2006**, *69*, 1295–1299.
- 73 Shah R., Singh G.; Mann P. S.; Shri A.S. *Int. J. Institutional Pharm. Life Sci.*, **2011**, *1*, 267–278.
- 74 Whitmore, T.C.; Ng, F. S. P. In *Elaeocarpacea*, Tree flora of Malaya: a manual for foresters, Longman, Volume 4, 1989, pp. 82–96
- 75 Manandhar N. P. In *Elaeocarpacea*, Plants and people of Nepal; Timber Press: Oregon, 2002, 192, pp. 526–527.
- 76 Zhou C.; Wang X.; Mo J.; Zhang J.; Gan L. *Helv. Acta*, **2011**, *94*, 347–354.
- 77 Johns S. R.; Lambertson J. A.; Sioumi A. A. *Aust. J. Chem.*, **1969**, *22*, 793–800.
- 78 Katavic P. L.; Venables D. A.; Rali T.; Carroll A. R. *J. Nat. Prod.*, **2007**, *70*, 872–875.
- 79 Ray A. B.; Chand L.; Pandey V. B. *Phytochemistry*, **1979**, *18*, 700–701.

- 80 Johns R. I.; Lamberton S.R.; Sioumis J.A.; Soares A.A.; Willing H. *Aust. J. Chem.*, **1971**, *24*, 1679–1694.
- 81 Aggarwal, S.; In *Elaeocarpus* L.: Plant Resources of South-East Asia No. 12(2): Medicinal and poisonous plants 2; Valkenburg, J.L.C.H., Bunyaphatsara, N. (Eds); Backhuys Publishers: Leiden, The Netherlands, 2001, pp. 241–246.
- 82 Robertson G. B.; Tooptakong U.; Lamberton J. A.; Geewananda Y. A.; Gunawardana P.; Ralph I.; Bick C. *Tetrahedron Lett.*, **1984**, *25*, 2695–2696.
- 83 Poulter C. D.; Muscio O. J.; Goodfellow R. *J. Biochem.*, **1974**, *13*, 1530–1538.
- 84 Rivera S. B.; Swedlund B. D.; King G. J.; Bell R. N.; Hussey C. E.; Shattuck-Eidens D. M.; Wrobel W. M.; Peiser G. D.; Poulter C. D. *Proc. Natl. Acad. Sci. U. S. A.*, **2001**, *98*, 4373–4378.
- 85 Posner G. H.; Asirvatham E.; Hamill T. G.; Webb K. S. *J. Org. Chem.*, **1990**, *55*, 2132–2137.
- 86 Gribble G. W.; Switzer F. L.; Soll R. M. *J. Org. Chem.*, **1988**, *53*, 3164–3170.
- 87 Lehn J. M. In *Nitrogen inversion: Dynamic Stereochemistry*; vol. 15/3; Fortschritte der Chemischen Forschung; Springer: Berlin, Heidelberg, 1970, pp. 311–377
- 88 Bradshaw B.; Luque-Corredera C.; Bonjoch J. *Chem. Commun.*, **2014**, *50*, 7099–102.
- 89 Lamberton J. A.; Geewananda Y. A.; Gunawardana P.; Bick I. R. *C. J. Nat. Prod.*, **1983**, *46*, 235–247.
- 90 Wilds A. L.; Beck L. W.; Close W. J.; Djerassi C.; Johnson J. A. Jr.; Johnson T. L.; Shunk C. H.; *J. Am. Chem. Soc.*, **1947**, *69*, 1985–1994.
- 91 Dieter R. K.; Chen N.; April R. V. *J. Org. Chem.*, **2006**, *71*, 5674–5678.
- 92 Crabb T. A. *Org. Magn. Reson.*, **1972**, *4*, 259–281.
- 93 Buckel W.; Thauer R. K. *Angew. Chemie. Int. Ed.*, **2011**, *50*, 10492–10494.
- 94 Cortinovis C.; Caloni F. *Toxins.*, **2015**, *7*, 5301–5307.

## APPENDIX



Appendix 1: UV spectrum for tectoricine (1).



Appendix 2: IR spectrum for tectoricine (1).

Data: ERL 5

Sample Name:

Description:

Ionization Mode: ESI+

History: Determine m/z/Peak Detect(Centroid,30,Area),Correct Base(0.5%),Correct Bas...

Charge Number: 1

Element: <sup>12</sup>C: 3 .. 60, <sup>1</sup>H: 5 .. 60, <sup>14</sup>N: 0 .. 5, <sup>16</sup>O: 0 .. 15

Tolerance: 15.00(ppm), 5.00 .. 15.00(mmu)

Unsaturation Number: 0.0 .. 25.0 (Fraction...

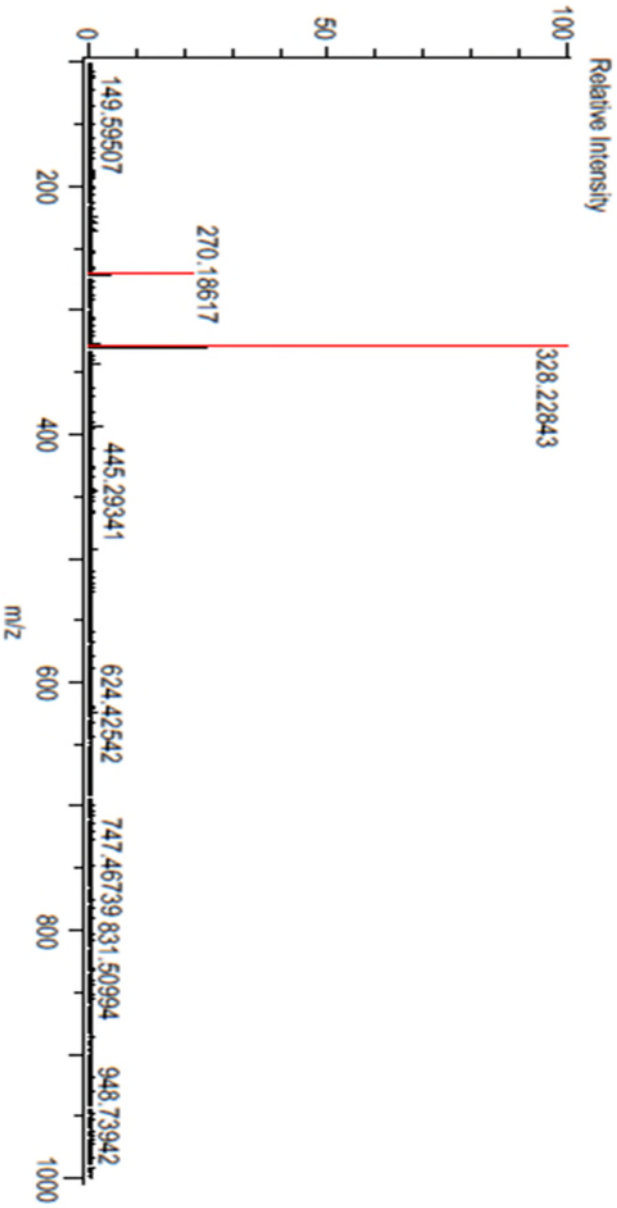
Acquired: 2/11/2015 2:40:14 PM

Operator: AccuTOF

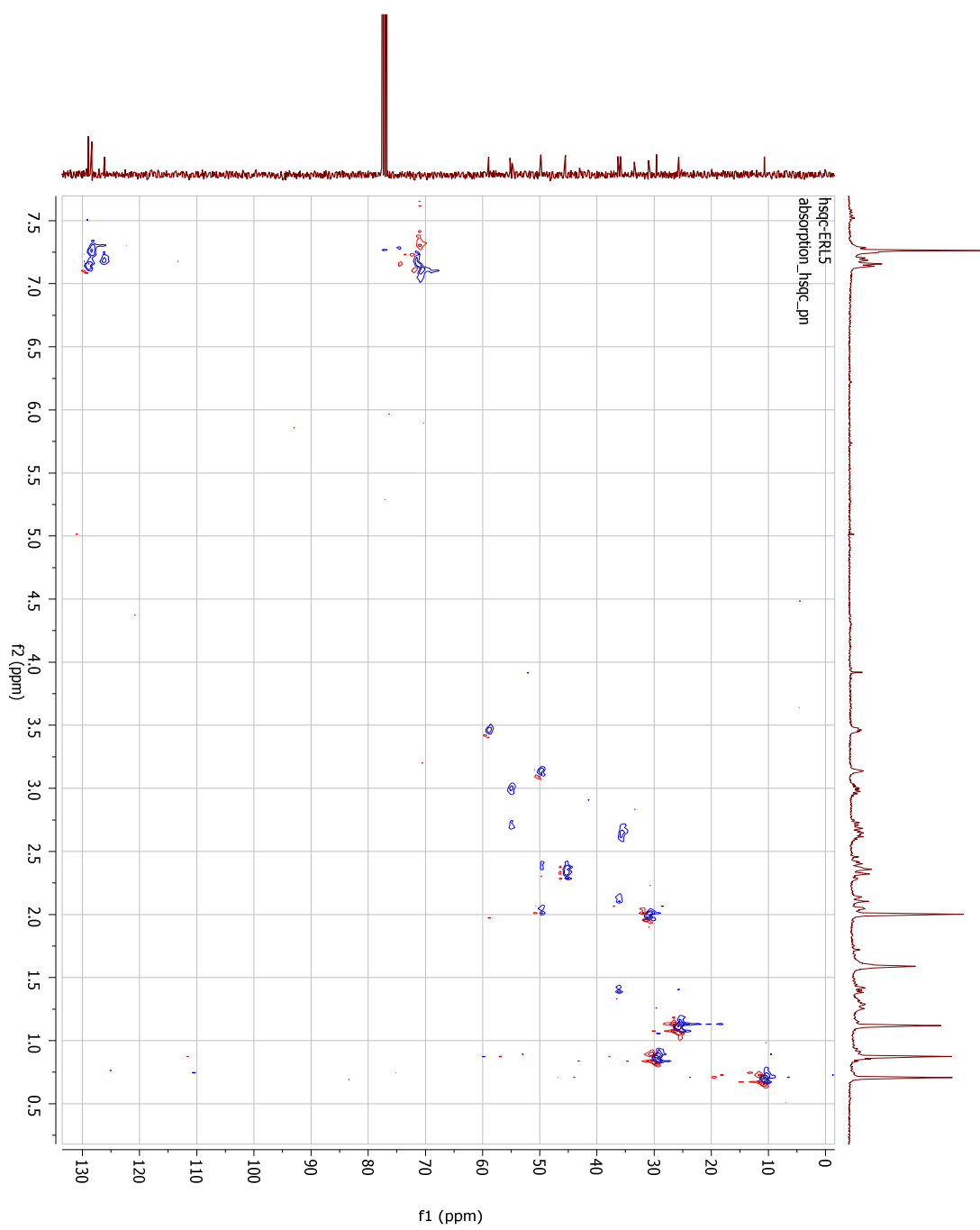
Mass Calibration data: Calibration

Created: 2/11/2015 4:14:46 PM

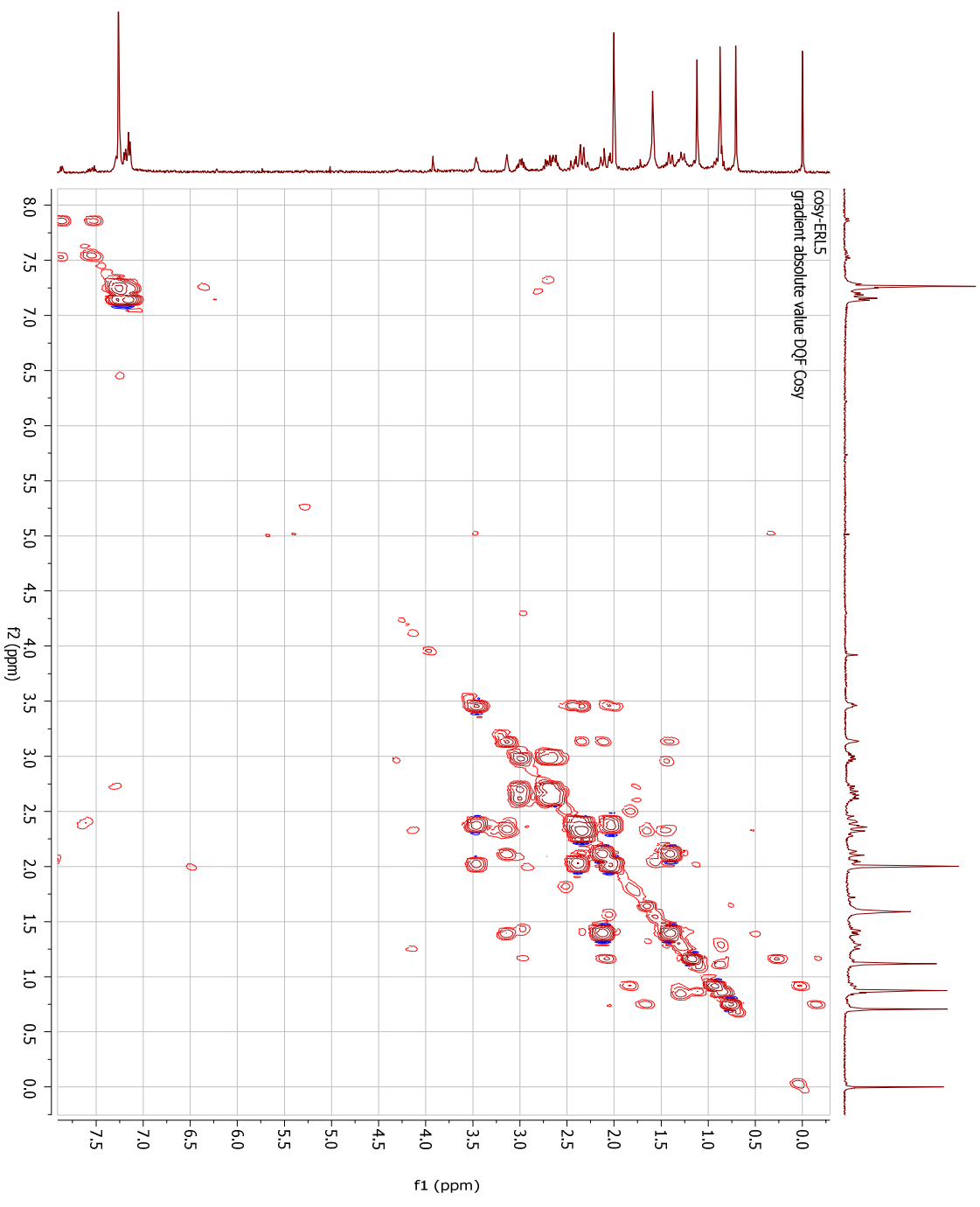
Created by: AccuTOF



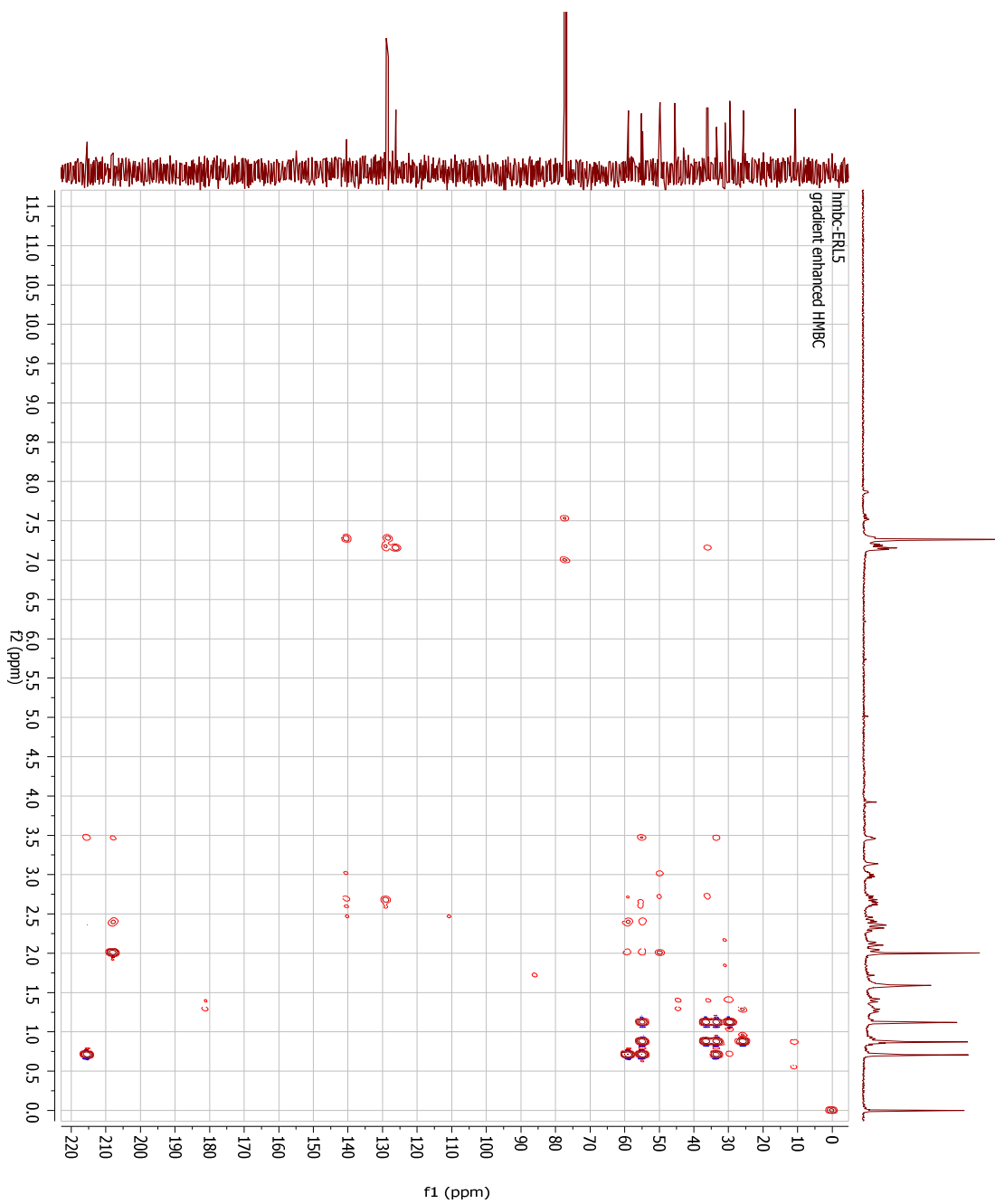
Appendix 3: MS spectrum for tectoricine (1).



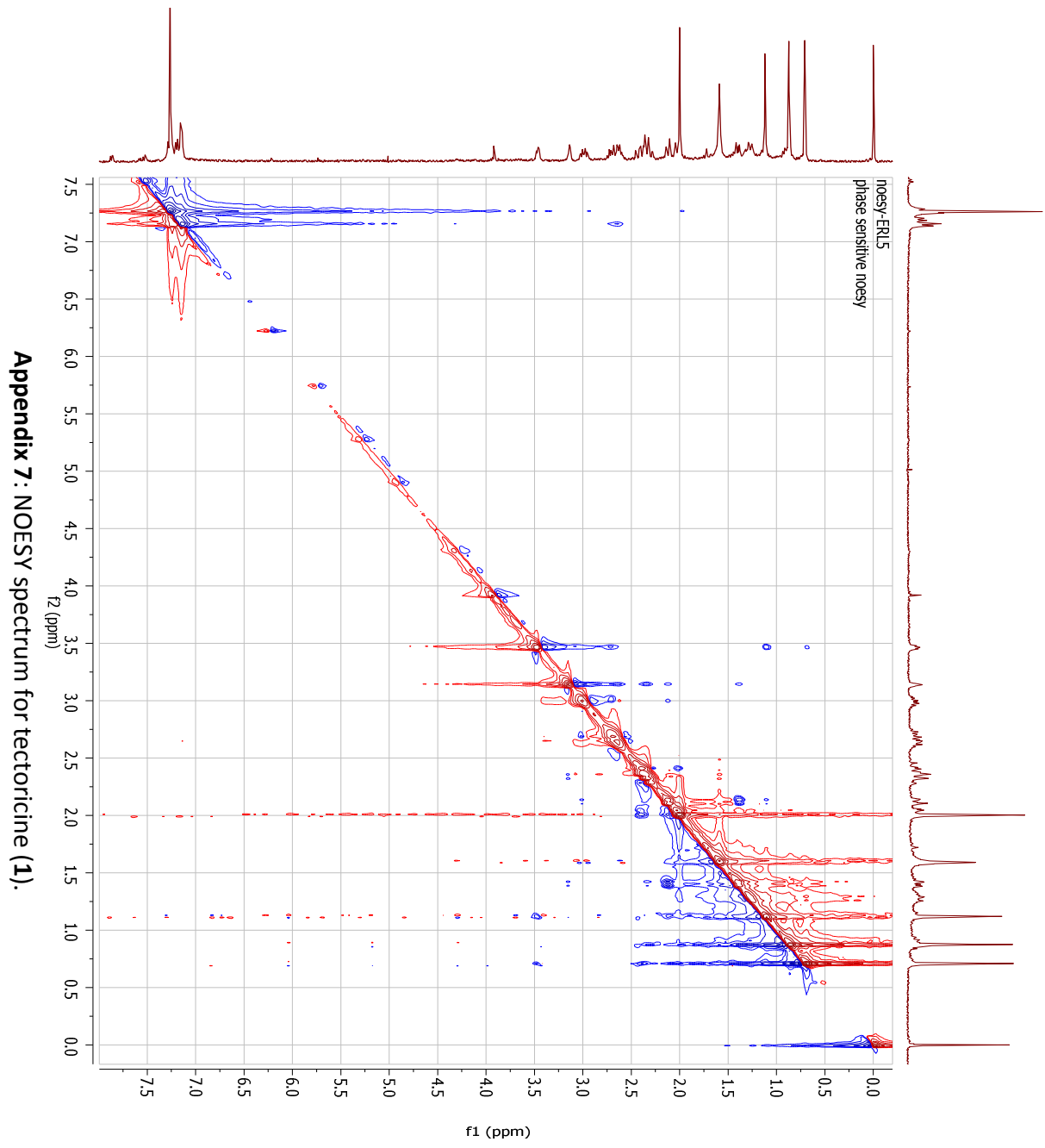
**Appendix 4:** HSQC spectrum for tectoricine (**1**).



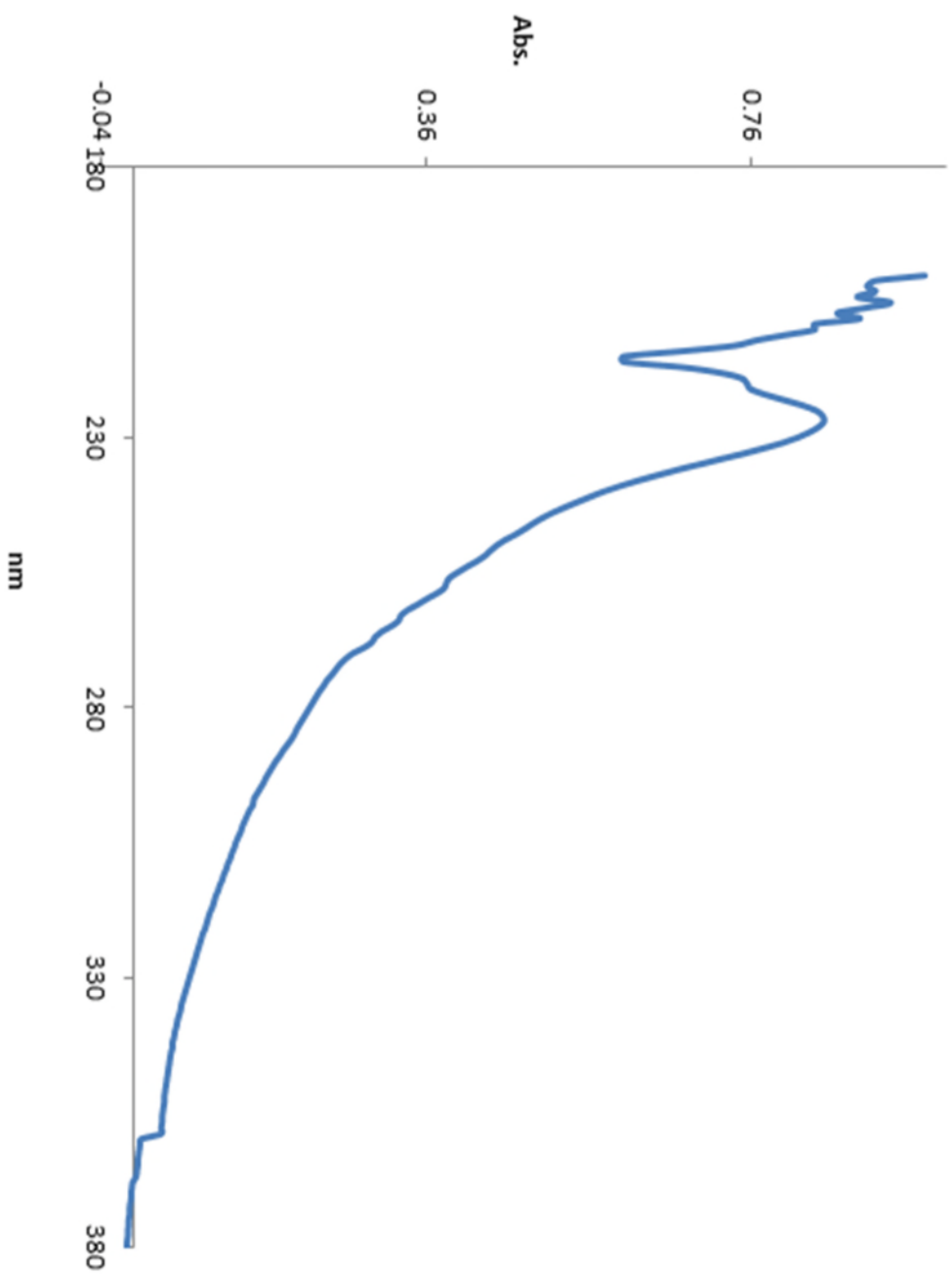
**Appendix 5: COSY spectrum for tectoricine (1).**



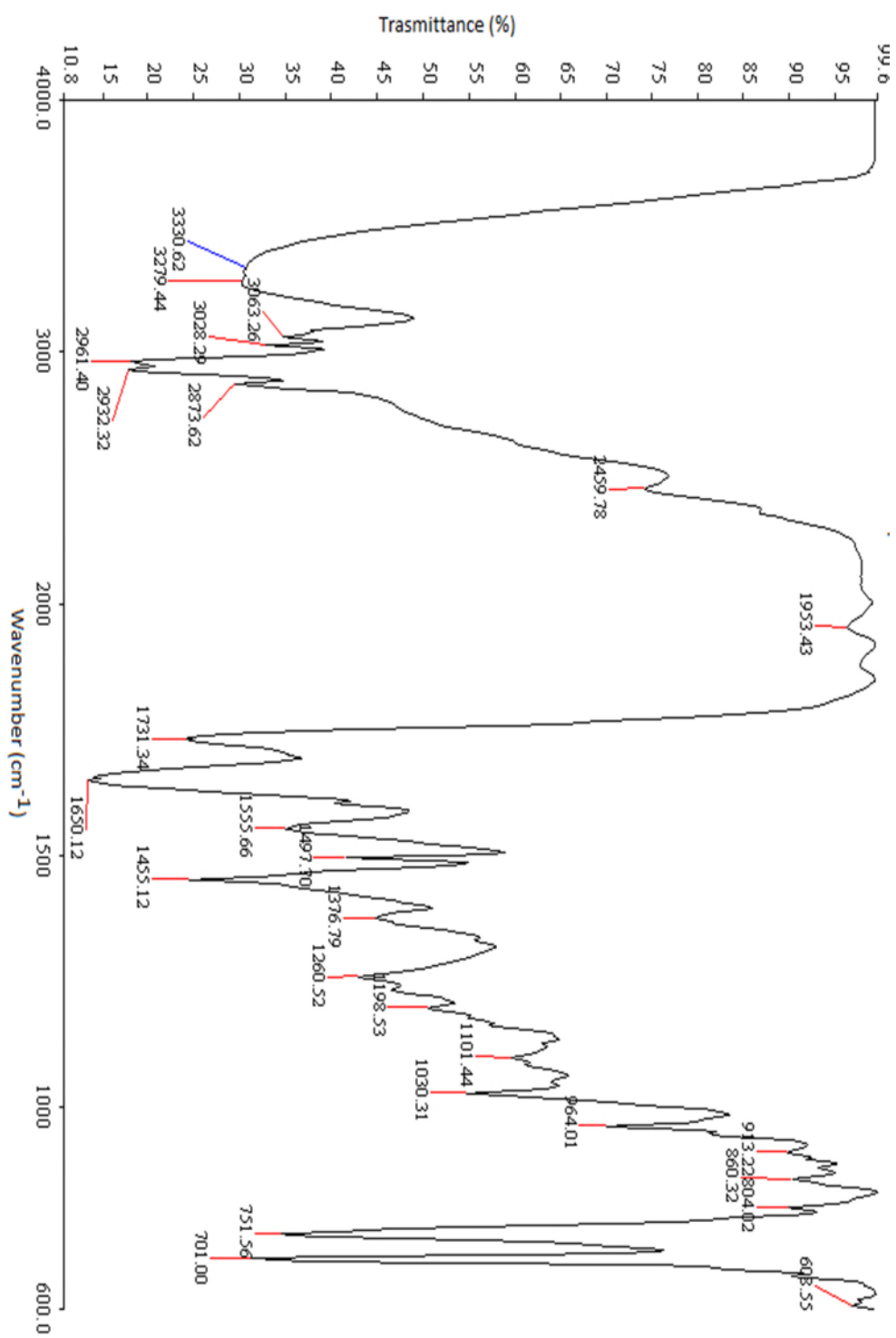
Appendix 6: HMBC spectrum for tectoricine (1).



**Appendix 7 : NOESY spectrum for tectoricine (1).**

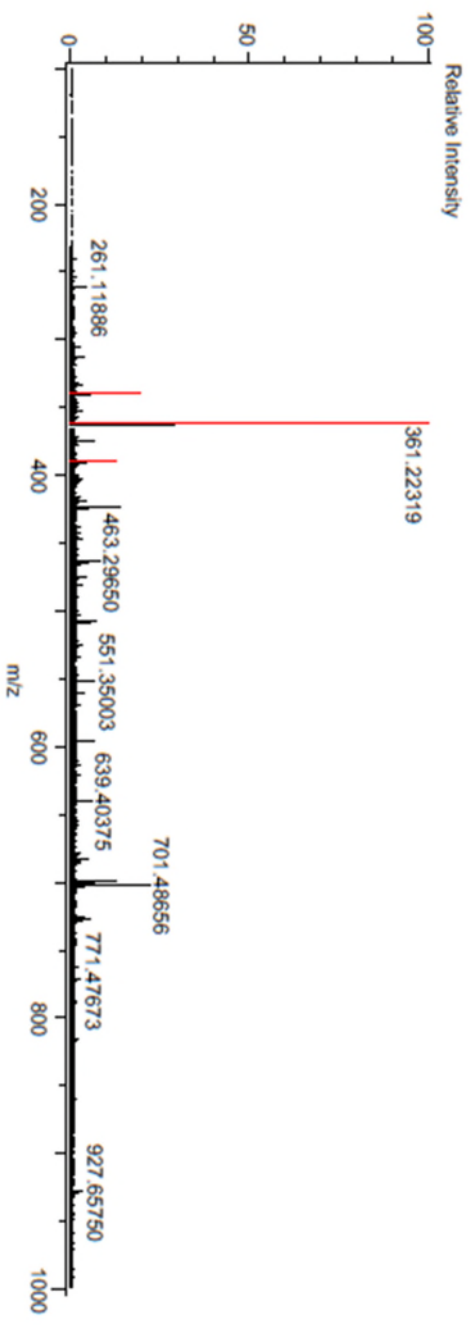


**Appendix 8: UV spectrum for tectoraline (2).**

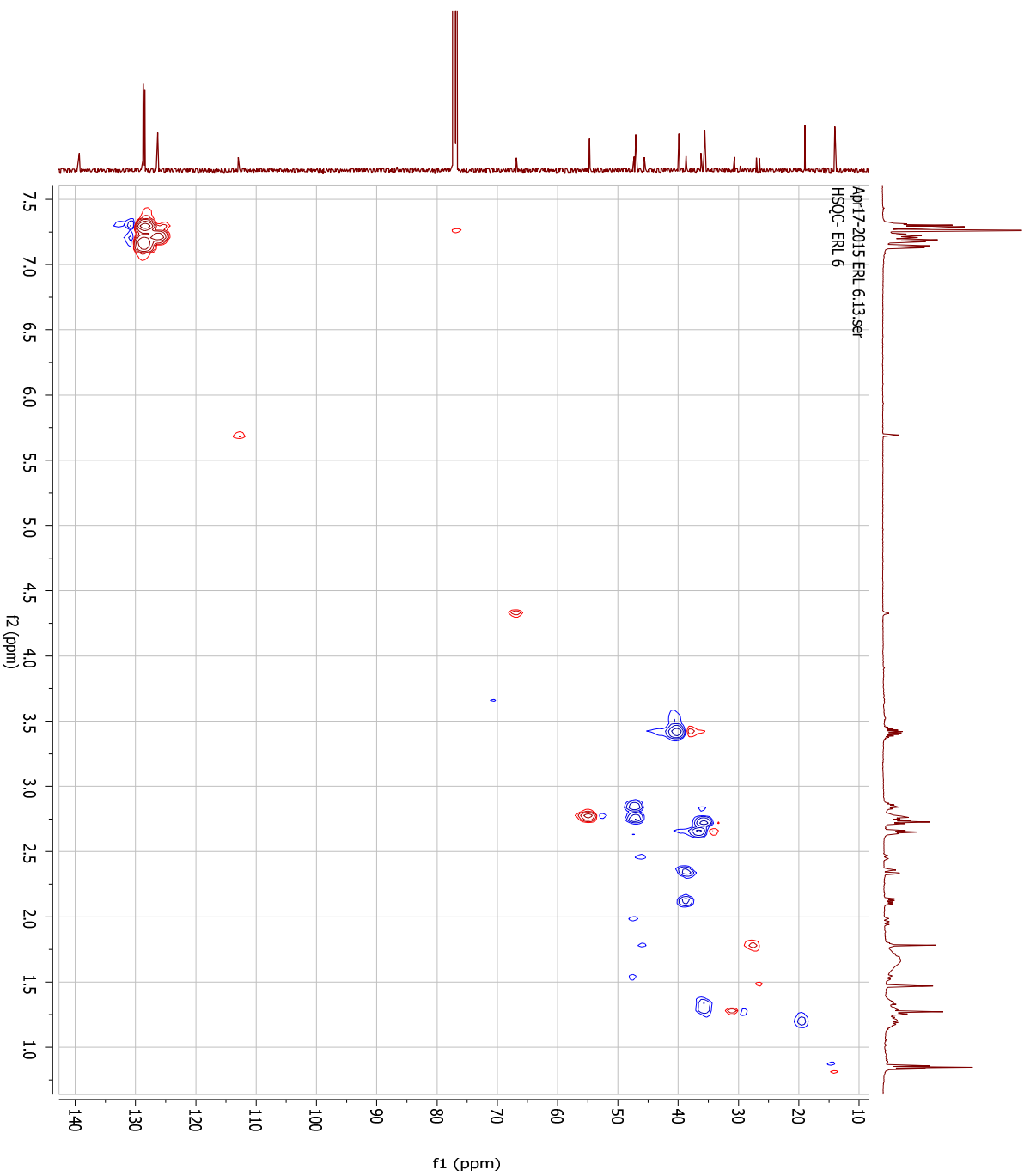


Appendix 9: IR spectrum for tectoraline (2).

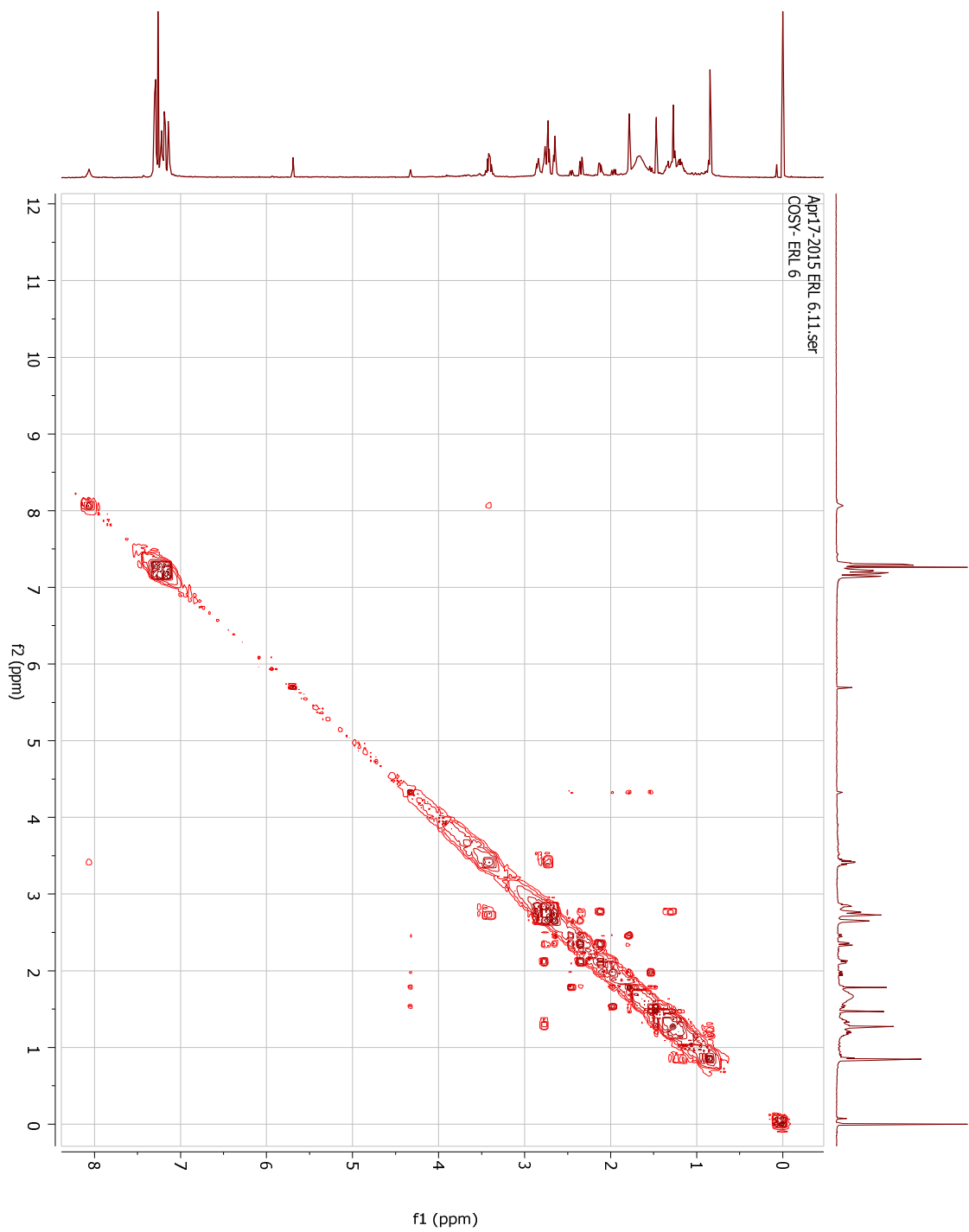
Data: ERL6  
 Sample Name:  
 Description:  
 Ionization Mode: ESI+  
 History: Determine m/z[Peak Detect(Centroid:30,Area);Correct Base(0.5%)];Correct Base(5.0%];...  
 Charge number: 1  
 Element: <sup>12</sup>C:10 .. 60, <sup>1</sup>H:10 .. 60, <sup>14</sup>N:0 .. 5, <sup>23</sup>Na:0 .. 1, <sup>16</sup>O:0 .. 10  
 Tolerance: 15.00(ppm), 5.00 .. 15.00(mmu)  
 Unsaturation Number: 0.0 .. 25.0 (Fraction:Both)



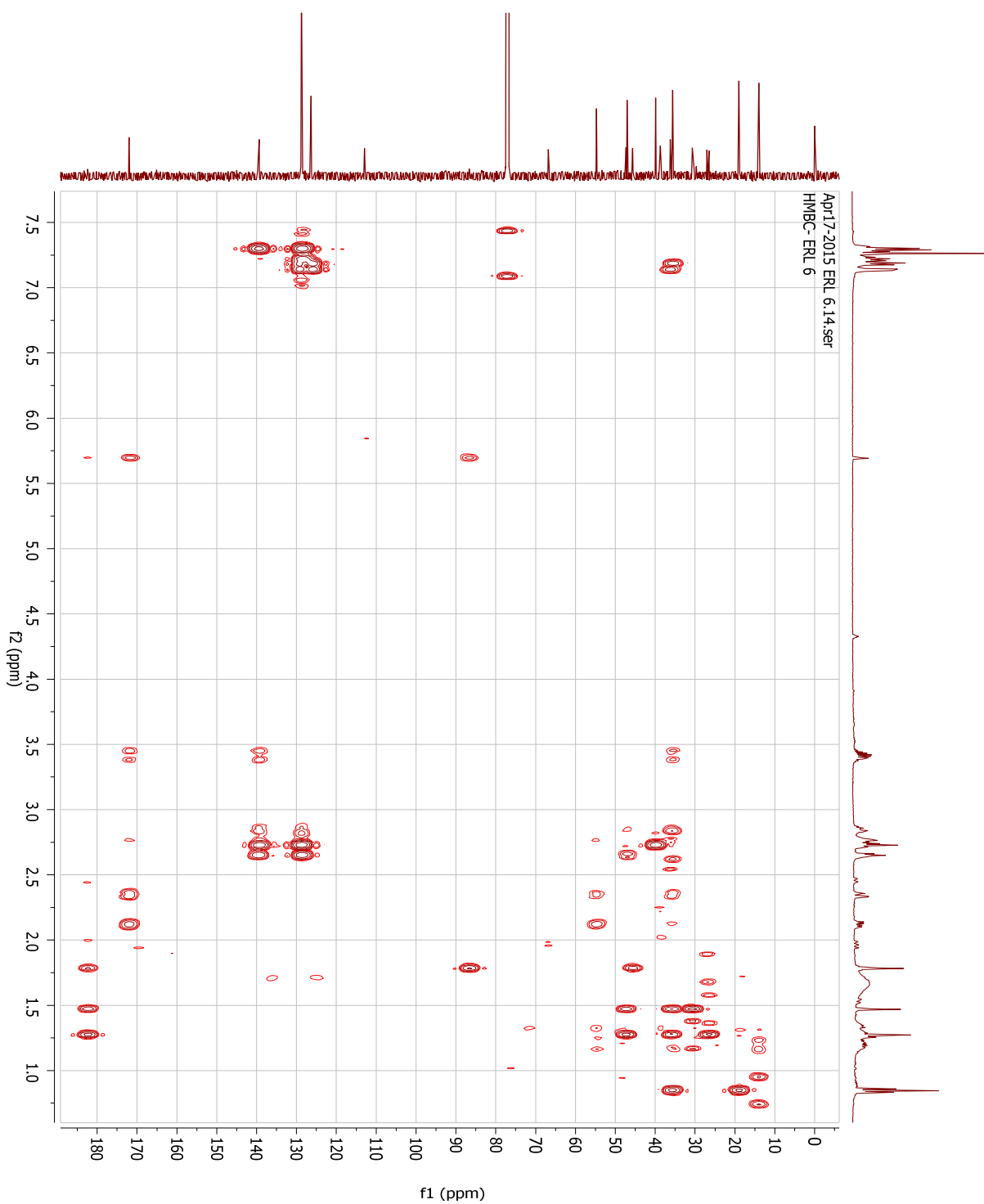
Appendix 10: MS spectrum for tectoraline (2).



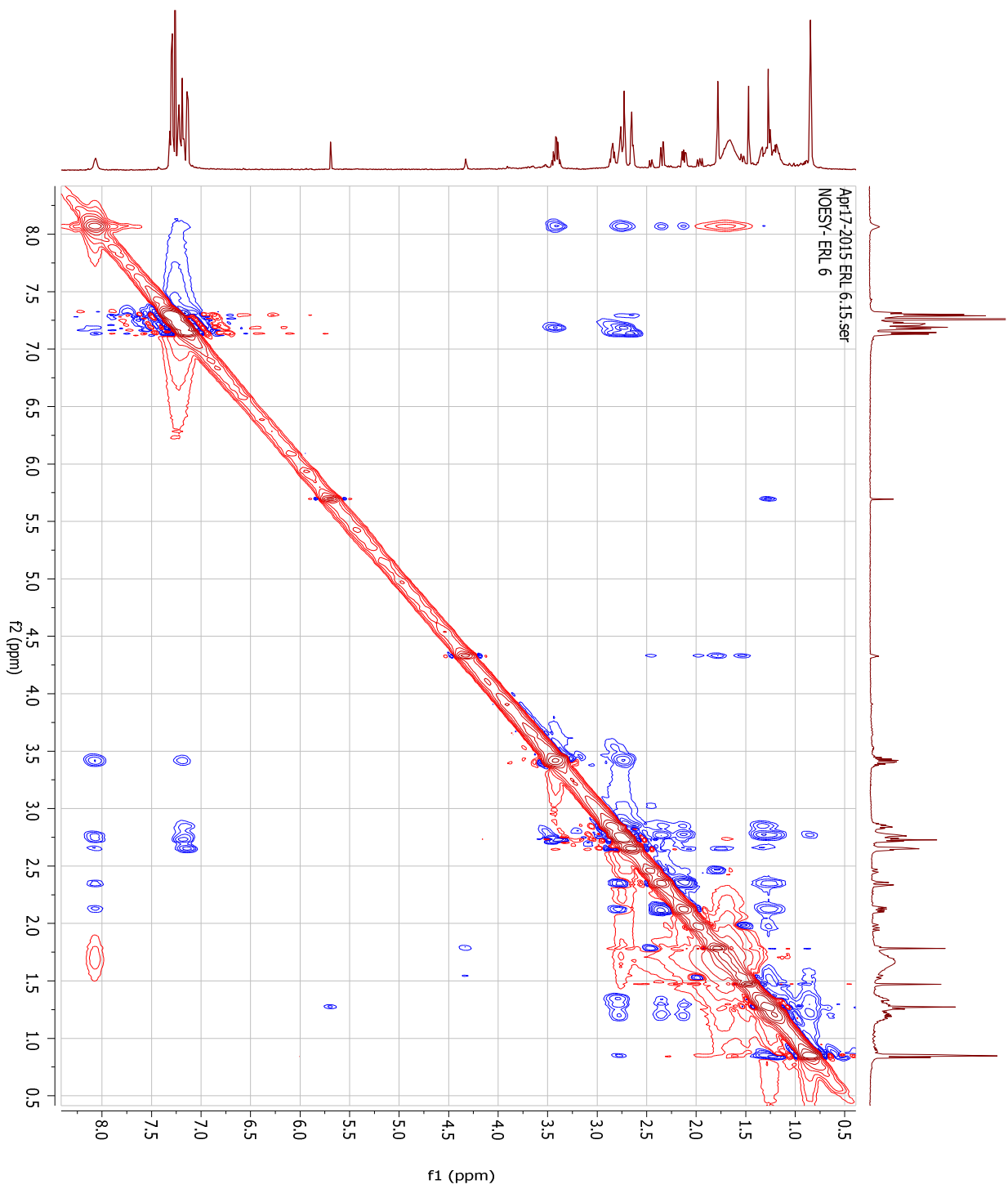
Appendix 11: HSQC spectrum for tectoraline (2).



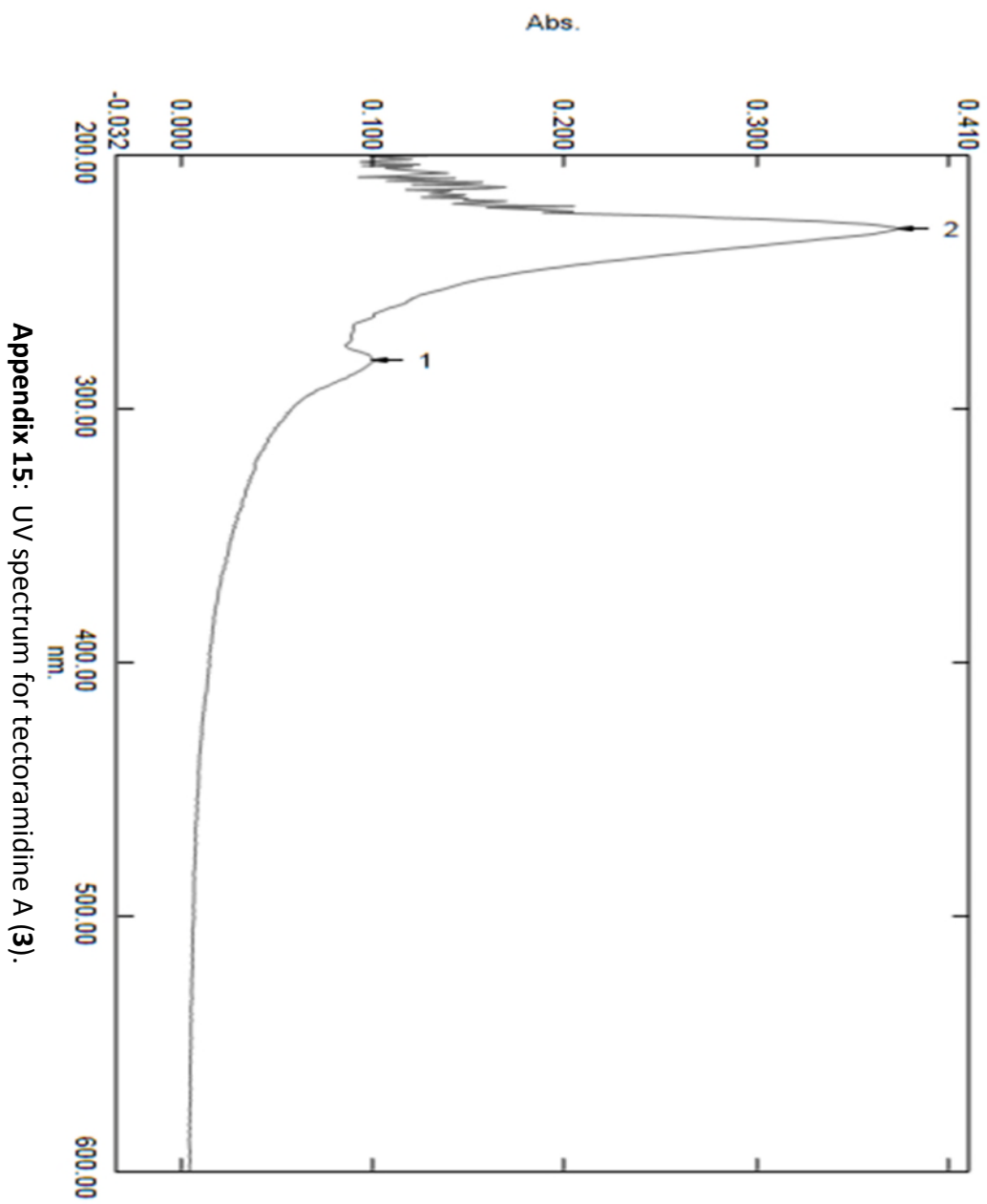
**Appendix 12: COSY spectrum for tectoraline (2).**



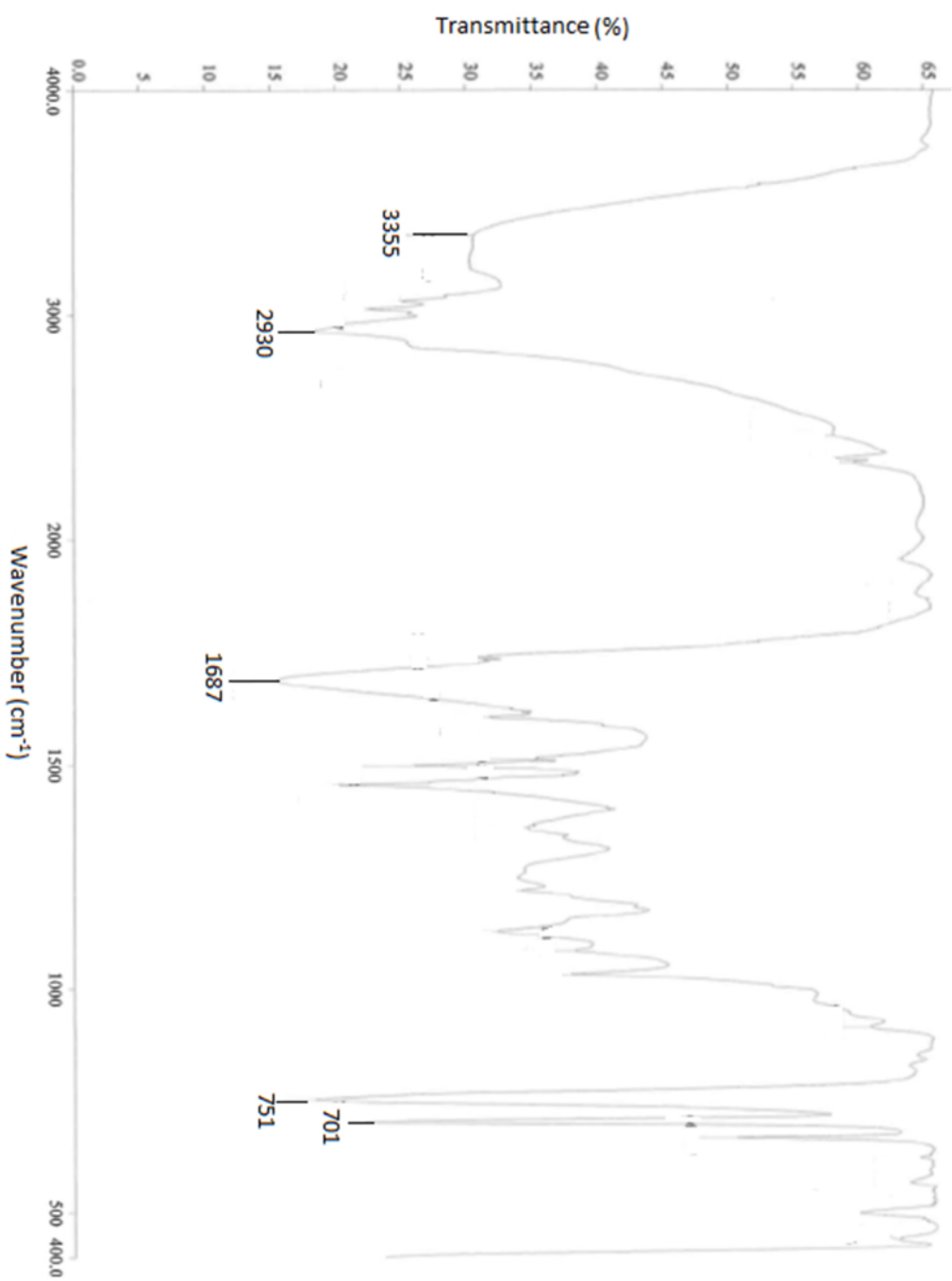
Appendix 13: HMBC spectrum for tectoraline (**2**).



Appendix 14: NOESY spectrum for tectoraline (2).



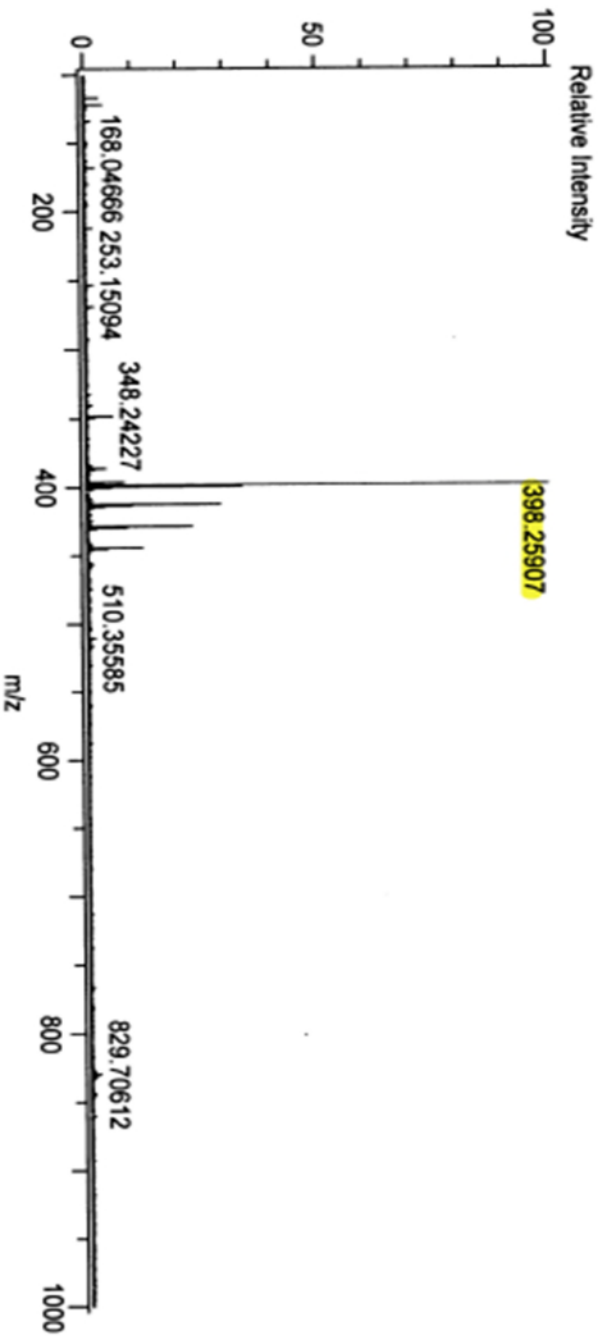
Appendix 15: UV spectrum for tectoramidine A (**3**).



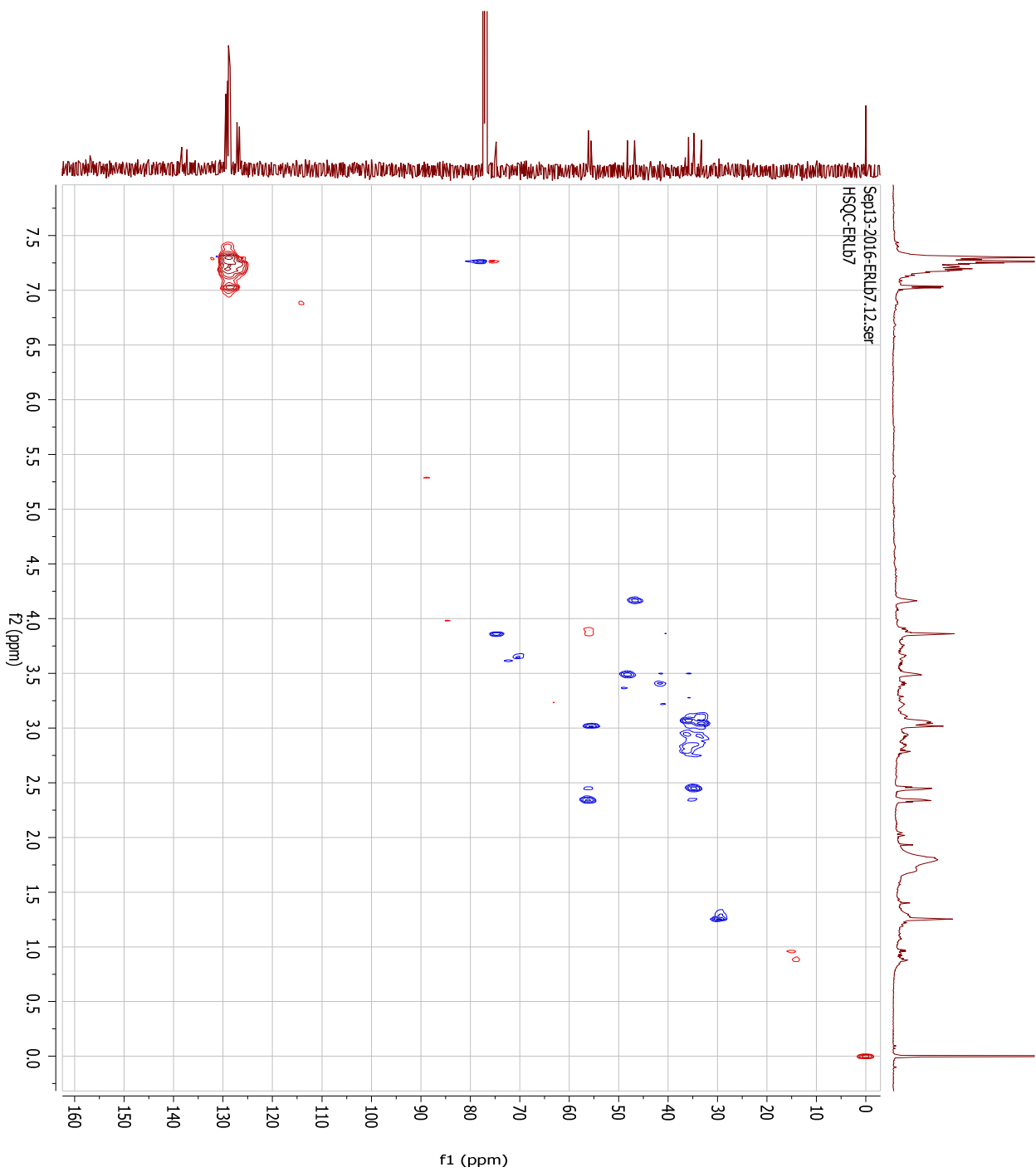
**Appendix 16:** IR spectrum for tectoramidine A (**3**).

Data: ERLb7  
Sample Name:  
Description:  
Ionization Mode: ESI+  
History: Determine m/z|Peak Detect|Centroid,30,Area|Correct Base|0.5%|Correct Ba...  
Acquired: 7/15/2016 2:14:03 PM  
Operator: AccuTOF  
Mass Calibration data: Calibration2  
Created: 7/18/2016 11:35:57 AM  
Created by: AccuTOF

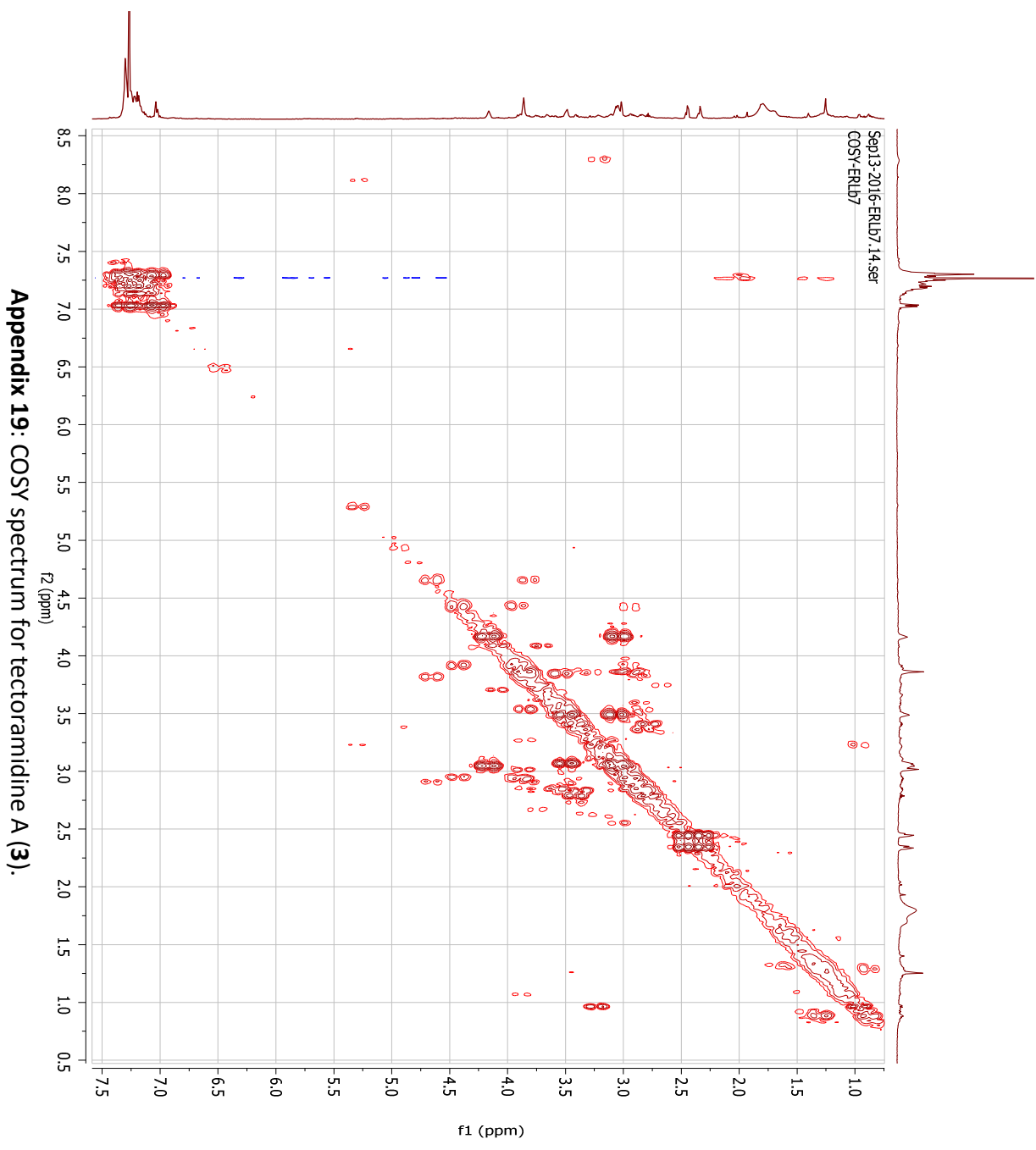
Charge number: 1  
Tolerance: 50.00(ppm), 5.00 .. 15.00(mmu)  
Element: <sup>12</sup>C:0 .. 50, <sup>1</sup>H:0 .. 100, <sup>14</sup>N:1 .. 10, <sup>16</sup>O:0 .. 15  
Unsaturation Number: 0.0 .. 25.0 (Fractio...



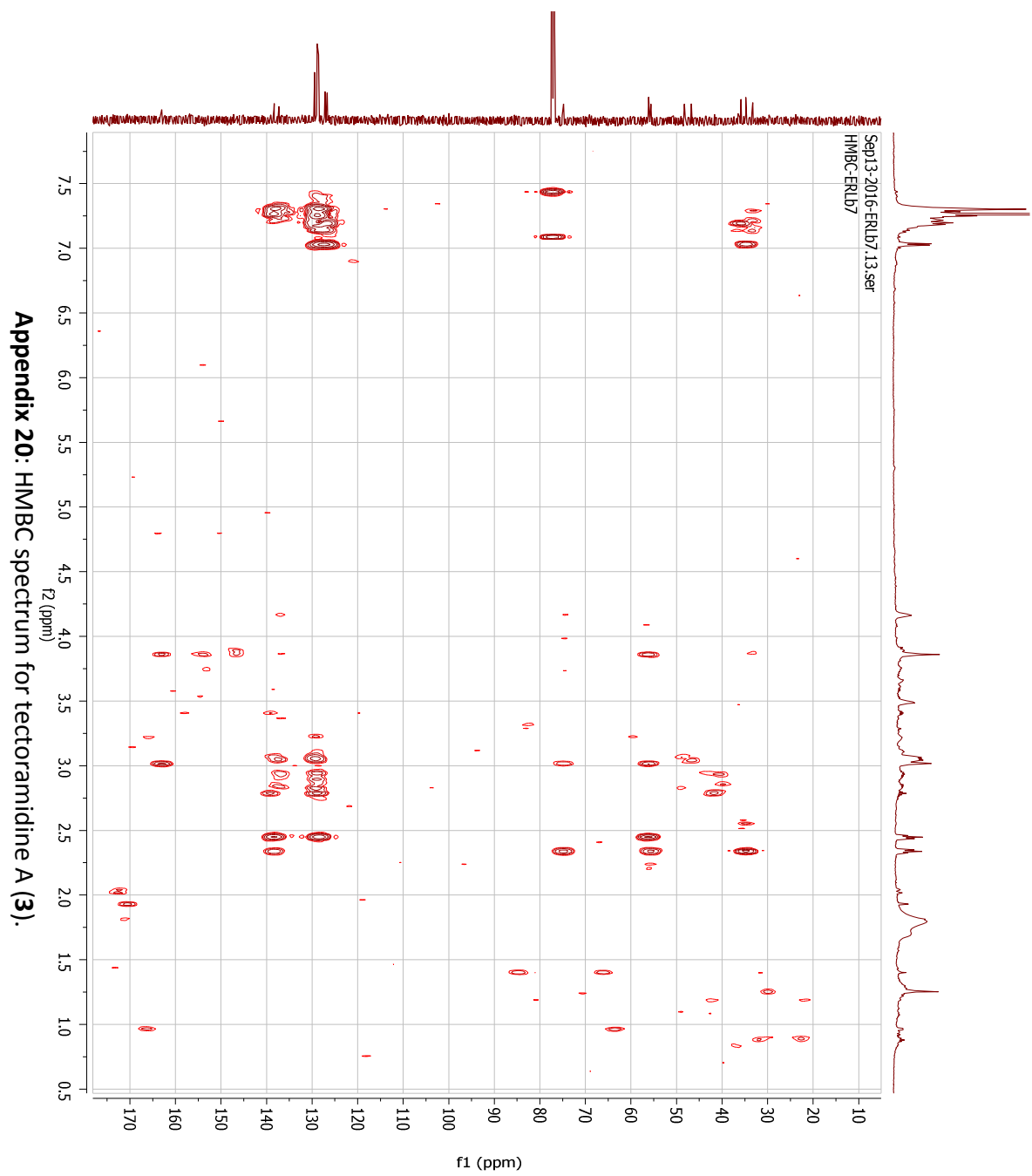
Appendix 17: MS spectrum for tectoramidine A (3).

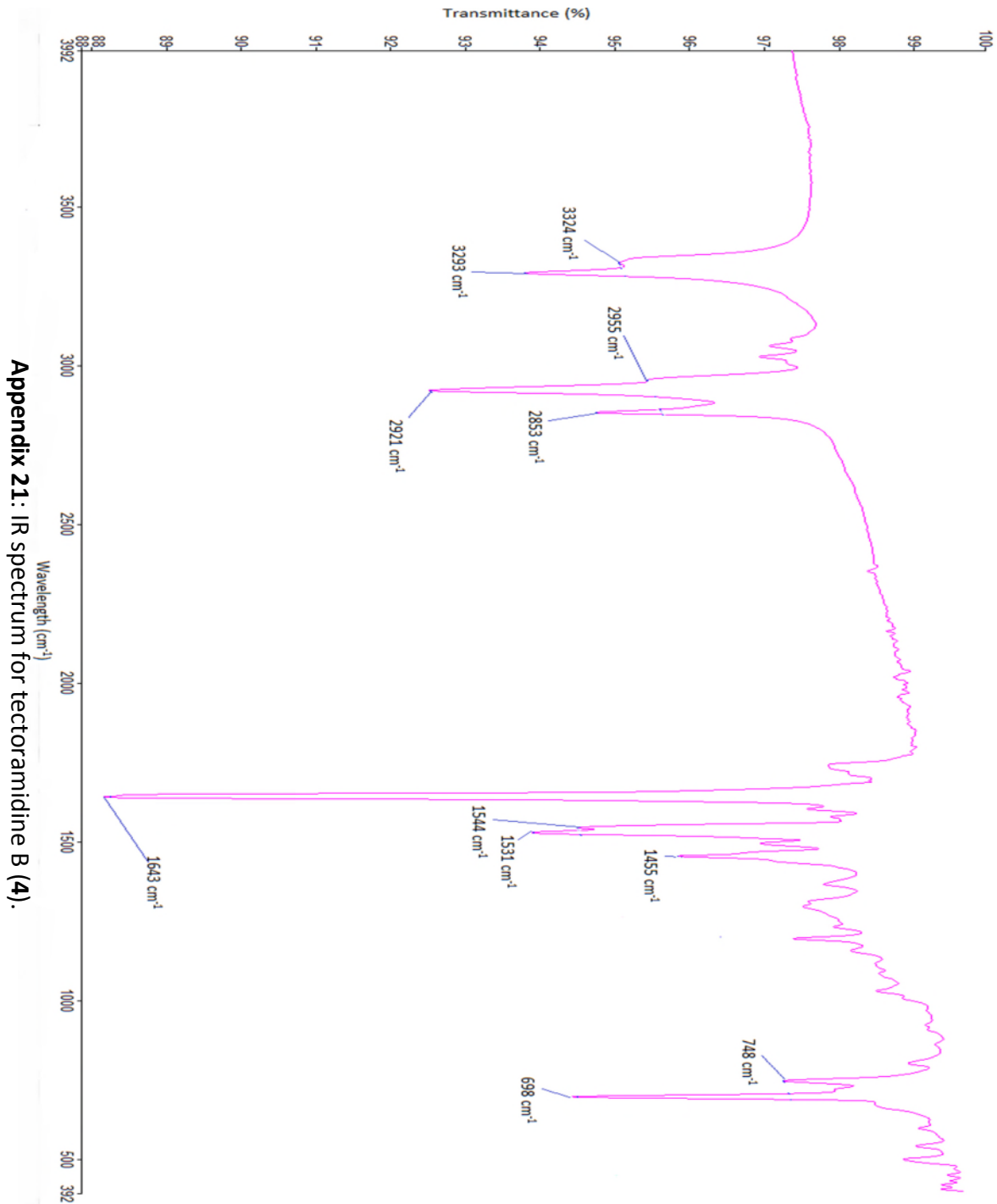


**Appendix 18:** HSQC spectrum for tectoramidine A (**3**).



**Appendix 19: COSY spectrum for tectoramide A (3).**





Appendix 21: IR spectrum for tectoramidine B (4).

Data:ERLb8

Sample Name:

Description:

Ionization Mode:ESI+

History:Determine m/z[Peak Detect[Centroid,30,Area],[Correct Base[0.5%]];Correct Ba...

Acquired:7/29/2016 11:22:19 AM

Operator:AccuTOF

Mass Calibration data:Internal Calib 2907...

Created:7/29/2016 1:40:36 PM

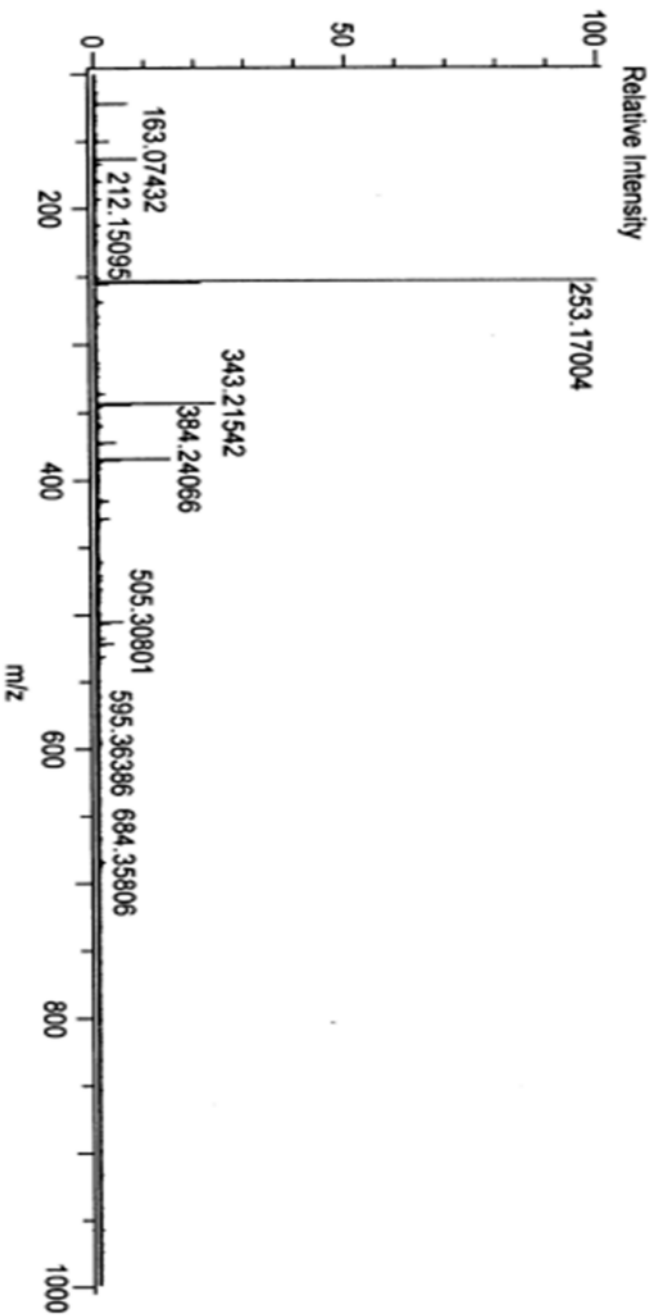
Created by:AccuTOF

Charge number:1

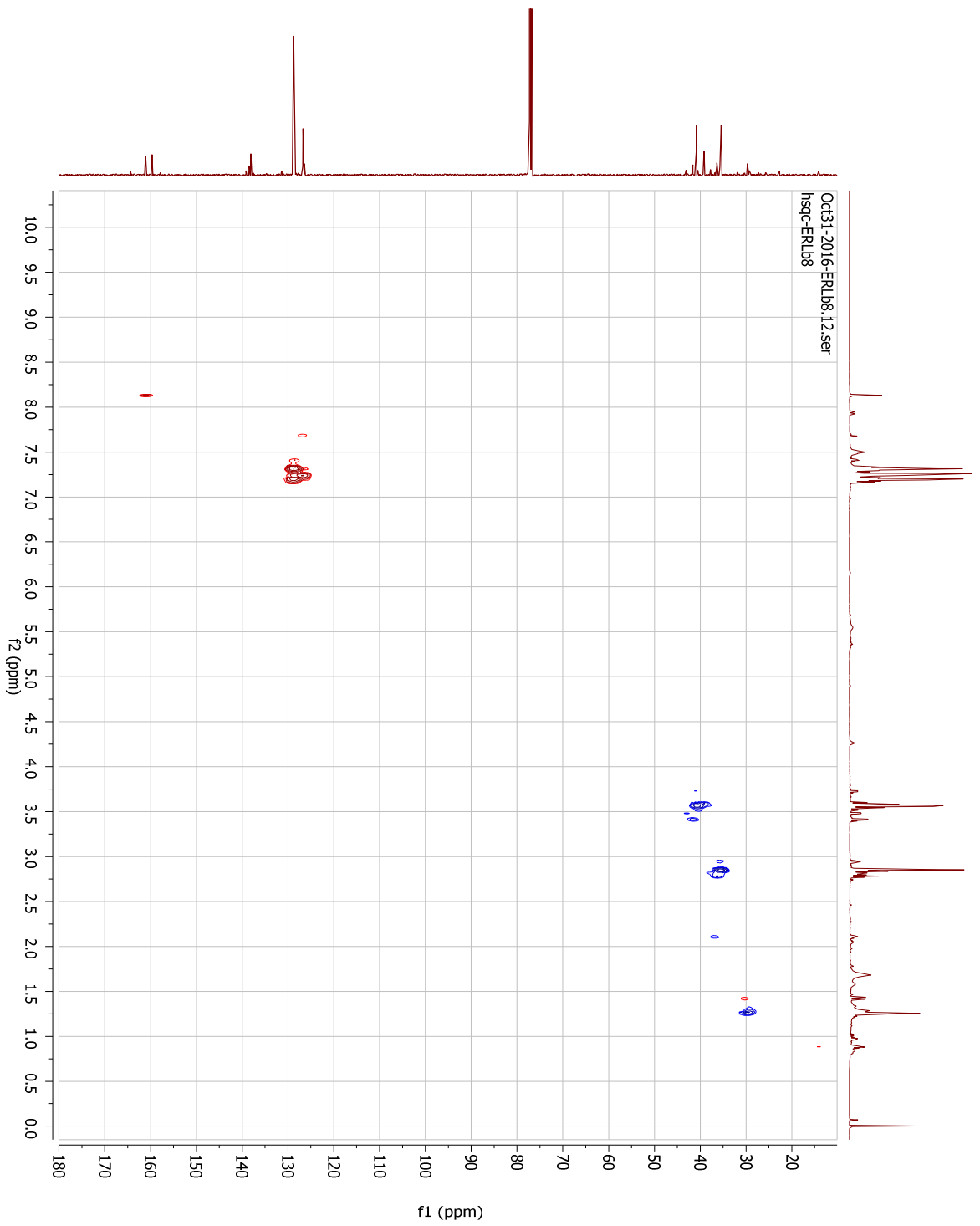
Tolerance:50.00(ppm), 5.00 .. 15.00(mmu)

Unsaturation Number:0.0 .. 25.0 (Fractio...

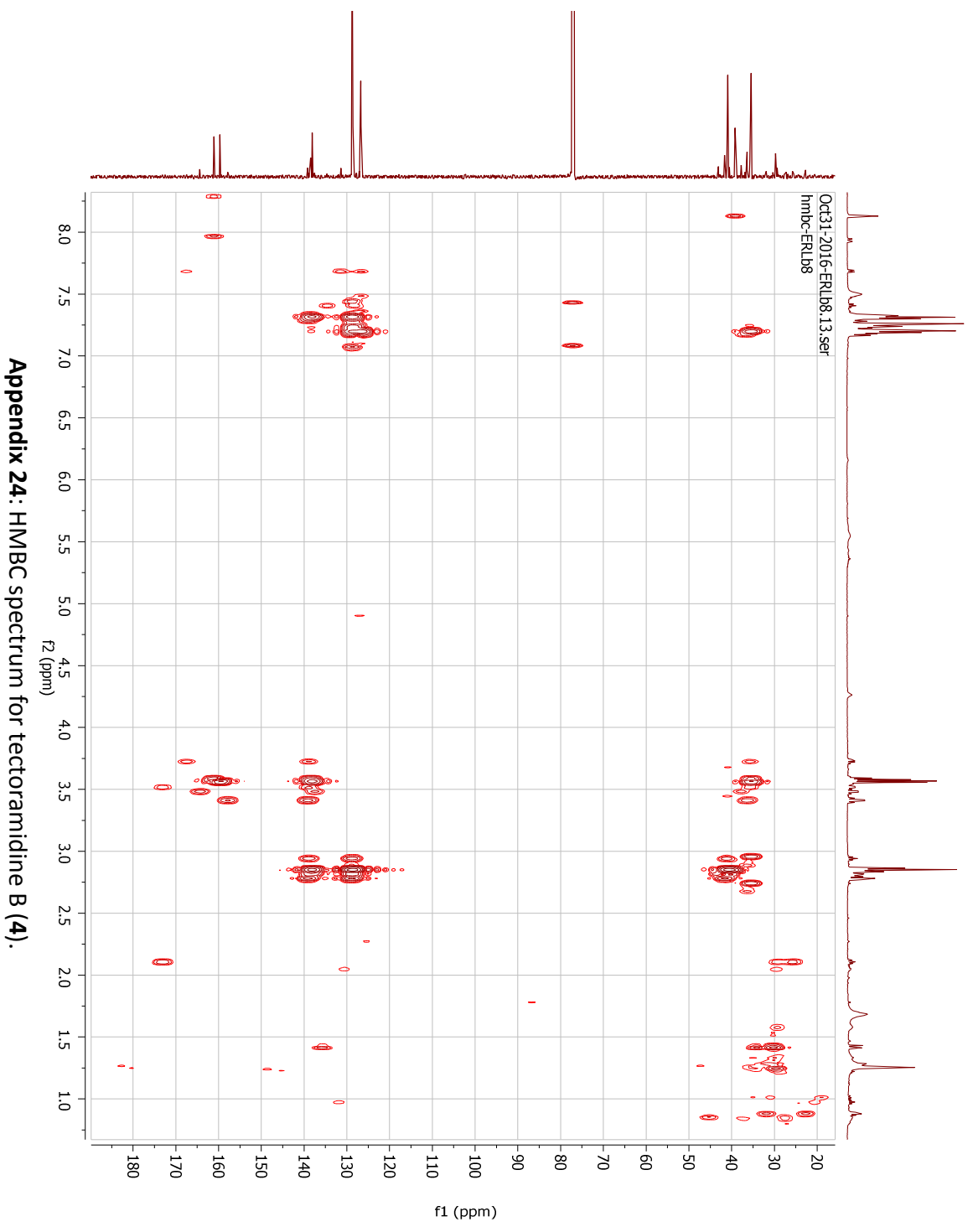
Element:<sup>12</sup>C:0 .. 50, <sup>1</sup>H:0 .. 100, <sup>14</sup>N:1 .. 10, <sup>16</sup>O:0 .. 15



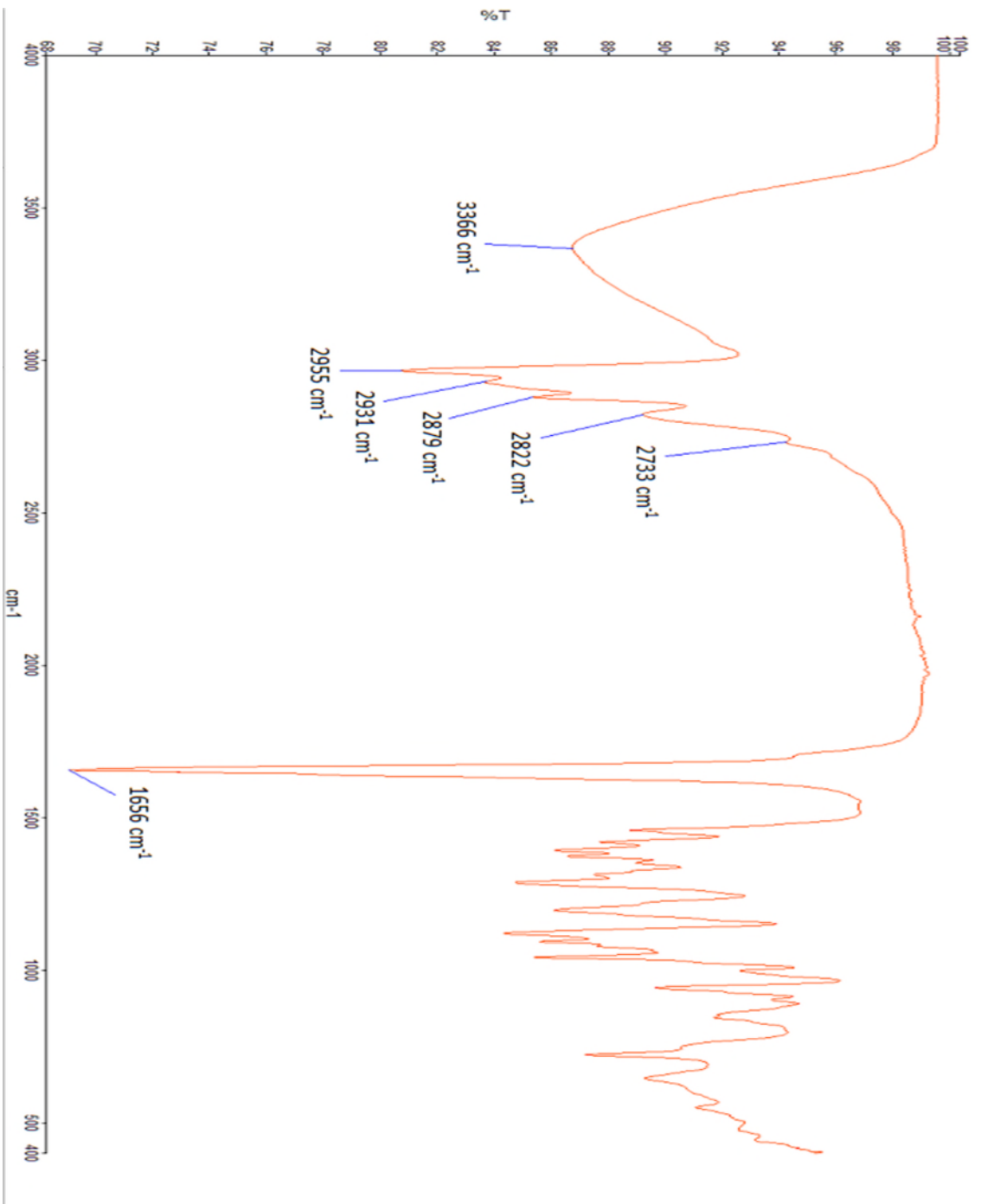
Appendix 22: MS spectrum for tectoramidine B (4).



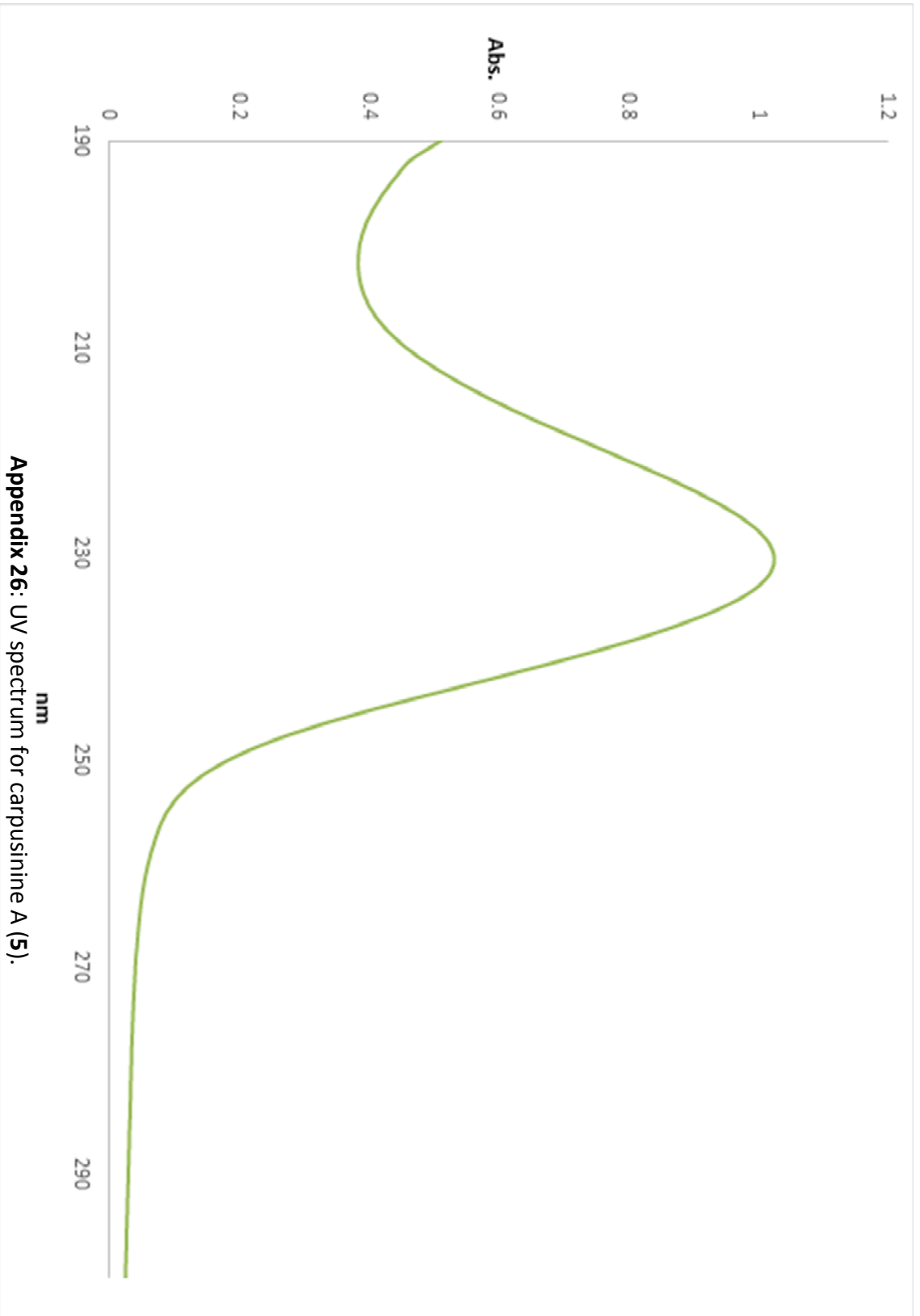
Appendix 23: HSQC spectrum for tectoramidine B (**4**).



Appendix 24: HMBC spectrum for tectoramide B (4).

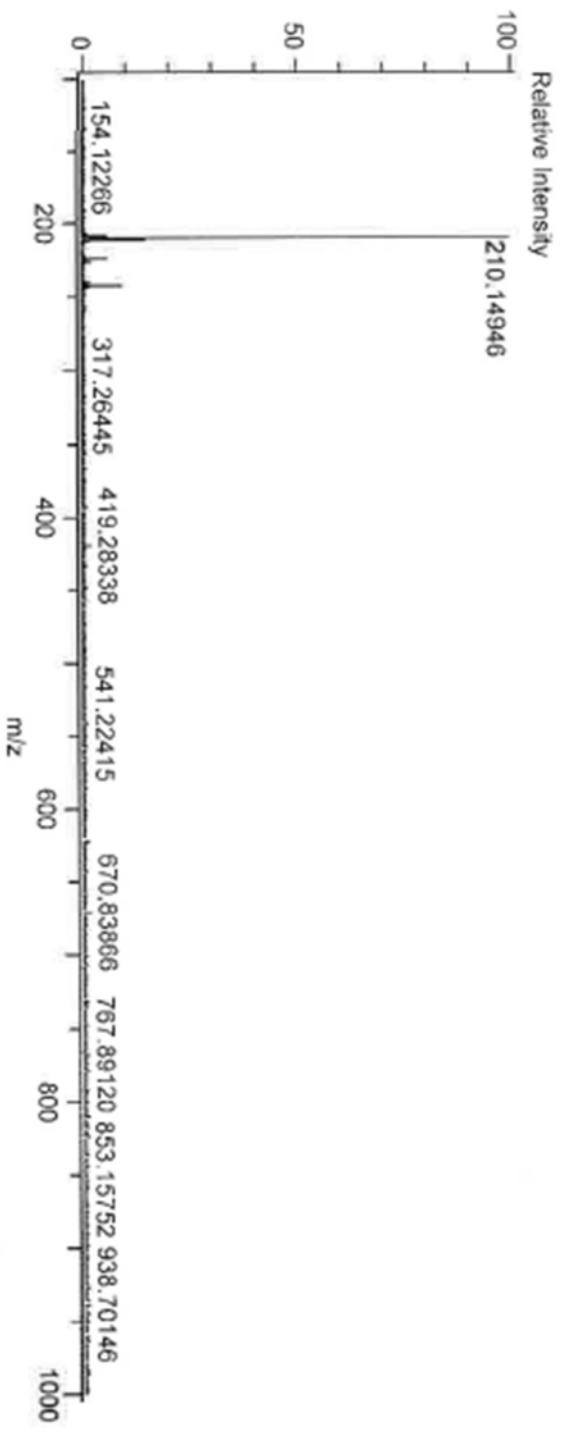


**Appendix 25:** IR spectrum for carpusinine A (5).

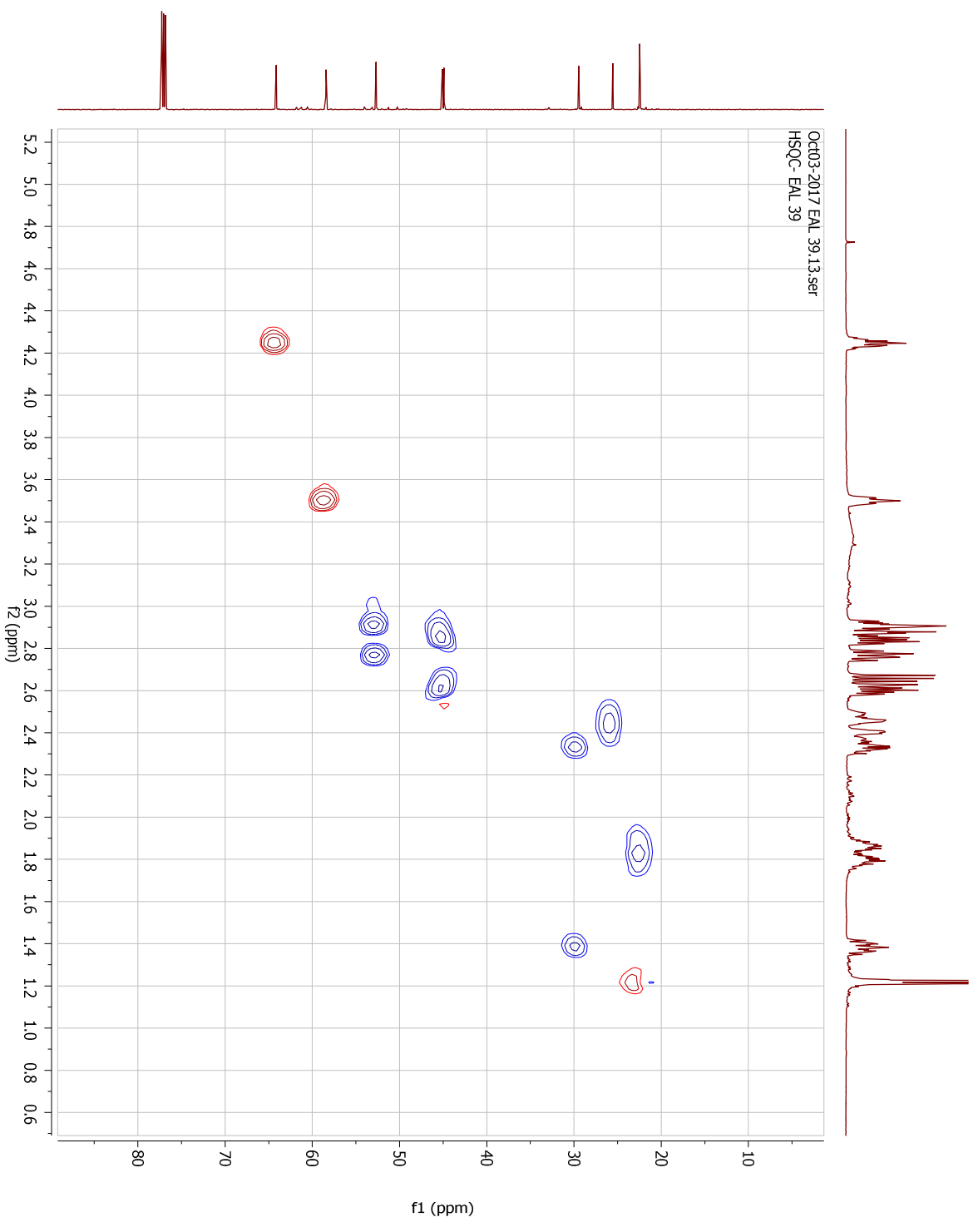


**Appendix 26:** UV spectrum for carpusinine A (5).

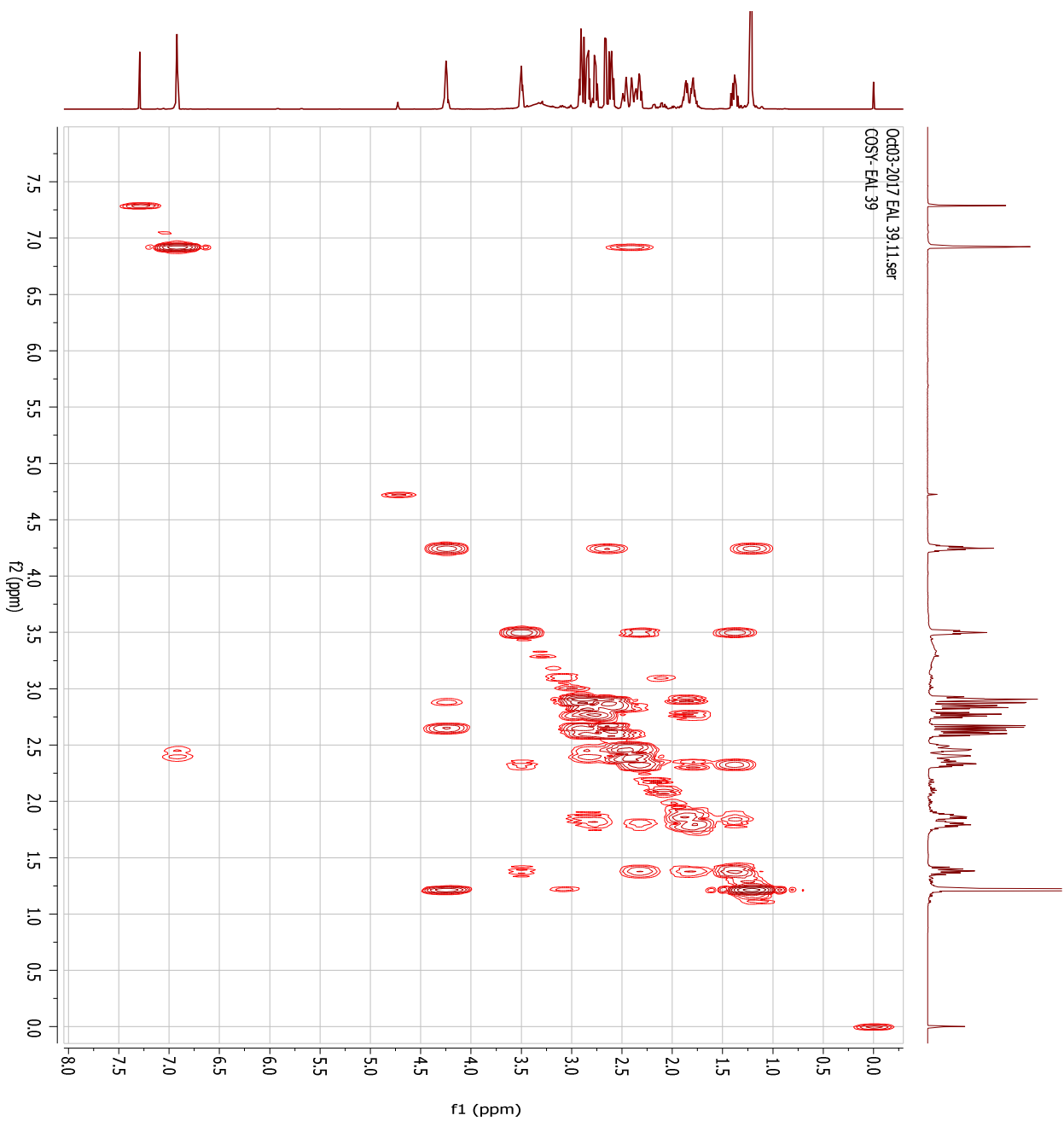
Data: EAL39  
 Sample Name:  
 Description:  
 Ionization Mode: ESI+  
 History: Determine m/z|Peak Detect(Centroid,30,Area);Correct Base[0.5%];Correct Ba...  
 Charge number: 1  
 Element: <sup>12</sup>C:0 .. 20, <sup>1</sup>H:0 .. 30, <sup>14</sup>N:0 .. 5, <sup>16</sup>O:0 .. 5  
 Tolerance: 20.00(ppm), 0.00 .. 30.00(mmu)  
 Unsaturation Number: 0.0 .. 25.0 (Fractio...  
 Acquired: 11/22/2017 10:54:03 AM  
 Operator: AccuTOF  
 Mass Calibration data: DART\_Calib\_2211...  
 Created: 11/22/2017 11:22:47 AM  
 Created by: AccuTOF



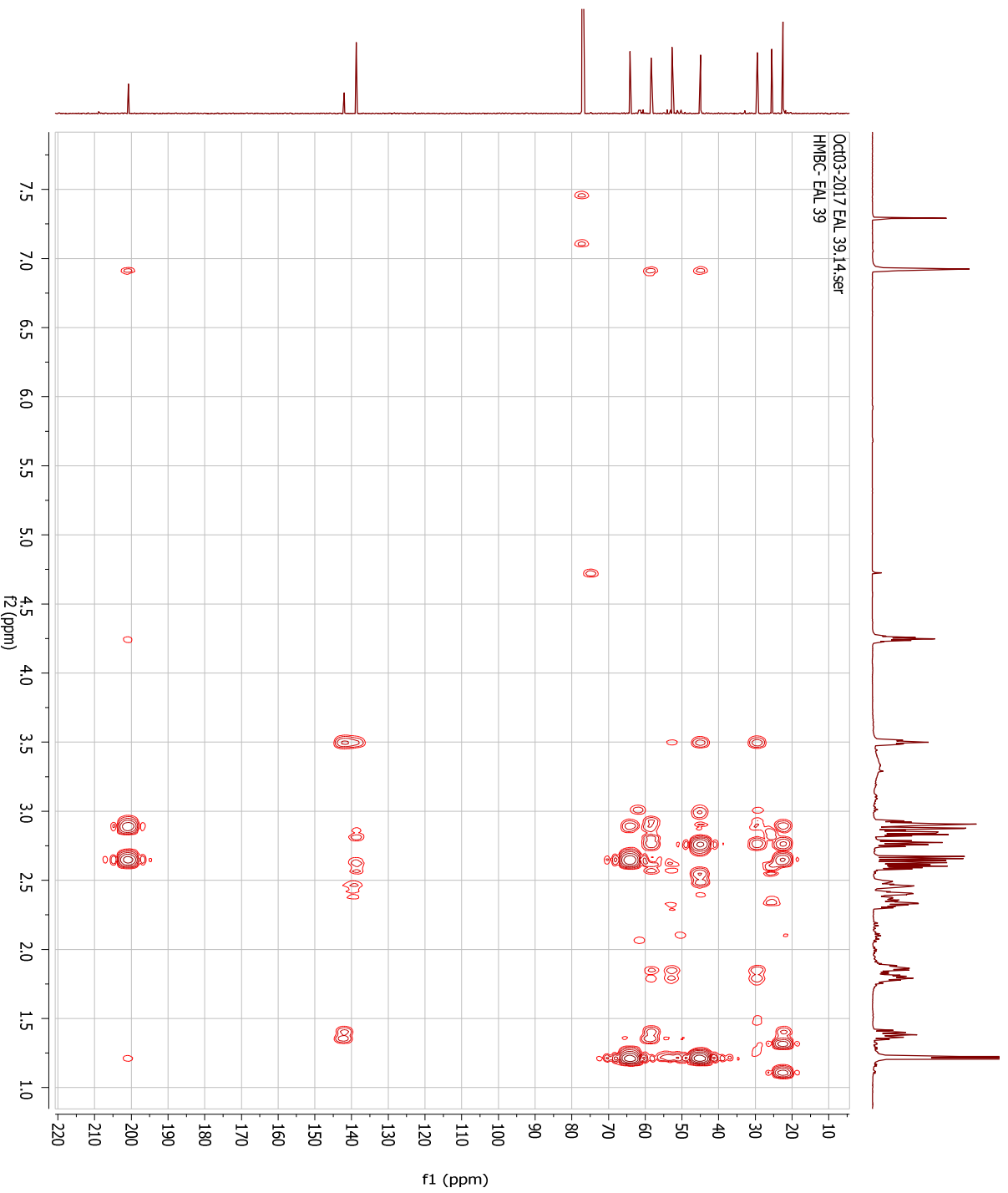
Appendix 27: MS spectrum for carpusinine A (5).



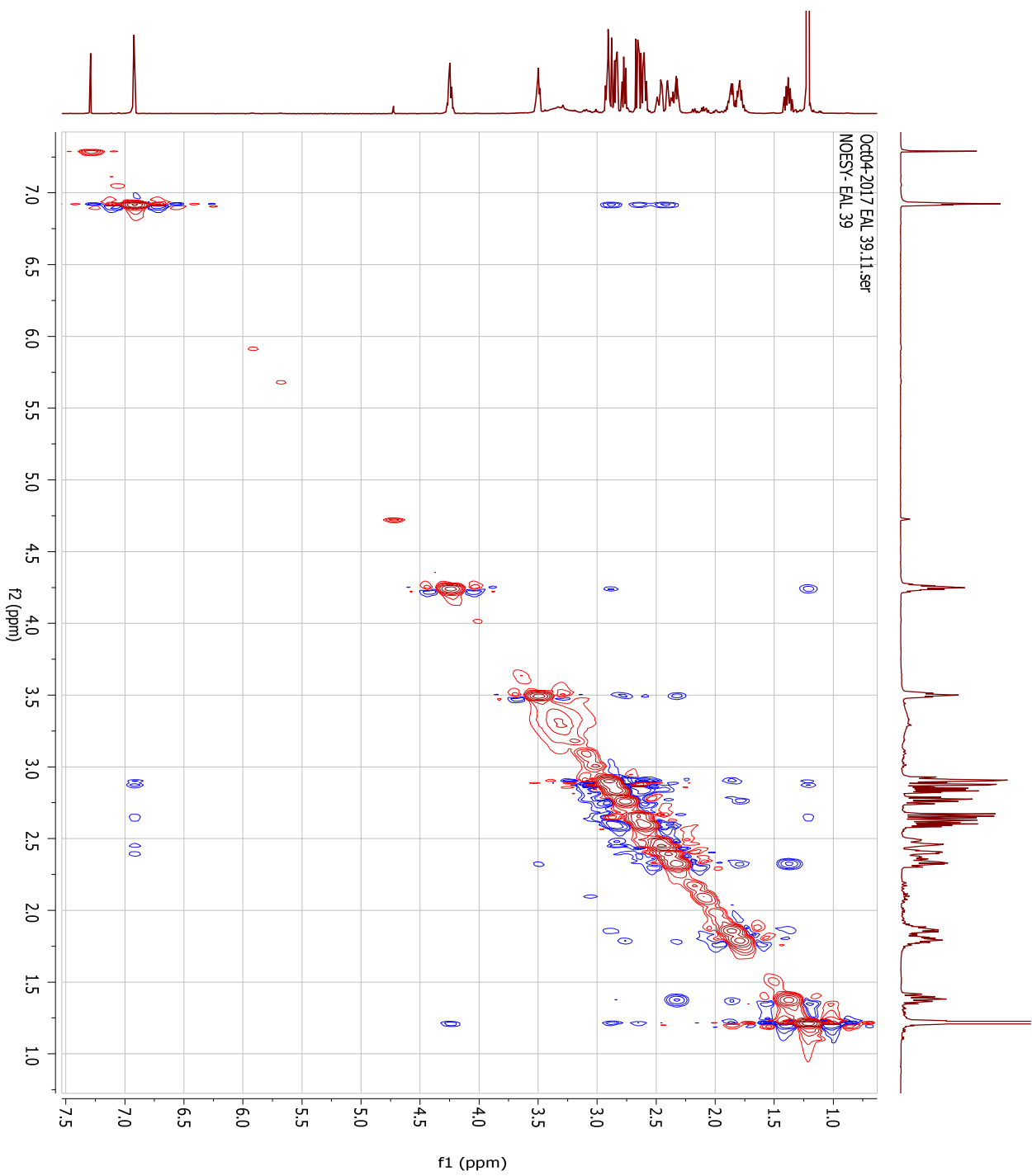
Appendix 28: HSQC spectrum for carpusinine A (5).



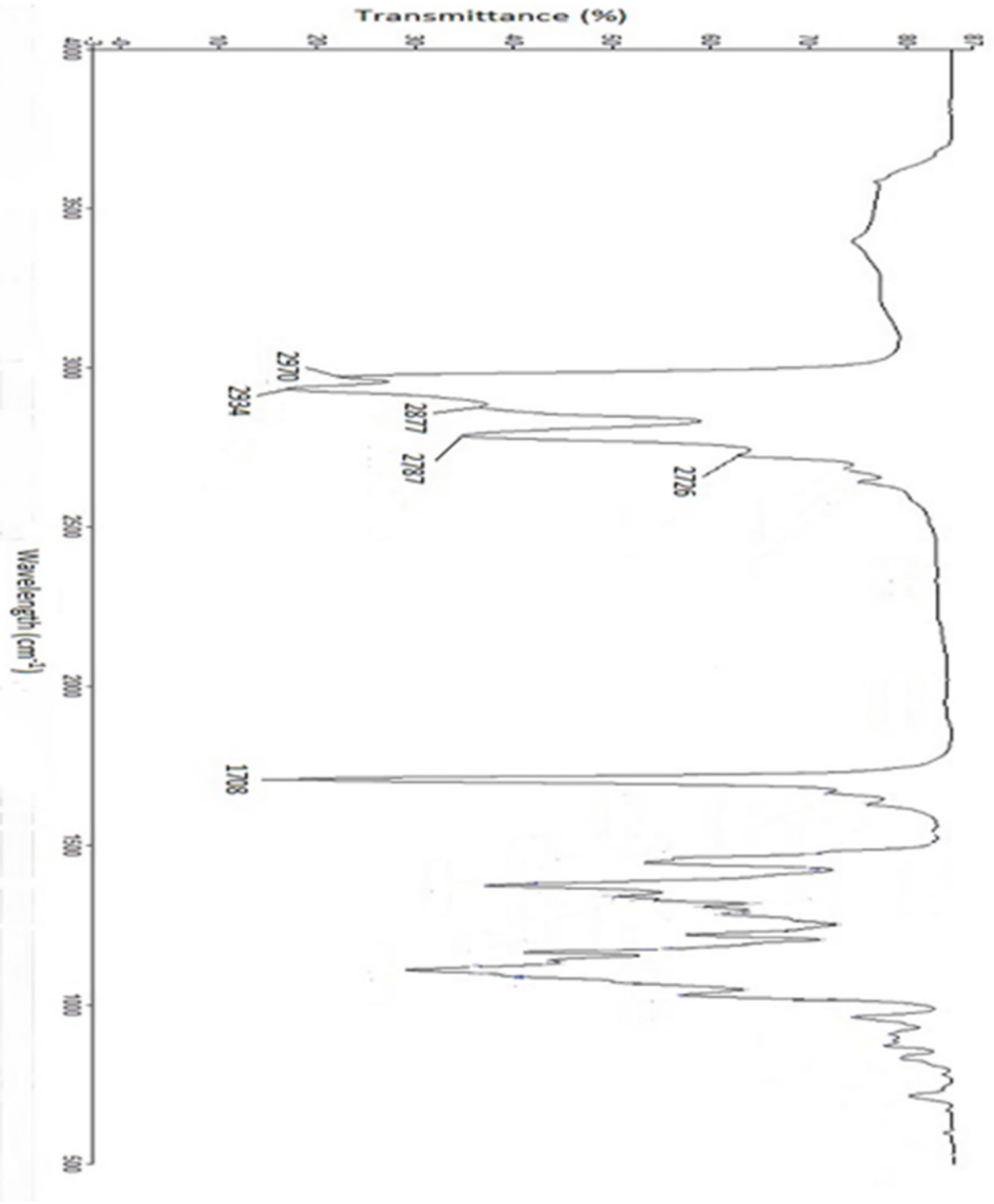
**Appendix 29:** COSY spectrum for carpusinine A (5).



Appendix 30: HMBC spectrum for carpusinine A (5).



**Appendix 31:** NOESY spectrum for carpusinine A (5).



Appendix 32: IR spectrum for carpusinine B (6).

Data: EAL26

Sample Name:

Description:

Ionization Mode: ESI+

History: Determine m/z/Peak Detect(Centroid,30,Area),Correct Base(0.5%),Correct Ba...

Acquired: 3/22/2017 2:15:04 PM

Operator: AccuTOF

Mass Calibration data: Int Calib 220317

Created: 3/22/2017 3:01:25 PM

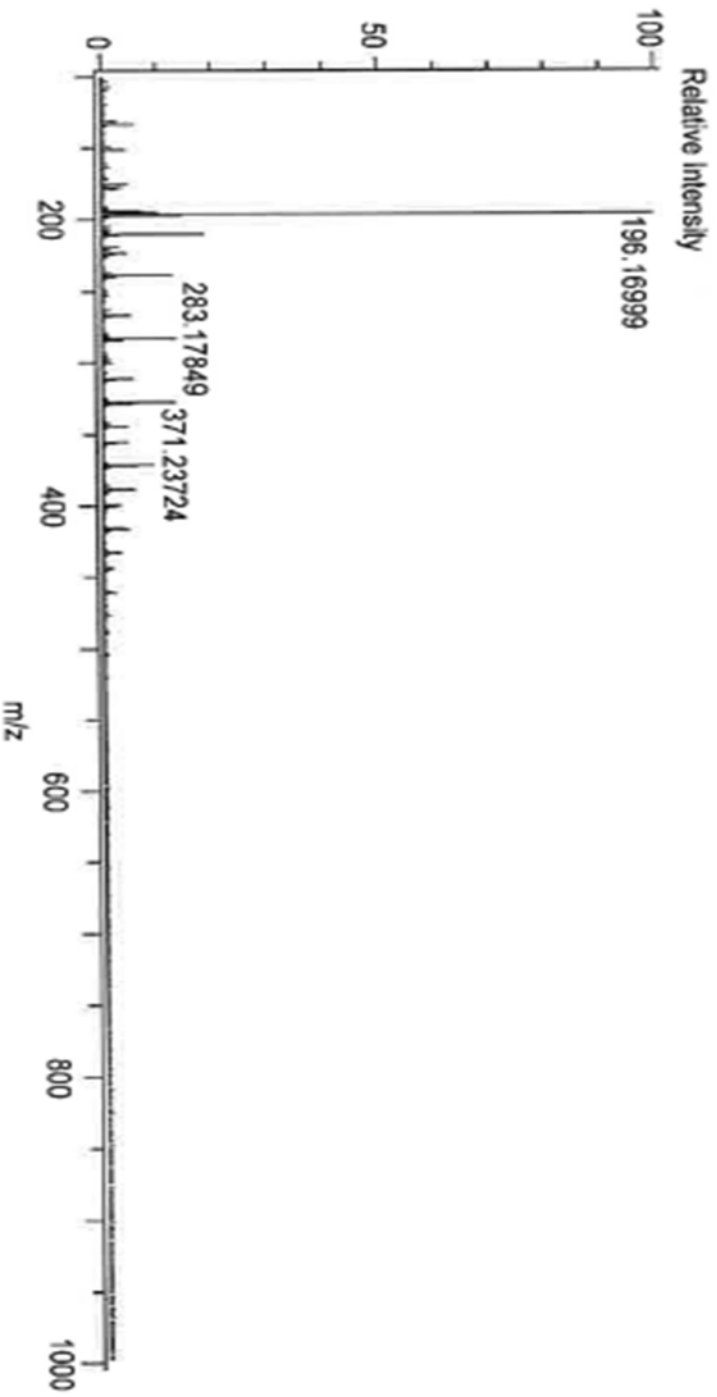
Created by: AccuTOF

Charge number: 1

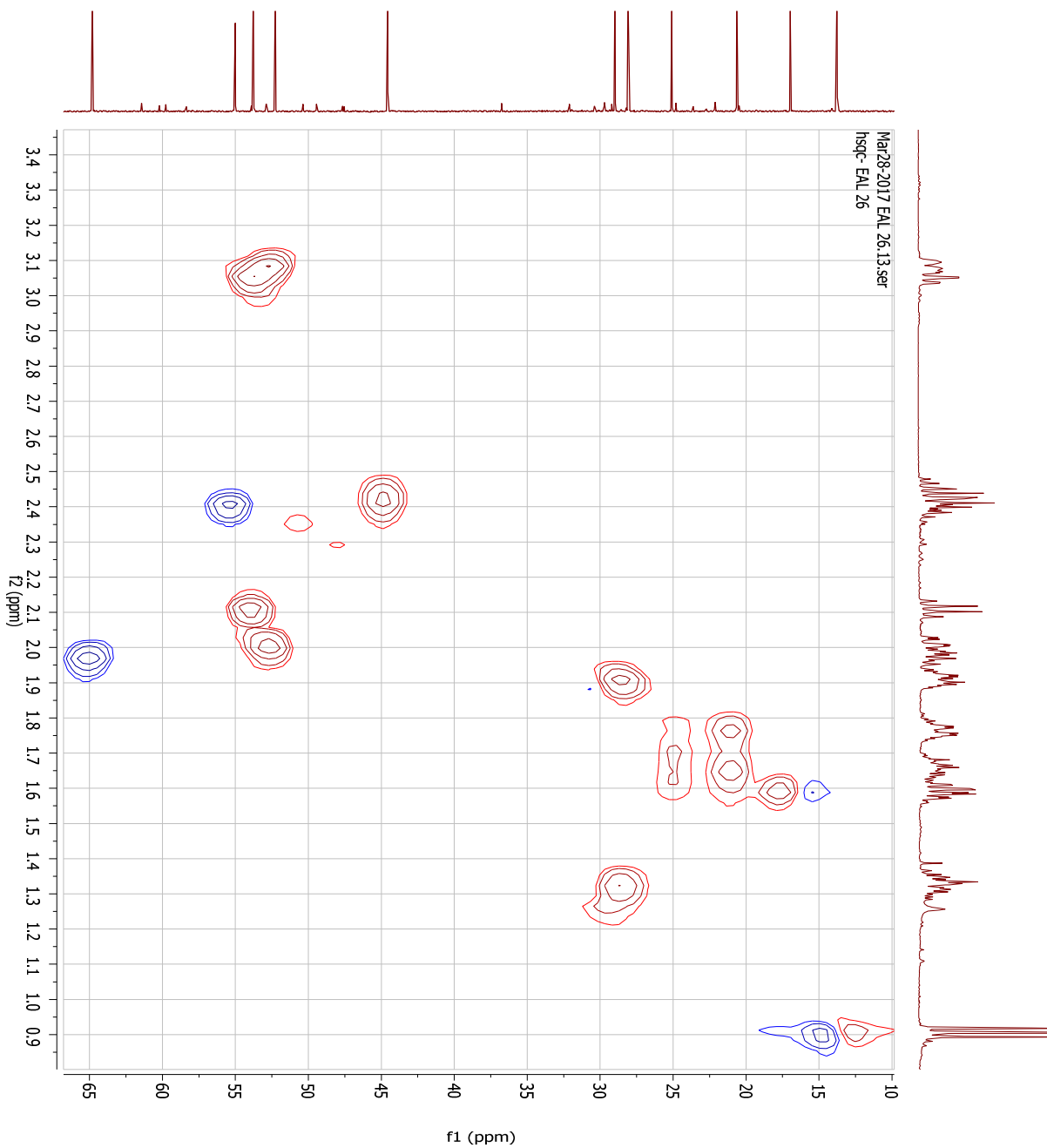
Tolerance: 10.00(ppm), 0.00 .. 30.00(mmu)

Unsaturation Number: 0.0 .. 25.0 (F-ratio...

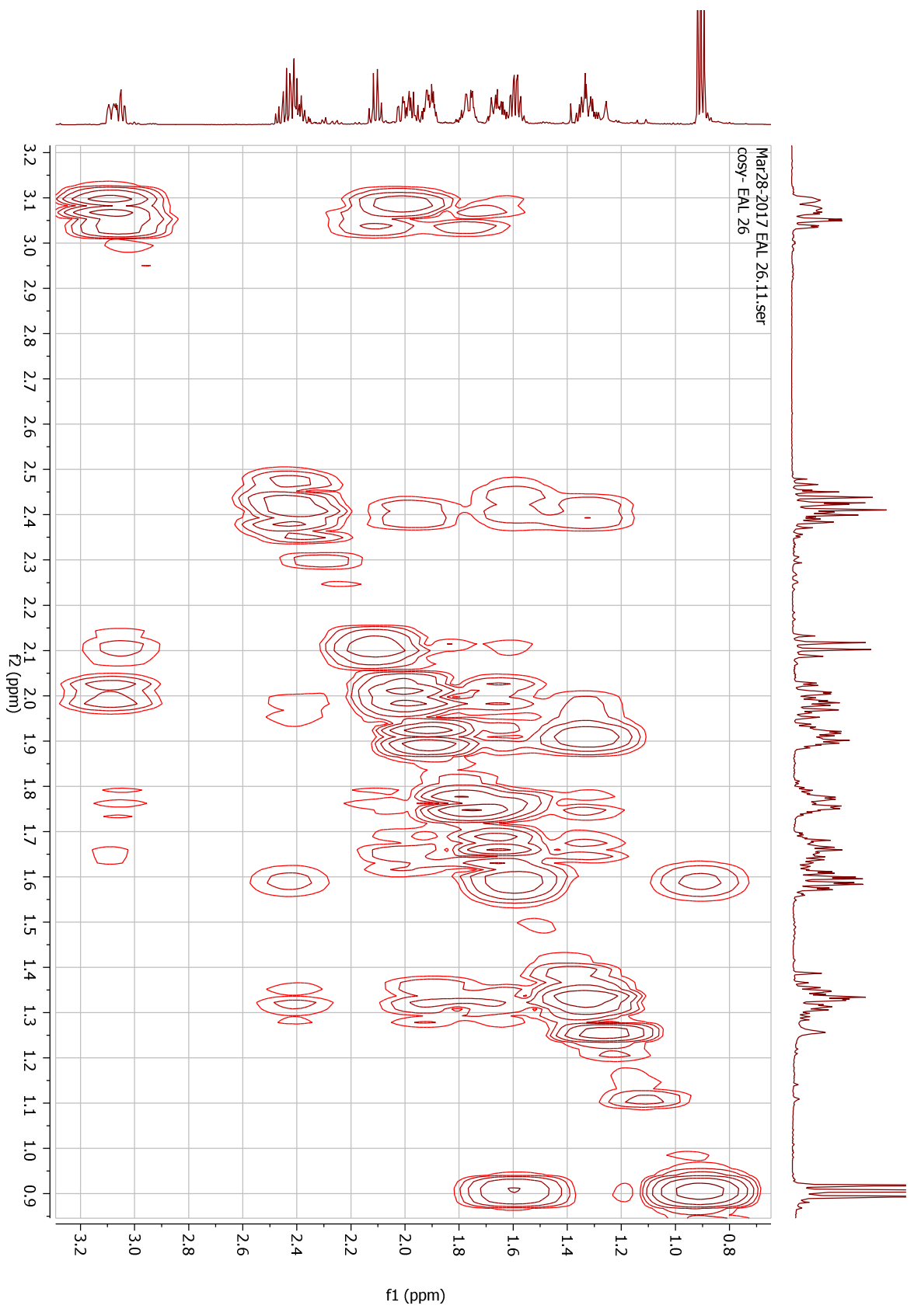
Element: <sup>12</sup>C: 0 .. 30, <sup>1</sup>H: 0 .. 30, <sup>14</sup>N: 0 .. 5, <sup>16</sup>O: 0 .. 5



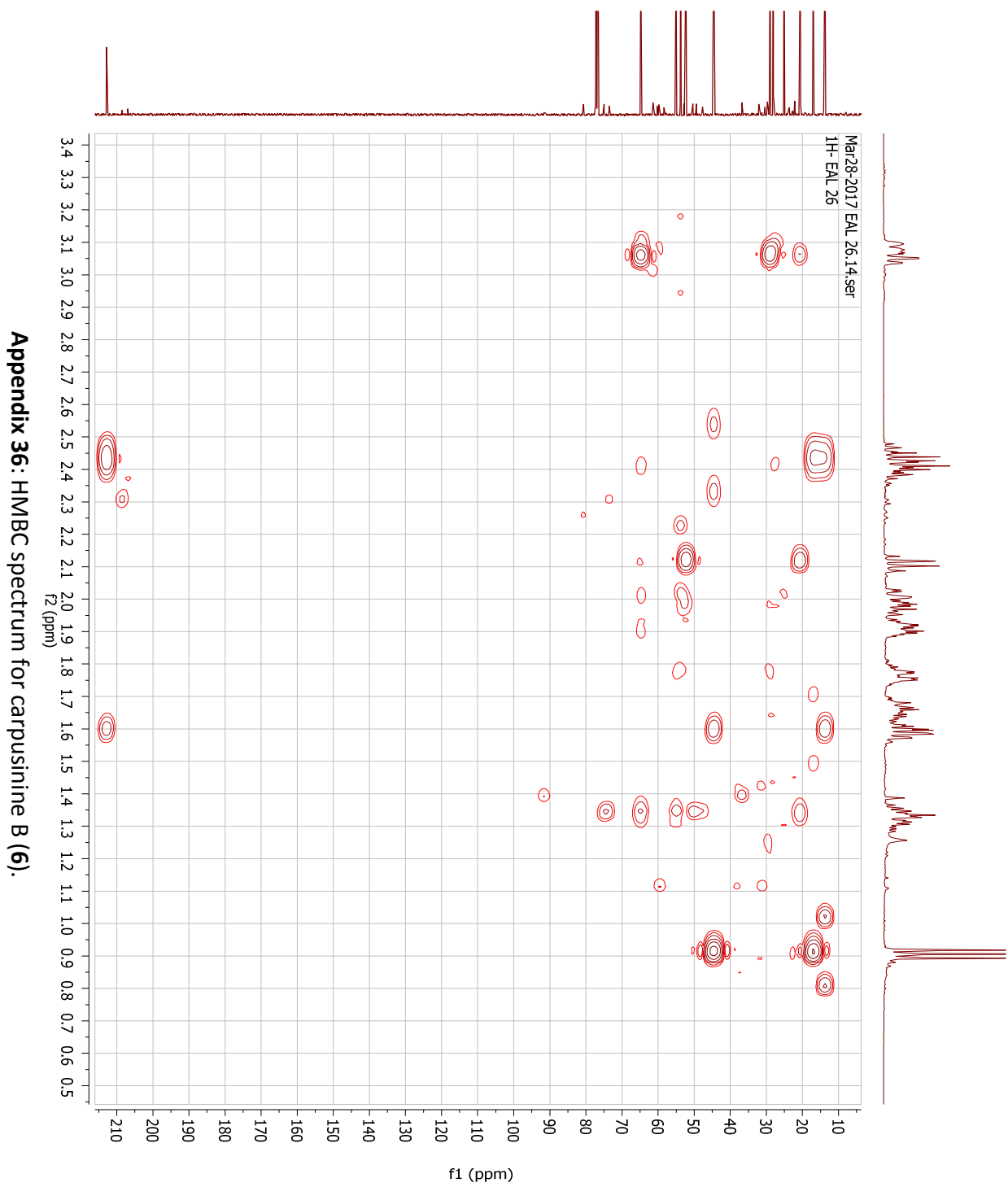
Appendix 33: MS spectrum for carpusinine B (6).



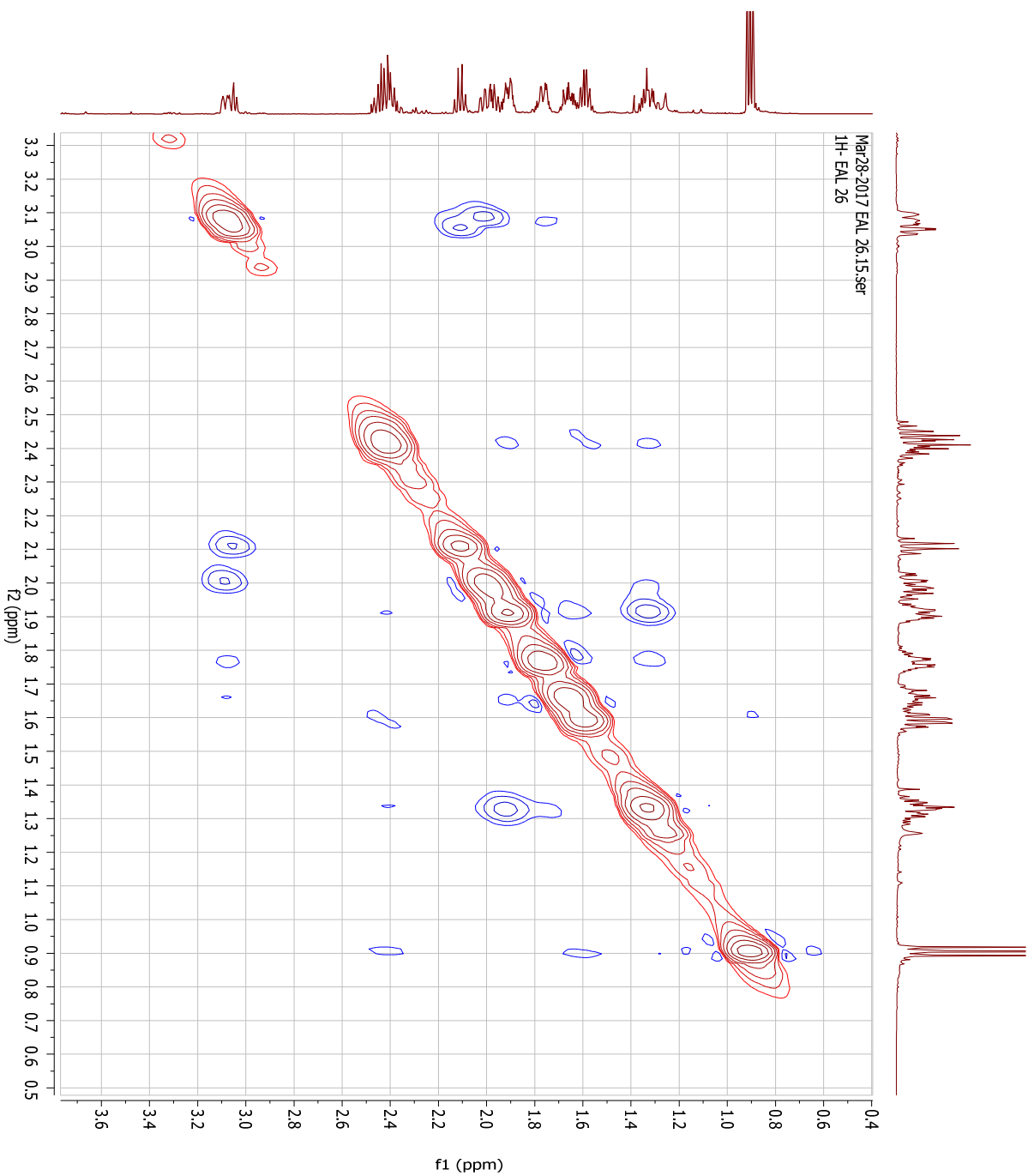
**Appendix 34:** HSQC spectrum for carpusinine B (6).



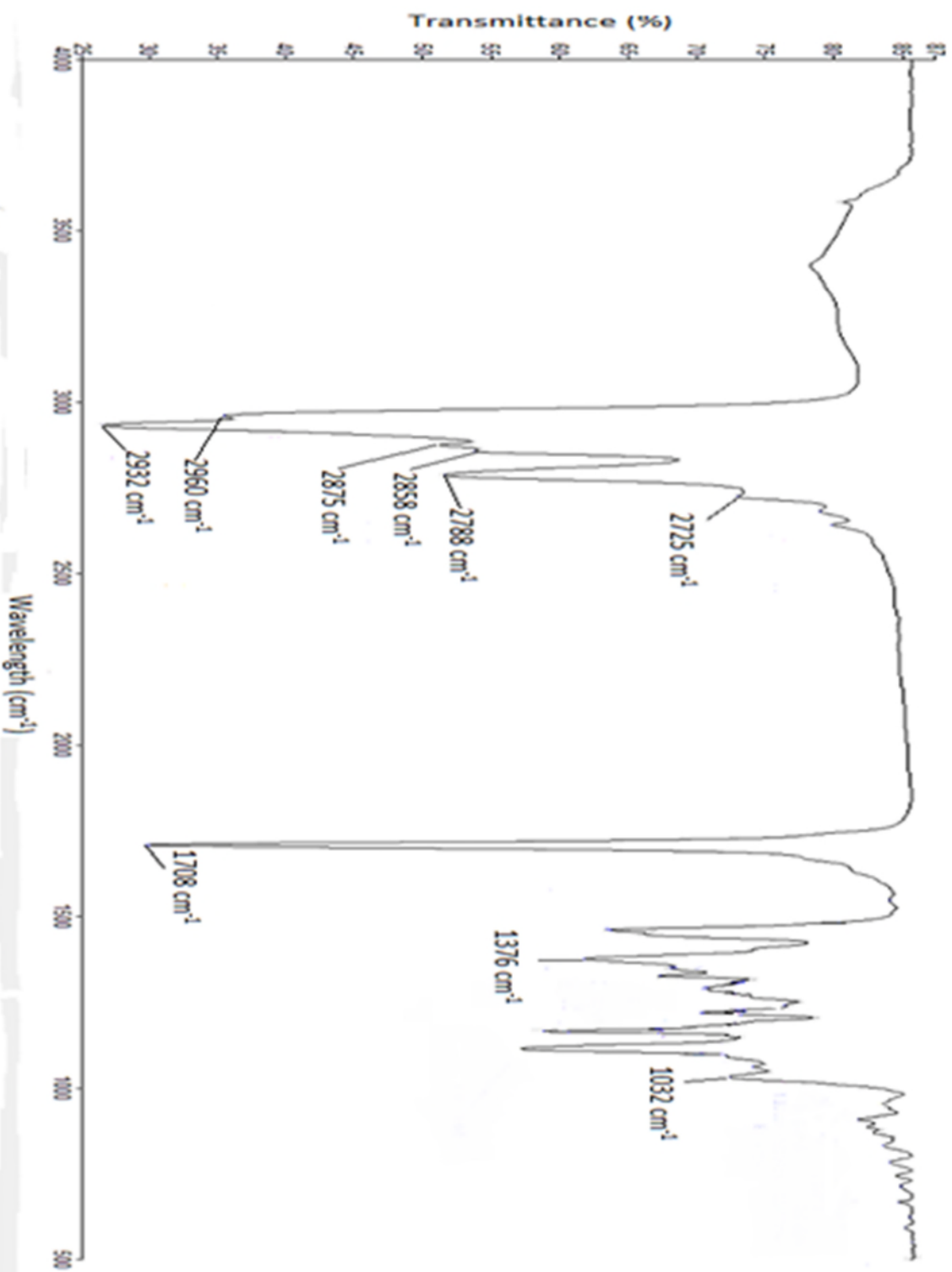
**Appendix 35: COSY spectrum for carpusinine B (6).**



Appendix 36: HMBBC spectrum for carpusinine B (6).



**Appendix 37: NOESY spectrum for carpusinine B (6).**



Appendix 38: IR spectrum for carpusinine C and epicarpusinine C (**7a** and **7b**).

Data: EAL27

Acquired: 3/22/2017 2:16:54 PM

Sample Name:

Operator: AccuTOF

Description:

Mass Calibration data: Int Calib 220317

Ionization Mode: ESI+

Created: 3/22/2017 3:13:23 PM

History: Determine m/z [Peak Detect [Centroid, 30, Area], Correct Base [0.5%]], Correct Ba...

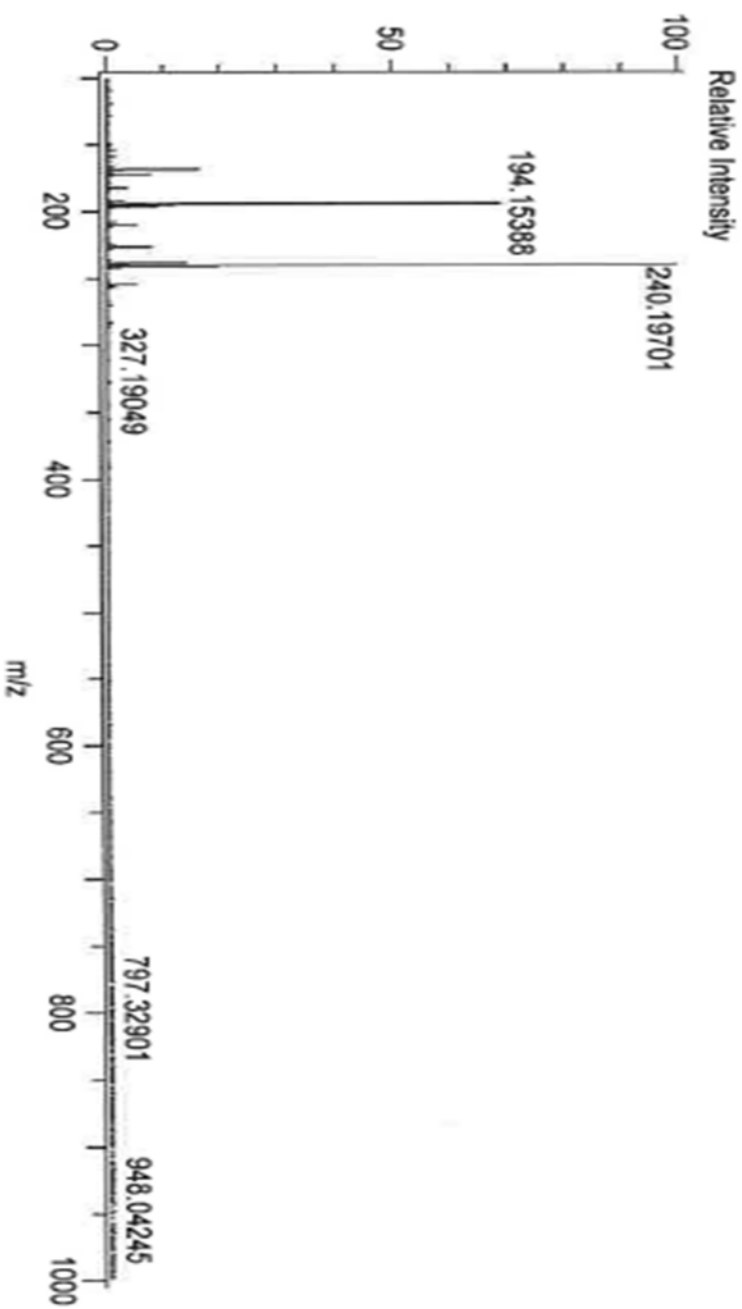
Created by: AccuTOF

Charge number: 1

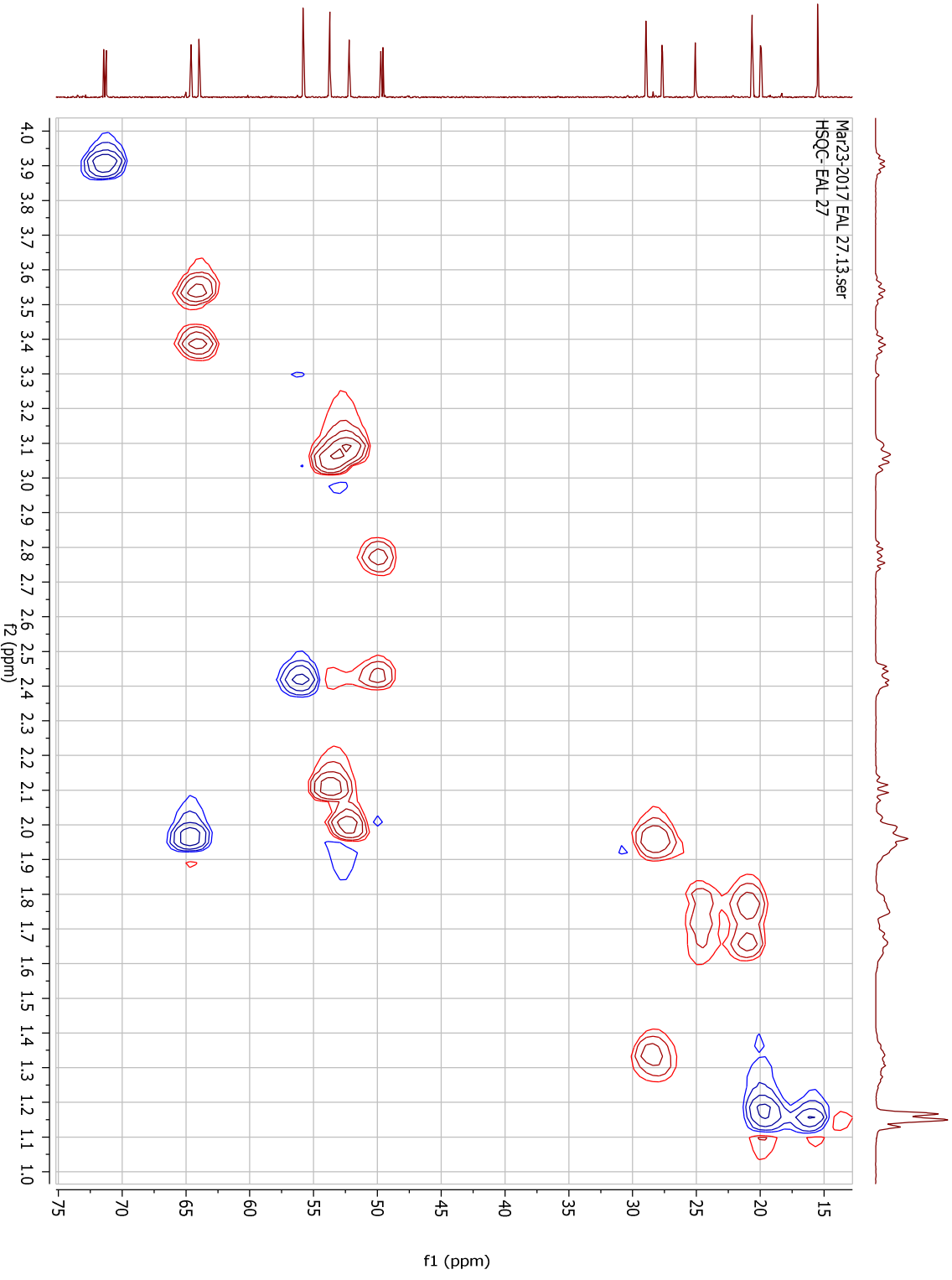
Tolerance: 10.00 (ppm), 0.00 .. 30.00 (mmu)

Unsaturation Number: 0.0 .. 25.0 (Fracio...

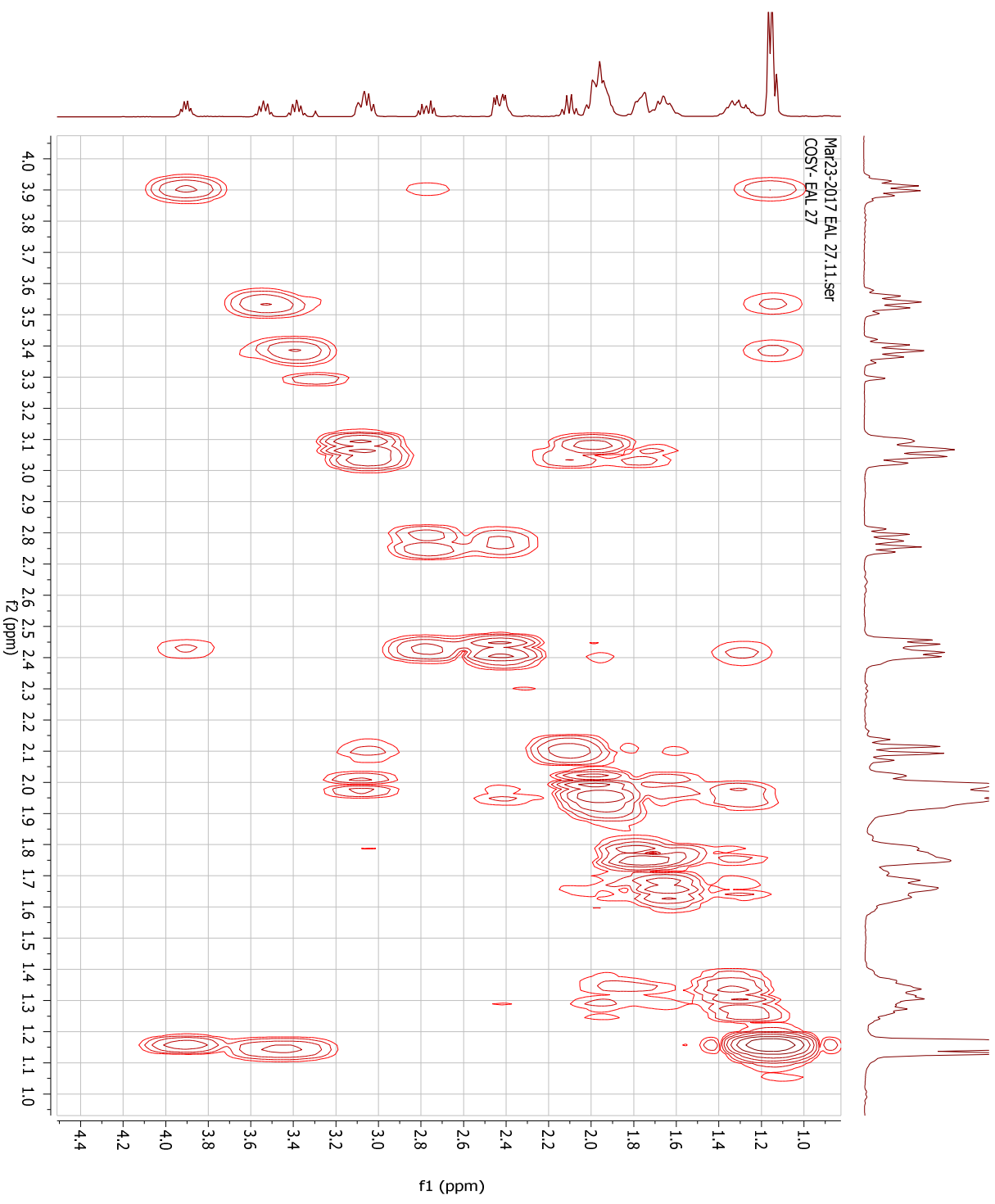
Element: <sup>12</sup>C: 0 .. 30, <sup>1</sup>H: 0 .. 30, <sup>14</sup>N: 0 .. 5, <sup>16</sup>O: 0 .. 5



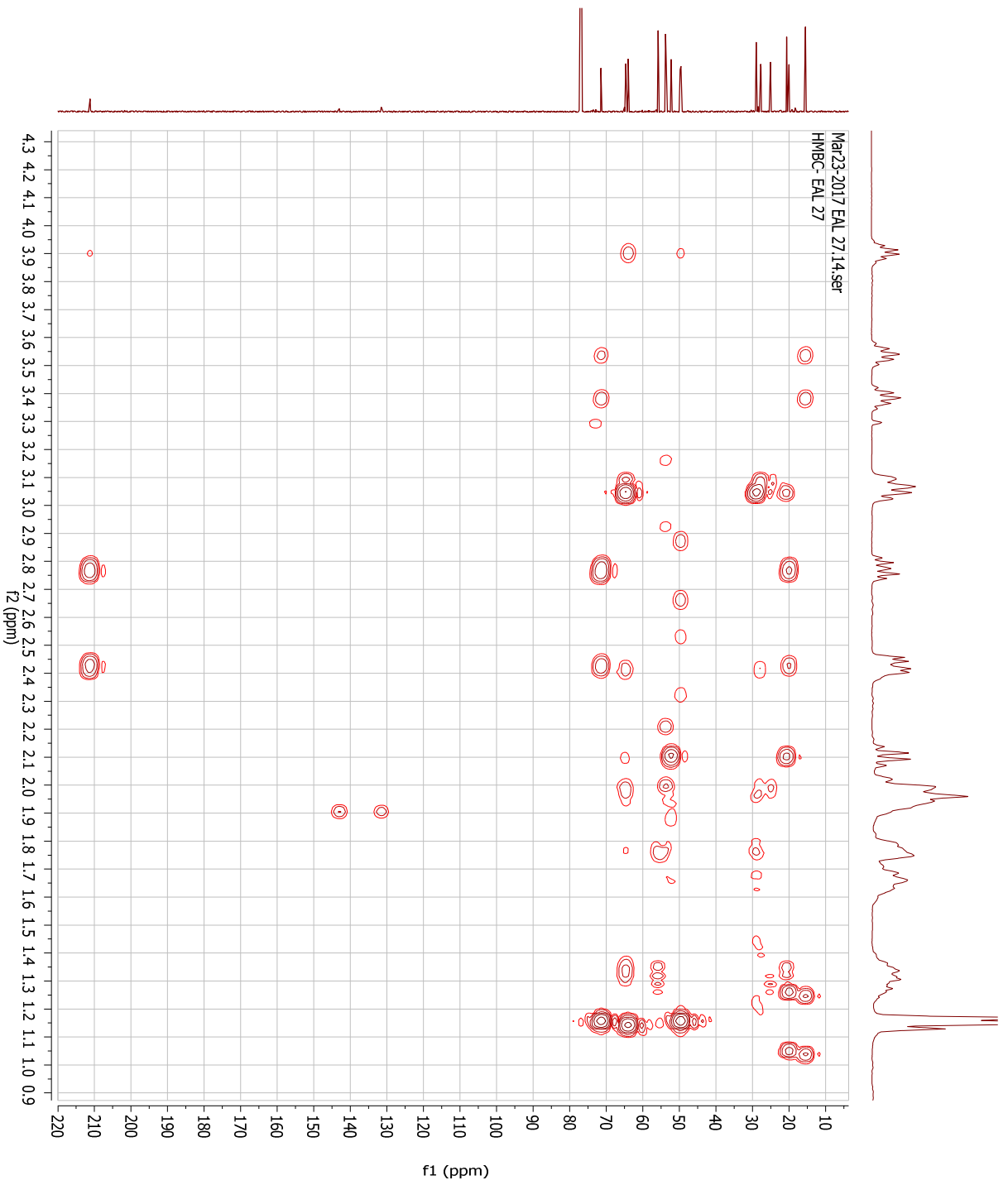
Appendix 39: MS spectrum for carpusinine C and epicarpusinine C (7a and 7b).



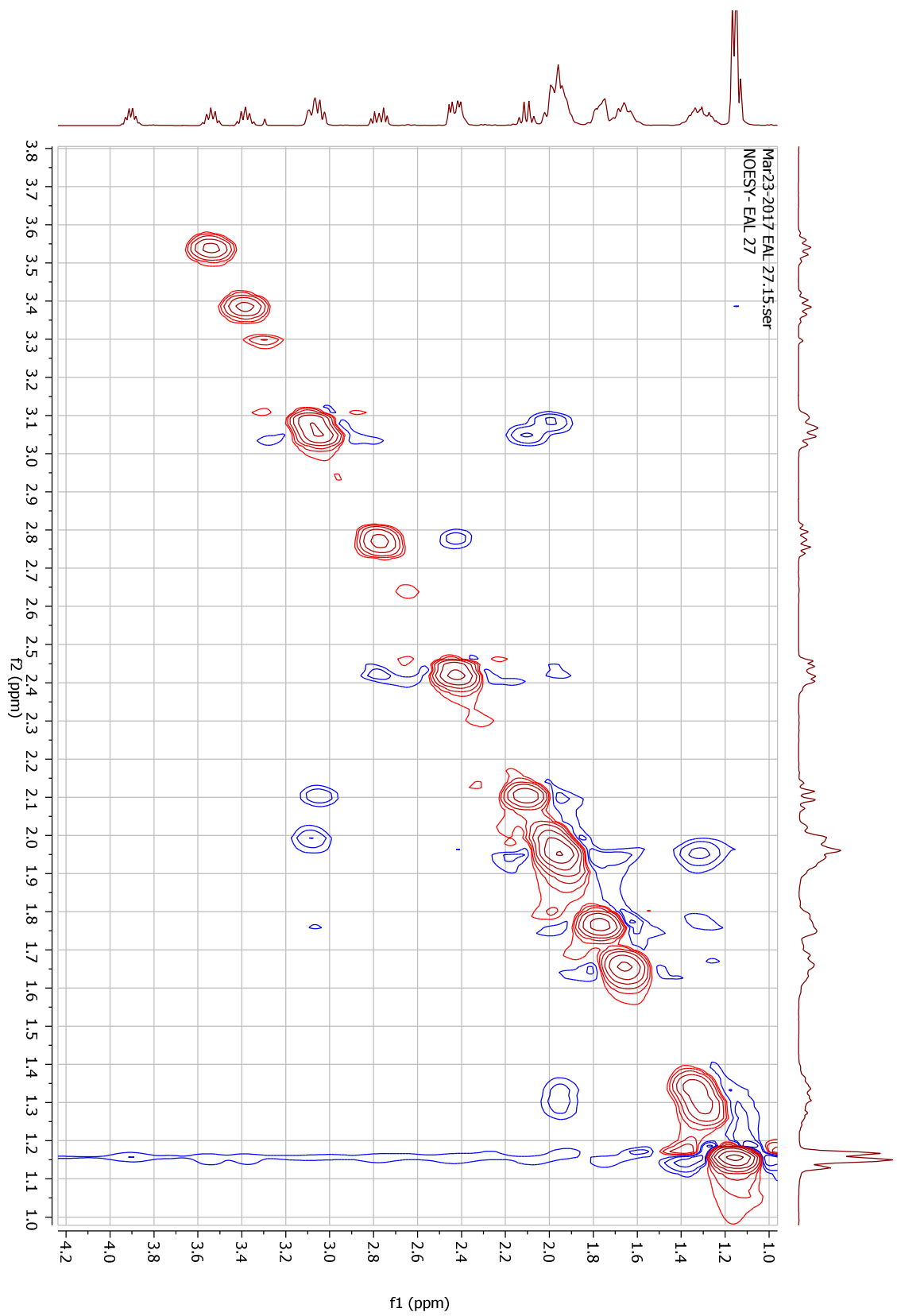
**Appendix 40: HSQC spectrum for carpusinine C and epicarpusinine C (7a and 7b).**



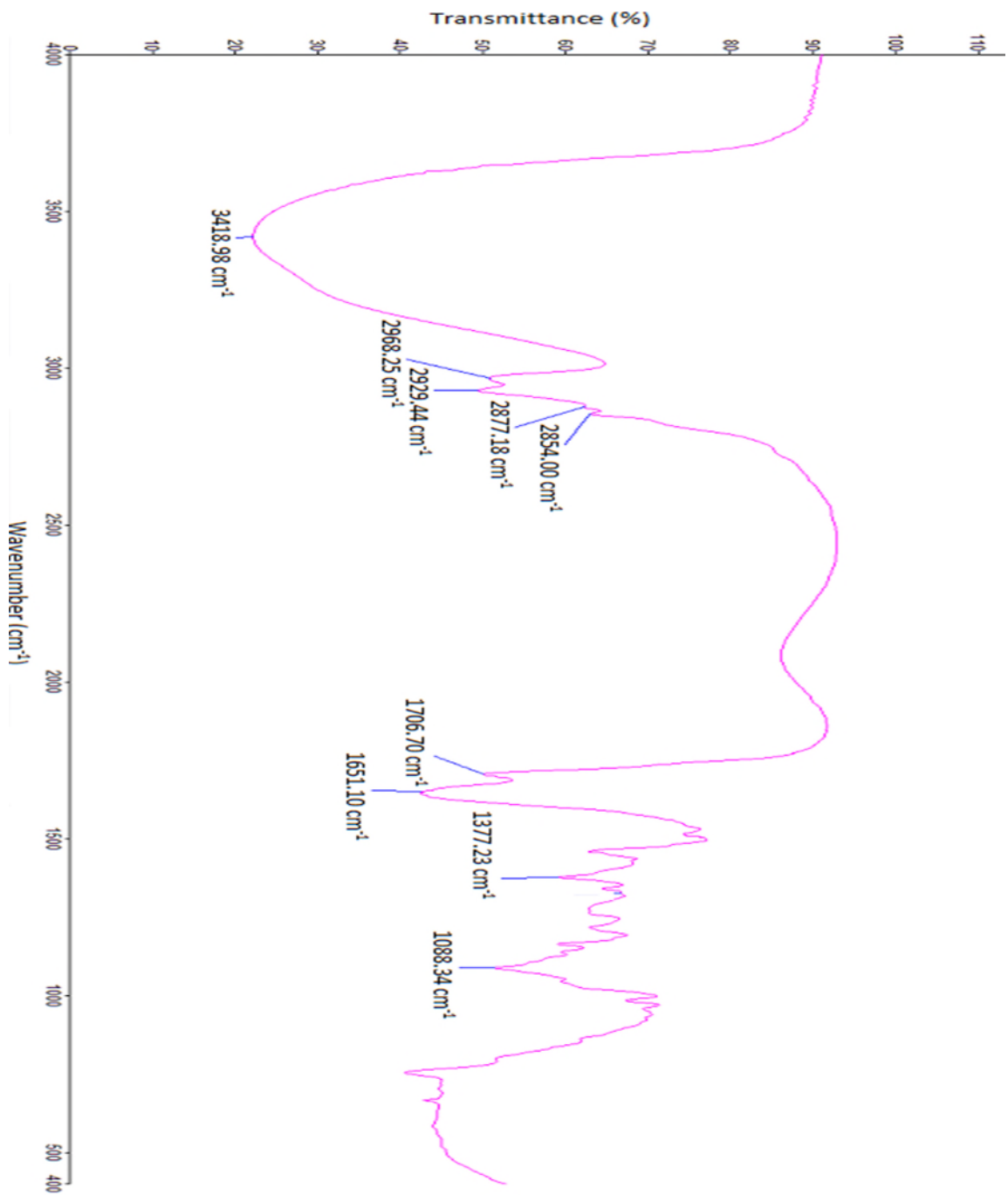
**Appendix 41:** COSY spectrum for carpusinine C and epicarpusinine C (**7a** and **7b**).



**Appendix 42: HMBC spectrum for carpusinine C and epicarpusinine C (7a and 7b).**



**Appendix 43: NOESY spectrum for carpusinine C and epicarpusinine C (7a and 7b).**



**Appendix 44:** IR spectrum for carpusinine D (**8**).

Data: EAL3\_291116

Acquired: 11/29/2016 11:32:09 AM

Sample Name:

Operator: AccuTOF

Description:

Mass Calibration data: Int Calib 291116

Ionization Mode: ESI+

Created: 12/1/2016 10:08:21 AM

History: Determine m/z Peak Detect(Centroid,30 Area),(Correct Base[0.5%]); Correct Ba...

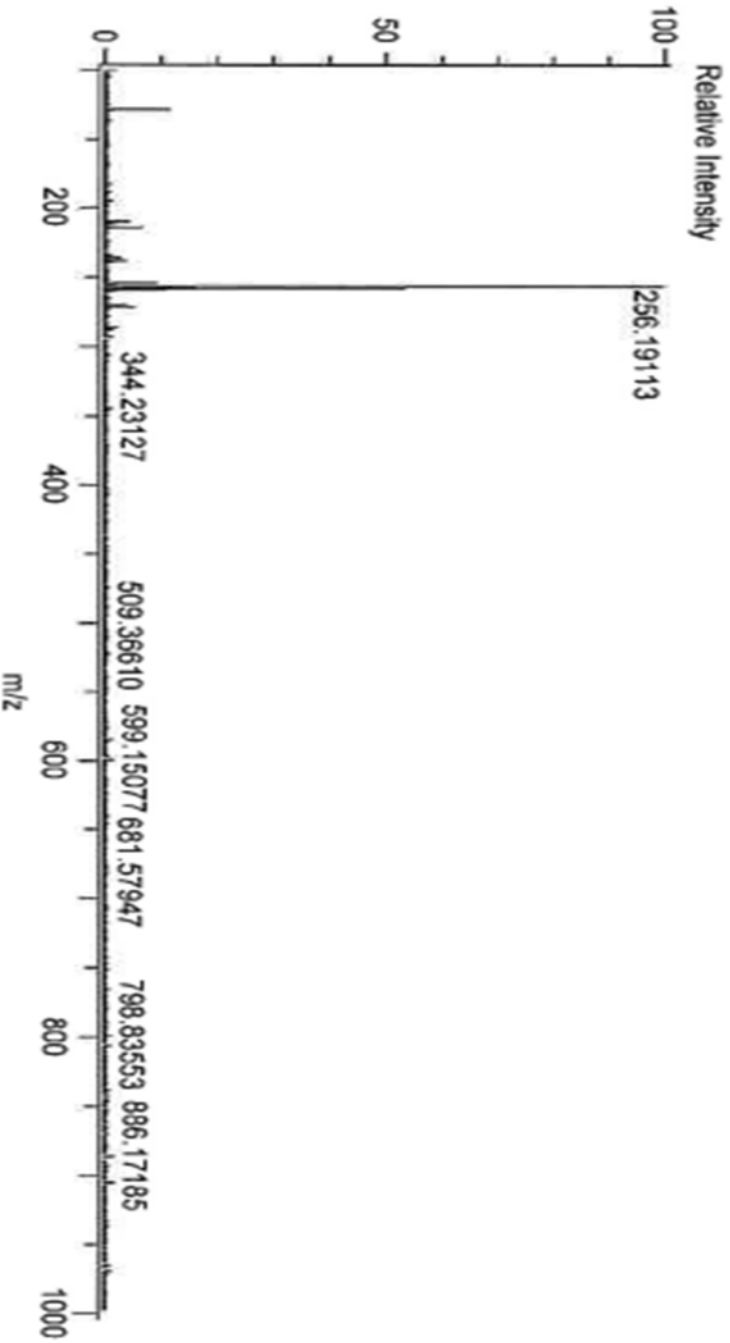
Created by: AccuTOF

Charge number: 1

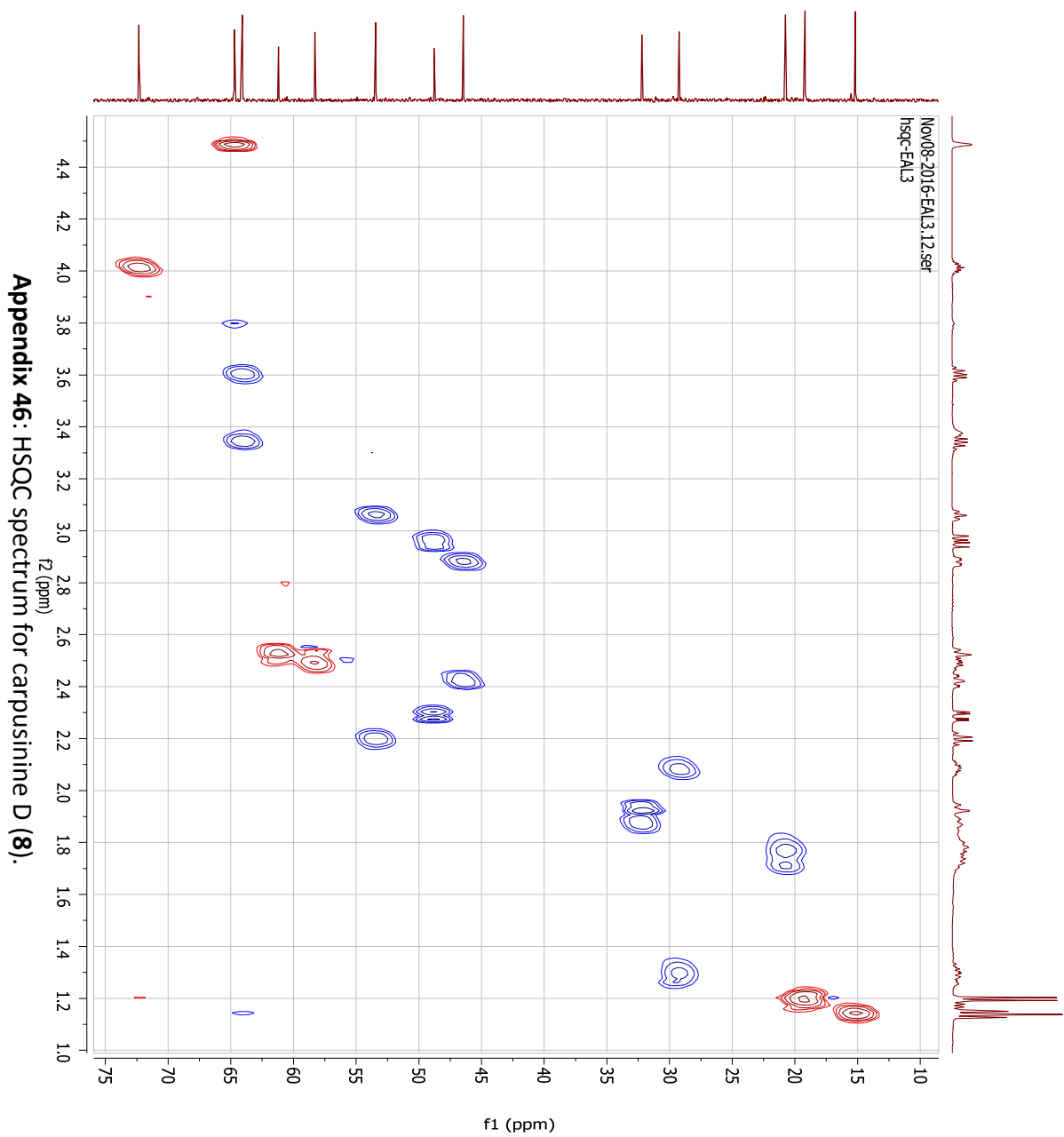
Tolerance: 30.00(ppm), 5.00 .. 15.00(mmu)

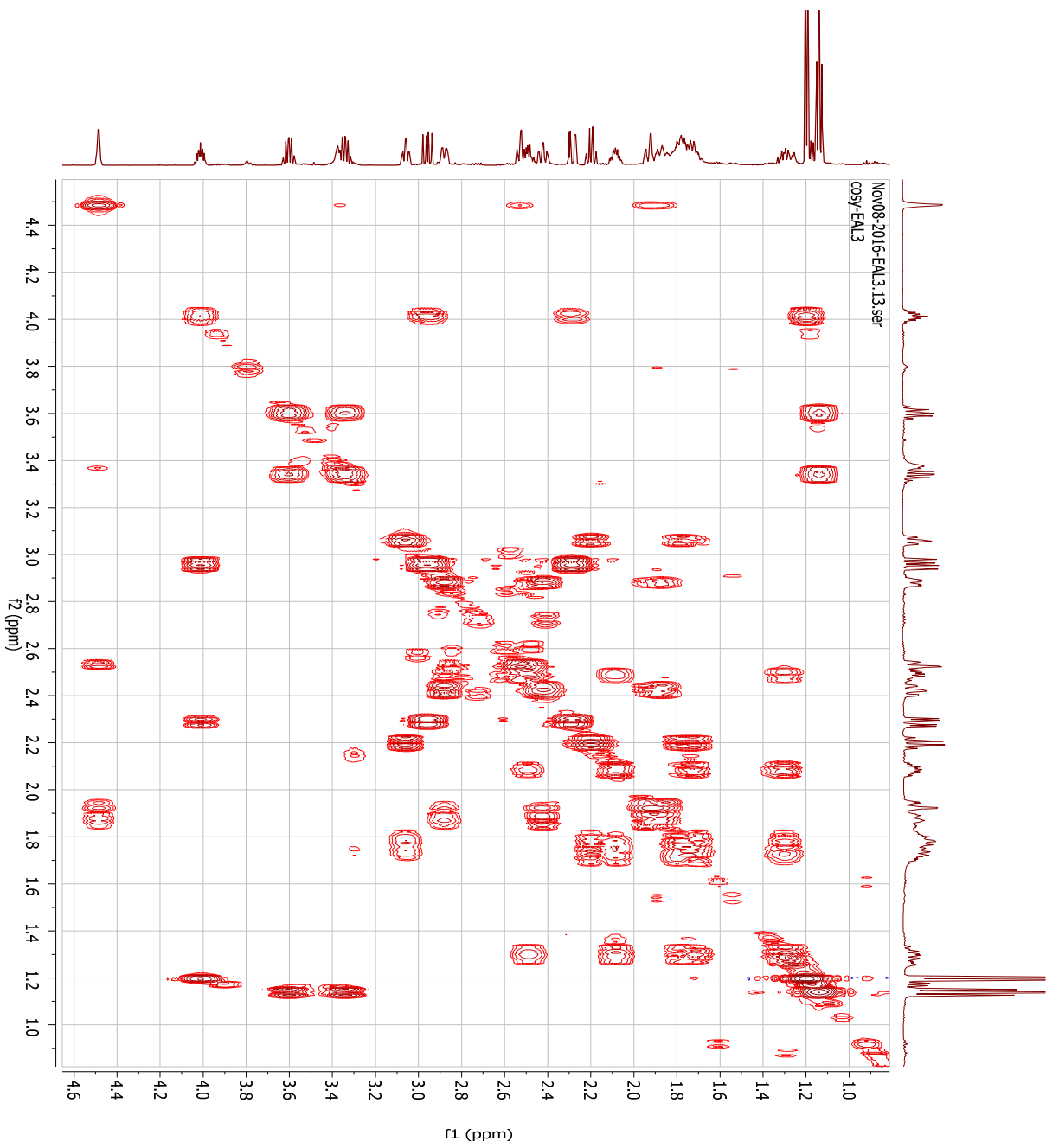
Unsaturation Number: 0.0 .. 25.0 (Fractio...

Element: <sup>12</sup>C: 0 .. 30, <sup>1</sup>H: 0 .. 40, <sup>14</sup>N: 0 .. 5, <sup>16</sup>O: 0 .. 5

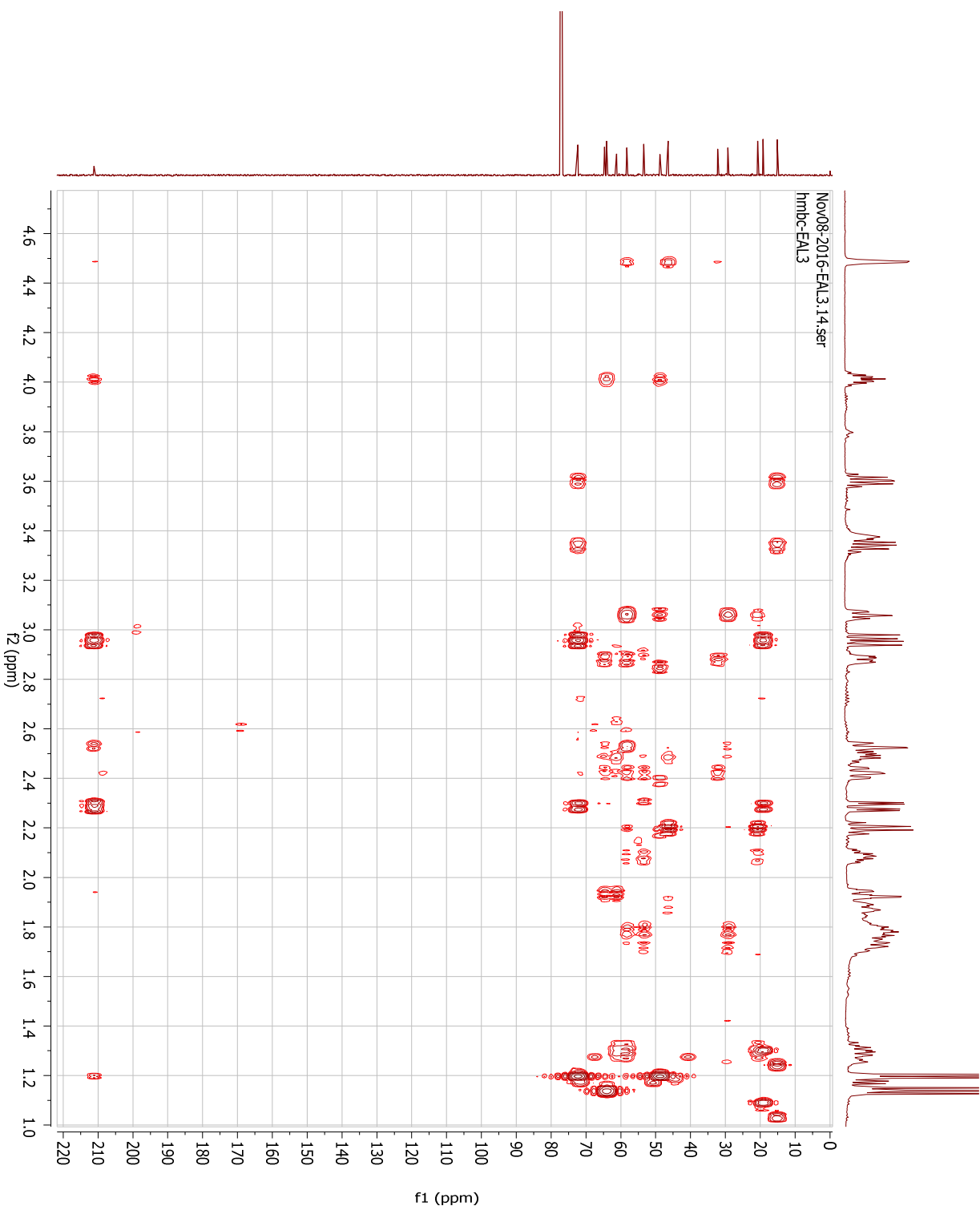


Appendix 45: MS spectrum for carpustinine D (8).

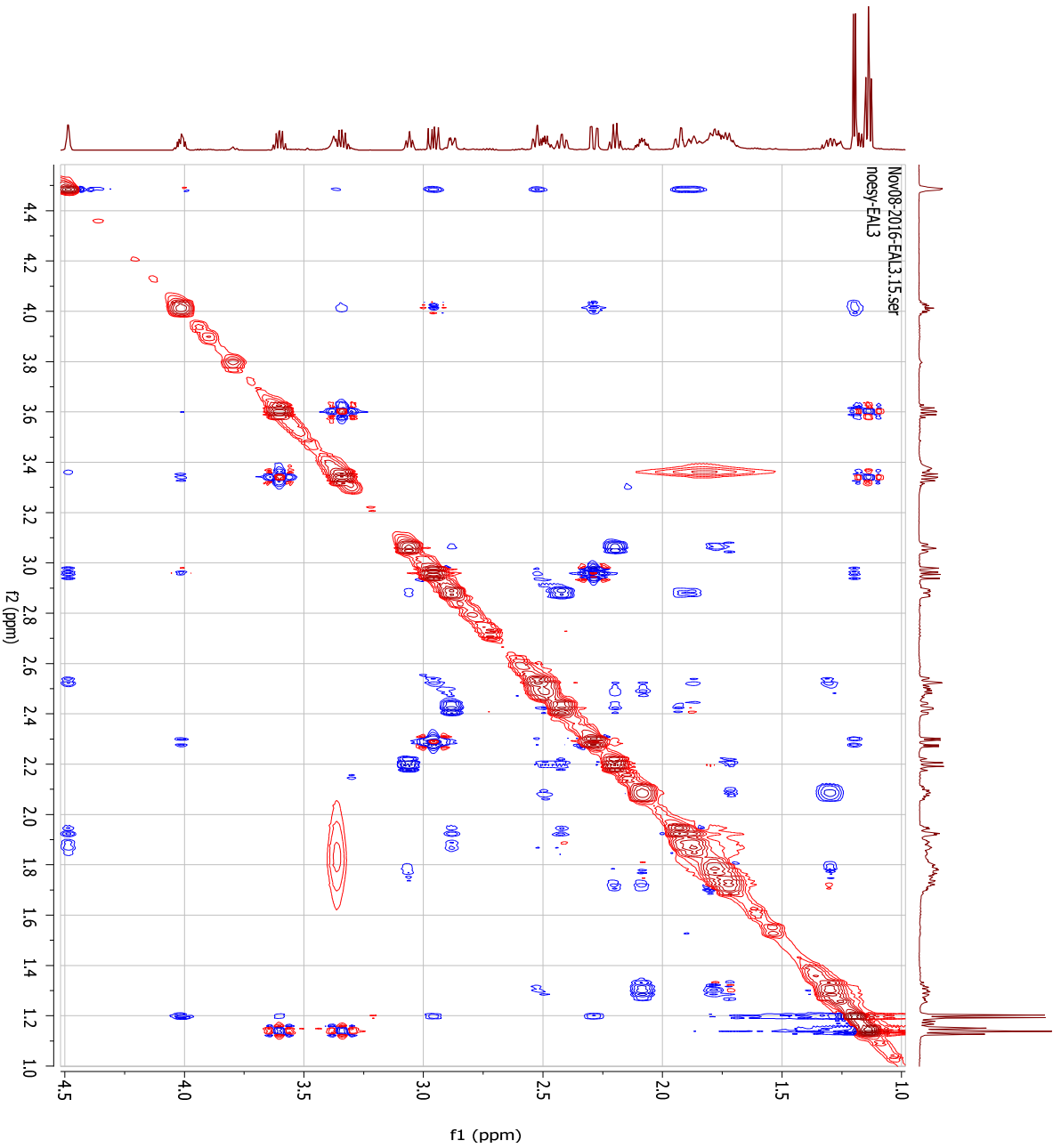




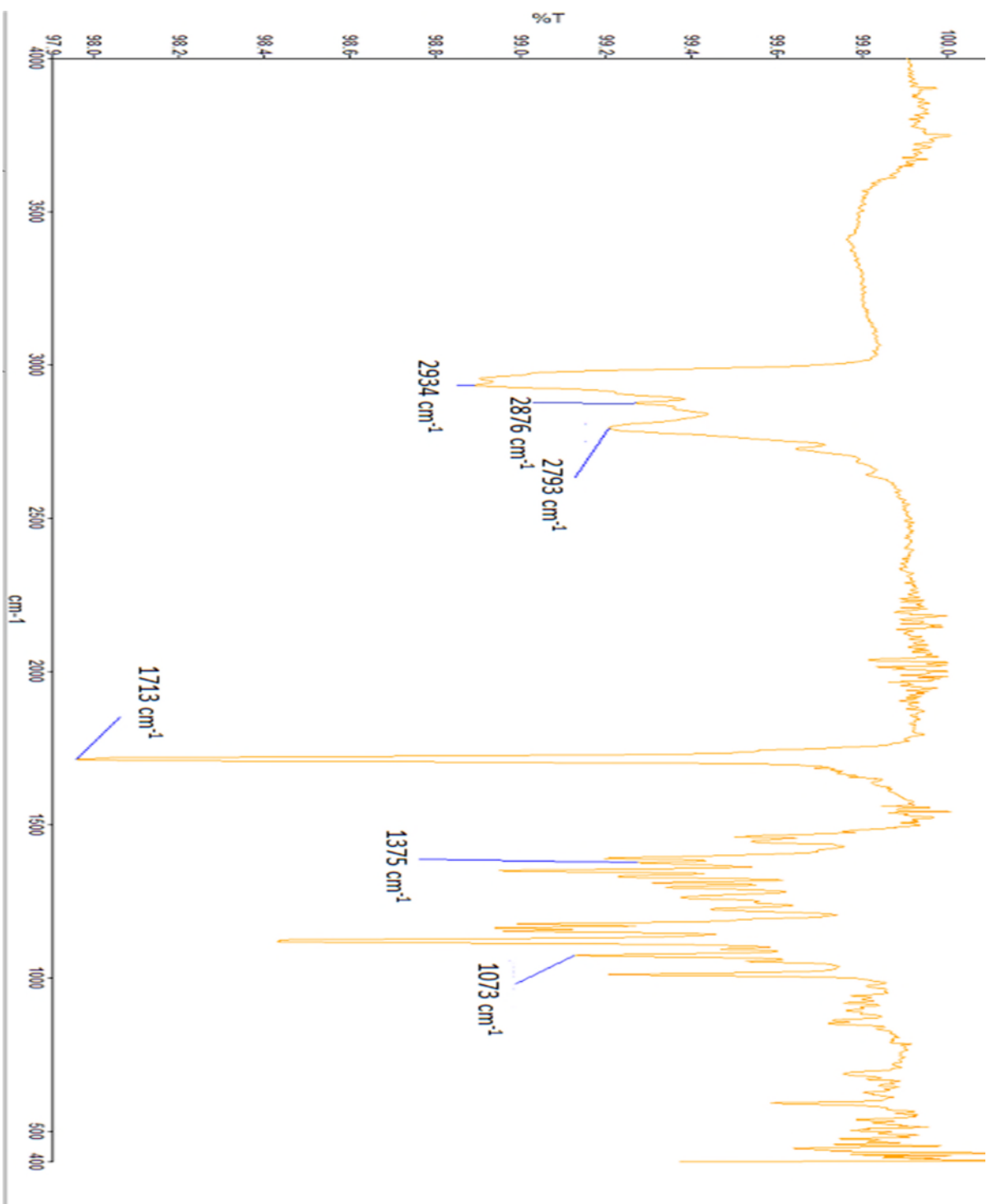
**Appendix 47: COSY spectrum for carpusinine D (8).**



Appendix 48: HMBC spectrum for carpusinine D (8).



Appendix 49: NOESY spectrum for carpusinine D (8).



**Appendix 50:** IR spectrum for carpusinine E (**9**).

Data: EAL17

Sample Name:

Description:

Ionization Mode: ESI+

History: Determine m/z[Peak Detect][Centroid,30,Area]; Correct Base[0.5%]; Correct Ba...

Acquired: 3/22/2017 2:13:16 PM

Operator: AccuTOF

Mass Calibration data: Int Calib 220317

Created: 3/22/2017 2:58:13 PM

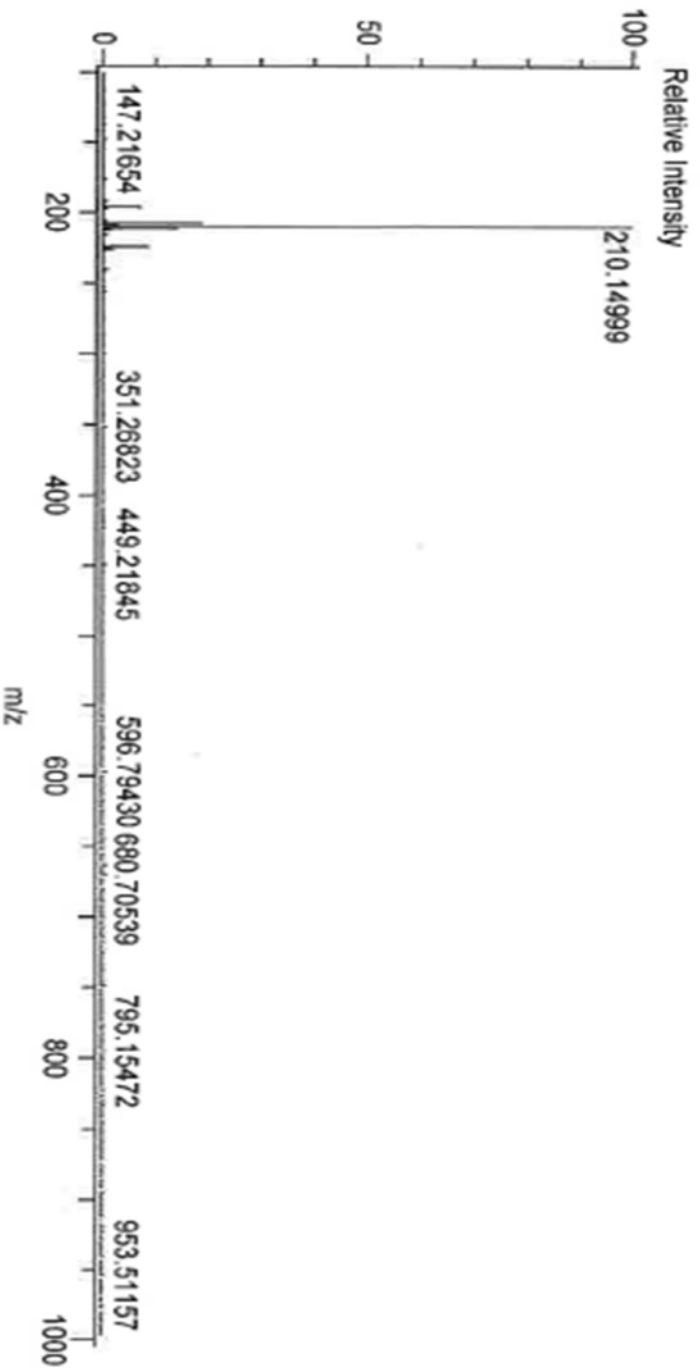
Created by: AccuTOF

Charge number: 1

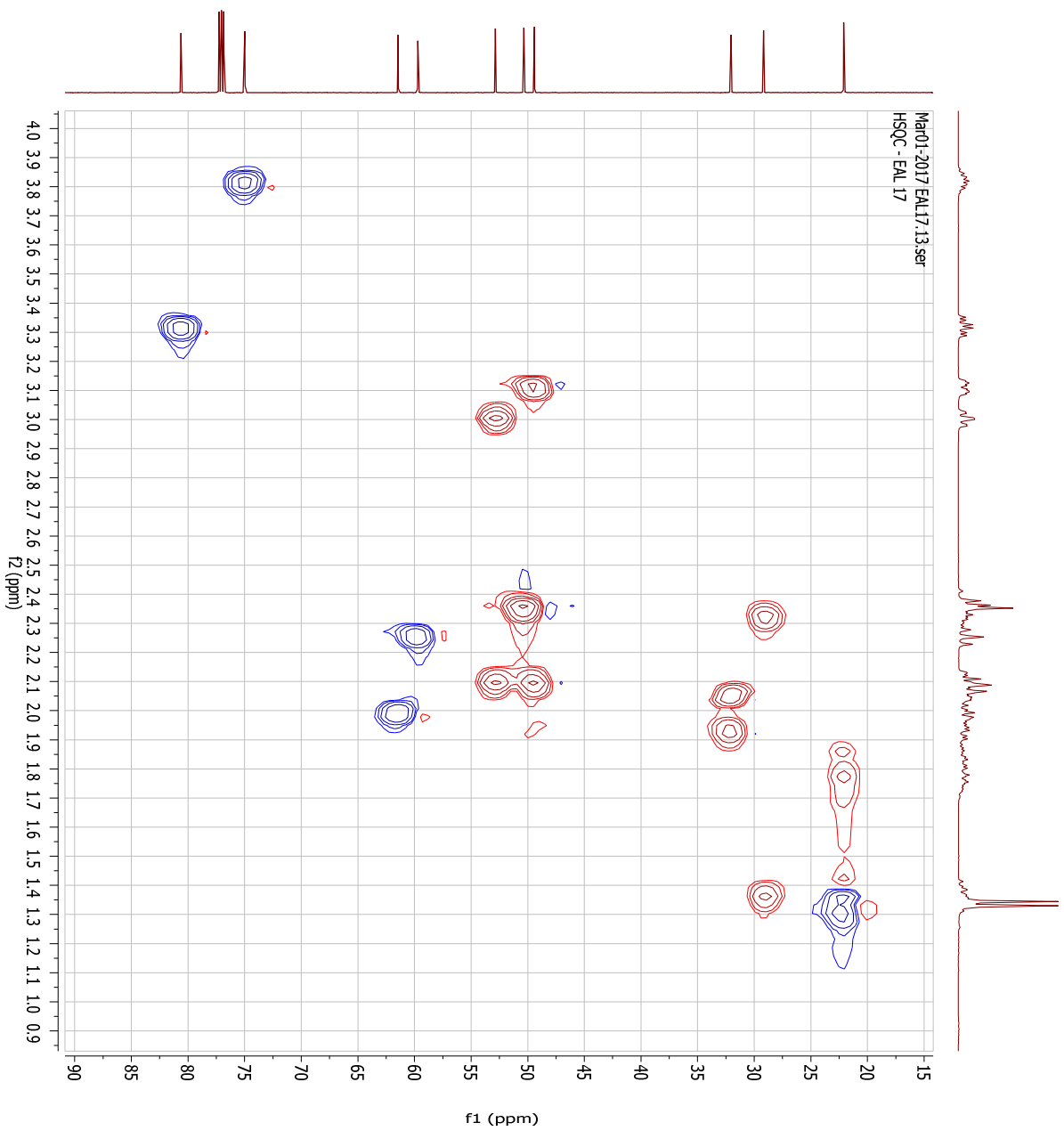
Element: <sup>12</sup>C:0 .. 30, <sup>1</sup>H:0 .. 30, <sup>14</sup>N:0 .. 5, <sup>18</sup>O:0 .. 5

Tolerance: 10.00(ppm), 0.00 .. 30.00(mmu)

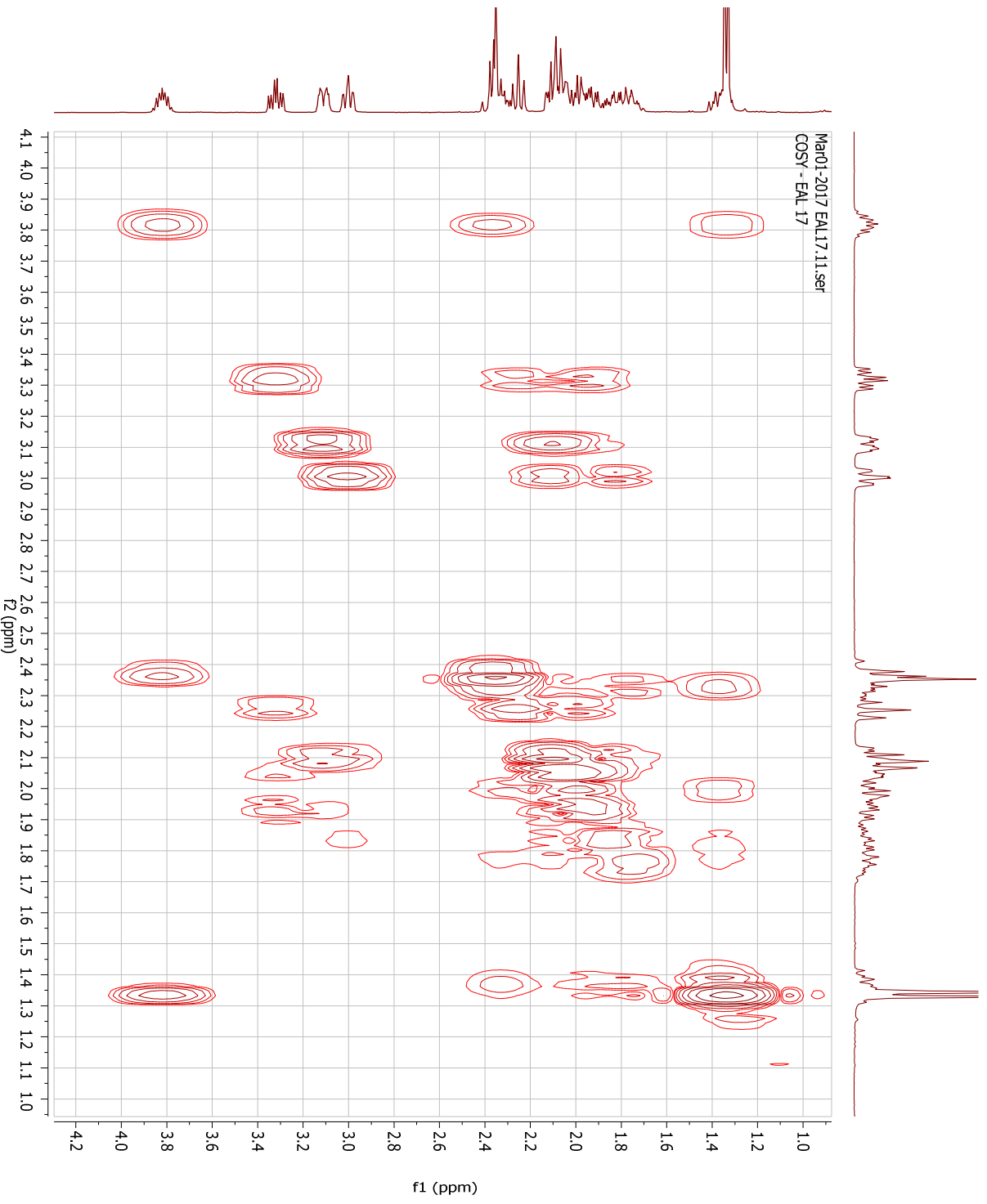
Unsaturation Number: 0.0 .. 25.0 (Fractio...



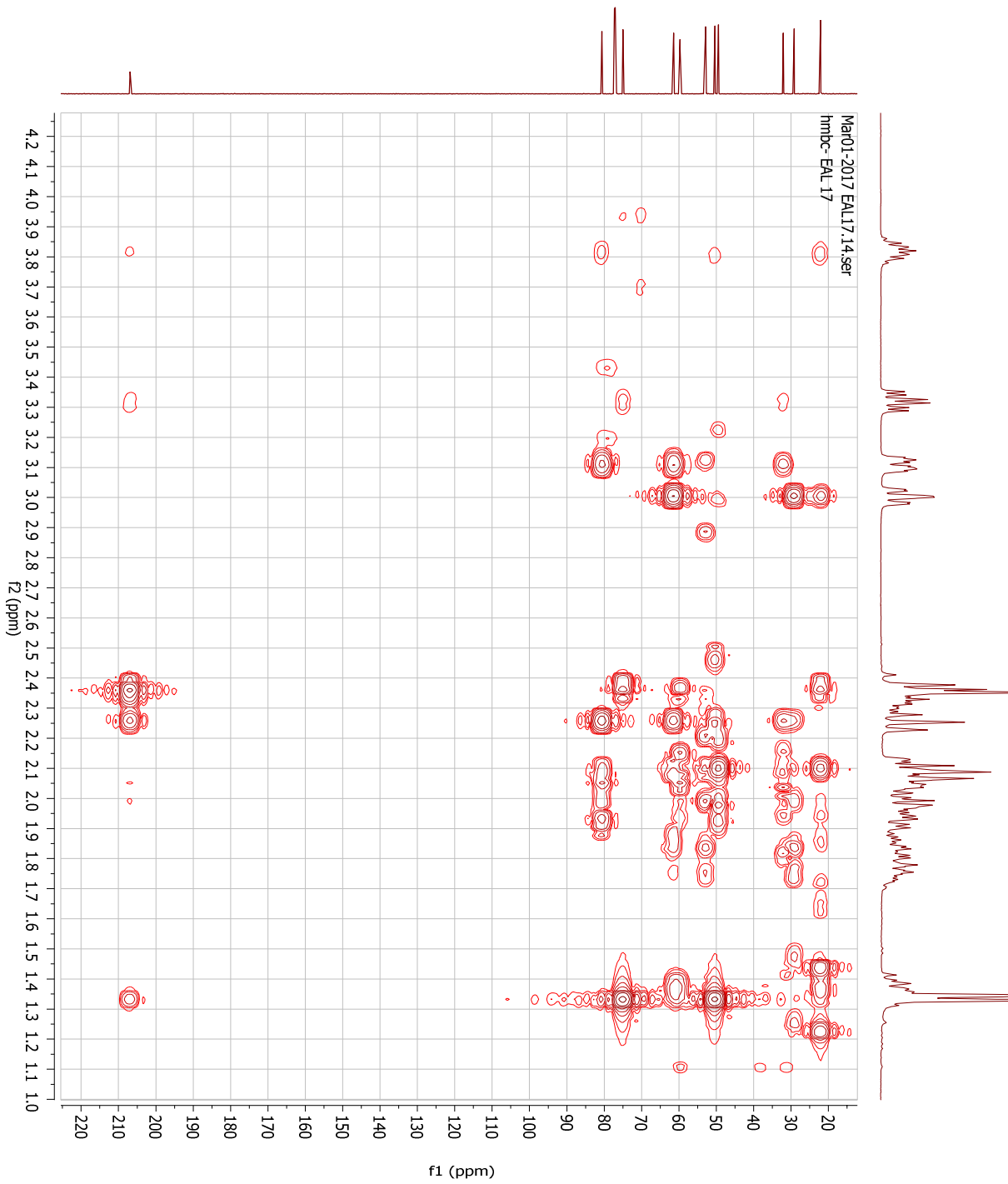
Appendix 51: MS spectrum for carpusinine E (9)



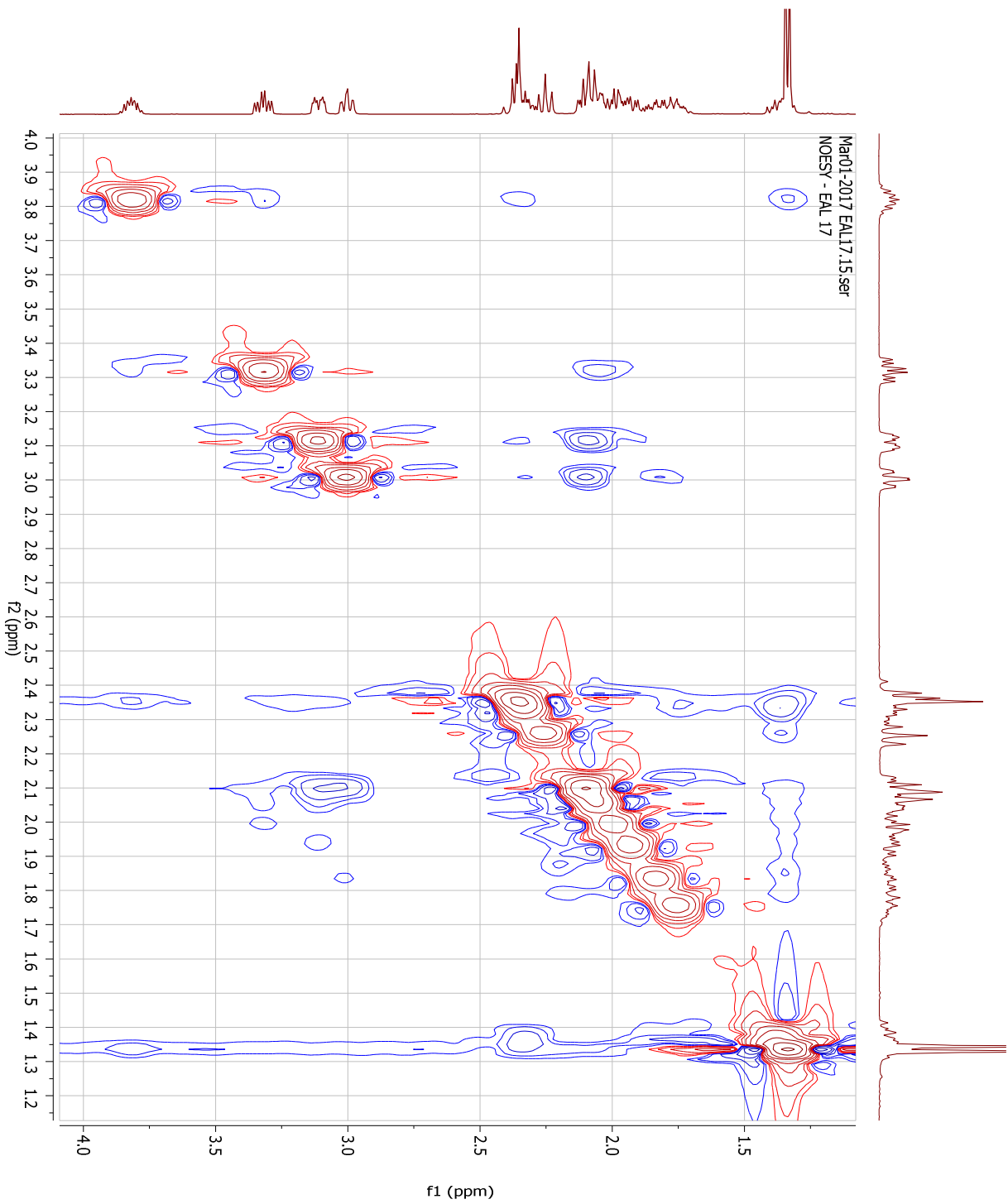
**Appendix 52:** HSQC spectrum for carpusinine E (**9**).



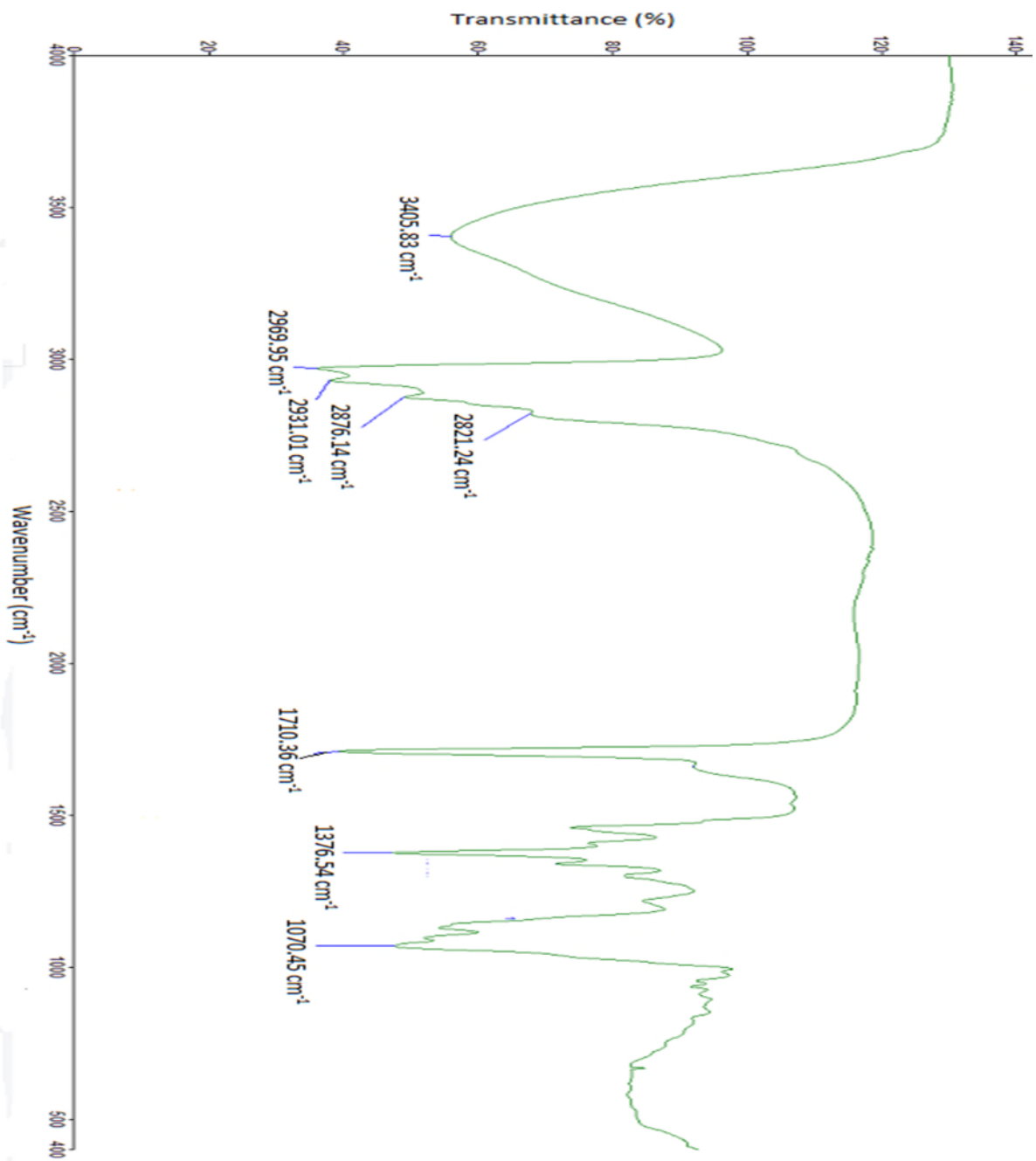
**Appendix 53: COSY spectrum for carpusinine E (9)**



**Appendix 54:** HMBC spectrum for carpusinine E (9).



Appendix 55: NOESY spectrum for carpusinine E (9).



**Appendix 56:** IR spectrum for carpusinine F and epicarpusinine F (**10a** and **10b**).

Data: EAL10\_291116

Sample Name:

Description:

Ionization Mode: ESI+

History: Determine m/z/Peak Detect(Centroid,30,Area);Correct Base(0.5%);Correct Ba...

Acquired: 11/29/2016 11:28:01 AM

Operator: AccuTOF

Mass Calibration data: Int Calib 291116

Created: 12/1/2016 10:01:49 AM

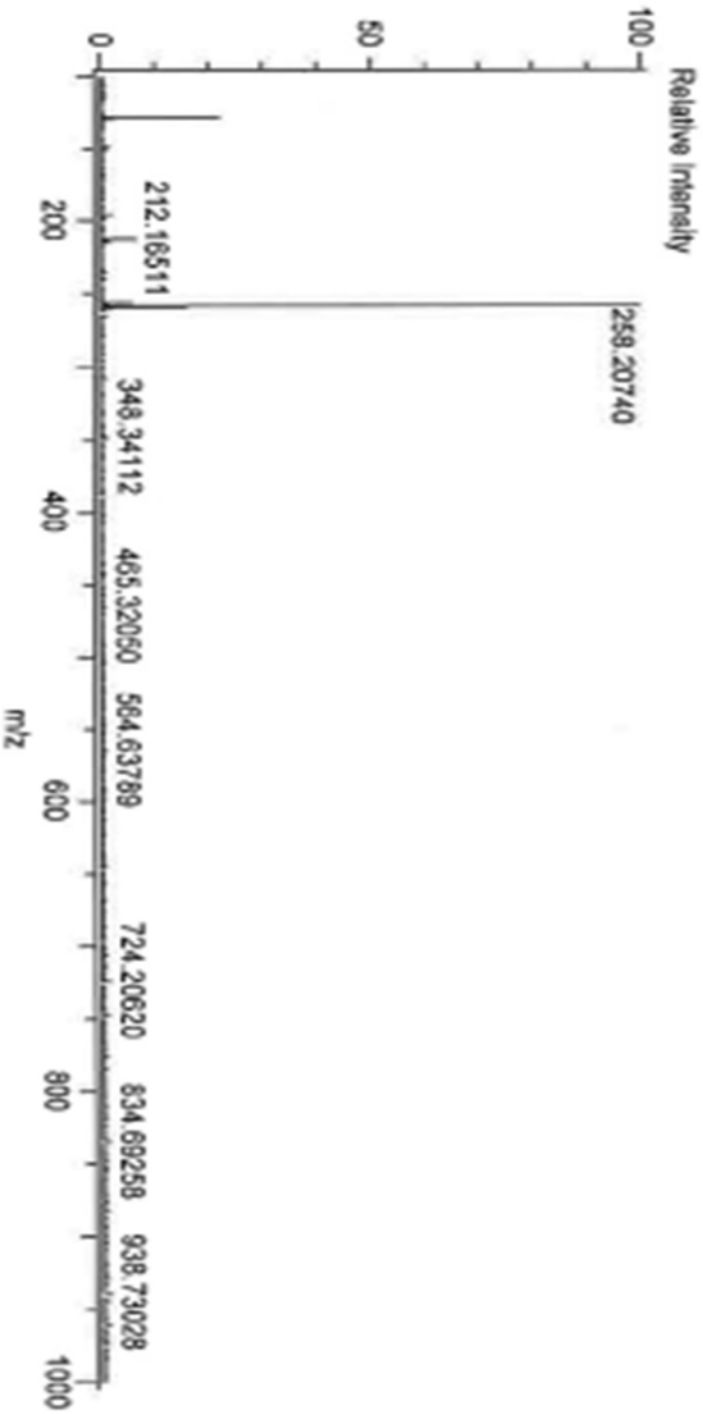
Created by: AccuTOF

Charge number: 1

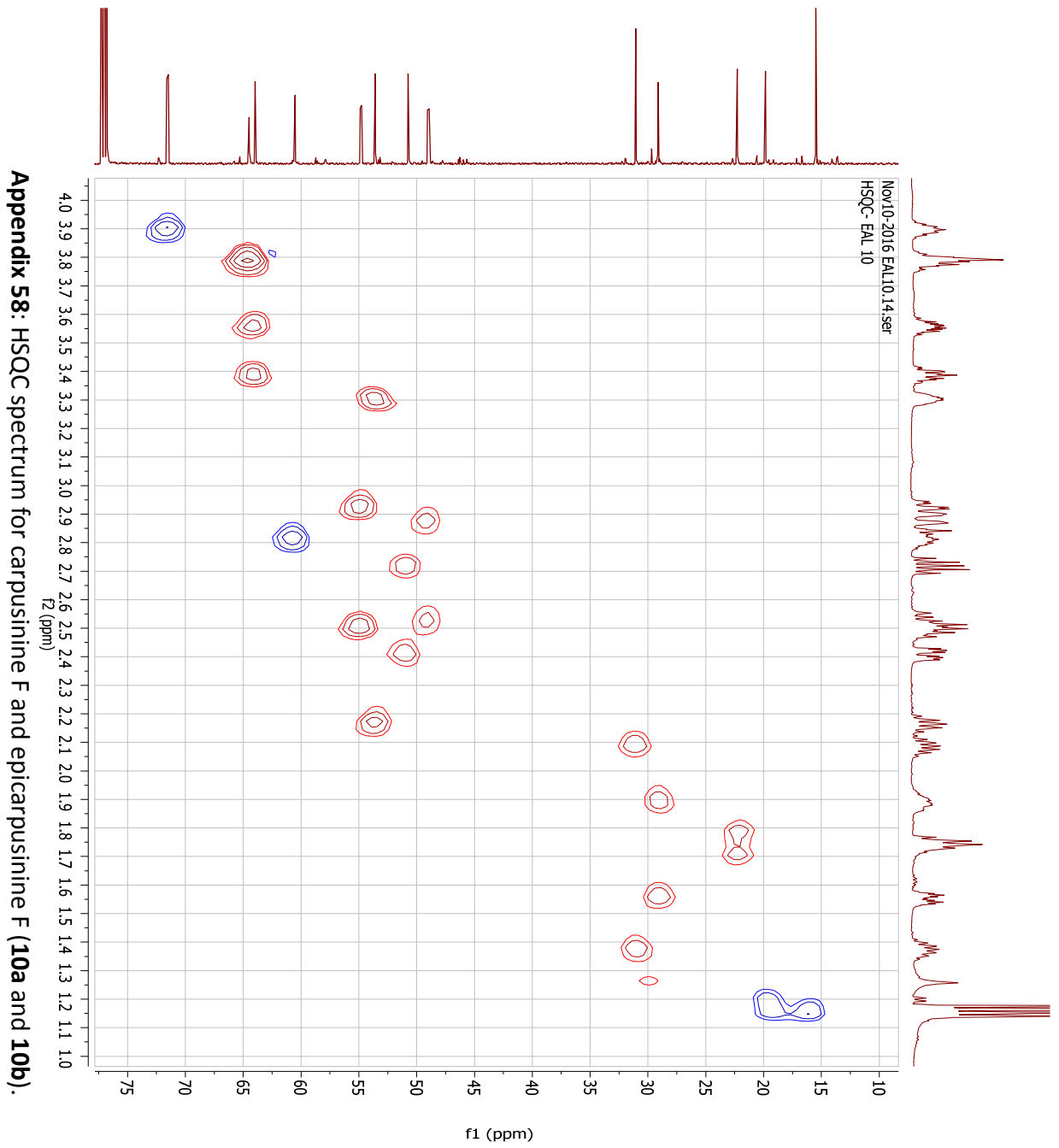
Tolerance: 30.00(ppm), 5.00 .. 15.00(mmu)

Unsaturation Number: 0.0 .. 25.0 (Fractio...

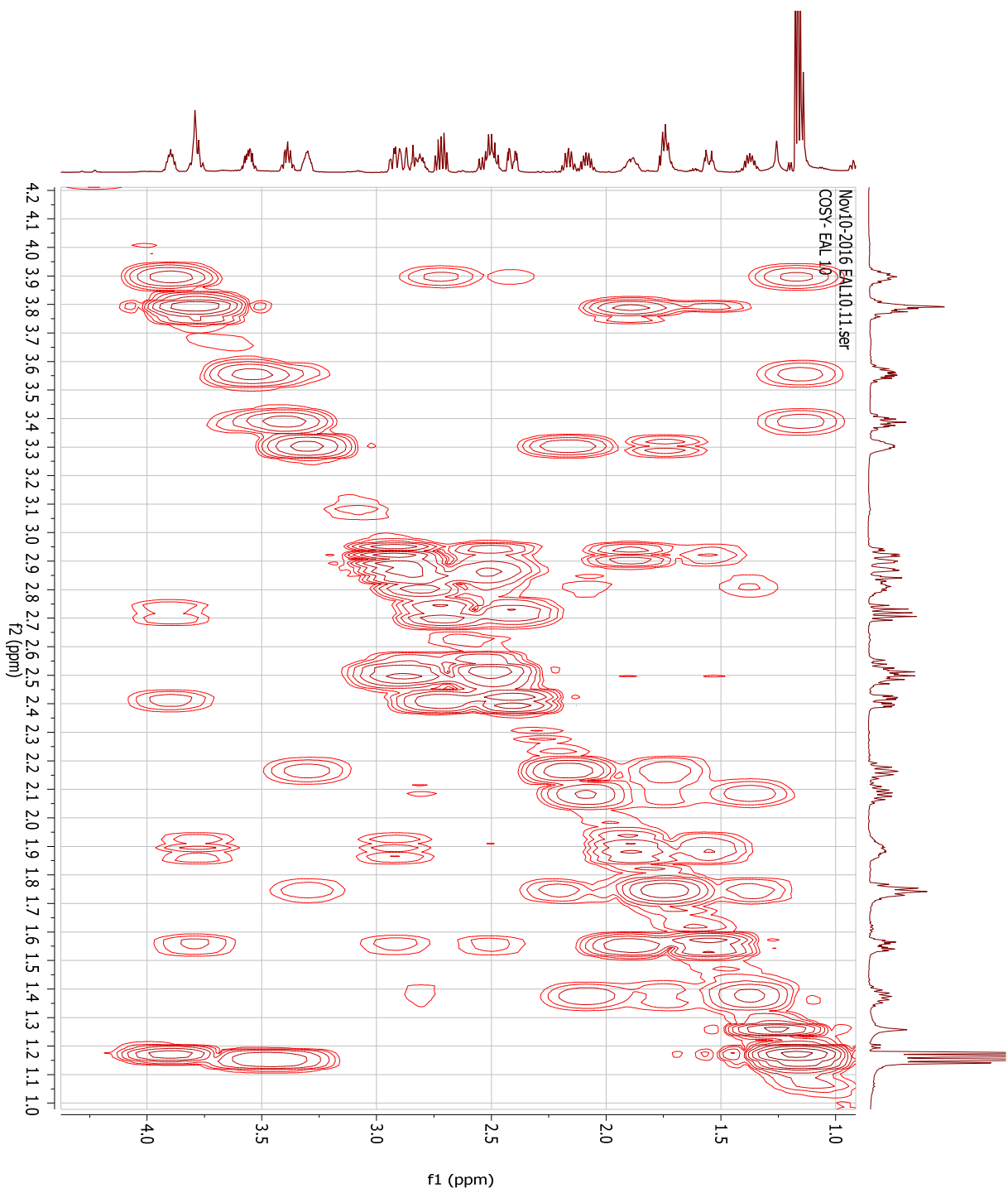
Element: 12C: 0 .. 30, 1H: 0 .. 40, 14N: 0 .. 5, 16O: 0 .. 5



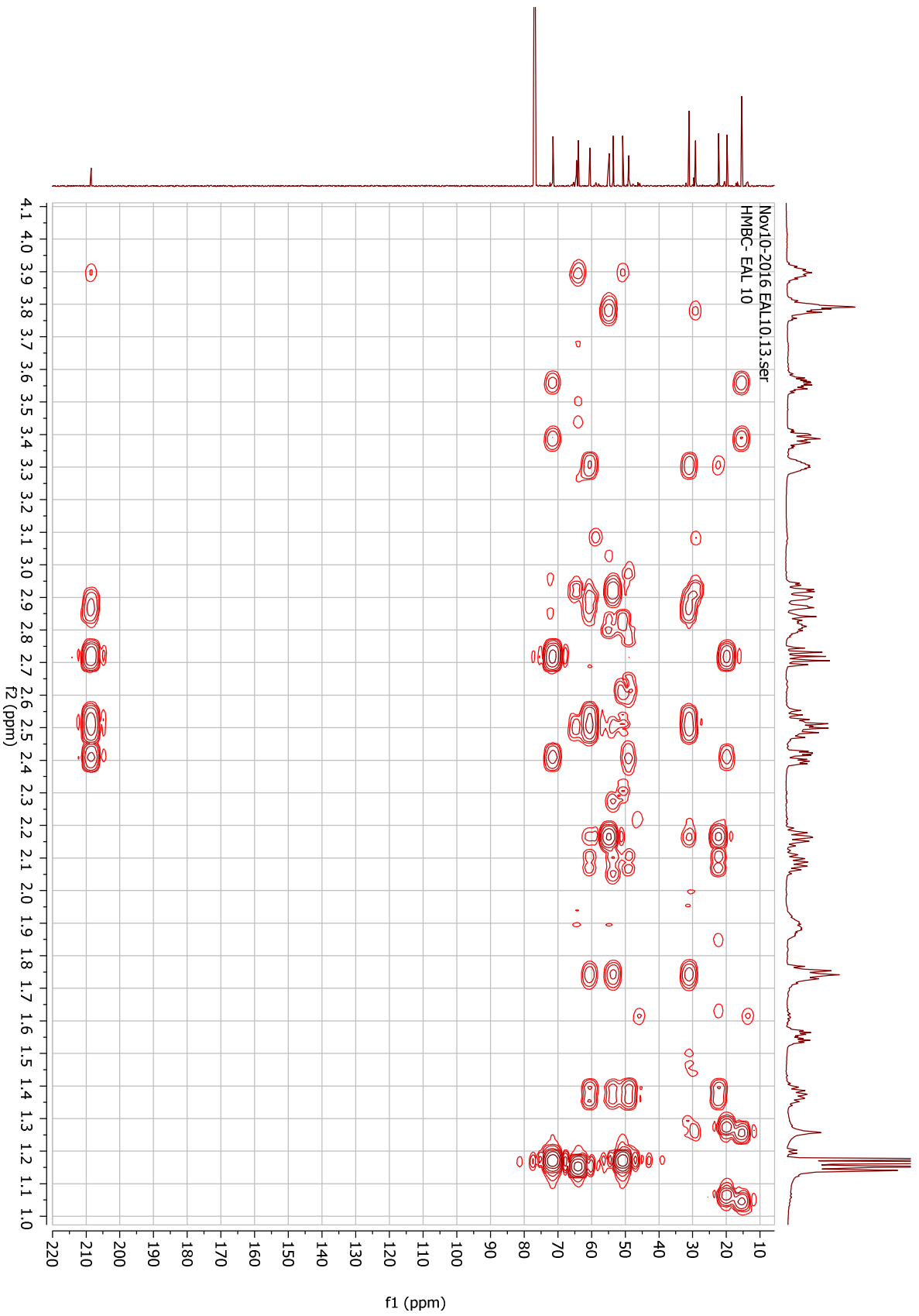
Appendix 57: MS spectrum for carpusinine F and epicarpusinine F (10a and 10b).



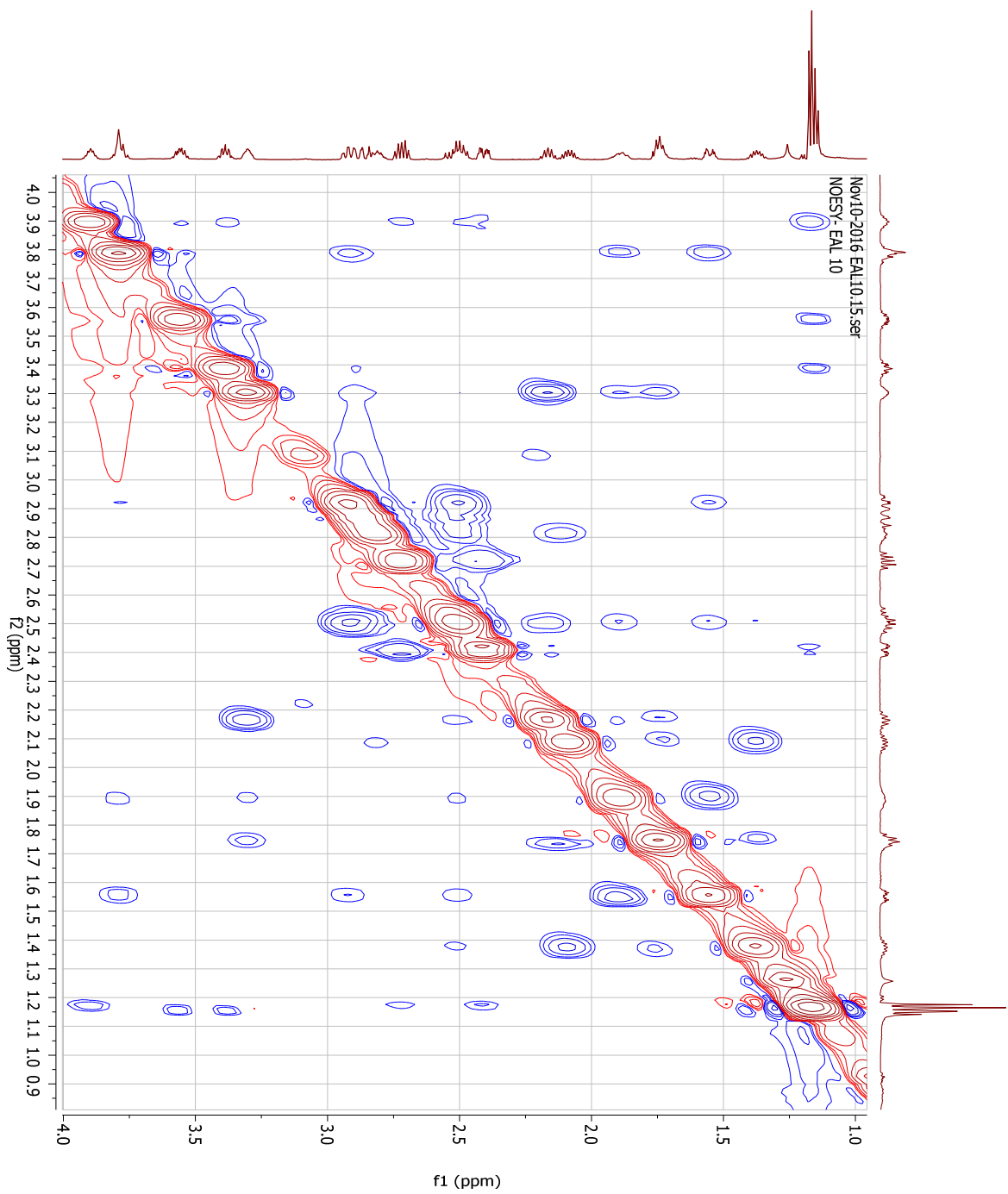
Appendix 58: HSQC spectrum for carpusinine F and epicarpusinine F (**10a** and **10b**).



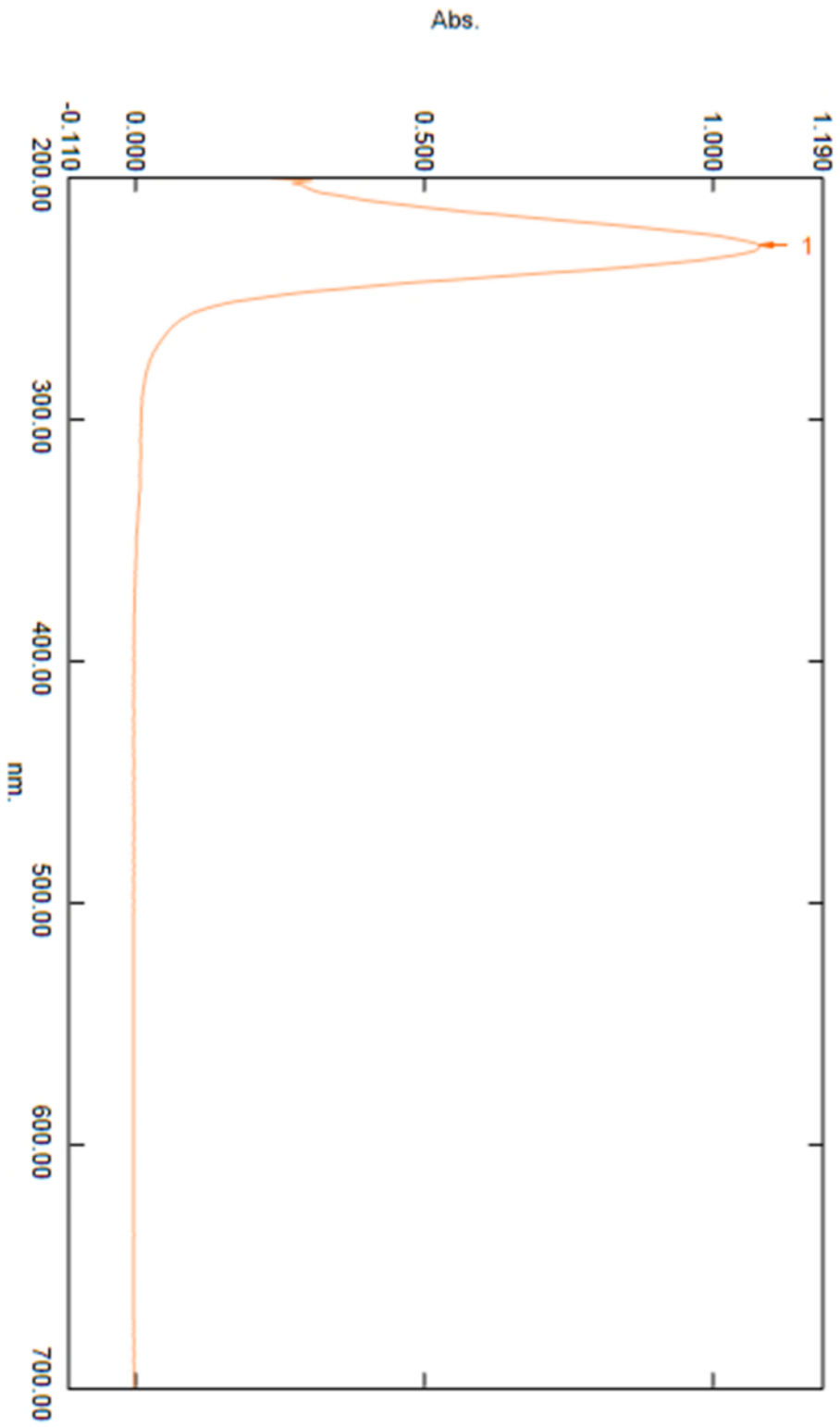
**Appendix 59: COSY spectrum for carpusinine F and epicarpusinine F (10a and 10b).**



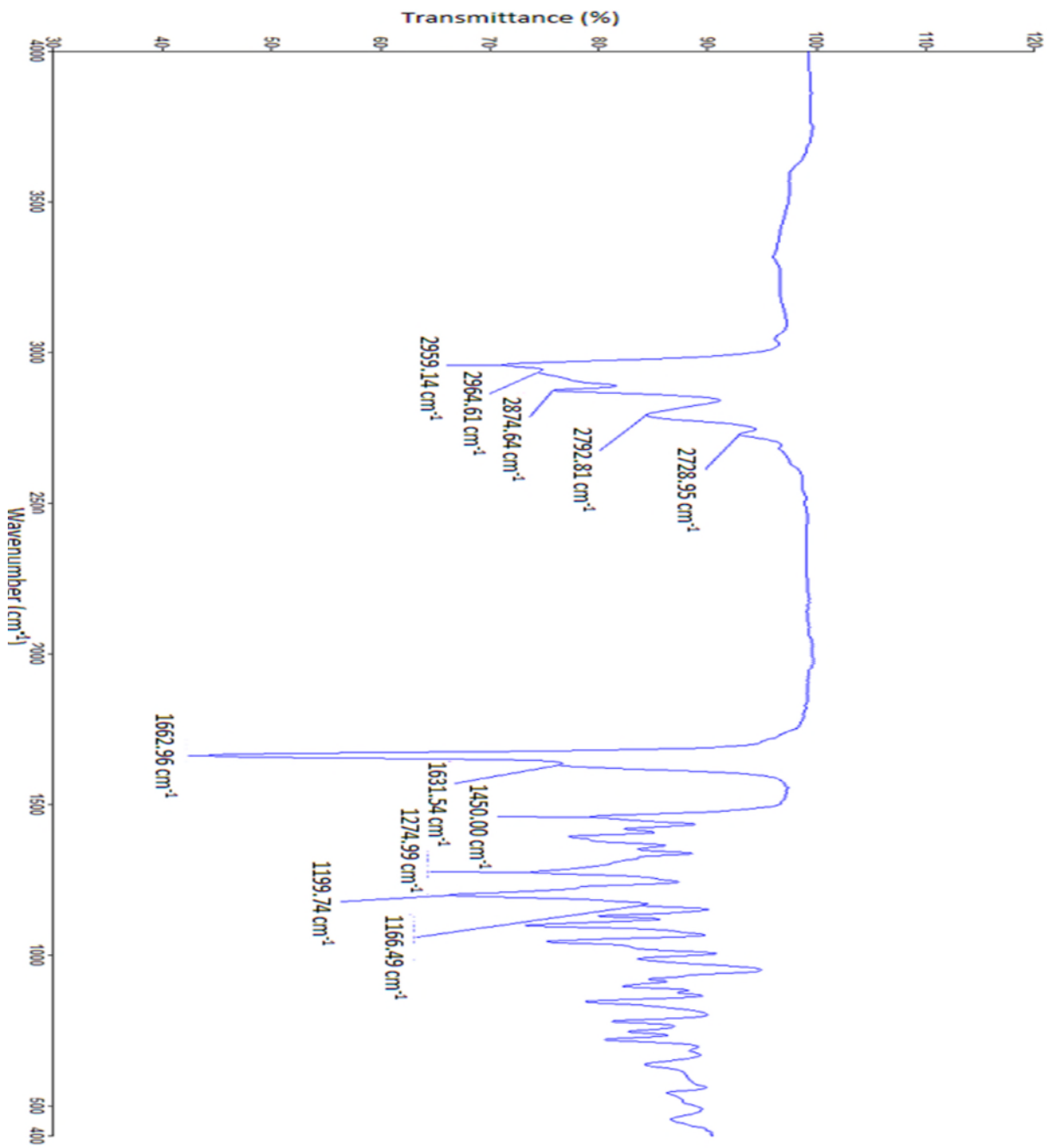
**Appendix 60: HMBC spectrum for carpusinine F and epicarpusinine F (10a and 10b).**



Appendix 61: NOESY spectrum for carpusinine F and epicarpusinine F (10a and 10b).

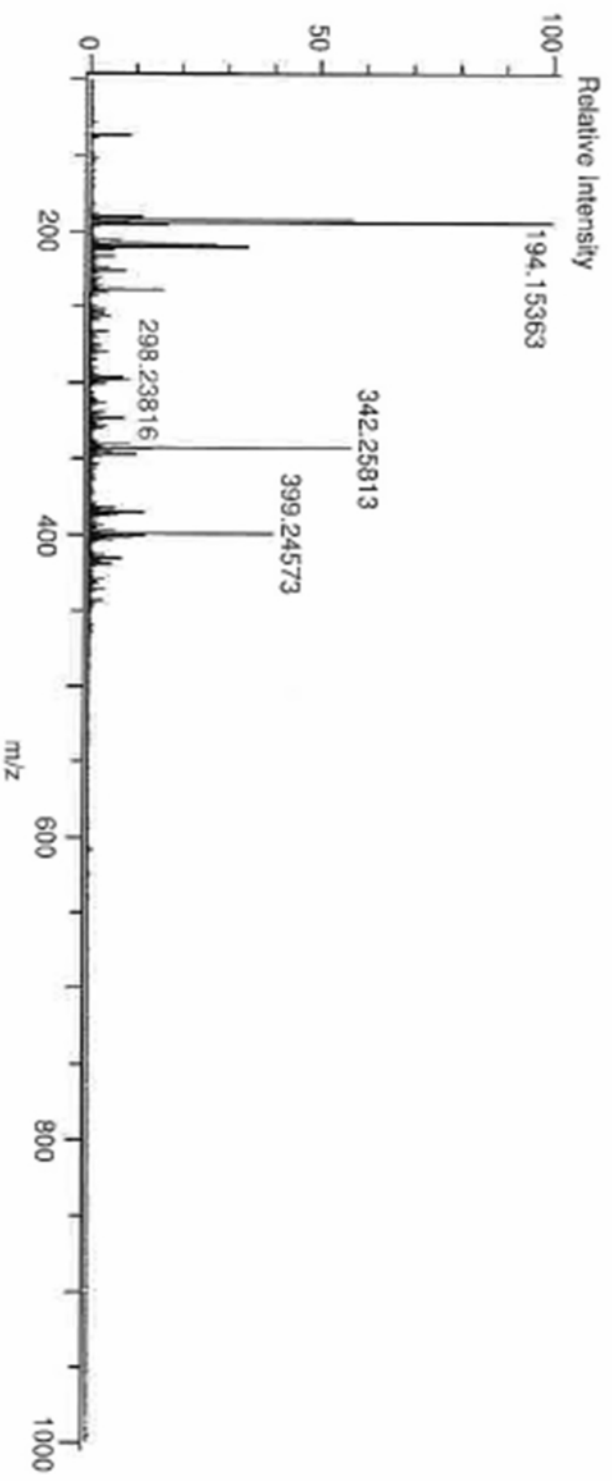


Appendix 62: UV spectrum for elaeokanine A (11)

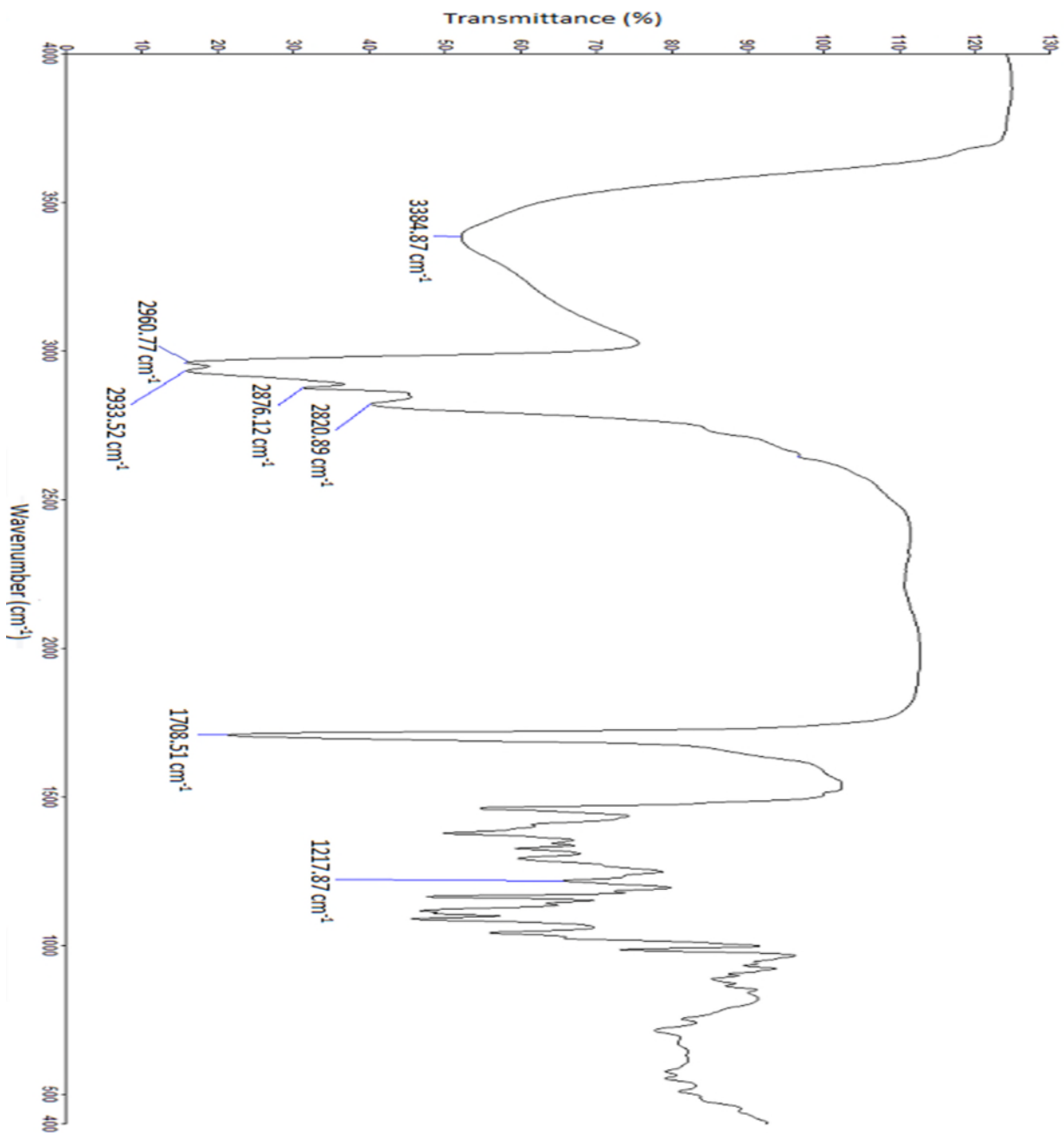


Appendix 63: IR spectrum for elaeoquinine A (11)

Data: EAL1  
Sample Name:  
Description:  
Ionization Mode: ESI+  
History: Determine m/z/Peak Detect(Centroid,30 Area);Correct Base[0.5%];Correct Ba...  
Charge number: 1  
Element: <sup>12</sup>C: 0 .. 20, <sup>1</sup>H: 0 .. 30, <sup>14</sup>N: 0 .. 5, <sup>16</sup>O: 0 .. 5  
Tolerance: 30.00(ppm), 0.00 .. 30.00(mmu)  
Unsaturatation Number: 0.0 .. 25.0 (Fractio...  
Acquired: 1/24/2017 11:21:04 AM  
Operator: AccuTOF  
Mass Calibration data: Int Calib 240117  
Created: 1/24/2017 12:44:46 PM  
Created by: AccuTOF



Appendix 64: MS spectrum for elaeokanine A (11)



**Appendix 65:** IR spectrum for elaeoquinine C (12)

Data: EAL14

Sample Name:

Description:

Ionization Mode: ESI+

History: Determine m/z[Peak Detect][Centroid,30,Area],[Correct Base[0.5%]]; Correct Ba...

Charge number: 1

Element: <sup>12</sup>C: 0 .. 20, <sup>1</sup>H: 0 .. 30, <sup>14</sup>N: 0 .. 5, <sup>16</sup>O: 0 .. 5

Tolerance: 30.00(ppm), 0.00 .. 30.00(mmu)

Unsaturation Number: 0.0 .. 25.0 (Fractio...

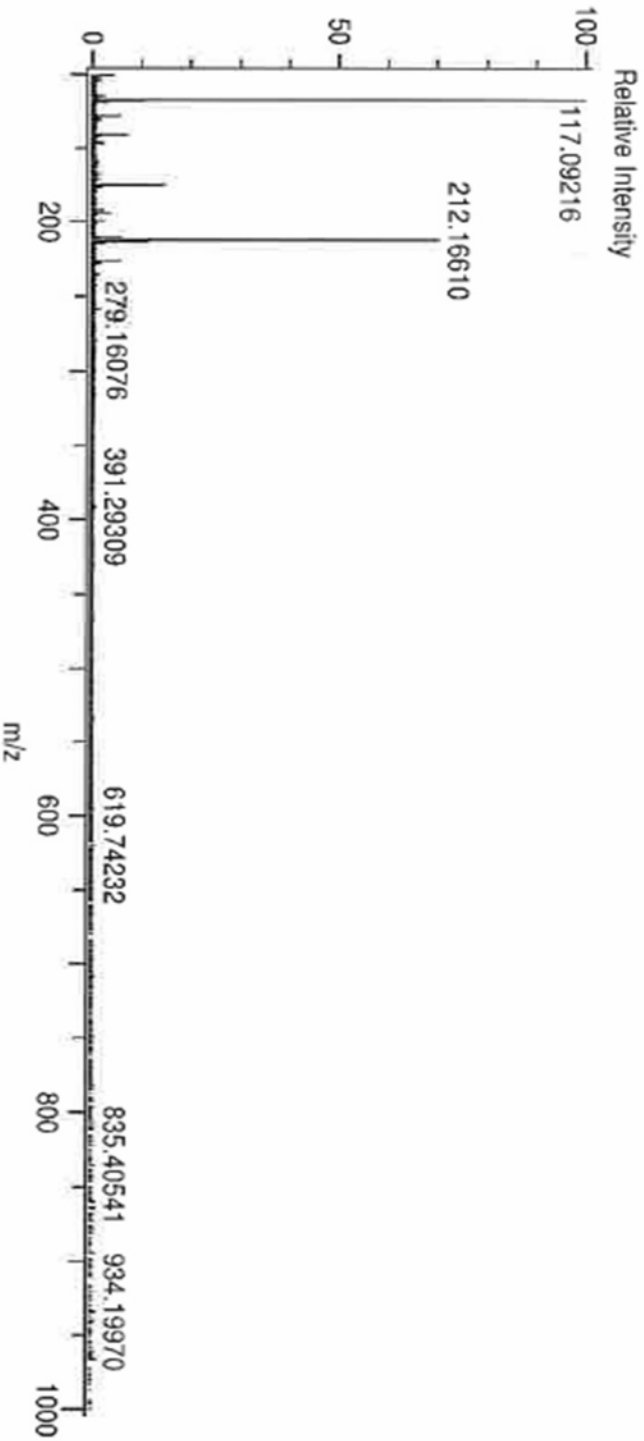
Acquired: 1/24/2017 11:23:11 AM

Operator: AccuTOF

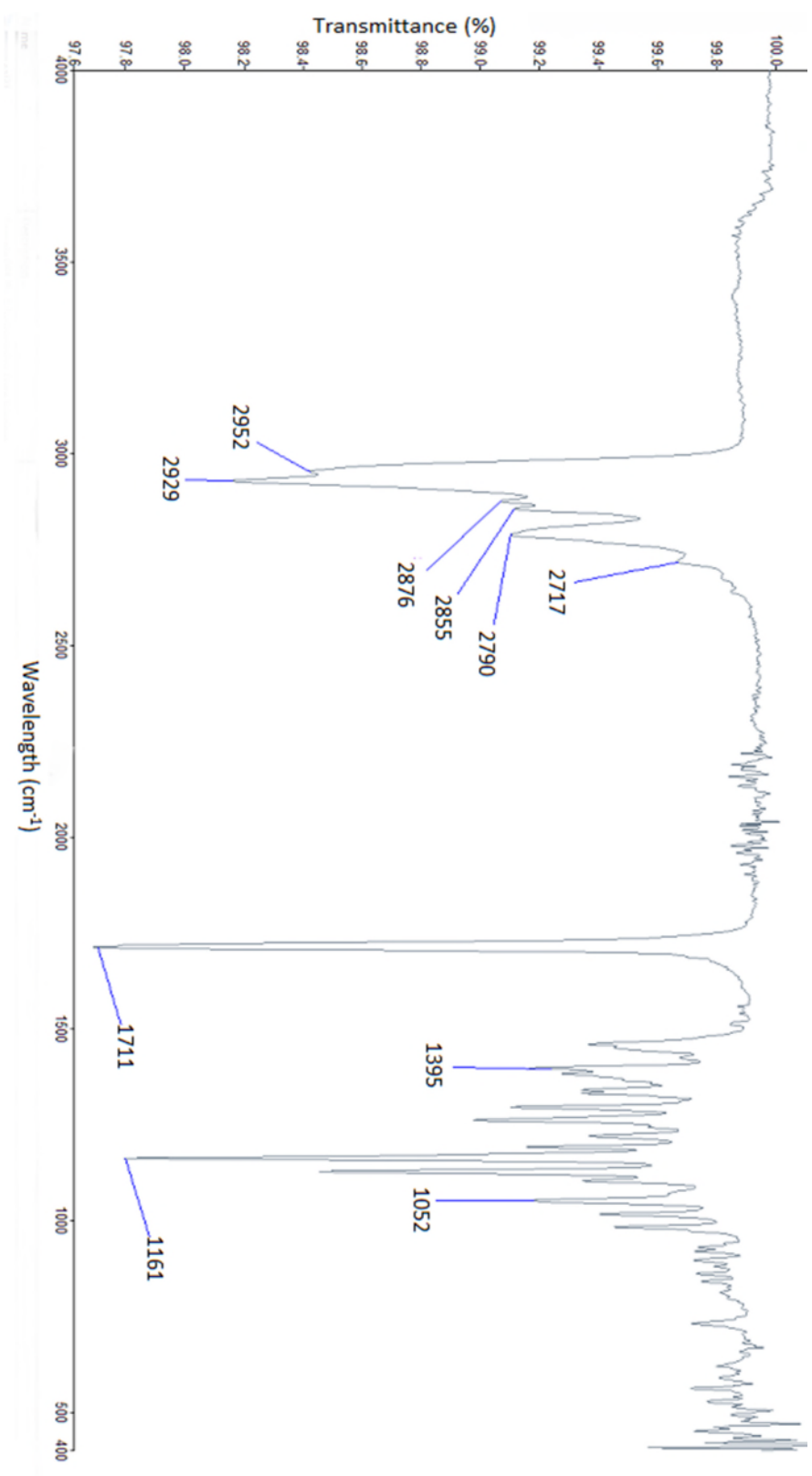
Mass Calibration data: Int Calib 240117

Created: 1/24/2017 2:22:32 PM

Created by: AccuTOF

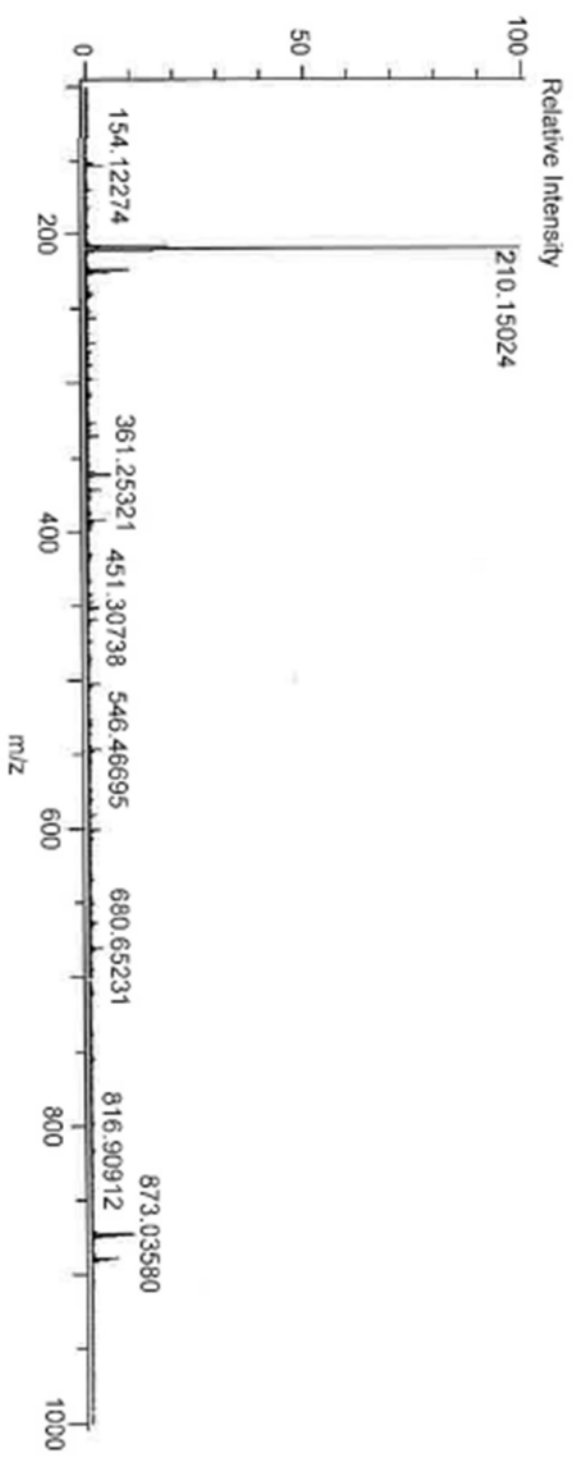


Appendix 66: MS spectrum for elaeoakanine C (12)

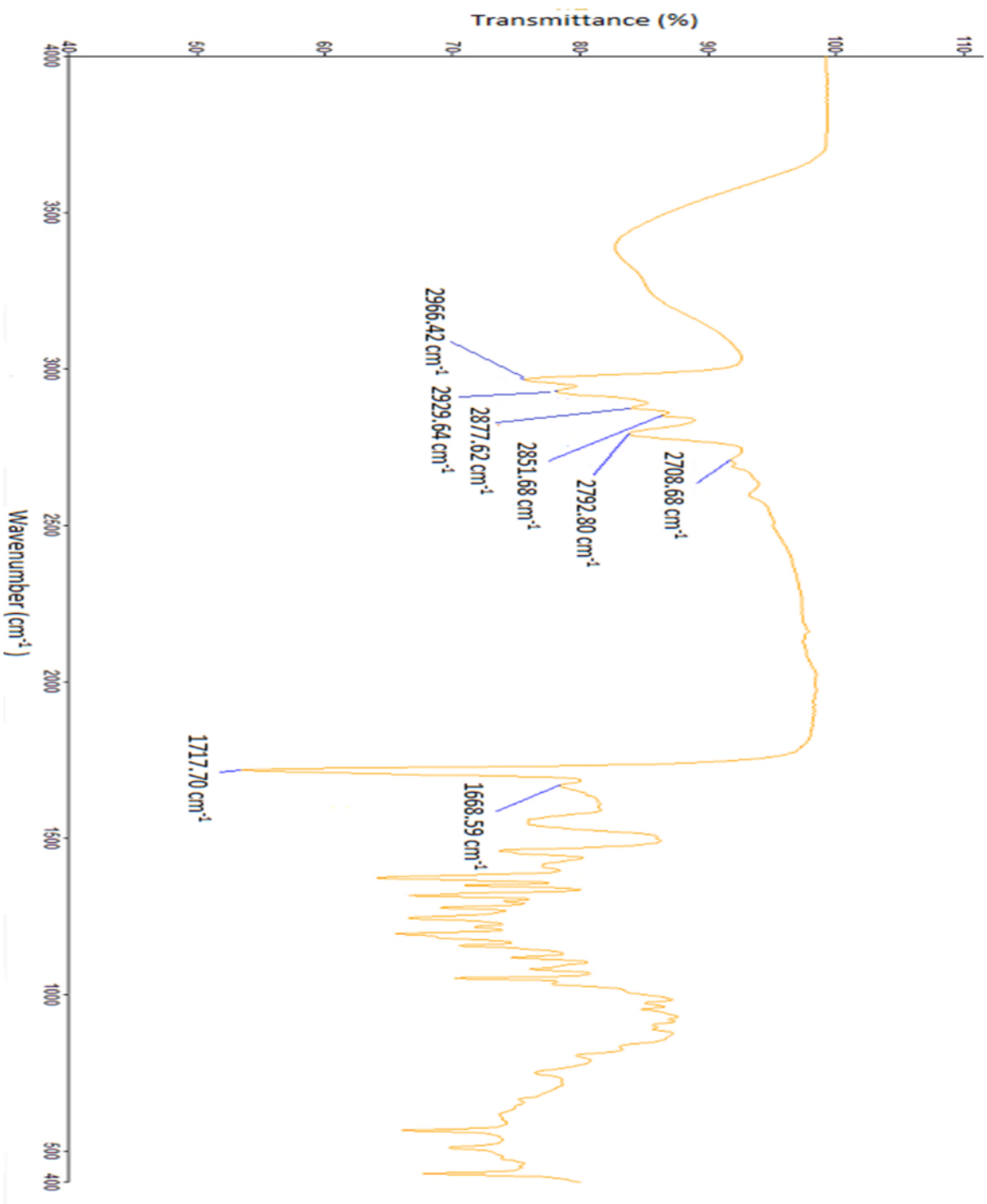


Appendix 67: IR spectrum for elaeoakanine D (13)

Data: EAL.31  
 Sample Name:  
 Description:  
 Ionization Mode: ESI+  
 History: Determine m/z Peak Detect [Centroid, 30, Area]; Correct Base [0.5%]; Correct Ba...  
 Charge number: 1  
 Tolerance: 20.00 (ppm), 0.00 .. 30.00 (mmu)  
 Element: <sup>12</sup>C: 0 .. 20, <sup>1</sup>H: 0 .. 30, <sup>14</sup>N: 0 .. 5, <sup>16</sup>O: 0 .. 10  
 Unsaturatation Number: 0.0 .. 25.0 (Fracitio...)  
 Created by: AccuTOF  
 Operator: AccuTOF  
 Mass Calibration data: DART\_Calib\_2211...  
 Created: 1/22/2017 11:53:27 AM  
 Acquired: 1/22/2017 10:51:08 AM

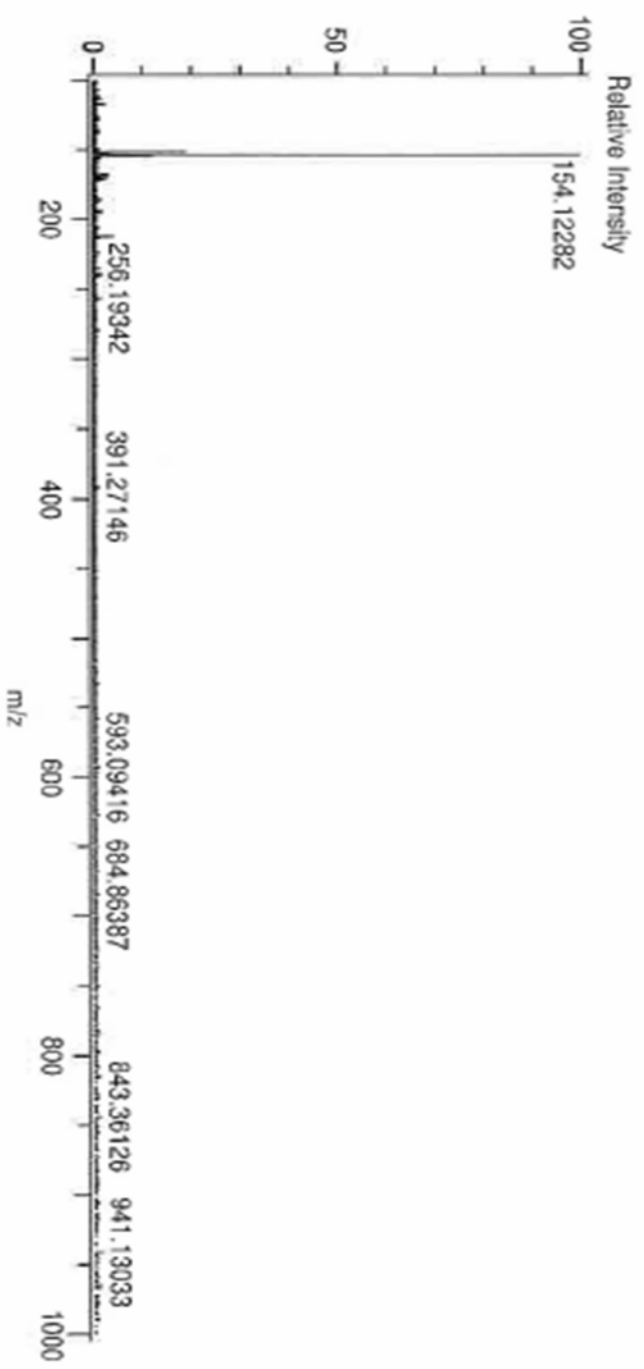


Appendix 68: MS spectrum for elaeokanine D (13)

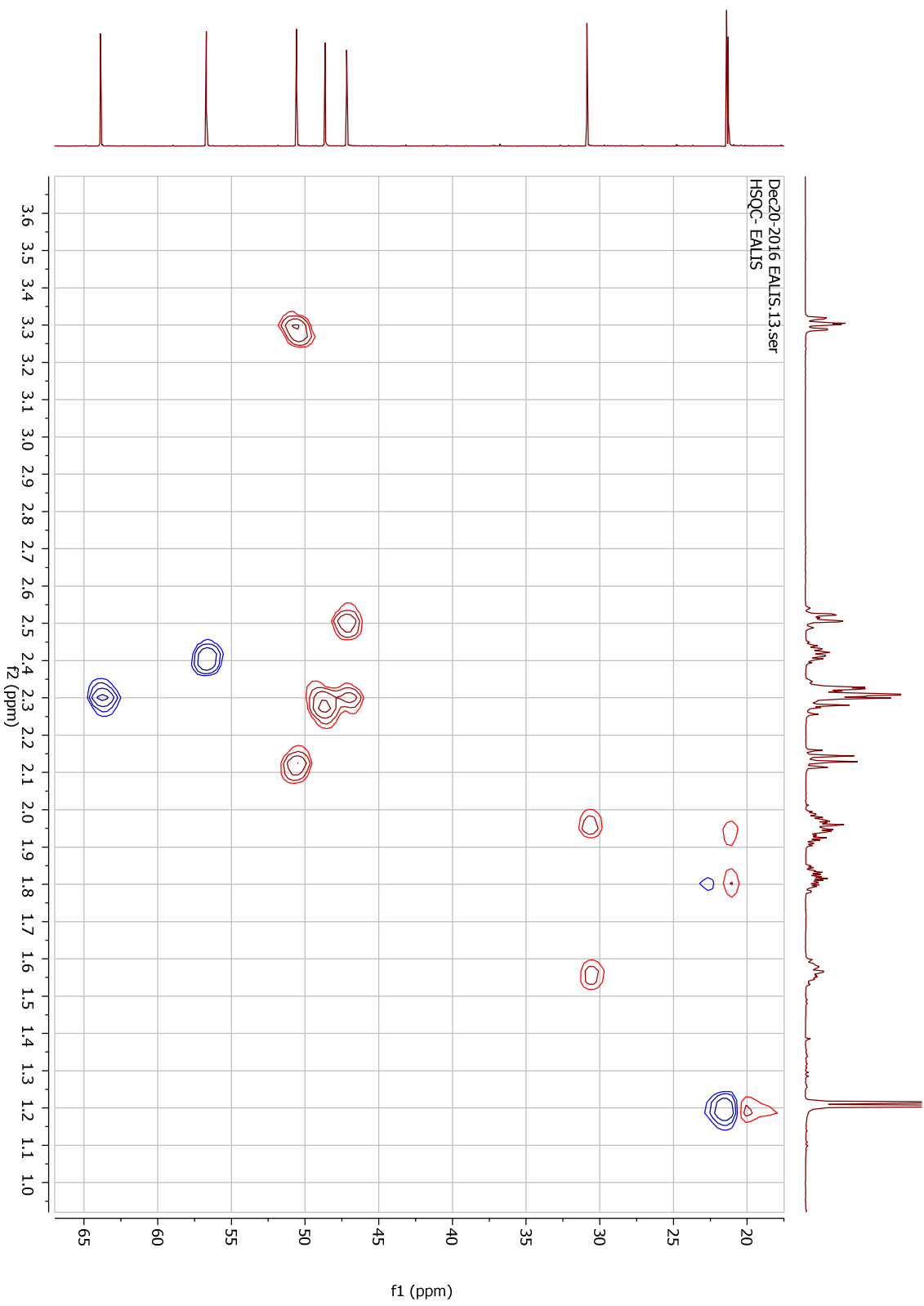


**Appendix 69:** IR spectrum for carpusidine (**14**).

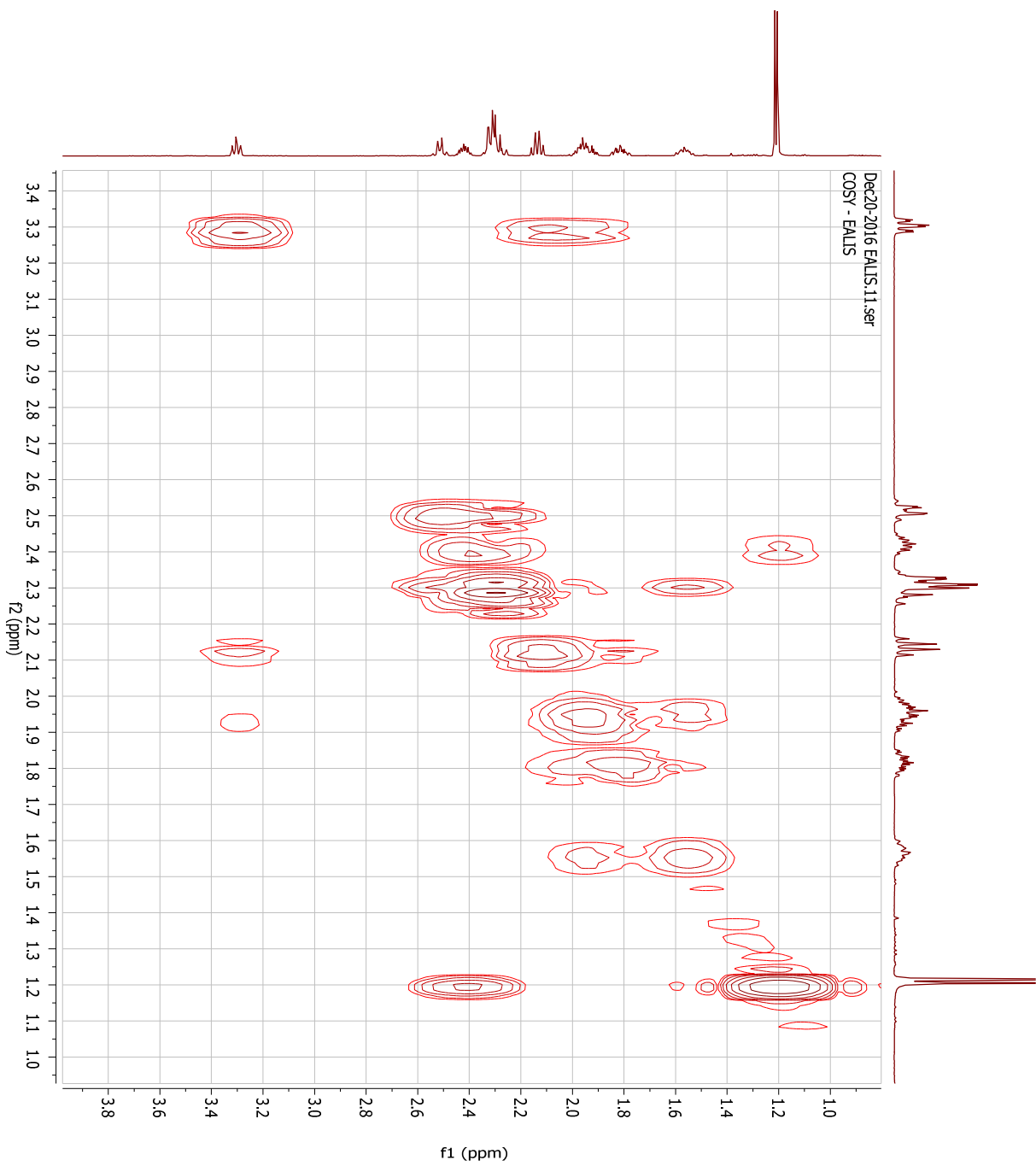
Data: EAL15  
Sample Name:  
Description:  
Ionization Mode: ESI+  
History: Determine m/z [Peak Detect (Centroid, 30, Area), Correct Base (0.5%), Correct Ba...  
Charge number: 1  
Element: <sup>12</sup>C: 0 .. 20, <sup>1</sup>H: 0 .. 30, <sup>14</sup>N: 0 .. 5, <sup>16</sup>O: 0 .. 5  
Tolerance: 30.00 (ppm), 0.00 .. 30.00 (mmu)  
Ursaturation Number: 0.0 .. 25.0 (Fractio...  
Acquired: 1/24/2017 11:25:24 AM  
Operator: AccuTOF  
Mass Calibration data: Int Calib 240117  
Created: 1/24/2017 2:36:08 PM  
Created by: AccuTOF



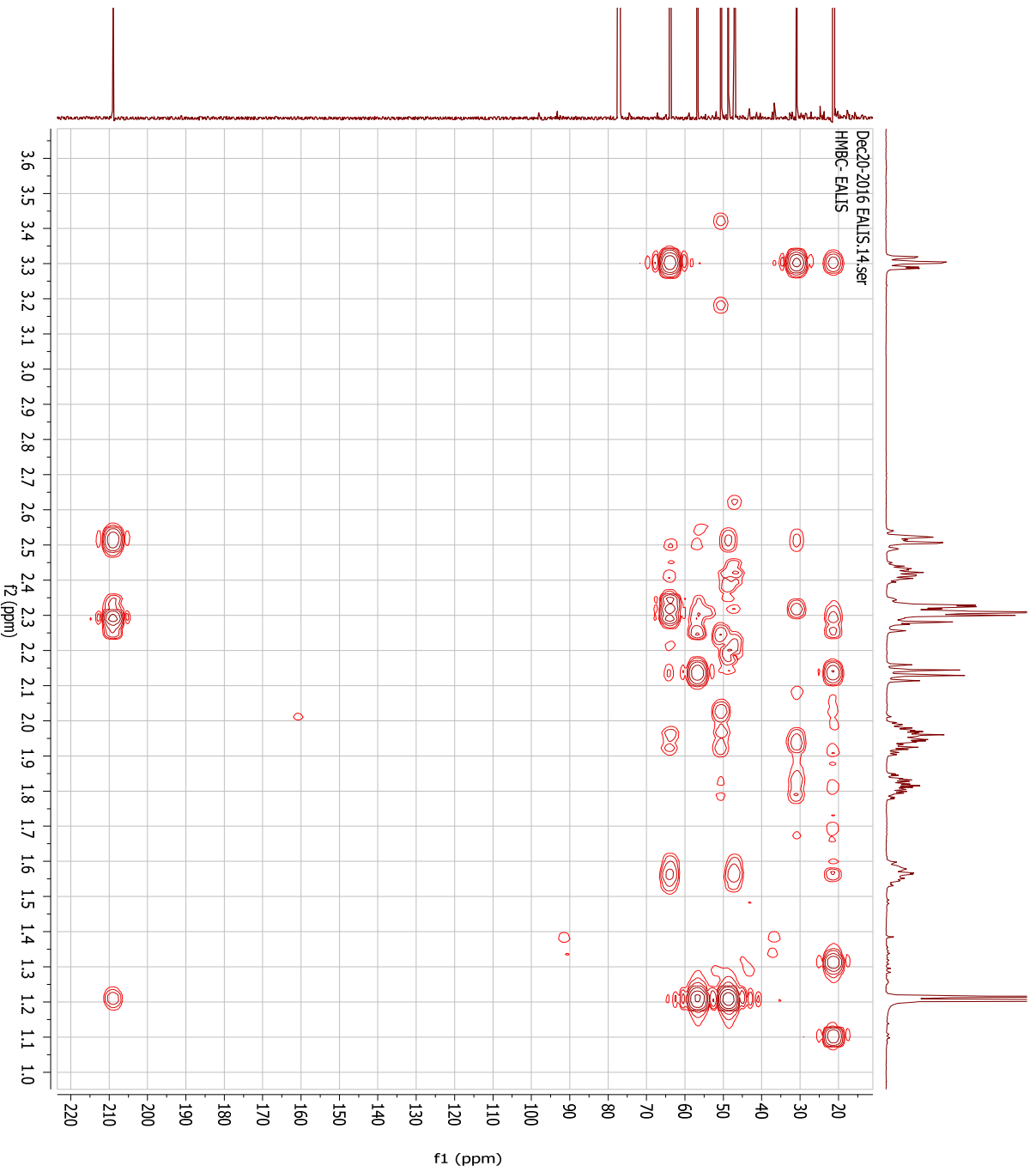
Appendix 70: MS spectrum for carpusidine (14).



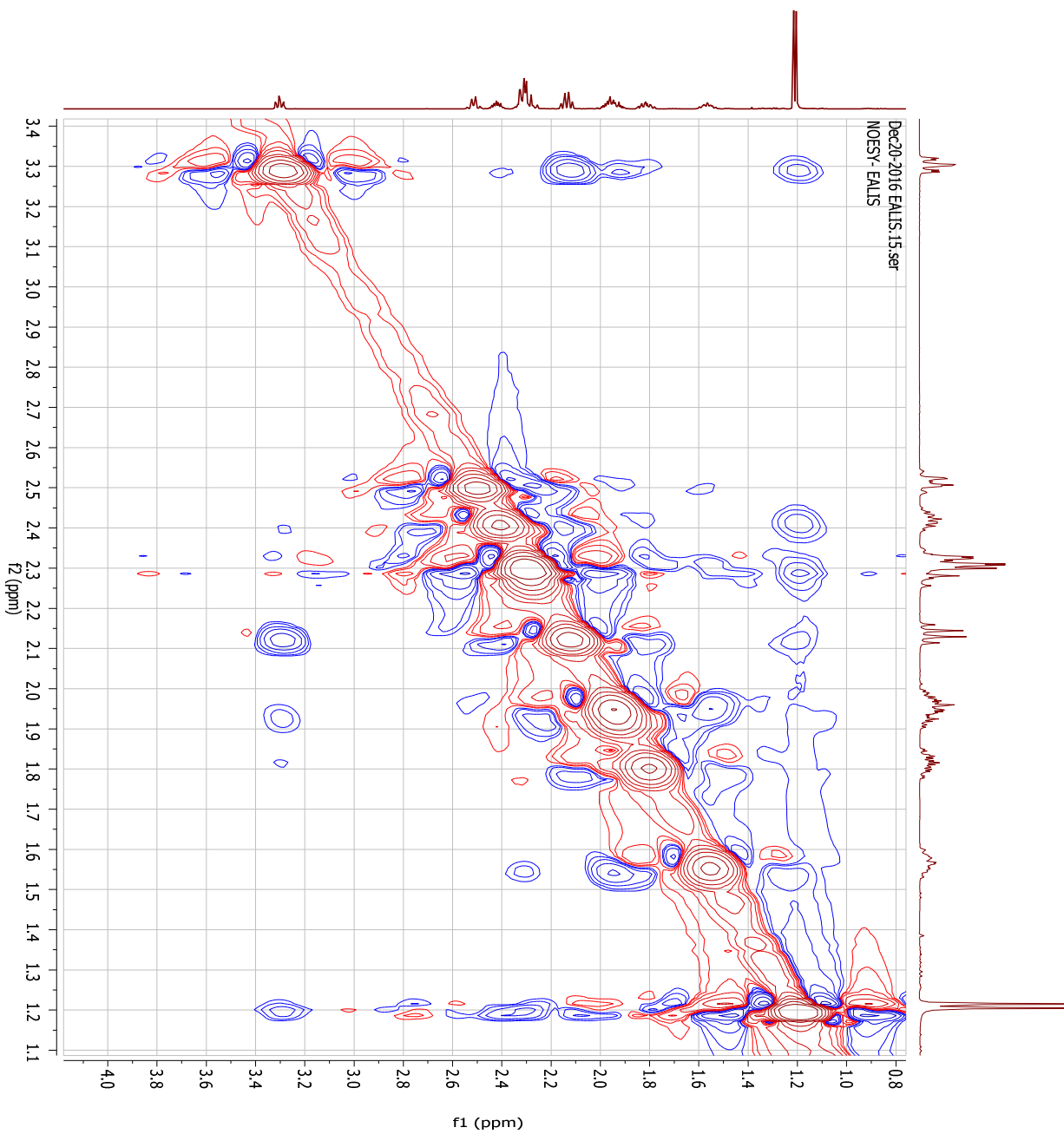
Appendix 71: HSQC spectrum for carpusidine (**14**).



**Appendix 72: COSY spectrum for carpusidine (14).**



Appendix 73: HMBC spectrum for carpusidine (**14**).



Appendix 74: NOESY spectrum for carpusidine (**14**).